Impacts of Large-Scale Reforestation Programmes on Regional Climate Change: A Regional Climate Modelling Study on the Loess Plateau, China

Lang Wang MSc BSc

April 2015

Department of Environmental Sciences, Macquarie University

This thesis is presented for the degree of Doctor of Philosophy.

The Loess Plateau, China after reforestation in June 2008

Abstract

Reforestation has been considered as a strategy for alleviating diverse environmental degradation problems and mitigating anthropogenic global warming in recent years. The 'Grain for Green Project' in China is one of the key reforestation programmes that have been implemented in recent years. The primary goal of the project is to mitigate soil erosion problems across the Loess Plateau region through converting erodible crop lands into forests. The large changes from agricultural land to forest can modify important biophysical characteristics of the land surface, potentially resulting in climate change at a variety of spatial scales.

The Loess Plateau, located in the northern part of China, is considered one of the world's most sensitive areas to global climate change. The plateau is located in the semi-arid transition zone and is characterized by complex topography. The extensive reforestation in the plateau would lead to further complex conditions in the local climate. The local climate is critical for the rain-fed agriculture and natural vegetation primarily through affecting the water availability in this semi-arid area. However, relatively few studies explicitly documented the potential climatic effects of reforestation over the Loess Plateau.

The primary aim of this research was to understand the local climate features and predict the potential impacts of the reforestation programme on the climate over the Loess Plateau. The Regional Climate Model version 4.3 (RegCM4.3) was applied based on its generally good performance. The model was firstly validated over the Loess Plateau region. The simulation overall represented the major climate features well, including surface

temperature, precipitation and regional circulation features at the near-surface level over the Loess Plateau. However the model was found with pronounced cold biases during winter. Analyses indicated that biases were generally caused by the combined effects of deficiencies in interior dynamical processes of the model and were exaggerated by uncertainties among the observational datasets.

Secondly, the major sensitivities of RegCM4.3 in simulating the regional climate over the Loess Plateau were examined. A series of simulations using different configurations were applied to investigate the model sensitivity to several critical model parameterizations. Results showed that the model simulation was significantly sensitive to the convective scheme and the land surface model (LSM). In general, the Grell convection scheme with Fritsch-Chappell closure combined with the LSM of Biosphere Atmosphere Transfer Scheme (BATS) and the Emanuel convective scheme combined with the LSM of Community Land Model (CLM) generated the most accurate simulation among all the configurations. Meanwhile, using higher horizontal resolution of 20 km could also effectively improve the spatial representation of the surface variables compared with the 50 km resolution.

Finally, the two best configurations selected from the sensitivity study in simulating the regional climate were applied to predict the climate responses to reforestation over the Loess Plateau. The conversion from agricultural land to forest led to pronounced changes in the local climate according to the BATS simulations, but only moderate changes in the CLM experiments. When the BATS was used, the surface temperature increased and precipitation decreased significantly during both summer and winter seasons. These

patterns were particularly evident over the southeast of the plateau. In contrast, in the CLM simulations reforestation generally produced a warmer winter, as well as a cooler and more humid summer. The opposite climate responses to the same land change scenario were primarily caused by the different representation of the irrigated crop in the two LSMs. Furthermore, changes in surface albedo, evapotranspiration, and roughness length from agricultural land to forest also played important roles in the climate responses to reforestation.

Beyond the main aim, this study improved on past studies by providing regional model simulation guidance regarding the performance in such climate transitional zones with very complex topography. This study has also revealed the model's strengths and weaknesses, and identified the key mechanisms that drove the simulated biases, which could help to explore future modelling efforts to produce more accurate climate information. The opposite climate responses to reforestation between two LSMs highlight the need for better descriptions of land surface characteristics in climate models in order to enable the reliable prediction of climate responses to land surface change. This study is a part of the efforts in improving our understanding of the local climate over the Loess Plateau, which could provide important references for future reforestation strategies and help reducing economic and ecological losses.

Statement of Candidate

I certify that the work in this thesis entitled ‘Impacts of Large-scale Reforestation Programs on Regional Climate Change: A Regional Climate Modelling Study on Loess Plateau, China’ has not previously been submitted for a degree nor has it been submitted as part of requirements for a degree to any other university of institution other than Macquarie University.

I also certify that the thesis is an original piece of research and it has been written by me. Any help and assistance that I have received in my research work and the preparation of the thesis itself have been appropriately acknowledged.

In addition, I certify that all information sources and literature used are indicated in the thesis.

Lang Wang (42491037)

April 2015

Acknowledgements

First and foremost, I would like to thank my PhD research supervisors: Dr Kevin Cheung and Dr Chih Pei Chang. For all the opportunities and doors you have opened throughout this research project I am extremely grateful. I have thoroughly enjoyed working with, and learning from you both. I have greatly valued your patience, encouragement, guidance and eternal optimism throughout this journey.

Also thanks to Dr Xuejie Gao, Dr Huqiang Zhang, Dr Yingping Wang and Dr Zongliang Yang, for your valuable advice for the initial model settings and the critical model processes. In conjunction Dr Yubin Li, Guoping Zhang, Dr Joachim Mai and Dr Steph Gardham – for your help with the computer skills, model configurations and thesis writing – I am very grateful!

For your supporting in the two critical training courses of my PhD, thanks to Dr Giorgi Filippo, the organizer of the training course, and Dr Graziano Giuliani, the main trainer – I couldn't know the model well and would probably have been struggling each model parameter until now without your help; it was greatly appreciated!

I also want to thank Dr Michael Chang and Dr Alana Grech, who provide me the opportunity to be a GIS lab tutor that was another critical and fulfilling experience during my PhD study. Thank you!

Finally, I want to say thanks to my family and friends…you know who you are…so many sparking moments with you guys during this journey, I will remember them for life long. Thanks to Hangwei. I am so happy that you have been here keeping me firmly grounded and giving me perspective through my many moments of PhD-associated panic.

Contents

Chapter 1. Introduction

“In studies of past and possible future climate change, terrestrial ecosystem dynamics are as important as changes in atmospheric dynamics and composition, ocean circulation, ice sheet extent, and orbital perturbations”

(Pielke et al. 1998)

1. Reforestation programmes and their implementation around the world

The Intergovernmental Panel on Climate Change (IPCC) Special Report on Land Use, Land-Use Change and Forestry states that reforestation and afforestation practices are considered to be a mitigation option for greenhouse gas (GHG) emissions (Watson et al. 2000), and their associated warming, due to the resultant carbon sequestration into forest biomass (Metz et al. 2007). Afforestation refers to the establishment of forests on land that has previously never been forested naturally; while reforestation consists of rebuilding forests on land from which a forest was previously removed (IGBP 1998). Both practices are combined and referred to as reforestation in this study.

a. Reforestation programmes around the world

Reforestation projects are used to solve a range of environmental problems, beyond mitigating climate change; these include maintaining biodiversity, improving water quality, reducing soil erosion and reducing desertification over particular regions (Foley et al. 2003; Jackson et al. 2005). For all these reasons, various reforestation projects have been implemented around the world in recent years. For example, the Conservation Reserve Program, implemented in the United States, converted around 18 million ha of erodible crop land into natural vegetation by 1990, which effectively reduced soil erosion and enhanced wildlife habitats (Ribaudo et al. 1990). Furthermore, a congressional project of reforestation is planned for the southeast of the United States to help mitigate global warming; around 7 million ha of land will be converted into forest by 2020 in the southeast and more reforestation will occur in regions within the Great Lake states and the Corn Belt states (Watson 2009). A series of reforestation projects have also been planned over West Africa (Abiodun et al. 2012) and southern South America (World Bank 2000), with the primary aim of mitigating against future climate change. Moreover, millions of trees are

planted each year in Western Australia, the African Sahel and the Pampas of Argentina, with the intention of controlling dryland soil salinity (George et al. 1999; Walker et al. 2002; Jobbagy and Jackson 2004).

b. Reforestation programmes over China and the Loess Plateau

During the most recent decades, China has implemented six key reforestation programmes to reduce atmospheric concentrations of GHGs, as well as alleviate severe land degradation and other environmental problems (Table 1; Fig. 1) (Cao et al. 2011). These reforestation programmes targeted 75 million ha of land for reforestation, which covered more than 97% of China's counties (Wang et al. 2007). Under these programmes, significant progress has been achieved in reforestation, such as the establishment of 28 million ha of plantations, between 2000 and 2005 (Chazdon 2008). The total forest coverage in China has increased from 16.6% to 18.2% since 2000. By 2050, an aggressive goal has been set to increase forest coverage by up to 26% of China, through these reforestation programmes (Wang et al. 2007).

TABLE 1 The major afforestation programmes in China in recent decades (Cao et al. 2011).

Six key afforestation projects	Region	Project dates	Project goals	Planted area (million ha)
Three North Shelter Forest System Project (Phase IV)	Northern and western provinces	2001–2010	Desertification control	27.5
Natural Forest Conservation Program	Northern and central China; 17 provinces	2000–2010	Soil and water conservation	4.4
Sand Control Program	Northern China; 5 provinces	2001–2010	Desertification control	5.2
Grain for Green Project	All of China except the southeastern provinces	2001–2010	Soil and water conservation	32
Forest Industrial Base Development Program	Areas of eastern China where precipitation is more than 400 mm; 17 provinces	2001–2015	Wood production	13.3
Wildlife Conservation and Nature Reserves Development Program	All of China	2001–2010	Wildlife conservation and the development of nature reserves	-

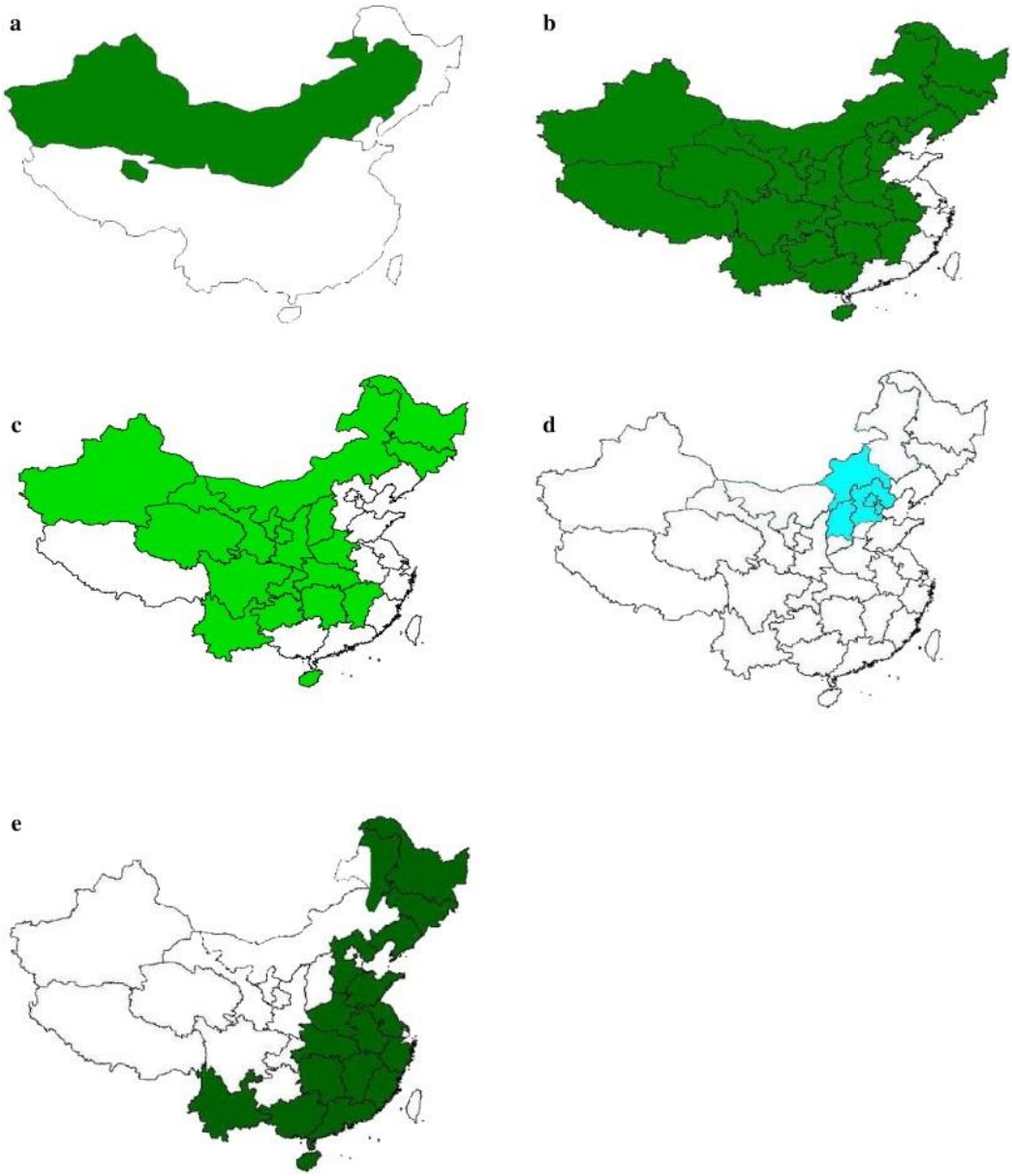

FIGURE 1 The distribution of the areas affected by the afforestation conducted under (a) the Three North Shelter Forest System Project, (b) the Grain for Green Program, (c) the Natural Forest Conservation Program, (d) the Sand Control Program for areas in the vicinity of Beijing and Tianjin, and (e) the Forest Industrial Base Development Program (collated from information/figures of Cao et al. (2011); Li (2001); Yang (2004); Liu et al. (2008a) and Piao et al. (2010).

The 'Grain for Green Project' (GGP), over the Loess Plateau in Northern China, is one of the key reforestation programmes. The Loess Plateau, located in the northern part of China and 64.87 million km^2 in size, is considered one of the world's most sensitive areas.

The GGP started in 1999, with the primary aim of conserving water and soil resources that are impacted by severe soil erosion; this is caused over the Loess Plateau, by a series of natural and anthropogenic factors, including the local loose soil texture, hilly and gully terrains and summer extreme rainfalls, as well as low vegetation coverage and highly erodible cultivation practices. The GGP is primarily concerned with anthropogenic effects on soil erosion and has focussed on an improvement of vegetation coverage and reduction in the area of erodible cultivation practices. Consequently, the crop lands and bare lands with slopes over 25˚, that are more vulnerable to erosion, were replaced by natural vegetation, such as forest, bush land and grassland through the GGP (e.g., Li 2004; McVicar et al. 2007; Lü et al. 2012).

Accordingly, the land surface over the Loess Plateau has experienced a significant change since 1999. By the end of 2008, the area of farming land had decreased from 40.80% to less than 30%, of the total area of the plateau. Meanwhile the area of woodland (forest and bush land) had increased from 11.91% to over 16%; and grassland had increased from 38.97% to over 43% of the total plateau area (Lü et al. 2012). Over the next two decades, it is proposed that, through the GGP, another 17% of the erodible areas on the plateau will be converted to natural vegetation (NDRC et al. 2010). However, before embarking on such massive reforestation activities, there is a need to investigate the influence of the GGP, especially on global and regional climate change. This would guide policymakers on the pros and cons of creating such reforestation belts over these regions, from the view of global climate change.

2. Potential effects of reforestation programmes on the climate

Extensive land cover changes caused by reforestation impact the climate through direct and indirect interactions with atmospheric systems on a variety of spatial scales.

Directly, reforestation increases the sequestration of carbon. Indirect interactions occur through the modification of land surface properties, which play critical roles in the biophysical feedback mechanisms (Foley et al. 2003; Field et al. 2007; Bonan 2008; Anderson et al. 2010); such land surface properties that are affected include soil water content, evapotranspiraton (ET), surface albedo and surface roughness (Bonan 2008).

a. Carbon sequestration

The Kyoto Protocol considered that reforestation could partly offset the GHG concentrations in the atmosphere through carbon sequestration, although this sequestration was viewed as a temporary reservoir (IGBP 1998; Metz et al. 2007). Since the Kyoto Protocol, a series of studies have shown that reforestation leads to substantial carbon uptake, particularly through the conversion of crop lands and bare lands to woodlands (Unruh 1995; Betts 2000; Fang et al. 2001; Jackson et al. 2005; Metz et al. 2007). For example, Fang et al. (2001) found that carbon storage in China has increased significantly, mainly due to reforestation programmes, since the late 1970s; they studied this through a forest biomass database, obtained from direct field measurements. Furthermore, Jackson et al. (2005) used a GHG model to estimate the area of reforestation, and found that 72 million ha of land would initially need to be converted into forested land in the United States for carbon sequestration at the simulated price of $ 100 per Mg Carbon.

b. Change in albedo

The albedo mechanism describes the change in radiative forcing as a result of the surface albedo effect. Charney (1975) and Charney et al. (1977) first postulated this vegetation-atmosphere interaction, through investigating the effects of albedo in semi-arid regions, and their studies have been followed by a series of studies (e.g., Sud and Fennessy

1982; Laval and Picon 1986). Through these studies, it has been shown that vegetated areas generally have a lower surface albedo, compared to bare soil or snow covered ground, and this results in an increase in the amount of energy absorbed by the surface; the higher energy absorption in turn favours an increase surface air temperatures and may enhance precipitation. Particularly, over boreal areas, which have large snow coverage, the albedo mechanism has been shown to strongly affect the local climate; Bonan (2008) found that over such regions, forests tend to have a local warming effect, since forested land is significantly darker and reflects much less solar radiation back into space, compared to crop land, in which any extensive snow cover is exposed (Fig. 2c). Betts (2000) also found that in some areas of boreal forests, the warming effect of the change in albedo, caused by reforestation, was equivalent to the cooling effect of carbon sequestration, resulting in a neutral total forcing.

Forested lands are also darker than other land types over tropical and temperate regions, but they induce more complex climate conditions, compared to the general warming effect over boreal regions (Figs. 2a, b) (Bonan 2008). For example, over the subtropical rainforest in South America, the darker forest maintained a higher level of surface latent and sensible heat flux, due to the sufficient absorbed surface radiation energy; this resulted in more intensive convection and precipitation, compared to grassland areas (Dirmeyer and Shukla 1994). Enhanced rainfall as a result of reforestation has also been found over the Sahel region, due to changes in albedo (Xue and Shukla 1996). Over temperate regions, in some areas a general warming effect of reforestation has been found, but in others this has not been shown (Fig. 2b) (Snyder et al. 2004; Bonan 2008). At the global scale, converting from crop land to forest is likely to induce a cooling effect, primarily caused by changes in the surface albedo leading to a re-balancing of the Earth's radiation budget (Lenton and Vaughan 2009). The global radiative forcing as a result of

changes in albedo may be comparable with that that occurs due to anthropogenic aerosols, solar variation and several of the GHGs.

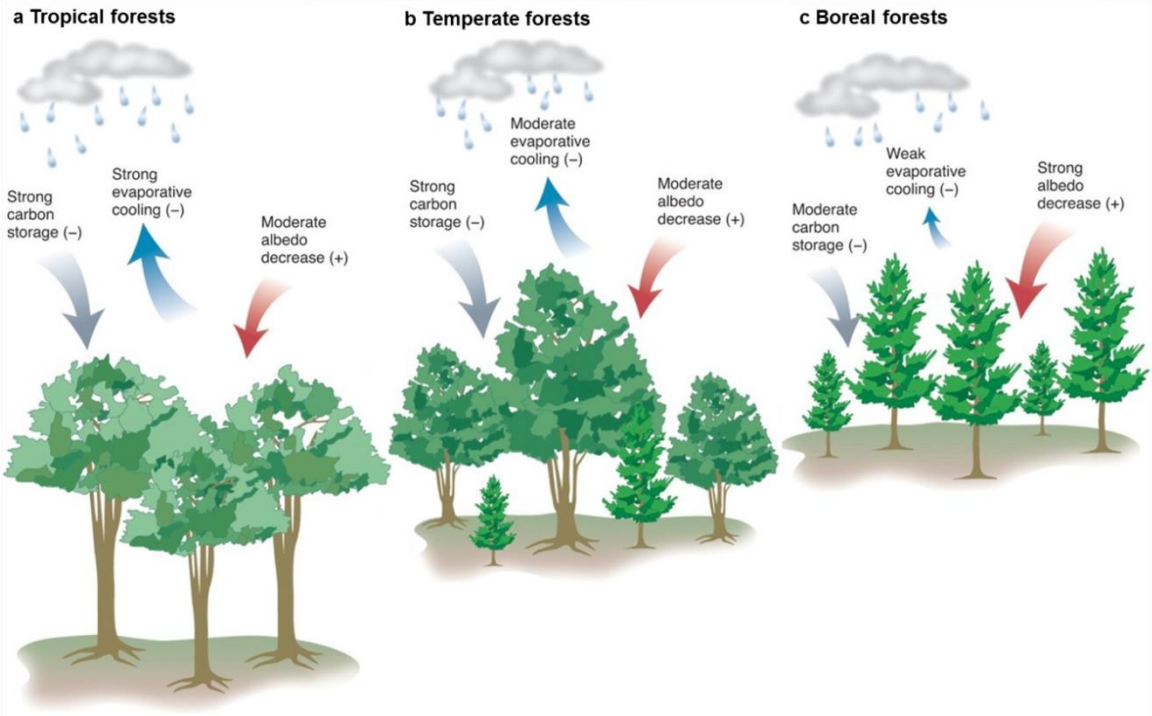

FIGURE 2 Climate services in (a) tropical forests, (b) temperate forests, and (c) boreal forests, copied from Bonan (2008).

c. Change in evapotranspiration

Vegetation that is more efficient at ET and partitions more energy into latent heat, is more likely to lead to a decrease in surface temperatures and possibly an increase in precipitation (Shukla and Mintz 1982; Bounoua and Krishnamurti 1993; Zeng et al. 1999). For example, forests with higher ET rates (because they have deeper roots that allow trees to access deeper soil water for maintaining high ET during dry seasons) are more likely to have a cooling effect than other land types in tropical regions (Fig. 2a) (Bonan 2008). Jackson et al. (2005) used a Regional Atmospheric Modelling System (RAMS) to simulate the climatic effects of reforestation over the eastern United States; their results showed that conversion from crop land to forest cooled down summer temperatures by 0.3˚C, primarily

through enhanced ET rates (> 0.3 mm day^{-1}). However, the simulated precipitation in their study generally decreased by 30 mm $month^{-1}$. The increase in ET rates did not generate more rain, primarily because the temperate regions modelled did not have sufficient energy to elevate the additional atmospheric moisture high enough for it to condense and form clouds. Furthermore, the lack of sensible heating over areas in which the vegetation was converted, reduced the energy available for convection; this resulted in a reduction in total precipitation in general, and the convective component in particular.

d. Change in roughness length

A higher roughness length of vegetation, such as forest land compared with crop land, on the one hand results in an increase in turbulent mixing in the boundary layer (latent heat and sensible heat), thus reducing surface air temperature. On the other hand, it results in more mass convergence, associated with an anomalous lower pressure, which increases upward moisture transport and convective clouds, thus increasing precipitation (Dickinson and Henderson-Sellers 1988; Sud et al. 1988; Bonan 1997).

Higher roughness length can also reduce near surface wind, thereby decreasing temperature and moisture advection (Zhang et al. 2009; Zhang and Gao 2009; Liu 2011). For instance, using a global circulation model (GCM), Xue and Shukla (1996) found that precipitation increased by 0.8 mm day^{-1} (27%), over the reforested area in the Sahel, primarily caused by the changes in moisture convergence, which was forced by changes in roughness length and latent heat. Liu (2011) evaluated the potential climatic effect of the congressional afforestation project over the southeast United States, by replacing crop lands with forest, using the regional climate model (RegCM); they found that precipitation increased during the winter months over the reforestation area, but decreased during the summer. The changes in precipitation were mainly caused by the increased surface

roughness of the forest that reduced the prevailing winds in both seasons. These climatic effects of surface roughness on prevailing winds are also the main cause for the increase in the simulated precipitation over northern China, where the reforestation region was located in the middle latitudes, with westerly prevailing winds. The cool and dry westerly winds decreased, due to the higher roughness length of the planted trees, thus generating more precipitation locally (Liu et al. 2008c).

e. Change in other biophysical mechanisms

Several other mechanisms, resulting from changes in vegetation that lead to effects on the climate, have also been examined. For example, the effect of changes in the leaf area index (LAI) on climate was investigated by means of a general circulation model (GCM) (Chase et al. 1996); a higher LAI of forest compared with crops, was found to increase the surface latent heat flux and decrease the sensible heat flux, during both winter and summer seasons, on a global scale (forests have a higher maximum LAI and stem area index than crops). Xue et al. (1996) replaced crop lands with broadleaf deciduous trees in a GCM, coupled with the Simplified Simple Biosphere (SSiB) model. They also found an increase in latent heat flux and a decrease in sensible heat flux over the reforested region in the central United States, as well as a summer cooling effect of up to 2˚C and enhanced precipitation. The increase of the LAI was the determining parameter in the magnitude of these changes in climate. An increase in the LAI was also found to be the main factor involved in cooling of the local temperature, due to reforestation, over Western Australia in a climate simulation (Pitman and Narisma 2005).

Changes in the leaf-scale stomatal resistance is another key mechanism; it influences the ease with which water can pass from a plant to the atmosphere (Xue et al. 1996). Crop lands, especially irrigated crop lands, generally have the lowest stomatal resistance,

followed by broadleaf deciduous trees and grassland. An increase in stomatal resistance (by conversion from crop land to natural vegetation) is likely to result in less transpiration and lower ET rates, and thus influences the simulated climate through ET (Fig. 3) (Findell et al. 2007). The rooting depth also impacts on modelled ET rates due to similar physical processes: a decrease in the rooting depth effectively reduces the maximum soil water holding capacity of the grid cell. For a given rainfall event, a small soil water holding capacity is more likely to become saturated than a large soil water holding capacity. Thus, rainfall is more likely to be removed by surface runoff, leaving less moisture available for ET (Findell et al. 2007). According to global studies of climate change, the local climate may also respond to land surface disturbances that occur in regions distant from the local area, through changes in atmospheric circulations and teleconnections (Chase et al. 2000; Feddema et al. 2005; Pielke 2001).

f. The combined influence of biophysical mechanisms

Clearly, there are several mechanisms that influence the local and global climate; as a result, it is still a major scientific challenge to accurately predict the potential responses of the local climate to large-scale land surface changes, such as reforestation programmes. This is mainly due to the fact that land surface change is an extremely complex system, with many processes operating simultaneously and interacting at various temporal and spatial scales. In general, reforestation, by converting bare land or crop lands into forest, leads to a decrease in albedo and an increase in ET rates and roughness length, along with increases in the LAI and rooting depth (Fig. 4) (Sellers 1992; Jackson et al. 1996; Pitman 2003; Liu 2011). Decreases in the albedo tend to generate higher surface air temperatures, based on the albedo radiation mechanism; in contrast, increases in ET rates and roughness length are more likely to cool temperatures.

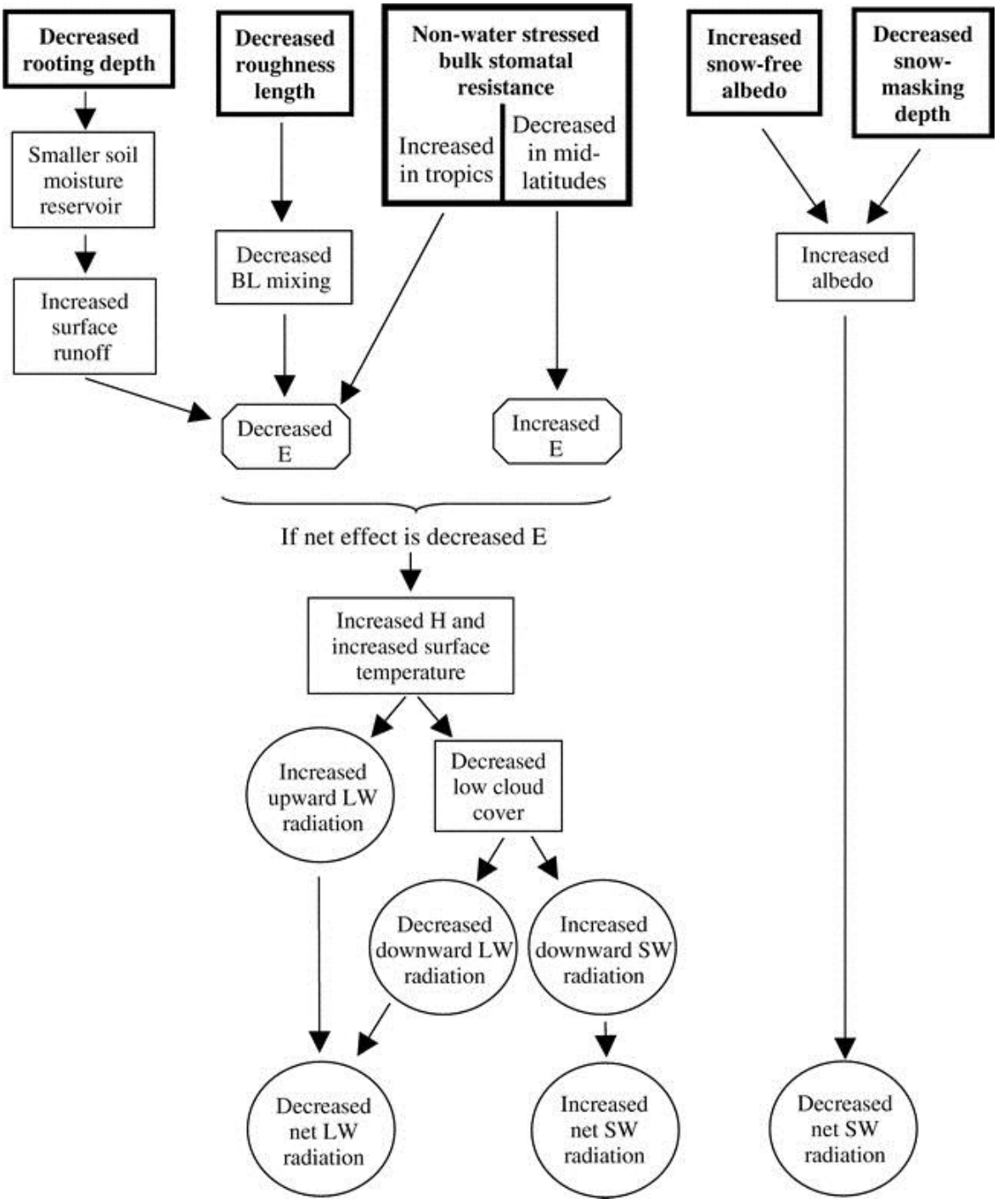

FIGURE 3 Idealized schematic of the physical processes that are influenced by the conversion of forests to grasslands. Model-prescribed physical parameters are in bold; BL: boundary layer, E: evapotranspiration, H: sensible heat flux, LW: longwave, and SW: shortwave. All radiative fluxes (in circles) are surface fluxes (positive towards the surface) (Findell et al. 2007).

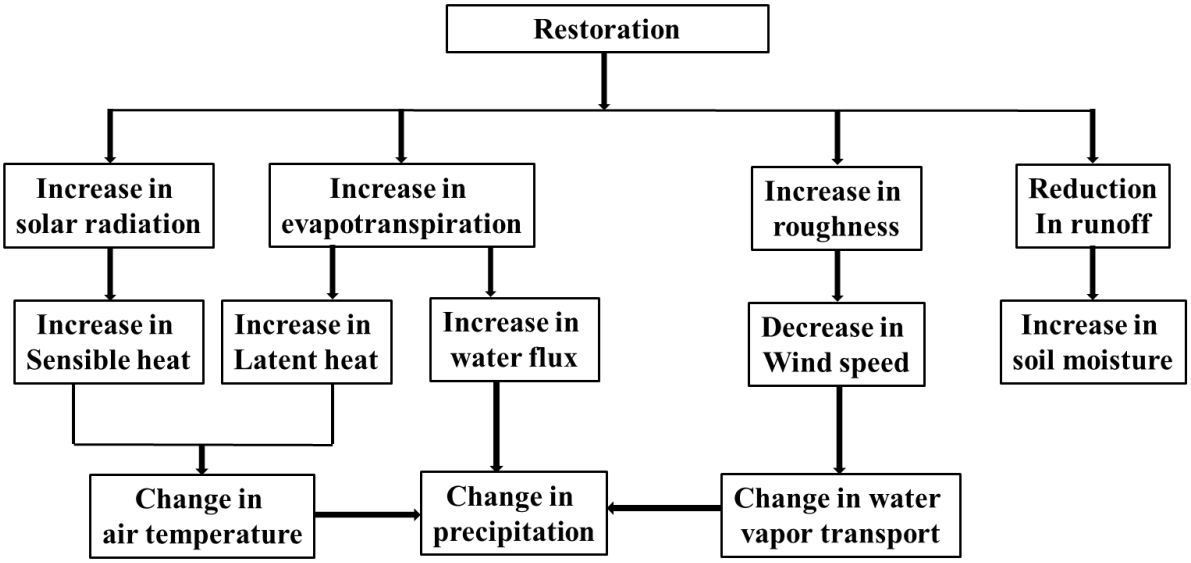

FIGURE 4 Forested lands have a smaller albedo and larger evapotranspiration rates, roughness, and water capacity than cultivated lands. A smaller surface albedo leads to more solar radiative energy absorbed on the ground, which is converted into larger sensible and latent heat fluxes and air temperature changes. Larger evapotranspiration moves soil water in the root layer into the atmosphere, through leaf stomata. Larger roughness reduces prevailing wind speeds on the ground and therefore changes water vapour transport in the atmosphere. Greater holding capacity of soil moisture contributes to a reduction in runoff. Precipitation, determined by water vapour availability, vertical velocity, and thermal instability, is modified in response to the changes in temperature and vertical and horizontal transport of water (Liu 2011).

1) THE EVALUATION OF BIOPHYSICAL EFFECTS OF REFORESATION

It is difficult to evaluate the biophysical feedback mechanisms through observations, although some observational approaches have been applied to assess reforestation effects on the global or regional climate. For instance, Brooks (1928) suggested that replacing bare soil with forest would increase local precipitation by 1–2%, based on observational data. Stebbings (1935) proposed a forest band across West Africa, to bind the blowing sand, and following its implementation showed that the conditions of the local hydro-climate were improved. Anthes (1984) suggested that reforestation in semi-arid

regions, initially irrigated by aquifer water, could enhance both the total and convective precipitation rates locally, driven by favourable mesoscale circulations, based on statistical analyses of observational data.

Furthermore, a global analysis of observational data from 504 annual catchments found that reforestation substantially decreased surface runoff within a few years of implementation (Jackson et al. 2005). Using satellite based indices, present day vegetation feedback mechanisms on the global or regional climate have also been assessed (Kaufmann et al. 2003; Liu et al. 2006; Notaro et al. 2006; Notaro and Liu 2008). Particularly, Notaro et al. (2006) found that reforestation in the United States leads to a cooling of surface air temperatures and an increase in precipitation.

Although observational approaches can be used, most of our understanding on how reforestation and other land surface changes affect the climate has come from model simulations. A large number of studies have been published of the climatic impacts on land surface changes recent years (e.g., Nobre et al. 1991; Fu and Yuan 2001; Zhang et al. 2001; Findell et al. 2007; Pitman et al. 2009; Pitman and de Noblet-Ducoudré 2011; Boisier et al. 2012; de Noblet-Ducoudré et al. 2012; Pitman et al. 2012). In these studies, the climatic impacts of reforestation have mainly been explained through changes in the albedo, ET mechanism and the roughness length.

The overall effects of reforestation on the local climate vary significantly across regions with different climate backgrounds and climate models with different physical processes. For example, over the United States, Xue et al. (1996) found reforestation generally cooled summer temperatures and increased precipitation, with a GCM simulation. In contrast, Bonan (1997) and Oleson et al. (2004a) found that forests in the same area increased the summer temperature, while Copeland et al. (1996) similarly showed that forests led to lower temperatures, but conversely decreased precipitation, in the summer.

There is therefore a pressing need to improve our climate simulation capacity and achieve a better predictive ability, with regard to the impacts of land surface properties on local and global climate change (Copeland et al. 1996). This study comprises part of the efforts in improving this understanding, by investigating the potential impacts of reforestation on the local climate over the Loess Plateau.

3. The current status of climate modelling

The recent IPCC Fifth Assessment Report concluded that there is considerable confidence that current fully coupled GCMs can provide credible quantitative estimates of future climate change at the continental and larger scales (Stocker et al. 2013). However, GCMs, with a horizontal resolution typically at hundreds of kilometres, have a limited capacity to represent topography and land surface heterogeneity and a lack of skill in simulating regional scale climate and mesoscale processes, such as convective storms. Thus, high-resolution regional climate models (RCMs), together with statistical downscaling, have been used for simulating detailed changes in regional climates (Takle et al. 1999; Fu et al. 2005; Christensen et al. 2007; Schmidli et al. 2007; Stocker et al. 2013; Mearns et al. 2012). Particularly in the last decade, the development of RCMs using dynamical downscaling has increased tremendously. RCMs can achieve great detail of the physical processes, and represent more realistic local processes affecting the climate; thereby they have become a better tool for understanding the climate at the regional scale, in comparison to GCMs (e.g., Giorgi and Mearns 1999; Sen et al. 2004; Pal et al. 2007).

The RCM technique was first developed in the late 1980s, in the United States National Centre for Atmospheric Research (NCAR) and was based on the standard NCAR/Penn State University (PSU) Mesoscale Model Version 4 (MM4) (Anthes et al. 1987; Dickinson et al. 1989; Giorgi and Bates 1989). RCMs began to be used in the 1990s

to improve the results from GCMs, with a focus on Europe, North America, East Asia and Australia (e.g., Giorgi and Mearns 1991; McGregor 1997; Giorgi and Mearns 1999). Nowadays, RCMs cover most geographical regions of the globe for a range of applications, allowing downscaling of the outputs from GCMs (for climate change studies, physical analyses of the climate, seasonal forecasting, etc.) and can use observational data (reanalysis; e.g., NCEP, ERA-Interim) as their initial and boundary conditions (e.g., Christensen et al. 2007). A series of RCMs have been extensively used recent years, primarily: the RegCM (Giorgi et al. 2012); the non-hydrostatic version of the PSU Mesoscale Model version 5 (MM5), coupled with the NCAR Community Land Model version 3 (CLM3) (MM5-CLM3) (Oleson et al. 2004b); the climate version of the weather research and forecast (WRF) model (Liang et al. 2012); the Regional Spectral Model (RSM) (Juang and Kanamitsu 1994); the RAMS (Cotton et al. 2003); the Hadley Centre regional climate modelling system (Jones et al. 1995); and the Canadian regional climate model (CRCM) (Laprise et al. 2003). The evaluation, development and application of these RCMs have been outlined in several studies (e.g., Wang et al. 2004; Giorgi et al. 2009; Rummukainen 2010; Evans et al. 2012; Hong and Kanamitsu, 2014).

Despite the advances of RCMs in recent years, there are some limitations in the modelling technique, which have been outlined in several review studies (Rummukainen 2010; Leung et al. 2003; Laprise et al. 2008). First of all, RCMs are driven by GCMs and/or reanalysis; therefore, any errors in lateral conditions will be passed on to the RCMs (McDonald 1997; Warner et al. 1997; Seth et al. 2007; Sylla et al. 2010). Secondly, information deficiencies of the complexity of the land surface in a region can limit the ability of the RCMs to reproduce important features in the atmosphere (Im et al. 2010; Wang et al. 2009). Particularly, soil moisture and snow are among the data elements for which very limited information is available in some areas. This could lead to errors in the

simulation of soil moisture, albedo and ET. Thirdly, domain size and domain choice also affect the performances of RCMs (Warner et al. 1997; Antic et al. 2004; Seth and Giorgi 1998). Different parameter configurations can also lead to very different simulation results (Pal et al. 2000; Fernandez et al. 2006; Frei et al. 2006; Jacob et al. 2007; Yhang and Hong 2008). An additional complication is that driven by the same boundary conditions; there are various simulation results from RCMs, reflecting each individual model's uncertainty.

A number of RCMs have previously been validated and used for the East Asia and China region, and have been shown to effectively improve the climate simulation, relative to GCMs (e.g., Zhang et al. 2006b; Gao et al. 2008; Wang et al. 2014). In particular, the RegCM, developed by the Earth System Physics (ESP) section of the Abdus Salam International Centre for Theoretical Physics (ICTP), has been extensively used, based on its good performance at least in comparison to the MM5-based models (Leung et al. 1999; Fu et al. 2005). The RegCM began to be utilized over the East Asia and China region in the 1990s, to simulate the observed features of the present climate (Giorgi et al. 1993a; Giorgi et al. 1993b; Liu et al. 1994; Hirakuchi and Giorgi 1995; Giorgi et al. 1999; Kato et al. 1999).

Use of the RegCM has increased in recent years, to address objectives, such as: investigations of the model's ability to simulate the regional climate (e.g., Im et al. 2006; Gao et al. 2011; Park et al. 2008); evaluations of the use of different initial and boundary condition forcings, as well as different physical parametrizations (Pan et al. 2001; Singh et al. 2006; Steiner et al. 2005); validations of the simulated diurnal cycle of precipitation (Gao et al. 2006; Gao et al. 2008; Gao et al. 2012); evaluations of the model's ability when coupled with an aerosol-chemistry model, to simulate specific climatology of atmospheric systems (Qian et al. 2001; Giorgi et al. 2003a); explorations of future climate scenarios

(Gao et al. 2001; Gao et al. 2002; Gu et al. 2012); and evaluations of land surface change scenarios (Gao et al. 2003; Gao et al. 2007; Wu et al. 2012).

4. Climate effects of reforestation programmes over China and the Loess Plateau

There have been a number of studies of the climatic impacts of vegetation change in the regions in the vicinity of the Loess Plateau. Liu et al. (2008c) used an early version of the RegCM to simulate the impact of reforestation in northern China; they found that overall, reforestation increased precipitation, ET fluxes, relative humidity and root-layer soil moisture, and reduced air temperatures and wind speed over the reforested regions. Xue (1996) used a GCM, coupled with SSiB, to study the impacts of desertification in the Mongolian and Inner Mongolian region, the simulation domain of which included the northern part of the Loess Plateau. Their results suggested that, compared with bare soil, vegetated land would likely have higher precipitation rates, particularly over the northern Loess Plateau parts of the degraded region. Over a similar region of the Mongolian plateau, Zheng et al. (2002) used the RegCM version 2 and found that, with grassland the local climate tended to be more humid than with bare land; they showed that changes of roughness length played a more important role than changes of surface albedo in precipitation, surface air temperatures, and atmospheric circulation patterns. They considered that further conversion, from grassland to forest, would possibly lead to a greater reduction in precipitation, especially over the outer belts of the vegetation conversion (Zheng et al. 2002).

There have also been a series of studies of the climatic impacts of vegetation change over the China and East Asia regions. Xue and Fennessy (2002) provided a review of studies investigating the impacts of land surface change on local and regional climate in East Asia. Fu et al. (2002) also evaluated some studies that investigated the interactions

between the atmosphere, land surface and regional climate systems in the East Asian monsoon region. Furthermore, Fu and Yuan (2001) used a regional integrated environmental model system (RIEMS) to simulate a change from crop land to natural vegetation over China and found that natural vegetation tended to have a cooling effect (by around 1˚C), over the Loess Plateau region, and an increase of precipitation by around 1–2 mm day^{-1} during the summer season. Their results were confirmed by Gao et al. (2003) that used the RegCM forced by a GCM over China. They found that the natural vegetation, with large areas of grass and bush land over the Loess Plateau region, was likely to produce more rainfall and lower temperatures during summer, compared with the current vegetation patterns which comprised extensive areas of crop land. Their results also suggested that changes of roughness length would be the primary forcing, which would also influence the wind circulation, and the maximum and minimum temperatures. Wang et al. (2003) also investigated the climatic impact of land surface changes during the period comprising 1700, 1750, 1800, 1850, 1900, 1950, 1970 and 1990, over China using a high resolution regional model. Their simulated results were consistent with Gao et al. (2003) and Fu and Yuan (2001), and showed that forests and grasslands were more likely to lead to a significant increase in humidity and cooling effect over large areas of China, compared with crop lands, during June.

Despite the previous research, uncertainties of local climate changes in response to changes in vegetation always affect model simulation results. The magnitude, location, and direction of the changes in climate vary among the models and studies and appear to be dependent on the specifics of the parameterizations in biophysical processes. For example, Xue et al. (2004) applied two different land surface schemes to a GCM (one using SSiB with explicit biophysical processes and the other without); they found that land surface processes represented by the two schemes had different effects on the development of the

East Asian monsoon and circulation in 1987. Furthermore, Zhang et al. (2009) studied the impact of vegetation changes from natural vegetation to the current vegetation, using the Australian Bureau of Meteorology Research Centre (BMRC) model, and found that natural vegetation tended to generate a warm and humid winter, but less precipitation during summer over China. In contrast, Zhang and Gao (2009) used the RegCM to simulate the same vegetation forcing, but found a conflicting response of the simulated summer precipitation, which was more humid over the area where the vegetation was changed. The major factors that explained how the vegetation changes may affect the local climate remained the same in the two models (the roughness length mechanism played a critical role in both climate responses), but the modelled monsoon spatial pattern varied between the two models and that directly led to the differences in the summer precipitation simulated (Fig. 5). The study with the RegCM (Zhang and Gao 2009) was more consistent with other studies of vegetation change in East Asia (e.g., Zhao and Pitman 2005). Therefore, more accurate climate models are required to simulate changes in climate and gain confidence in our understanding of the impact of land surface changes under current and future climate conditions.

In summary, changes in vegetation will impact on the local and global climate. It is recommended that, before implementing the large-scale reforestation programme in the next round of the GGP, the effects on the climate, as well as the risks associated with the reforestation should be well understood. A series of studies have focused on the direct and potential climate effects of major reforestation programmes over the world, through observations and climate simulations. However, large uncertainties of the climate responses to reforestation remain in all these studies, and relatively few studies have explicitly investigated the large-scale reforestation over the Loess Plateau region. In this

regard, the present study aims to investigate the potential climate effects of reforestation over the Loess Plateau in China, with a more precise model.

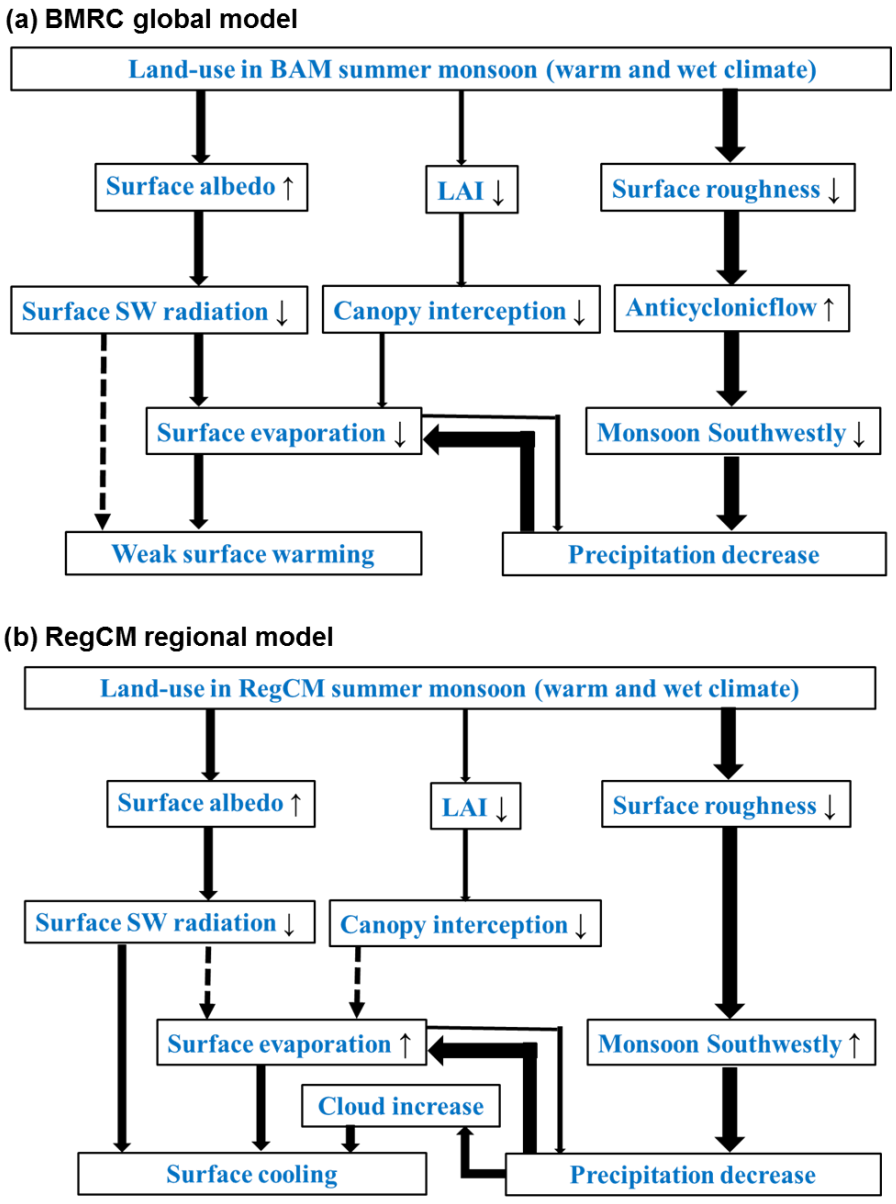

FIGURE 5 Schematic diagram showing the physical processes that lead to the differences between the RegCM and BMRC model-simulated changes in rainfall and surface temperatures in summer: (a) processes simulated in the BMRC global model; and (b) processes simulated in the RegCM regional model. The thickness of the arrows reflects the relative importance of each process and dashed arrows mean the process has a negative contribution to the changes in surface temperature or rainfall (Zhang and Gao 2009); LAI is leaf area index.

5. The need for this research

The area comprising the Loess Plateau and its surrounding regions, is located in northern China and is considered one of the world's most climatic sensitive areas (Stocker et al. 2013). The plateau is located in the largest climate transition area in northern China, between the humid East Asian monsoon region and the continental semi-arid region (Huang et al. 2008). Climate interactions between these two regions result in complex conditions over the Loess Plateau, where a moderate change in the system would lead to a high variability in the local climate (e.g., Li et al. 2010; Zhou et al. 2010).

The complex climate conditions are further amplified by the complex topography of the Loess Plateau. On the one hand, two large orographic systems surround the plateau, including the Tibetan Plateau, 'the roof of the world', which lies to the southwest, and the Mongolian Plateau to the north. In particular, the Tibetan Plateau results in a sharp increase in the elevation over the southwest of the Loess Plateau, from 500 m to 3000 m; this can enhance the convection processes to a great degree at the local scale and regulates mesoscale circulation (Pielke and Avissar 1990; Pielke 2001; Dickinson 1995). On the other hand, the Loess Plateau has thousands of gullies, due to severe soil erosion, which has resulted in a highly heterogeneous land surface boundary.

Considering the high variability of the local climate and complex geophysical characteristics of the Loess Plateau, an understanding of the regional climate has become an essential scientific issue. However, there are few studies that have explicitly focussed on the local climate over the Loess Plateau, through climate modelling. Furthermore, the large-scale land surface changes induced by the reforestation programme may have, and in the future could further, alter water, heat and momentum exchanges between the land and atmosphere, as previously discussed, thus affecting the local climate substantially. It is important to be able to understand and predict such changes and their potential impacts on

the local climate. The local climate is also critical for the development of the economy and natural ecosystems, primarily through affecting water availability for rain-fed agriculture and natural vegetation in this semi-arid area.

Based on the reliable ability of the RegCM in reproducing major high-resolution spatial characteristics of the climate over China and East Asia, the RegCM approach has been taken to quantify the local climate and the climatic effects of the land surface changes that have occurred due to the reforestation programme, over the Loess Plateau. The RegCM allows the topographic variability to be well represented, including the complex orography and pronounced land surface changes, which is extremely important for robust climate prediction over the Loess Plateau (Giorgi et al. 1997).

6. Thesis aims and structure

The overall aim of this research was to identify the potential effects of the large-scale land surface changes, which have resulted from the reforestation programme, on the local climate over the Loess Plateau. In order to do this, the research was performed using the RegCM, and a series of observational data sets.

Chapters within this thesis have been written in a format for publication, with some additions that add value to the thesis. At the start of each chapter, the contributions of other individuals to the work presented are acknowledged.

Chapter 2: A Regional Climate Modelling Study over the Loess Plateau, China. Part I: Model Evaluation against the observed climatology

The aim of the work presented in this chapter was to validate the performance of the RegCM in simulating the local climate of the Loess Plateau, as well as analyse the origins of the model biases and identify the key mechanisms that drive the simulated biases. The

chapter describes details of the RegCM model, parameterization schemes, characteristics of the Loess Plateau, and an assessment of the model performance in predicting surface air temperature, precipitation, and wind circulation. Comparison with a series of observational datasets was provided. The work presented in this chapter revealed the strengths and weaknesses of the RegCM, identified uncertainties of driven reanalysis data sets and observational data sets for model validation, and provided reference for further climate simulation over the Loess Plateau.

Chapter 3: A Regional Climate Modelling Study over the Loess Plateau, China. Part II: Sensitivity Tests

The aim of the work presented in this chapter was to further evaluate the performance of the RegCM over the Loess Plateau, and characterise the key parameterizations that influenced the model simulation. A further aim was to provide a model configuration that was able to reproduce the local climate more appropriately for further application of simulating the potential effects of land surface changes on the climate over the plateau. With these considerations, a series of experiments using different parameterizations were designed through applying alternative convective schemes, horizontal resolutions, and domain locations. The work in this chapter assessed the level of accuracy that the RegCM could reach over the Loess Plateau and provided general guidance for simulations over areas in a mid-latitude zone with complex topography.

Chapter 4: A Regional Climate Modelling Study over the Loess Plateau, China. Part III: Impacts from the Community Land Model

The aim of the work presented in this chapter was to investigate the model sensitivity to the land surface model (LSM) in the RegCM system over the Loess Plateau. Generally,

the LSM is applied to represent the land surface conditions and provide biophysical feedbacks to the atmosphere; therefore, it plays a critical role in simulating the effects of reforestation on the local climate. The work presented in this chapter evaluated the performance of the RegCM configured with the two LSMs over the study area, and investigated the key processes and mechanisms that led to the differences between the simulations generated by the RegCM. Based on these analyses, an optimized configuration of the RegCM over the Loess Plateau was achieved, which could then be applied to model the potential climate impacts of the reforestation programme.

Chapter 5: A Regional Climate Modelling Study over the Loess Plateau, China. Part IV: Impacts of Reforestation Programmes

The aim of the work presented in this chapter was to investigate the potential climatic effects of reforestation over the Loess Plateau region, with a focus on land-atmospheric interactions and the modulations to climate variability. The two most appropriate RegCM configurations were used in the work presented in this chapter; these configurations were identified from the evaluations in Chapters 2 to 4. We explored the dominant atmospheric dynamical processes that were responsible for the simulated impacts of reforestation on the local climate, through a series of hypothetical reforestation scenarios. These scenarios led to changes in the surface albedo, ET fluxes, roughness length and stomatal resistance, which modified the land-atmosphere interactions and further influence the regional climate features. By performing these analyses, the potential impacts of reforestation on the local climate were revealed, including its impact of mitigating climate change and improving ecosystem conditions.

Chapter 6: Discussion

The discussion summarizes the findings of this research, and places it in context with other similar modelling studies and observational datasets. Within the chapter, future opportunities and directions for this research are also identified.

Chapter 2. A Regional Climate Modelling Study over the Loess Plateau, China. Part I: Model Evaluation against the Observed Climatology

The aim of the work presented in this chapter was to evaluate the performance of the RegCM in simulating the local climate of the Loess Plateau, as well as analyse the origins of the model biases and identify the key mechanisms that drive the simulated biases. The chapter describes details of the RegCM model, parameterization schemes, characteristics of the Loess Plateau, and an assessment of the model performance in predicting surface air temperature, precipitation, and wind circulation. Comparison with a series of observational datasets was provided. The work presented in this chapter revealed the strengths and weaknesses of the RegCM, identified uncertainties of driven reanalysis data sets and observational data sets for model validation, and provided reference for further climate simulation over the Loess Plateau.

Candidate's contribution to this paper

The data used in this paper were collected by the candidate, except the CN05.2 observational data was provided by the National Meteorological Information Centre of the China Meteorological Administration. The candidate also performs all the figure preparation and manuscript drafting. All the work was under supervision of Dr Cheung, who led the main direction of the work and guided the candidate to carry out the research.

A Regional Climate Modelling Study over the Loess Plateau, China.

Part I: Model Evaluation against the observed climatology

Lang Wang and Kevin K. W. Cheung

Department of Environmental Sciences, Macquarie University, Sydney, Australia

Prepared for Journal of Climate

Submitted February 2015

* Author for Correspondence: Kevin Cheung, Department of Environmental Sciences, Macquarie University, North Ryde, NSW 2109, Australia. Email: kevin.cheung@mq.edu.au

Abstract

This paper presents an evaluation study of the Regional Climate Model version 4.3 (RegCM4.3) over the Loess Plateau in northern China. The Loess Plateau is considered one of the world's most sensitive areas to global climate change, which is located in the semi-arid transition zone and characterized by complex topography. During recent years, a series of reforestation programmes have been implemented across the region for soil and water conservation. The programme induced extensive changes of land surface could lead to further complex conditions in the local climate. The local climate is critical for the rain-fed agriculture and natural vegetation, however, relatively few studies explicitly documented the local climate features.

The RegCM4.3 was applied to simulate the local climate over the plateau based on its generally good performance. The RegCM4.3 modelled the present-day climate from 1990 to 2009 with a 50 km horizontal resolution, driven by ECMWF-Interim reanalysis. A series of climate variables and processes were evaluated during the winter and summer seasons, such as 2m surface air temperature, precipitation, wind circulation, surface energy and water balance and cloud coverage, and were compared with gridded observations and reanalysis.

The RegCM4.3 simulation generally reproduced the major climate features. However, the model had pronounced cold biases during winter and underestimated precipitation during summer. Analyses indicated that the cold biases may have resulted from an insufficient energy budget and negative temperature advection by the seasonal circulation. These processes were primarily triggered by deficiencies in cloud-radiation feedback. The underestimated precipitation during summer was related to the weak southerly monsoon migration associated with less moisture advection. There was non-sufficient stratiform rainfall, as well as infrequent induction of convection in the Grell Fritsch-Chappell

parameterization. In addition, discrepancies among observational datasets resulted in temperature biases up to 2˚C and precipitation biases of 8 mm month^{-1} in comparison to a dataset collated from denser meteorological stations.

Model improvement on the above mentioned physical processes are needed over this complex region. Moreover, changes in land use over the plateau, which was induced by the reforestation programmes, are only partially presented in the RegCM4.3 database and should be considered for more accurate climate simulation.

Keywords:

Regional climate model; Loess Plateau; model validation; model bias; water and energy heat fluxes

1. Introduction

The regional climate change has been attracting increasing focuses during recent years because it is more closely related to living environment of human beings than general changes at the global scale (Moss et al. 2010). The recent Intergovernmental Panel on Climate Change (IPCC) Fifth Assessment Report concluded that quantitative estimates of reginal climate changes can be provided by a series of high-resolution reginal climate models (RCMs) with considerable confidence (Stocker et al. 2013). RCMs can achieve great detail of land surface heterogeneity, and represent relatively realistic local processes affecting the climate; thereby they have become a good tool for understanding the climate at the local scale (e.g., Giorgi and Mearns 1999; Sen et al. 2004; Pal et al. 2007). RCMs were used to describe regional climate features over a range of climatic vulnerable areas (e.g., Takle et al. 1999; Fu et al. 2005; Christensen et al. 2007; Schmidli et al. 2007; Mearns et al. 2012), but simulations over regions with complex climate and substantial land surface changes, such as the Loess Plateau, were still not explicitly documented (e.g., Nobre et al. 1991; Copeland et al. 1996; Fu and Yuan 2001; Zhao and Pitman 2005; Liu 2011).

The Loess Plateau and surrounding regions are considered one of the world's most sensitive areas to global climate change (Stocker et al. 2013). The plateau is located in the largest climate transition area in Northern China between the humid East Asian monsoon region and the continental semi-arid region (Huang et al. 2008). Climate interactions between these two regions have resulted in complex conditions over the Loess Plateau, where a moderate change in the system would lead to a high variability in the local climate (e.g., Li, et al. 2010; Zhou et al. 2010). For example, precipitation rates have significantly decreased in the central and southern areas of the plateau over the past four decades (Liu et al. 2008b). The plateau temperature has steadily increased by 0.12˚C per decade, as well as

solar radiation and evaporation rates dramatic decreases in the summer and spring seasons (Qian and Zhu 2001; Liu and Zeng 2004). It is important to understand and predict such changes of the local climate because they can significantly impact both the development of the economy and natural ecosystems primarily through affecting water availability in this semi-arid area.

In addition to the large-scale climate interactions, the complex topography of the region further increases the regional climate variability (An et al. 2001). The Loess Plateau is encompassed by the Tibetan Plateau (the earth's highest plateau) to the southwest and the Mongolian Plateau to the north. In particular, the Tibetan Plateau results in a sharp increase in the elevation over the southwest of the Loess Plateau; this can enhance the convection processes to a great degree at the local scale and regulates mesoscale circulation (Pielke and Avissar 1990; Pielke 2001; Dickinson 1995). Furthermore, the complex topography contains thousands of gullies, which has resulted in a highly heterogeneous land surface boundary.

The sensitive climate condition is further amplified by reforestation programmes across the region that has been implemented recent years with the primary goal of mitigating soil erosion. Particularly, the 'Grain for Green programme' (GGP) has been converting highly erodible crops and bare land into natural vegetation such as forest and grassland, which modified the local land surface considerably (Zhang 2000; Lü et al. 2012). The modified land surface can further alter water, heat and momentum exchanges between the land and atmosphere, thereby potentially affecting the local climate.

Considering the high variability of the local climate, complex geophysical characteristics and substantial land surface changes, an understanding of the regional climate over the Loess Plateau has become an essential scientific issue. To obtain reliable climate information over the Loess Plateau, a credible RCM can be used to reproduce

major climate variables and quantify potential climatic effects of GGP (Cui et al. 2008; Wang et al. 2013; Wang and Yu, 2013). One such RCM is the Regional Climate Model (RegCM) system, developed by the Abdus Salam International Centre for Theoretical Physics (ICTP). It has been used for a wide range of applications around the world (e.g., Pal et al. 2000; Giorgi et al. 2004; Steiner et al. 2005; Seth et al. 2007; Sylla et al. 2010), including China and the surrounding areas (e.g. Hirakuchi and Giorgi 1995; Leung et al. 1999; Im et al. 2006; Gao et al. 2011).

These RegCM simulations generally captured finer-scale structures of the local climate characteristics; however, inevitably substantial biases in simulating major climate features were still identified. In particular, the model is relatively weak over elevated topographic regions. For example, simulations with substantially cold biases were captured over the Alps and Apennine mountains (Im et al. 2010) and Czech mountains in Europe (Halenka et al. 2006), the Guinea Highlands and Cameroon mountains in West Africa (Afiesimama et al. 2006; Sylla et al. 2010), the Caribbean in Central America (Martinez-Castro et al. 2006) and the South and West American mountainous region (Fernandez et al. 2006; Pal et al. 2007; Wang et al. 2009). Such biases were largely attributed to a rapid increase in elevation that can trigger rapidly changing physical processes in the model. Therefore, complex topography of the Loess Plateau necessitates that a systematic model evaluation of the main climate features within RegCM would be important. This would allow an understanding of the model's strengths and weaknesses and provide the necessary information to refine the model prior for studying the possible consequences of GGP.

In the present study, RegCM was used to simulate climate conditions over 20 years from 1990 to 2009 in the Loess Plateau region. This first part of the study includes evaluation of the model performance and analysis of the model biases. Section 2 describes

the methods, including details of the RegCM, experimental design and observational datasets for model evaluation. The evaluated results are presented in Section 3 with assessments of the simulated surface air temperature, precipitation and wind circulation. Section 4 discusses possible origins of the biases such as the surface energy budget and cloudiness, as well as uncertainties in the lateral boundary conditions and observational datasets. Section 5 provides conclusions and summarizes the model limitations.

2. Methods and Datasets

a. The RegCM model

RegCM model version 4.3 (RegCM4.3) (Giorgi et al. 2012) is an evolution of the model originally developed by Giorgi et al. (1993a, b). RegCM4.3 has a dynamical core of the fifth generation Mesoscale Model (MM5) from the National Center for Atmospheric Research (NCAR) and Pennsylvania State University (Grell et al. 1994). It employs the radiation scheme of the Community Climate Model 3 (Kiehl et al. 1996), the second generation of the Biosphere-atmosphere transfer scheme (BATS) (Dickinson et al. 1993) as land surface processes and the modified planetary boundary layer scheme of Holtslag et al. (1990).

The Grell scheme (Grell 1993) with the Fritsch-Chappell (Fritsch and Chappell 1980) closure assumption (Grell-FC) was used for convective precipitation parameterization. A sensitivity analysis of four convective precipitation schemes found that the Grell-FC scheme yields the best results over the Loess Plateau (not shown). For large scale non-convective precipitation, the sub-grid explicit moisture scheme (SUBEX) (Pal et al. 2000) is used. This scheme takes the sub-grid variability of clouds into account in accordance with the work of Sundqvist et al. (1989), and also includes the evaporation and accretion processes for stable precipitation. Sensible and latent heat fluxes were computed

by BATS parameterizations using the bulk aerodynamic formulas (Dickinson et al. 1993). For soil variables (water content at three soil layers) the initial condition was supplied by climatological values in BATS over the simulation domain.

b. Experimental design

A simulation domain encompassing China and its surroundings was used (Fig. 1). The domain was centred at 107˚E, 35˚N, with a grid size of 50 km and 110 × 144 grid points, which is close to that recommended by the East Asian portion of the COordinated Regional climate Downscaling EXperiment (CORDEX) (Giorgi et al. 2012). The domain captures most of the prominent topographic features, such as the Tibetan Plateau, the Loess Plateau, the Mongolian Plateau and the eastern and northern plains. The simulation domain was sufficiently large to encompass the Loess Plateau and allowed for the development of internal model physical processes to generate climate features that were influenced by the local topography and circulation systems around the plateau. A smaller analysis domain, comprised of the immediate vicinity of the Loess Plateau (31˚N to 42˚N, 101˚E to 115˚E), was used for the statistical analyses and spatial distributions of the relevant climate features.

Lateral boundary conditions were supplied by the six-hourly ERA-Interim (EIN) reanalysis dataset with 1.5° latitude/longitude resolution, which was developed by the European Centre for Medium-Range Weather Forecasts (ECMWF). The dataset was an improvement on the previous dataset based on the ERA-40 reanalysis, although it still needs further refinement (Uppala et al. 2008; Dee et al. 2011).

The horizontal resolution utilized was 50 km, which took into account the necessary computational resource given the large size of the domain and the 20-year climatology to complete in each simulation. This resolution was marginally sufficient to analyze the

mesoscale convective systems, but may be too coarse to adequately represent details of the local topographic features. In the vertical resolution, there were 18 sigma levels with a higher resolution in the boundary layer and a constant model top pressure of 10 hPa. The model analyses spanned 21 continuous years, from 1 January 1989 to 31 December 2009, with the first year (1989) comprising the model spin-up period. This was long enough to demonstrate the present-day climatology and principle factors controlling interannual anomalies. In addition, it allowed an analysis of the potential effects of the GGP on the local climate, which will be found in our later parts of study.

A series of climate variables and processes in RegCM4.3 were evaluated by gridded observations and reanalysis. For example, the 2m surface air temperature, precipitation and wind circulation were evaluated as the major climate variables of the RegCM4.3 simulation over the plateau. The surface energy and water balance, as well as cloud coverage were also analysed for identifying primary factors responsible for the model biases. These simulated variables and their comparisons with observations were demonstrated via spatial distributions and interannual anomalies in the winter (December-January-February; DJF) and summer (June-July-August; JJA) seasons, along with annual cycles of major climate variables.

A series of statistical measurements were employed for model evaluation, including the spatial mean climatology (Mean), mean bias (MB) using the simulations minus the observations, root mean square error (RMSE), pattern correlation coefficient (PCC) and temporal correlation coefficient (TCC). The PCC is a measure of how the simulation spatially related to the observation, while the TCC is between the two time series that represent the interannual anomalies of the simulation and the observation. The statistical significance of TCC is further assessed by Student's *t*-test at the 90% and 95% confident levels. All these statistical measurements were calculated over the analysis domain.

c. Observational datasets for model validation

1) CRU DATASET

The Climate Research Unit (CRU) dataset (New et al. 2000) of the University of East Anglia was utilized to verify the model results. This dataset, with a horizontal resolution of 0.5˚ latitude/longitude, includes data throughout the simulation period from around 200 stations covering the entire China domain (with around 30 over the Loess Plateau). A series of climate variables were used, including monthly mean 2m air temperature, precipitation and cloud coverage, and monthly maximum and minimum temperatures (Tmax and Tmin, respectively) (Table 1).

2) CN05 DATASET

Another observational dataset was used to verify the model results. The National Meteorological Information Centre dataset version 05.2 (CN05) is from the China Meteorological Administration. It also has horizontal resolution of 0.5˚ latitude/longitude and uses a similar interpolation method as in the CRU dataset, but includes data from around 2400 stations over the China domain (with around 500 stations over the Loess Plateau) (Wu and Gao 2013). Four climate variables were applied in this model evaluation analysis, including monthly mean 2m air temperatures and precipitation, Tmax and Tmin (Table 1).

With a much higher meteorological station density compared to the CRU dataset the CN05 is likely to be more accurate. For instance, Xu et al. (2009) found significant differences in the mountain ranges when they compared the CN05 and CRU datasets on a monthly timescale. For example, colder temperatures were observed in the CN05 dataset during the winter season over the Loess Plateau and surrounding areas (Xu et al. 2009). Sun et al. (2014) also illustrated this difference, showing that in the China domain temperatures of the CN05 dataset were generally lower than those in the CRU dataset and

precipitation was significantly higher. In this study, CN05 was used as an additional observation dataset to comprehensively evaluate the RegCM4.3 simulation and examine the impacts from uncertainties of observations.

3) EIN REANALYSIS DATASET

The EIN reanalysis dataset (Uppala et al. 2008; Dee et al. 2011) was also used to evaluate the model for the following climate features: large-scale atmospheric circulation, cloud fraction, sensible and latent heat fluxes, specific humidity and convective and stratiform precipitation (Table 1). The EIN reanalysis grid was interpolated on the RegCM4.3 grid for comparison.

4) SURFACE RADIATION BUDBET (SRB) DATASET

Radiation fluxes and cloud coverage were evaluated by the Surface Radiation Budget (SRB) global dataset from the Global Energy and Water-Cycle Experiment (GEWEX) (Cox et al. 2004; Stackhouse et al. 2004) with 1˚ latitude/longitude resolution. The SRB dataset contains 3-hourly data extending from 1990 through 2007 (Table 1). Monthly averaged radiative flux errors are generally within ±10 Wm^{-2}, with larger errors over mountainous valleys where there are larger uncertainties in the input data. Cloud fraction in the SRB dataset comes from the International Satellite Cloud Climatology Project (Rossow and Schiffer 1999) and meteorological inputs from Goddard Earth Observing System reanalysis (Pawson et al. 2008). The SRB datasets are reprojected to the RegCM4.3 grid for comparison.

3. Results

a. Simulated 2m air temperature

1) EVALUATION BY CRU

During the winter season, the CRU dataset showed minimum 2m air temperatures over the north and warm temperatures over the southeast of the analysis domain (Fig. 2a). These temperatures were controlled by the high pressure system over the continent to the north of the analysis domain. Minimum 2m air temperatures were observed over the southwest due to the high altitudes close to the eastern edge of the Tibetan Plateau.

Similar 2m air temperature patterns were found in the EIN reanalysis and RegCM4.3 simulation. In general, the EIN reanalysis captured a slightly colder pattern over most of the region compared to CRU with the differences mostly ranging from -2 to 0˚C (Fig. 2b). Forced by the EIN reanalysis, the RegCM4.3 simulation inherited this predominantly cold pattern, but exaggerated it into a wider range from -4 to 0˚C compared with the CRU observations particularly over the northern and eastern plateau (Fig. 2c), which is consistent with Gao et al. (2011). Differences between the RegCM4.3 simulation and EIN reanalysis confirmed this magnified cold bias, with large biases in the northern and eastern regions of the analysis domain (Fig. 2d).

In the summer season, the CRU observations showed a temperature distribution with maximum temperatures (25–30˚C) located in the southeast, minimum temperatures (8–10˚C) in the southwest and northeast, and moderate temperatures (10–20˚C) in the central areas (Fig. 3a). The EIN reanalysis and RegCM4.3 simulation again showed a high consistency of spatial temperature patterns with the CRU, but they tended to produce slightly higher temperatures over certain areas.

A warm bias was evident over the northern and central regions, and a cold bias over the southern areas in the EIN reanalysis compared with CRU observations (Fig. 3b). Differences were within the range of ±2˚C. Correspondingly, the RegCM4.3 simulation reproduced most of the warm biases, but exaggerated their magnitude to the range of 0–4˚C compared to the CRU observations and expanded their extent to most of the analysis

domain (Fig. 3c). Differences between the RegCM4.3 simulation and EIN reanalysis confirmed that the RegCM4.3 simulation was slightly warmer over most of the analysis domain, except in the eastern regions (Fig. 3d).

2) EVALUATION BY CN05

CN05 temperature observations were generally in good agreement with the CRU patterns in both the winter and summer seasons, except for a band of colder temperatures in the CN05 observations during the winter season located predominantly over the high-altitude southwestern area (Fig. 4a). Considering the cold bias of the RegCM4.3 simulation in winter compared with the CRU observations, there was a much better agreement of the RegCM4.3 simulation with the CN05 observations, as the amount of the negative biases were reduced by the colder conditions recorded by the CN05 dataset (Fig. 4b). This is consistent with Xu et al. (2009), however, the RegCM4.3 still tends to under predict the 2m air temperature generally. In the summer season, the CN05 observations showed slight differences from the CRU observations with 0–2˚C warmer temperatures over the northern region and -2–0˚C colder temperatures for the other regions (Fig. 4c). As a result, the RegCM4.3 simulation showed a similar bias pattern when compared with the CN05 observations as it did with the CRU observations (Fig. 4d).

3) SEASONAL CYCLE AND INTERANNUAL ANOMALIES

The annual cycle of the regionally-averaged 2m air temperature showed a bell-shape distribution in both the observational datasets, EIN reanalysis and the RegCM4.3 simulation, with a peak in July and a minimum in January (Fig. 5a). The RegCM4.3 simulation exceeded the peak magnitudes of the observational datasets and EIN reanalysis by less than 1˚C during July and August, but over the rest of the year underestimated the surface air temperatures by approximately 0.5–2˚C.

In both the winter and summer seasons, the interannual anomalies of the 2m air temperature in the RegCM4.3 simulation generally agreed with the CRU, CN05 datasets and the EIN reanalysis, showing reasonable fluctuations of the season-average temperature from cold to warm periods (Figs. 5b, c). Nevertheless, a systematic cold bias of around -3˚C compared to the CRU observations, as well as -2.5˚C compared to the EIN reanalysis and -1.8˚C compared to the CN05 observations, was notable in the winter season. During the summer season, the RegCM4.3 simulation generated 2m air temperatures on average around 1.0˚C warmer than the observations and EIN reanalysis.

4) SUMMARY

In general, both the spatial and temporal patterns of temperature over the Loess Plateau were reproduced well by the RegCM4.3 simulation as summarized in Table 2. The spatial MB were lower in summer (0.76˚C) than in winter (-3.16˚C) compared to CRU, and the largest biases were found over the orographic region in winter (in excess of -4˚C) using the simulation minus the observations. PCCs between the RegCM4.3 simulation and the CRU observations were quite high, being 0.94 for winter and 0.91 for summer. The TCC (over the 20 seasons) with the CRU dataset was higher in summer (0.79) compared to that in winter (0.49); both of these coefficients were significant at the 95% confidence level.

Average minimum and maximum temperatures were further investigated to find out the dominant contributor to the potential bias. During winter, both Tmax and Tmin were underestimated by a similar degree (around 2.7˚C), which together resulted in the lower mean temperature of the RegCM4.3 simulation. Nevertheless, during the summer season, Tmax became the primary reason for the higher temperature in the RegCM4.3 simulation with 2.02˚C positive biases in contrast to only 0.50˚C positive biases of Tmin (Table 2).

The RegCM4.3 model simulation biases during the summer season were in line with those of other state-of-art regional models, considering that typical RCM biases for

seasonal 2m air temperatures are within the range of ±2˚C (e.g., Jones et al. 1995; Giorgi et al. 1998; McGregor et al. 1998), the uncertainties of the observational datasets and the high variability of the local temperature. The noticeable winter cold biases could be further attributed to a series of physical processes within the model, which was going to be discussed in Section 4c.

b. Simulated precipitation

1) WINTER PATTERNS

In winter, the CRU observations showed a predominantly dry feature over the north plateau with precipitation levels of less than 10 mm month^{-1} and relatively wet conditions (20–40 mm month^{-1}) over the southeastern region (Fig. 6a). The EIN reanalysis and RegCM4.3 simulation captured generally these major features, but both of them tended to extend the southern wet centre north, towards the interior region.

Spatial differences show that the EIN reanalysis captured slightly more rainfall over the entire domain compared with the CRU observations (Fig. 6b); most differences were in the range of 0–10 mm month^{-1}, but there were some with large ranges of 10–20 mm month^{-1} over the southwestern orographic areas. This pattern was inherited by the RegCM4.3 simulation, although the area of orographic biases was enlarged (Fig. 6c). Differences between the EIN reanalysis and the RegCM4.3 simulation (Fig. 6d) confirmed this overestimation, showing systematically higher values of 0–10 mm month^{-1} in the RegCM4.3 simulation over the analysis domain, which is consistent with Gao et al. (2011).

In addition to the aforementioned inconsistency, the RegCM4.3 simulation captured a lower convective precipitation rate (0.19 mm month^{-1}; 1.25% of the total precipitation) in comparison to the EIN reanalysis (1.98 mm month^{-1}; 17.98% of the total) (Table 2). Correspondingly, the non-convective precipitation rate in the RegCM4.3 simulation (15.01

mm month^{-1}, 98.75% of the total) was much higher than in the EIN reanalysis (9.03 mm month^{-1}, 82.02% of the total). This could have been the main contributor to the overestimated total precipitation in the RegCM4.3 simulation.

2) SUMMER PATTERNS

In the summer season, monsoon flows bring in large amounts of water vapour from the oceanic region to the plateau, which significantly influences the local precipitation patterns, producing a southeast-to-northwest decreasing gradient. This gradient was represented in the CRU observations, with intensive precipitation in the southeast (typically 150–200 mm month^{-1}) and less precipitation in the northwest (20–40 mm month^{-1}) (Fig. 7a). Similar patterns were captured by the EIN reanalysis and RegCM4.3 simulation, except that the EIN reanalysis generated more intensive gradients and the RegCM4.3 simulation displayed more isolated rainfall centres that were driven by the topography.

Compared with the CRU observations, both the EIN reanalysis and RegCM4.3 simulation captured less rainfall (10 mm month^{-1}) in the northwest region but excessive rainfall (>50 mm month^{-1}) over the southwest and northeast regions with rapid changes in the topography (Figs. 7b–7d). Moreover, the RegCM4.3 simulation generated a series of pronounced drier events (over 20 mm month^{-1}) over the south-eastern analysis domain.

Furthermore, two components of the total precipitation (convective and stratiform precipitation) were both underestimated by the RegCM4.3 simulation in comparison to the EIN reanalysis (Table 2). Convective precipitation was underestimated by 3.78 mm month^{-1} in the RegCM4.3 simulation, compared to 53.41 mm month^{-1} in the EIN reanalysis averaged during summer, while stratiform precipitation was only 30.74 mm month^{-1} compared to 49.38 mm month^{-1}, for each respectively. This significant underestimation of stratiform precipitation (18.64 mm month^{-1}) accounted for a large portion of the total

negative biases (22.42 mm month^{-1}), and the underestimation of stratiform precipitation was primarily found over the south-eastern plateau, which spatially corresponded well with the negative biases in total precipitation (not shown here). Such spatial consistency strongly indicates that the dry conditions in the RegCM4.3 simulation were largely caused by the underestimation of the stratiform precipitation.

Another important precipitation features simulated by RegCM was that over a series of areas outside the analysis domain, such as the north-eastern China and eastern Mongolia, precipitation was significantly overestimated compared with both CRU observations and EIN reanalysis. Such overestimation over these areas on the north of the Loess Plateau is different from the negative biases over the plateau (will be discussed in 4c).

3) EVALUATION BY CN05

The CN05 observations showed the same basic precipitation features as the CRU observations. Specifically in DJF, the CN05 observations have general differences within 0–10 mm month^{-1} from the CRU (Fig. 8a), which slightly reduced the positive bias of the RegCM4.3 simulation (Fig. 8b). In summer, the CN05 observations showed large-scale peaks of rainfall over the orographic areas, such as over the eastern edge of the Tibetan Plateau and the northeast highlands, which were not available in the CRU observations (Fig. 8c) but captured by the RegCM4.3 simulation (Fig. 8d). Thus, the RegCM4.3 simulation was more consistent with the CN05 compared to the CRU dataset over those areas. However, insufficient precipitation was again captured over the south-eastern analysis domain by the RegCM4.3 simulation compared to the CN05 observations, and this negative bias extent was even larger than the extent when compared with CRU. Particularly, Table 2 illustrated that CN05 captured averagely 8.15 mm month^{-1} excessive precipitation compared to CRU. These discrepancies between the two observational

datasets confirmed the impacts of uncertainties in precipitation to model evaluation (Xu et al. 2009; Sun et al. 2014).

4) SEASONAL CYCLE AND INTERANNUAL ANOMALIES

Both the CRU and CN05 datasets and the RegCM4.3 simulation showed a bell shape pattern for the annual precipitation cycle (Fig. 9a). The observations showed the peak value in July associated with the monsoon rainfall and the minimum value in December and January. The RegCM4.3 simulation captured the general trend, however, it brought the peak value one month advancement and resulted in negative biases of around 20 mm month^{-1} during July and August. The earlier peak value in June was also found by Giorgi et al. (1999) and was likely related to the early summer monsoon migration in the simulation. Further, during winter and spring, the RegCM4.3 simulation tended to overestimate precipitation by around 20 mm month^{-1}.

The RegCM4.3 simulation captured the interannual anomalies of precipitation during both winter and summer seasons by showing most of the interannual fluctuations (Figs. 9b, c). Exceptions include some inconsistencies in certain years such as much underestimating the humid summers of 1994 and 2000 (Figs. 9c), and overestimating the winters of 1990, 1998 and 2008 (Figs. 9b). Meanwhile, there are systematic biases in the RegCM4.3 simulation, with an overestimation in winter from 4.5 mm month^{-1} on average (compared to the EIN reanalysis) to 9.4 mm month^{-1} (compared to the CRU observations). In contrast, during the summer, a systematic underestimation of simulated precipitation was captured, with the largest bias magnitude when compared to the EIN reanalysis (21.5 mm month^{-1}) and the smallest magnitude compared to the CRU observations (6.5 mm month^{-1}). The biases compared with the CN05 observations were between the CRU observations and the EIN reanalysis during both seasons.

5) SUMMARY

Overall, RegCM4.3 could reproduce major precipitation patterns over the Loess Plateau in both seasons, but tended to produce conditions that were more humid in winter and drier in summer. The RegCM4.3 simulation generated precipitation MB of -6.55 mm $month^{-1}$ in summer compared to the CRU observations, which again were in line with those of other state-of-art regional models, especially considering the high variabilities and uncertainties of the local observed precipitation in this season. In contrast, the model simulated precipitation MB of 9.40 mm $month^{-1}$ compared to the CRU observations in winter was relatively large, demonstrating less agreement of rainfall during this dry season with averaged precipitation less than 10 mm $month^{-1}$. Nevertheless, the PCC between the RegCM4.3 simulation and the CRU observations were quite high (0.72 in winter and 0.65 in summer), and high TCC were also found (0.83 and 0.58, respectively), both TCCs passed the 95% statistical significant confidence limit.

c. Midlevel simulated wind field

1) WINTER PATTERN

Considering the high altitude of the Loess Plateau and surrounding area, the 500 hPa wind circulation is examined to avoid much influence from topography. During the winter season, the EIN reanalysis showed prevailing northwesterlies over the north of the plateau and westerlies over the south of the analysis domain (Fig. 10a). This wind field spatial pattern was primarily driven by the high pressure system around the Mongolian Plateau to the north and Tibetan Plateau to the west. The wind speed increased gradually from the west (12–14 m s^{-1}) to the east (18–20 m s^{-1}). This basic wind pattern was captured by the RegCM4.3 simulation (Fig. 10b), except that there was a spurious cyclone over the analysis domain (Fig. 10c). Due to this spurious cyclone, the overestimated northwesterlies

brought in the cold air from the north, which may have resulted in the low 2m air temperatures identified in the RegCM4.3 simulation. Moreover, the large-scale convergence associated with this cyclone may be related to the over prediction of precipitation in the RegCM4.3 simulation during winter, which could release additional rainfall over the Loess Plateau (Gao et al. 2012).

2) SUMMER PATTERN

In the summer season, the monsoon winds reached the southern border of the Loess Plateau, and the northwesterlies still occupied the northern domain at 500 hPa in the EIN reanalysis (Fig. 10d). The typical magnitude of the southwesterly monsoon wind ranged from 2–6 m s^{-1} at this level, while the northwesterlies were relatively stronger (6–8 m s^{-1}).

The RegCM4.3 simulation captured most of the wind pattern in EIN reanalysis, but tended to generate stronger northwesterly flow over the northern analysis domain (Fig. 10e). These stronger northwesterlies could resist the southeasterly monsoon migration into the inner plateau, resulting in insufficient moisture advection to the plateau, which in turn may account for underestimation of stratiform and total precipitation compared to EIN reanalysis during summer. Meanwhile, excessive southeasterlies were simulated by RegCM4.3 over the north-eastern China outside the analysis domain compared with EIN reanalysis. Such stronger southeasterlies with moisture-laden monsoon migration could be the main cause of the simulated excessive rainfalls there, which had been aforementioned in Section 3b (Fig. 10e).

In addition, convergence was found over the eastern Mongolia region when compared RegCM4.3 simulations with EIN reanalysis (Fig. 10f). This convergence pattern spatially corresponded to the precipitation overestimation over this inner land region. It may in turn reduce water vapour availability in the atmosphere surrounded the Loess

Plateau and potentially decrease the simulated precipitation over there through remote effects.

4. Discussion

To identify the primary factors responsible for the identified model biases along with uncertainties among the observation datasets, the physical processes in RegCM including surface energy and water balance, cloud coverage and convection, as well as large-scale atmosphere circulation inducing heat and moisture advection were considered in the following sections.

a. Surface energy budget over the Loess Plateau

1) RADIATION BUDGET

In the winter season, the net downward shortwave radiation (NS) fluxes in the RegCM4.3 simulation were quite close to the SRB observations but higher than EIN reanalysis (Table 3). The RegCM4.3 simulated 104.44 W m^{-2} of NS which was slightly overestimated by 2.18 W m^{-2} compared to the SRB observations; whereas the simulated NS was overestimated by 11.22 W m^{-2} compared with the EIN reanalysis. Since NS fluxes are the predominant energy input to the surface energy budget and can directly affect 2m air temperatures and heat fluxes, the larger NS simulated by RegCM4.3 tended to play a positive role in increasing simulated temperatures rather than generating significant cold biases. In other words, some other factors in the model may account for the simulated cold condition.

Downward long wave radiation (DL) also plays an important role in determining the 2m air temperature via increasing the effective radiative temperature of the atmosphere and releasing energy towards the land surface. The RegCM4.3 simulated DL fluxes of 209.59

W m^{-2} which were underestimated by 16.92 W m^{-2} in comparison with the SRB observations but by only 4.45 W m^{-2} compared with EIN reanalysis (Table 3). Such DL underestimations compared with both datasets could dominantly explain the simulated cold bias, particularly corresponding with the Tmin underestimation. Meanwhile, higher upward net long-wave radiation (NL) fluxes were generated by RegCM4.3 compared with two datasets, resulting in excessive infrared energy emitted from the surface to the atmosphere, which also in turn favoured to cold conditions in RegCM4.3.

In the summer season, the RegCM4.3 simulation significantly overestimated the NS fluxes compared to the SRB observation and EIN reanalysis (Table 3). The positive bias was 41.69 W m^{-2} compared with the SRB and 24.43 W m^{-2} compared with the EIN, which may have been associated with the warm bias of 2m air temperature, especially the overestimation of Tmax. On contrast, simulated NL and DL fluxes were slightly different from the two datasets (biases within 8 W m^{-2}), therefore, the amplified NS fluxes could be the major discrepancies of radiation fluxes simulated by RegCM4.3.

2) SENSIBLE AND LATENT HEAT FLUX

The RegCM4.3 simulation captured a reasonable amount of turbulence fluxes over the plateau during the winter season: 17.15 W m^{-2} sensible heat fluxes (SH) and 14.01 W m^{-2} latent heat fluxes (LH) (Table 3). Compared with the EIN reanalysis, the RegCM4.3 simulation reduced the SH by 1.74 W m^{-2}, but enhanced the LH by 3.70 W m^{-2}. As a result, the RegCM4.3 simulation favoured to impose excessive moisture feedback to the atmosphere, which was likely related to the overestimation of precipitation and underestimation of temperature.

In the summer season, LH occupied a larger component than SH of the total turbulence flux in the EIN reanalysis. However, RegCM4.3 captured LH fluxed slightly higher than SH fluxes, showing 66.33 W m^{-2} and 73.07 W m^{-2}, respectively. Meanwhile,

the simulated SH fluxes exceeded the reanalysis by a large amount of 20.48 W m^{-2}, along with a slight overestimation by 3.33 W m^{-2} of LH fluxes. Such significant overestimation of SH but similar values of LH compared with EIN could be an important reason for the tendency of higher temperature and lower precipitation simulated by RegCM4.3 during the summer season.

3) DIABATIC HEATING AND TEMPERATURE ADVECTION

As mentioned above, both energy fluxes and wind flows were able to impact upon the local climate via local-scale processes and large-scale advections. In order to obtain their quantitative effects on temperature, the diabatic heating rate and temperature advection were applied to the temperature tendency equation:

$$\frac{\partial T}{\partial t} = -V \cdot \nabla T - \omega(\gamma d - \gamma) + \frac{1}{Cp}\frac{dQ}{dt} \quad (1)$$

where $\frac{\partial T}{\partial t}$ is the surface air temperature tendency, V is the horizontal wind vector of the surface layer; ∇T is the temperature change; $\gamma d \; and \; \gamma$ are the atmospheric disturbance and stability, respectively that control the sign of ω; Cp is the specific heat capacity at constant pressure, $\frac{dQ}{dt}$ is the heating rate. The formula represents the contributions from horizontal advection of temperature ($-V \cdot \nabla T$), vertical transportation of temperature ($-\omega(\gamma d - \gamma)$) and diabatic heating rate ($\frac{1}{Cp}\frac{dQ}{dt}$) to the temperature tendency. The vertical transportation of temperature was not considered in this study as only the surface level was analyzed. The other two parts were both at the surface level.

During the winter season, both the diabatic heating rate and temperature advection were negative (-1.45×10^{-3} °C s^{-1} and -3.36×10^{-5} °C s^{-1}, respectively), which was in line with the cold temperatures of the RegCM4.3 simulation (Table 4). Further, the magnitude of diabatic heating rate was much larger than the temperature advection, which indicates its dominant role in determining the simulated temperature. In other words, the cold bias of

the RegCM4.3 simulation was primarily caused by the negative energy budget, followed by the intensive northerly wind flow.

During the summer season, conversely, both the diabatic heating rate and temperature advection were positive (0.24×10^{-3} ˚C s^{-1} and 1.83×10^{-6} ˚C s^{-1}, respectively), and again the diabatic heating rate played a dominant role in the local temperature (Table 4). The slightly warm tendency could possibly be attributed to the diabatic heating rate being associated with the positive energy budget.

b. Cloud fraction and cloud-radiation feedback

Cloud fraction (CF) plays an important role in the response of the surface radiation budget throughout its primary cloud-radiation control process and is crucial for accurate temperature and precipitation simulation in the RegCM. CF was lower in the RegCM4.3 simulation compared with the SRB observations in both seasons (Table 5). In the winter season, 43.69% CF was simulated in the RegCM4.3 simulation and 50.92% in SRB observations. In the summer season, the RegCM4.3 simulated 45.44% CF compared with 65.45% in the SRB observations.

The absence of water vapour associated with low-level relative humidity fundamentally accounted for the low cloud fraction, according to the relationship in the SUBEX model. The RegCM4.3 simulated a weak southerly summer monsoon flow that carries the water vapor to the Loess Plateau, furthermore, a large portion of convection effectively removed the moisture in the troposphere. Both processes thereby reduced moisture for the formation of cloud, which results in the underestimation of cloud fraction. The negative bias of CF could trigger two inverse radiative processes. On one hand, less cloud fraction increases the net solar radiation, which can then directly increase the 2m air temperature. On the other hand, less cloud fraction reduces the re-emitted radiation flux

toward the surface and thus decreases the effective radiative temperature of the atmosphere. These two cloud-radiation-temperature feedbacks in the RegCM4.3 simulation were consistent with the higher NS and lower DL compared with observations. However, in terms of temperature the RegCM4.3 simulation was more likely linked to the former feedback in summer with a warm condition when solar radiation heating was much stronger than infrared heating, followed by the latter feedback in winter with cold conditions when DL played an important role. Additionally, the significantly lower CF may be a key driver towards the low total precipitation produced during the summer season.

c. Moisture advection

There was a positive bias of precipitation in winter but negative one in summer in the RegCM4.3 simulation. Plausible reasons may have included wind circulation loading excessive water vapour from more humid areas, as mentioned above. Similar to temperature advection, moisture advection has been investigated to quantify the effects of wind circulation and the specific humidity on the precipitation bias. The tendency in specific humidity was calculated at 500 hPa:

$$\mathrm{Adv(rh)} = -V \cdot \nabla \mathrm{rh} \quad (2)$$

where Adv (rh) represents moisture advection, V is the horizontal wind field, ∇rh is the specific humidity gradient.

During the winter, both the RegCM4.3 simulation and EIN reanalysis captured the positive moisture input over the Loess Plateau, which indicated that the wind circulation at 500 hPa effectively brought extra water vapour to the local atmosphere. In particular, the RegCM4.3 simulated 5.98×10^{-2} g kg^{-1} s^{-1} moisture advection, which was larger than the

EIN reanalysis (2.25×10^{-2} g kg^{-1} s^{-1}) (Table 5). The excessive moisture flow may partially contribute to the overestimated precipitation by the RegCM4.3 simulation.

During the summer season, both the RegCM4.3 simulation and the EIN reanalysis captured the positive moisture input, however, the RegCM4.3 simulation produced a slightly lower moisture advection (34.24×10^{-2} g kg^{-1} s^{-1}) compared to the EIN reanalysis (39.91×10^{-2} g kg^{-1} s^{-1}) (Table 5). Less water vapour available for SUBEX may have resulted in the underestimation of precipitation, which was found in response to the southward shift of the monsoon flow in the large-scale circulation within the RegCM4.3 simulation.

d. Other potential mechanisms responsible for the model biases

1) DISCREPANCIES IN THE OBSERVATIONAL DATASETS

Uncertainties of the observational data can affect the analysis of the model performance. For example, precipitation measurement used in the CRU dataset may underestimate the actual precipitation amount (e.g., Kim and Lee 2003; Sun et al. 2014) due to the low density of meteorological stations especially over topography (Giorgi et al. 1999). The CN05 dataset has higher density of stations and is able to record higher precipitation rate (by around 8 mm $month^{-1}$) and higher temperatures (by around 2˚C) (Xu et al. 2009).

Discrepancies are also identified in the datasets of radiation fluxes. The SRB dataset is based on the interpolated meteorological station and remote sensing data with 1˚ grid size and was adopted for references in the first priority, while the EIN dataset is derived from satellite data and assimilation modelling with a 1.5˚ latitude/longitude grid size. These differences in input sources and horizontal resolution between the two datasets primarily resulted in notable differences in surface radiation fluxes.

More specifically, uncertainties of the surface NS fluxes were a major difference between the EIN and SRB datasets (Zhang et al. 2006a, 2007). Compared with EIN, SRB has an NS larger by 9.04 W m^{-2} during winter and smaller by 17.26 W m^{-2} during summer over the Loess Plateau (Table 4). The winter difference between the datasets meets the accuracy requirements for climatological studies of 10 W m^{-2} (Zhang, et al., 2007). Nevertheless, the weak NS fluxes of SRB in the summer were quite significant, which have previously been reported by Troy and Wood (2009). Previous studies attributed this weak NS to the large surface albedo in SRB using 'clear-sky' values (Briegleb et al. 1986; Pinker and Laszlo 1992; Zhang et al. 2007). Comparatively the surface albedo used in the EIN reanalysis is related to aerosols and humidity in the atmosphere (Henderson-Sellers and Wilson 1983). Thus, the EIN reanalysis was considered more realistic for NS fluxes and could effectively be used to reduce the large positive bias of NS in the RegCM4.3 simulation during the summer season.

2) CONVECTIVE AND NON-CONVECTIVE PRECIPITATION

Convective rainfall amounts were slightly underestimated over the Loess Plateau during the two seasons, which could be attributed to the characteristics of the Grell-FC scheme. The low convection during winter in the RegCM4.3 simulation was more likely linked to the low availability of buoyant energy considering the cold conditions that drove the convection process (Giorgi and Marinucci 1996). Conversely, the release of buoyant energy in the summer season was discontinuous with promoted action between 30 min and 1 hour timescale, which may account for the smaller convective magnitudes in the scheme, although the net solar radiation and sensible heat fluxes provided sufficient energy sources (Gochis et al. 2002; Ratnam and Kumar 2005; Im et al. 2006).

The non-convective precipitation is essentially determined by the SUBEX scheme, which generates rainfall when the cloud water content exceeds the auto-conversion

threshold (Pal et al. 2000). Hence, cloud water content, cloud fraction and auto-conversion threshold could be the main factors that determine the magnitude of non-convective precipitation. The first two factors are positively correlated with the local atmosphere humidity and moisture advection, while the auto-conversion threshold follows positive correlations with indices of atmosphere temperature (Pal et al. 2000).

During the winter season, the RegCM4.3 simulation generated excessive non-convective precipitation. Based on the primarily cold conditions in the RegCM4.3 simulation, the auto-conversion threshold tended to be relatively low, which triggered an increase in the conversion of cloud water to non-convective precipitation (Giorgi et al. 2012). In addition, positive moisture advection and lower convection rates could increase the atmospheric humidity and cloud water that lead to stratiform precipitation.

During the summer season, the RegCM4.3 simulation generated a negative bias of non-convective precipitation. This deficiency was probably caused by the high portion of deep convective precipitation, which removed too much atmospheric water vapour for convection, leaving a limited amount of water vapour for stratiform precipitation. The amount of convective precipitation simulated by the RegCM4.3 simulation was 61.75% of the total, and stratiform precipitation was only 38.25% of total (Table 2). Convective precipitation simulated by the RegCM4.3 was 9.79% higher, but stratiform was 10% lower than those in the EIN reanalysis, considering differences in grid resolution in the two datasets.

An underestimation of the cloud fraction could further account for such rainfall deficiencies. In addition, neglecting ice physics within clouds is a shortfall of SUBEX, which also results in the underestimation of non-convective precipitation since cloud ice increases the auto-conversion efficiency (Rogers and Yau 1989; Pal et al. 2000). Last but

not least, insufficient moisture advection associated with shifts of the humid monsoon winds could have also caused the underestimation in the RegCM4.3 simulation.

3) LAND SURFACE SHCEME

During the entire 20-year period, the ability of the RegCM4.3 to accurately simulate the climate variability over the Loess Plateau is related to the realistic variations in the land use across the region. For example, simulations from 1990 to 1994 represented the temperature and precipitation quite well, however, larger biases were identified around the year of 1999. A possible factor is the changes in the land surface that occurred around 1999 at the start of the 'Grain for Green' project. Our preliminary simulations on land surface sensitivity experiments showed that change from cropland to forest may have triggered warmer climate conditions primarily due to the lower surface albedo and larger roughness length of trees (Gao et al. 2003; Zhang et al. 2009). Since the BATS land surface scheme employed by RegCM4.3 is based on land use maps between 1992 and 1993, its land use database shows large area of cropland over the study area. That is, the increase in forest areas over time has not been incorporated into the model simulation, which probably led to the large cold biases during the reforestation years.

4) LATERAL BOUNDARY CONDITION AND CONVECTIVE SCHEMES

Model performance is also sensitive to lateral boundary conditions and other convective schemes (Giorgi and Mearns 1999). Performance of the model driven by a different lateral boundary condition from NCEP/NCAR was also evaluated (not shown) but showed no significant difference, which is consistent with previous studies such as Gu et al. (2012). Moreover, the model inherited but exaggerated cold biases of the large-scale forcing datasets (EIN) compared with observations, spectral nudging sensitive tests may push the model's solution back to the EIN forcing at defined time steps (von Storch et al. 2000). Nevertheless, our preliminary results showed that the cold biases were not

significantly corrected by spectral nudging. However, alternative convective schemes could substantially modify the simulation results. It is interesting to note that the cold condition in the winter season was not very sensitive to either the lateral boundary condition or the convective scheme. More detailed investigation is needed to understand this persistent bias and its related processes.

5) TOPOGRAPHIC EFFECT

The climate response to greenhouse forcing was not included in the present study of regional climate features. Since its forcing could significantly increase the surface air temperature and alter the large-scale circulation pattern, this aspect should be taken into account for local climate simulations especially considering the cold bias identified in the present study. On the other hand, with a 50-km resolution major differences exist between the simulated topography and the actual topography at the Loess Plateau. One consequence of this was that orographic precipitation was suppressed and the model failed to generate sufficient rainfall particularly during summer. In addition, unrealistic altitudes can account for the temperature bias via temperature laps rate. This indicates the importance of topographic control on the local climate characters of the Loess Plateau, which needs an elevation correction and finer resolution for better topographic representation.

6) OTHER FACTORS

The factor of the modified planetary boundary layer scheme of Holtslag et al. (1990), could be also considered as the reason for obvious temperature biases. The original Holtslag scheme before modification in previous versions of the RegCM appeared to generate excessive vertical transport of heat, moisture, and momentum in the stable conditions, such as the winter season over the northern hemisphere high latitude regions (Giorgi et al. 2012). It was found that in such conditions, the scheme led to large warm winter biases (>10˚C) over several regions such as northern Siberia and northern Canada.

To address this problem, the RegCM4.3 modified the Holtslag parameterization through weakening vertical transport of heat and momentum in high latitude winter conditions. Our simulation domain over China and surroundings included a part of such high latitude regions where the vertical transport was potentially limited by the modified Holtslag scheme. As a consequence, the winter temperature cold biases may be generated over the Loess Plateau in Northern China.

The other concern of the cold bias was the aerosol radiative transfer calculation. The radiatively interactive aerosols (particularly the desert dust) had substantial impacts on long-term regional climate simulations. Solmon et al. (2012) and Zanis et al. (2012) studied of the Sahel and European region, respectively, both showing potential impacts of aerosols on their local temperature. The lack of the aerosols in the simulations may possibly result in the temperature bias over the Loess Plateau surrounded by desert and semi-desert regions.

Last but not least, high resolution simulations of the model were capable of capturing the fine-scale climatic signal in distinct climate regimes with complex topography. A sub-grid land surface configuration could be used for improving the temperature simulation over the Loess Plateau. The sub-grid configuration divides each grid in the model into a regular sub-grid and land surface processes are calculated at each sub-grid point taking into account the local topography and land cover. This scheme has been shown to be useful in model simulations particularly over mountainous areas (Giorgi et al. 2003b). However, the RegCM4.3 is still a hydrostatic model that limits its application for studies requiring very high resolution. The model is being developed for a new non-hydrostatic dynamical core as the base for the next version of the RegCM system.

5. Conclusion

A two-decade-long simulation using the new version of RegCM4.3 was performed over the Loess Plateau, China in order to evaluate the model's capability in reproducing the major regional climate features. This is a unique study exclusively focused on the present-day climate over Loess Plateau that is one of the most climatically sensitive regions in China with complex topography and intensive anthropogenic activities. The analysis presented included identification of simulation biases and their primary causes.

RegCM4.3 captured the major climate variables in both spatial distribution and temporal pattern, including the 2m air temperature, precipitation, wind circulation, surface radiation and turbulence fluxes and total cloud coverage. Statistical evaluation showed high pattern and temporal correlation coefficients for both temperature and precipitation. The wind field within the RegCM4.3 simulation inherited largely from the forcing data from the EIN, but has also developed its own local features. The RegCM4.3 simulation was found to be more consistent with the CN05 observational dataset in comparison to the CRU dataset, the former of which has taken into account more surface station observations.

Deficiencies did exist in the simulation of the precise location and overall magnitudes of major climate variables. Biases were generally caused by the combined effects of deficiencies in interior dynamical processes of the model and were exaggerated by uncertainties among the observational datasets. First, the noticeable cold temperature biases in winter were mostly related to the deficiency of the downward long wave radiation fluxes and excessive latent heat fluxes, as well as the added factor of negative heating advection driven by the simulated seasonal circulation. The slightly warm bias in summer was predominantly caused by the excessive solar radiation and sensible heat fluxes. RegCM4.3's treatment is not sophisticated in certain key processes for accurate 2m air

temperature simulation in winter such as cloud-radiation feedback, which is key in determining the radiation and energy budget. These processes are important and demonstrate this area of the model is in need of improvement.

RegCM4.3 also produced excessive precipitation in winter but underestimated precipitation in the summer. The over effective large-scale precipitation scheme and positive moisture advection on seasonal time scale largely accounted for the wet conditions in winter. Nevertheless, during summer, a tendency for reduced convection frequency in the Grell-FC explained the insufficient total precipitation, along with weak monsoon migration that carried insufficient moisture into this semi-arid region.

Over the present study area, uncertainties of observation were also identified. For the 2m air temperature, the CN05 dataset reduced the simulated cold bias by at least 1–2˚C and 0.5–1˚C in the winter and summer seasons, respectively, in comparison to the CRU dataset. In addition, over the orographic complex region, RegCM4.3 captured certain fine-scale information of climate features that were largely missed out by CRU observations but captured within the CN05 dataset.

In order to meet the accuracy requirements for climatology studies and even future climate projection over such topographic areas, more accurate energy and water cycles of the model are needed, as well as a higher density of meteorological stations. In addition, the disadvantages of a low-resolution grid, inadequate representation of the land surface, and greenhouse gases are all factors that need to be considered.

By evaluating the RegCM4.3 simulation with major climate features during recent decades, this study has revealed the model's strengths and weaknesses, and identified the key mechanisms that drove the simulated biases. The study could help to explore future modelling efforts to produce more accurate climate information. The study also has significant implications for model simulations interacting with the reforestation program

and changing landscapes in general. Understanding the local climate could provide reference for water management and reforestation strategies and help reduce economic and ecological losses.

Acknowledgement. The first author (LW) is supported by the China Scholarship Council, the International Macquarie Research Excellence Scholarship, and Higher Degree Research support fund from Macquarie University. Computational facilities are provided by Intersect Inc., NSW and the National Computational Infrastructure of Australia. We would like to thank Prof. C.-P. Chang of the US Naval Postgraduate School and the National Taiwan University for co-supervising LW and his many valuable comments on this work.

List of Figures

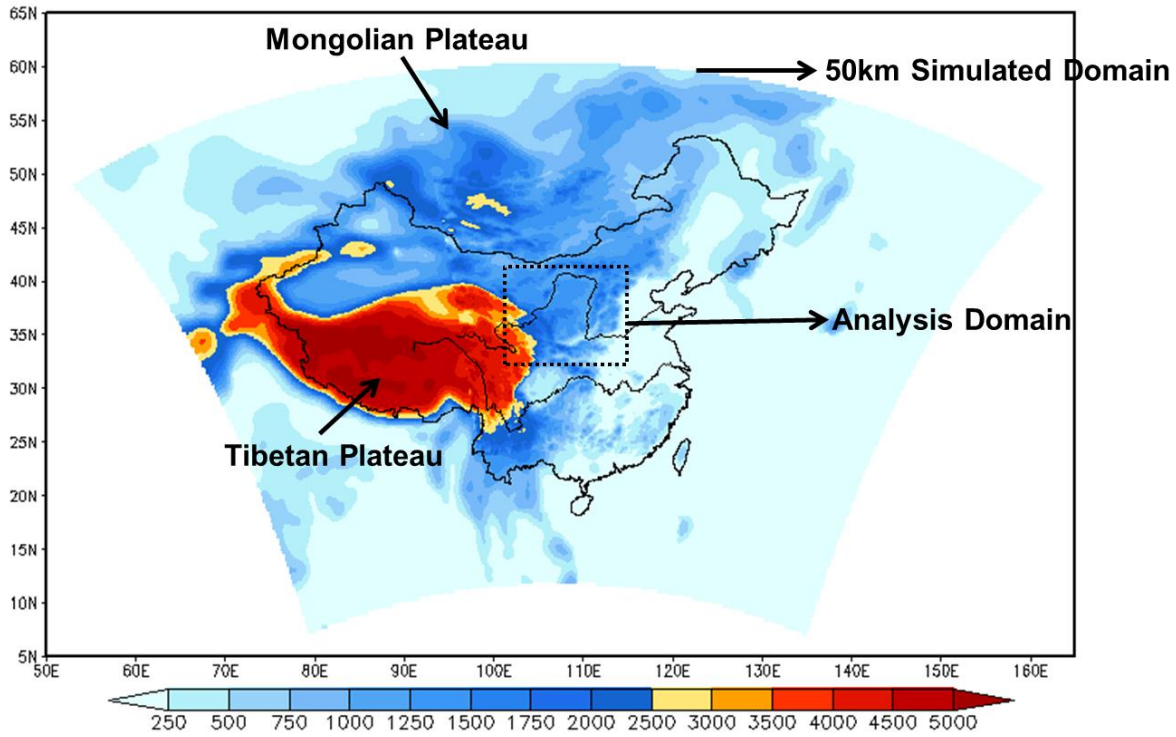

FIGURE 1 The RegCM4.3 simulation and analysis domain with elevations (unit: m).

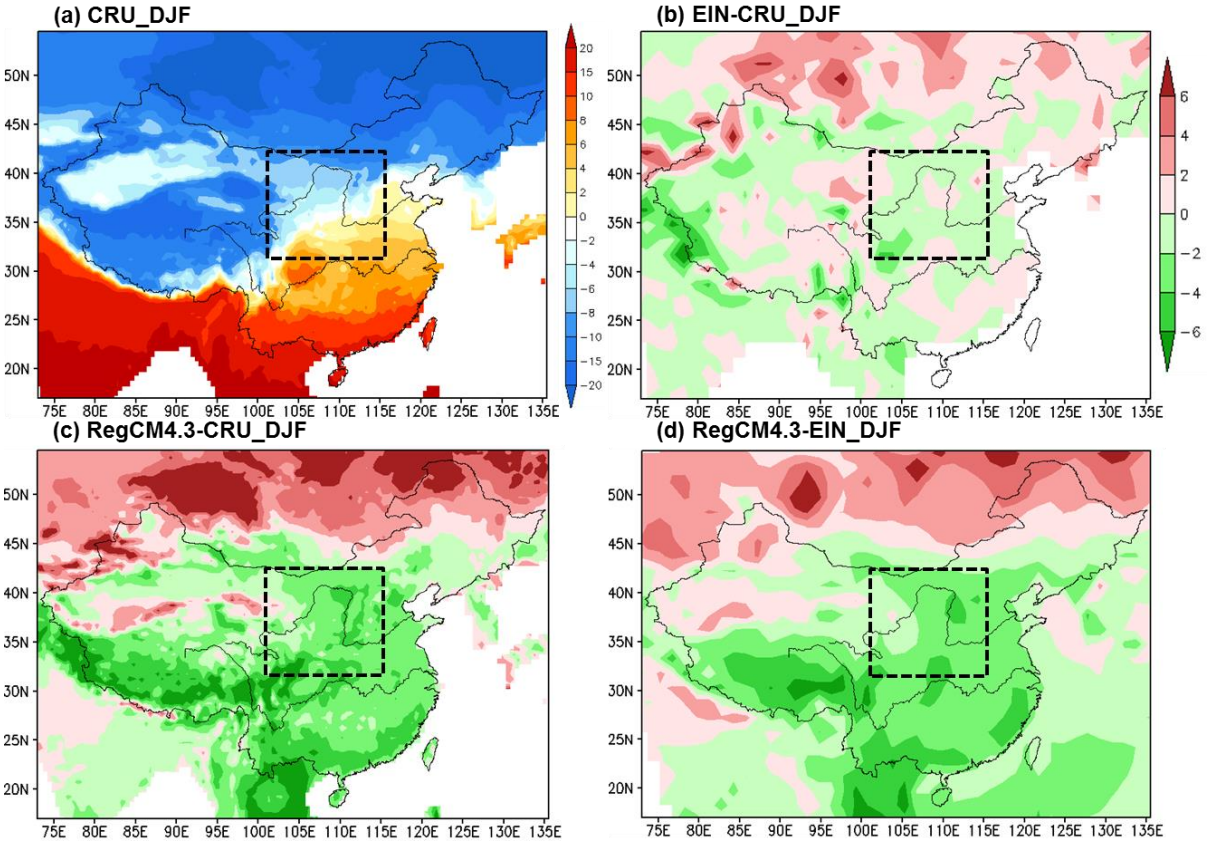

FIGURE 2 Spatial distribution of 2m air temperature (˚C) in winter (DJF) over the entire domain with the analysis domain in the dashed box: (a) CRU observation, differences of (b) EIN from CRU, (c) RegCM4.3 from CRU and (d) RegCM4.3 from EIN.

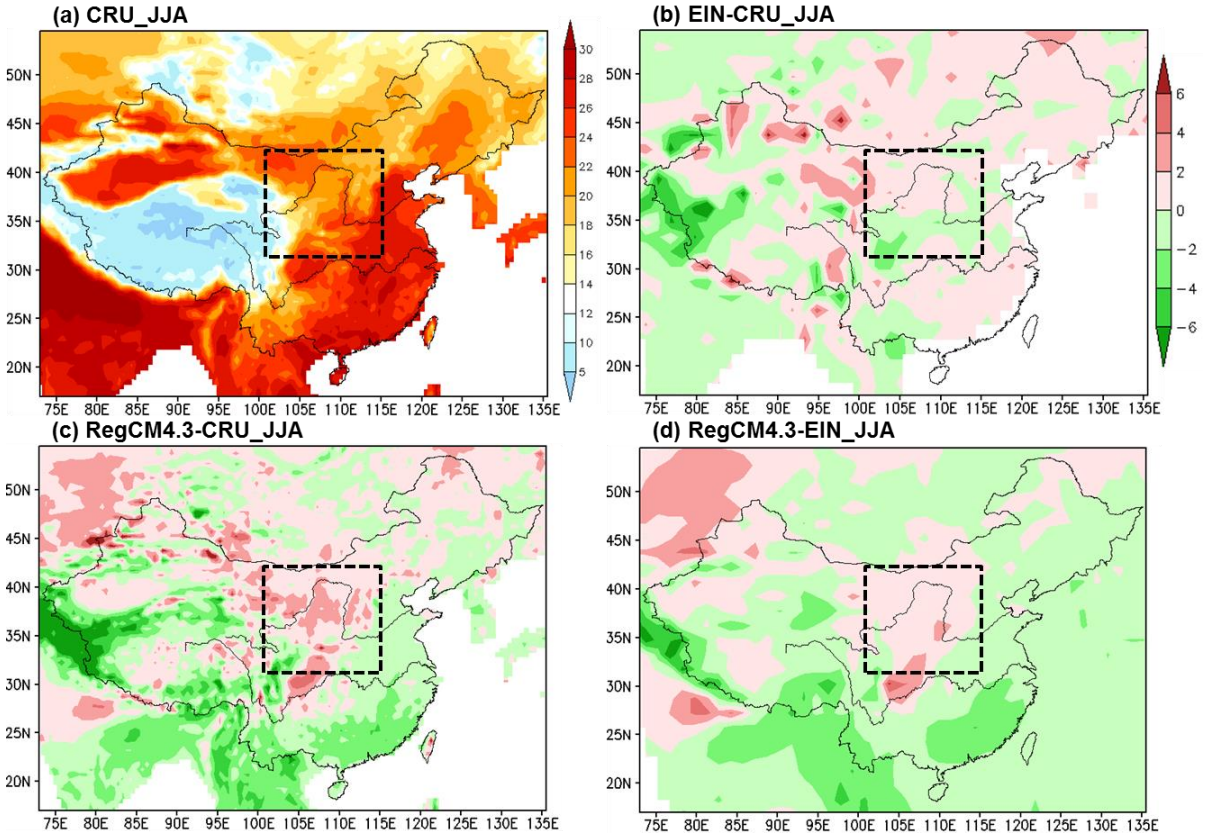

FIGURE 3 As in FIGURE 2, except for summer (JJA) 2m air temperature (˚C).

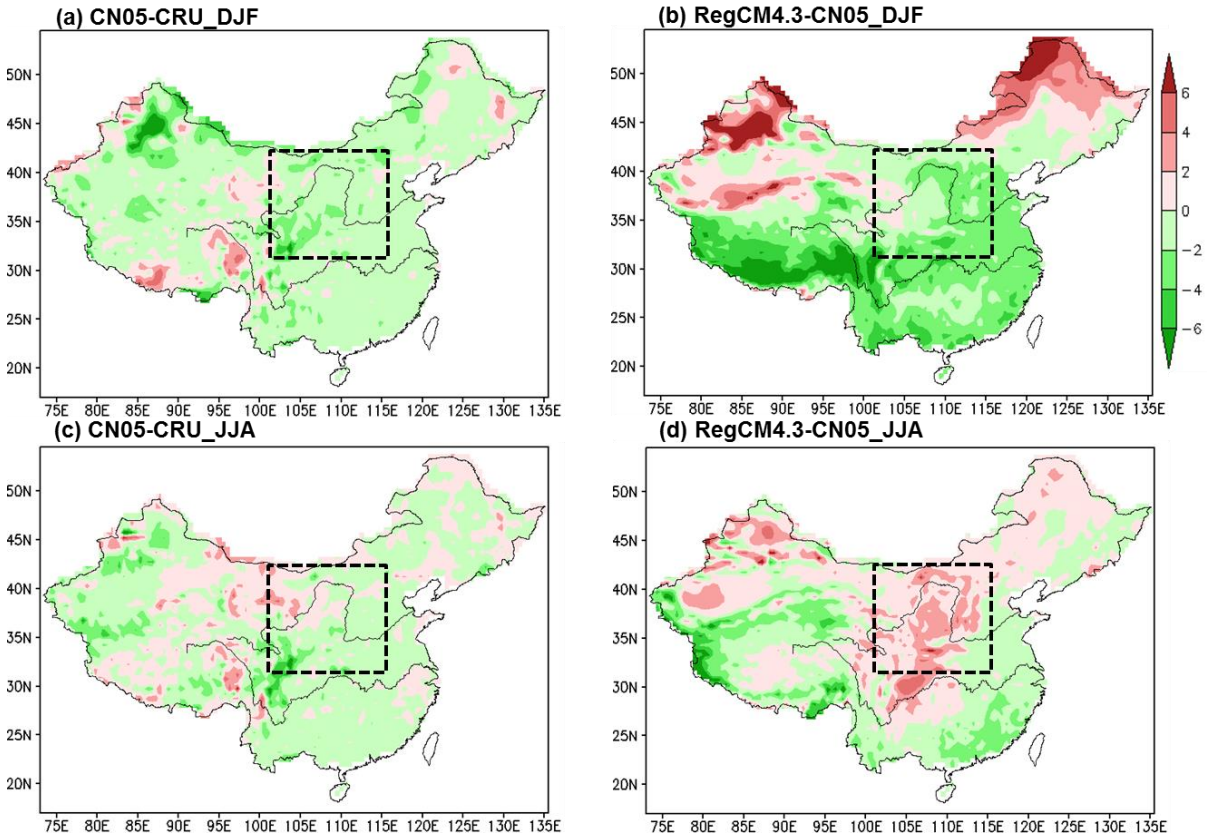

FIGURE 4 Spatial distribution of 2m air temperature (˚C) over China domain with the analysis domain in the dashed box: differences of (a) CN05 from CRU in DJF, (b) RegCM4.3 from CN05 in DJF, (c) CN05 from CRU in JJA and (d) RegCM4.3 from CN05 in JJA.

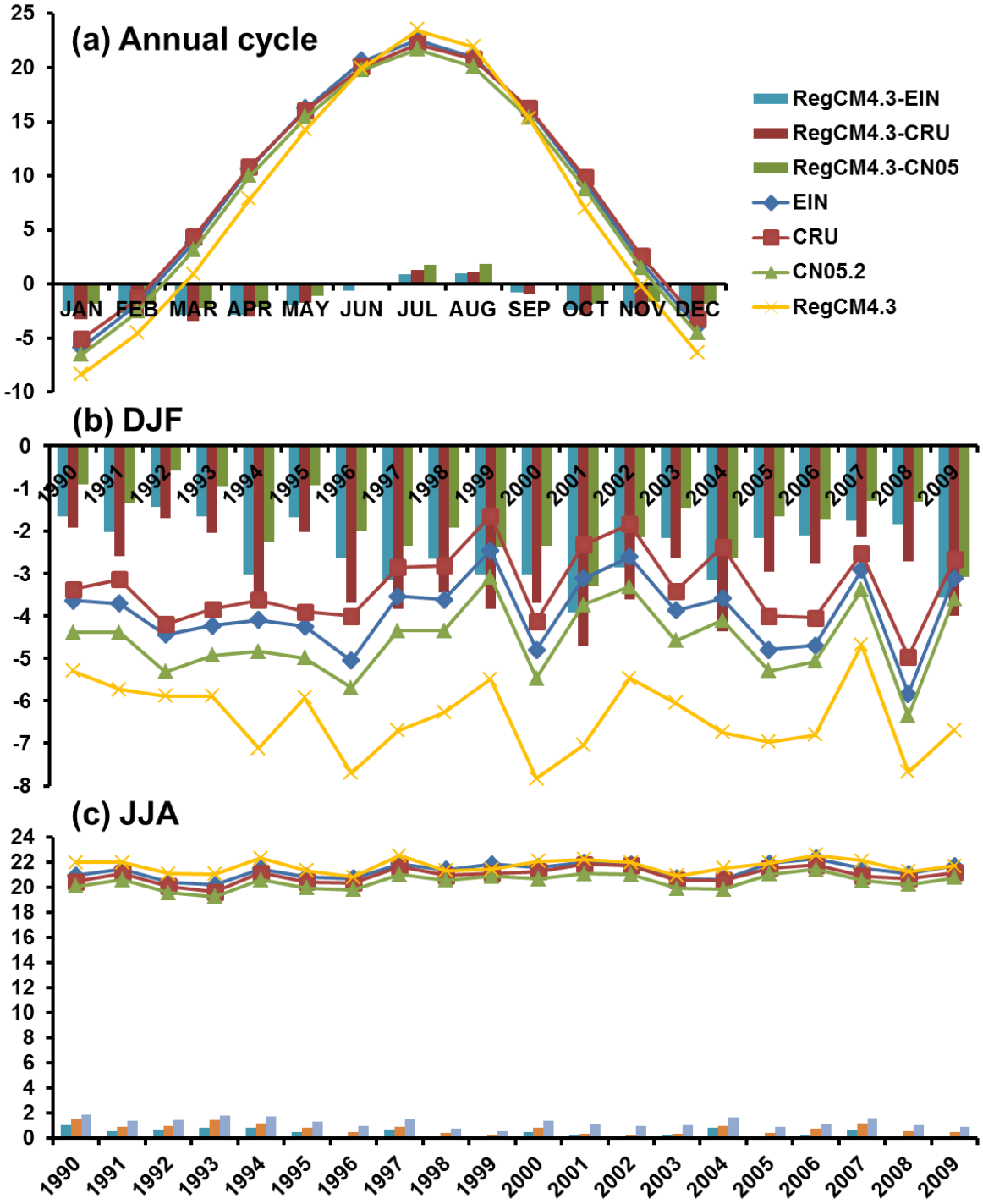

FIGURE 5 (a) Average annual cycle and interannual anomalies over the analysis domain during the season of (b) DJF and (c) JJA of observed (CRU and CN05.2), EIN reanalysis and RegCM4.3 simulated surface air temperature.

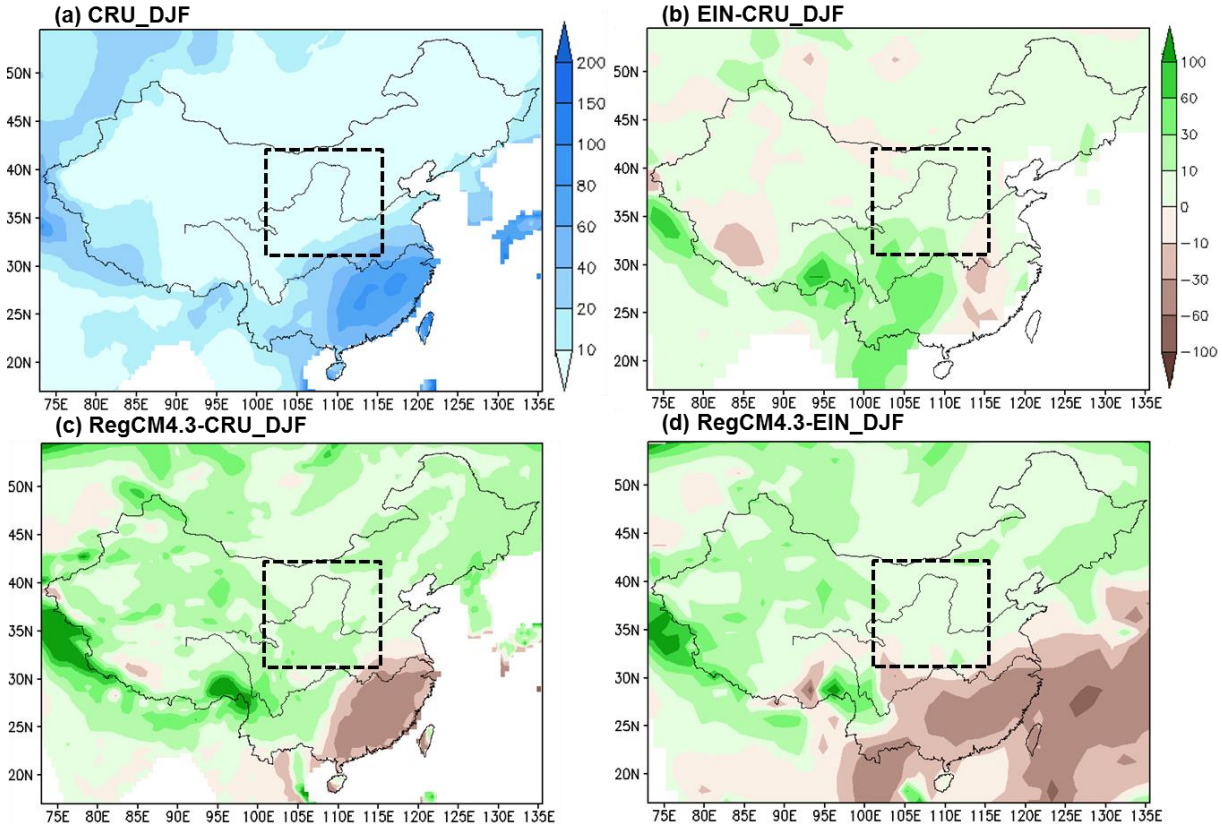

FIGURE 6 As in FIGURE 2, except for winter precipitation (mm month^{-1}).

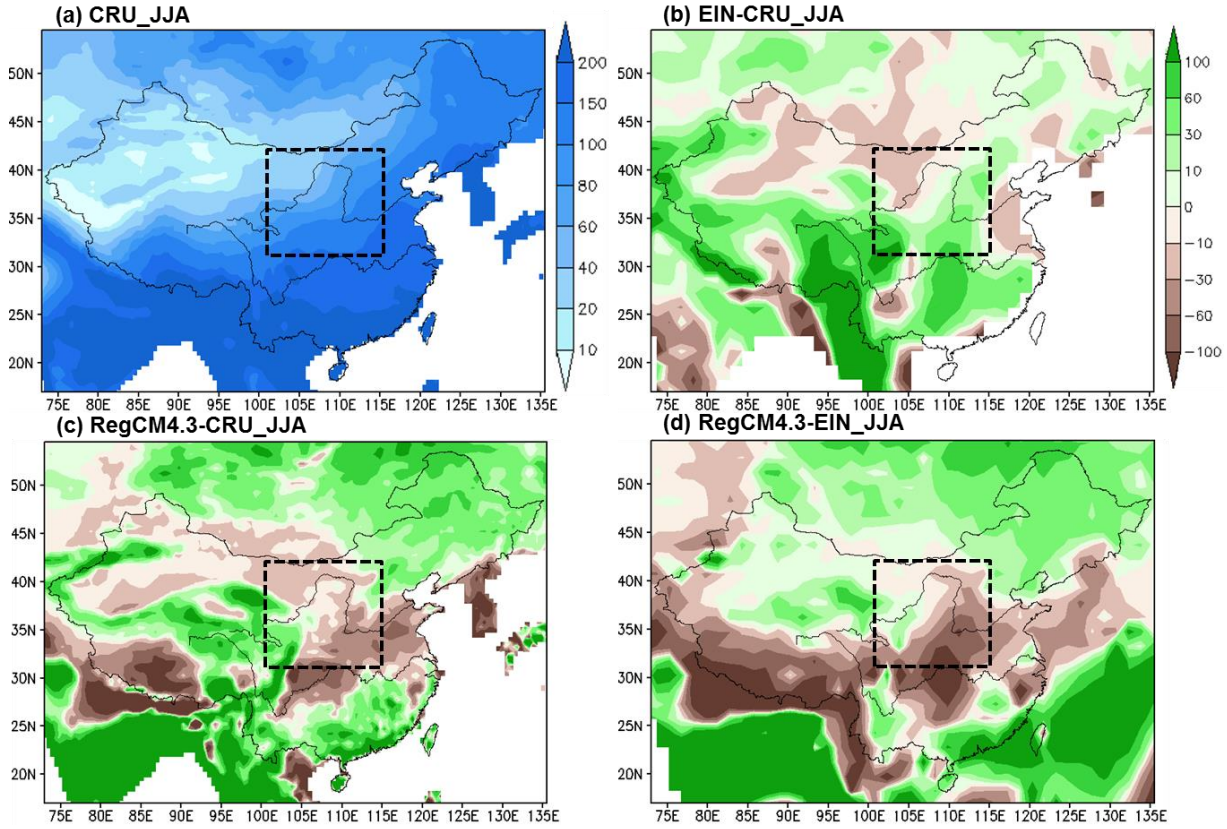

FIGURE 7 As in FIGURE 3, except for summer precipitation (mm month^{-1}).

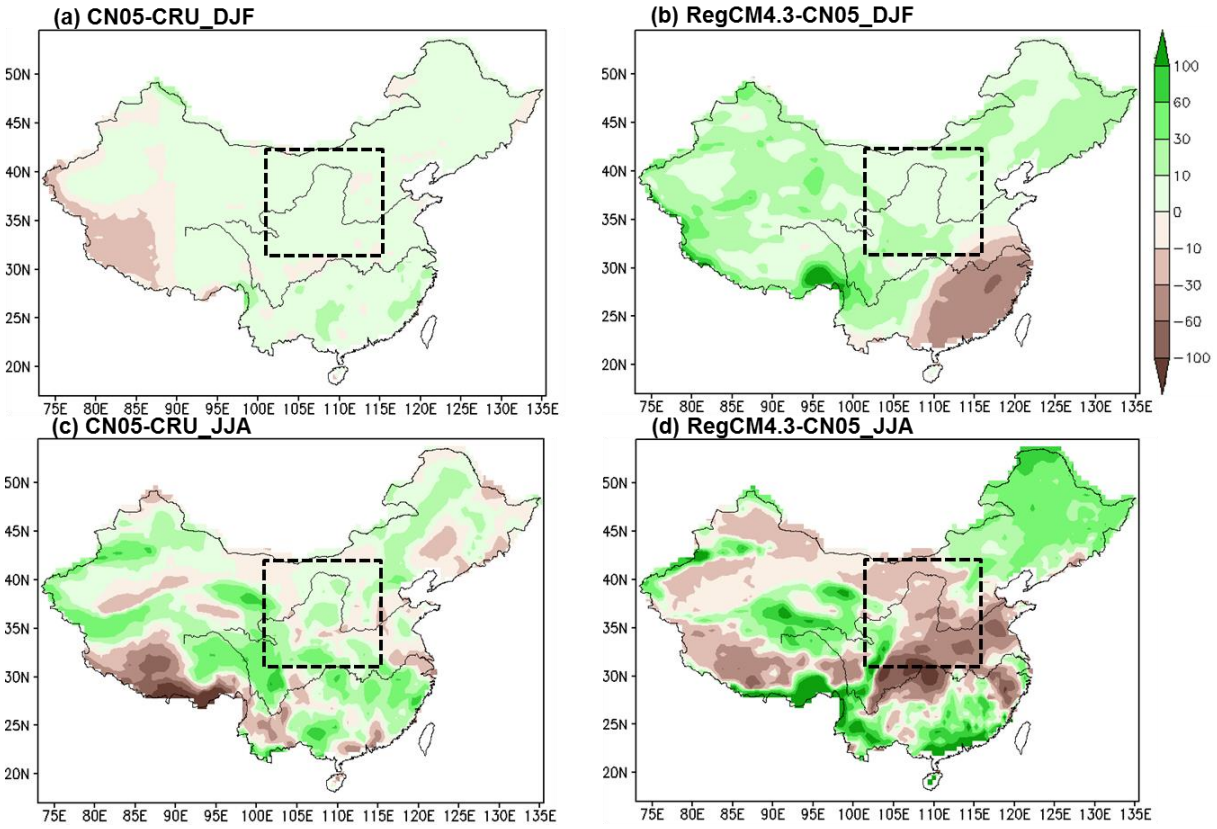

FIGURE 8 As in FIGURE 4, except for precipitation (mm month^{-1}).

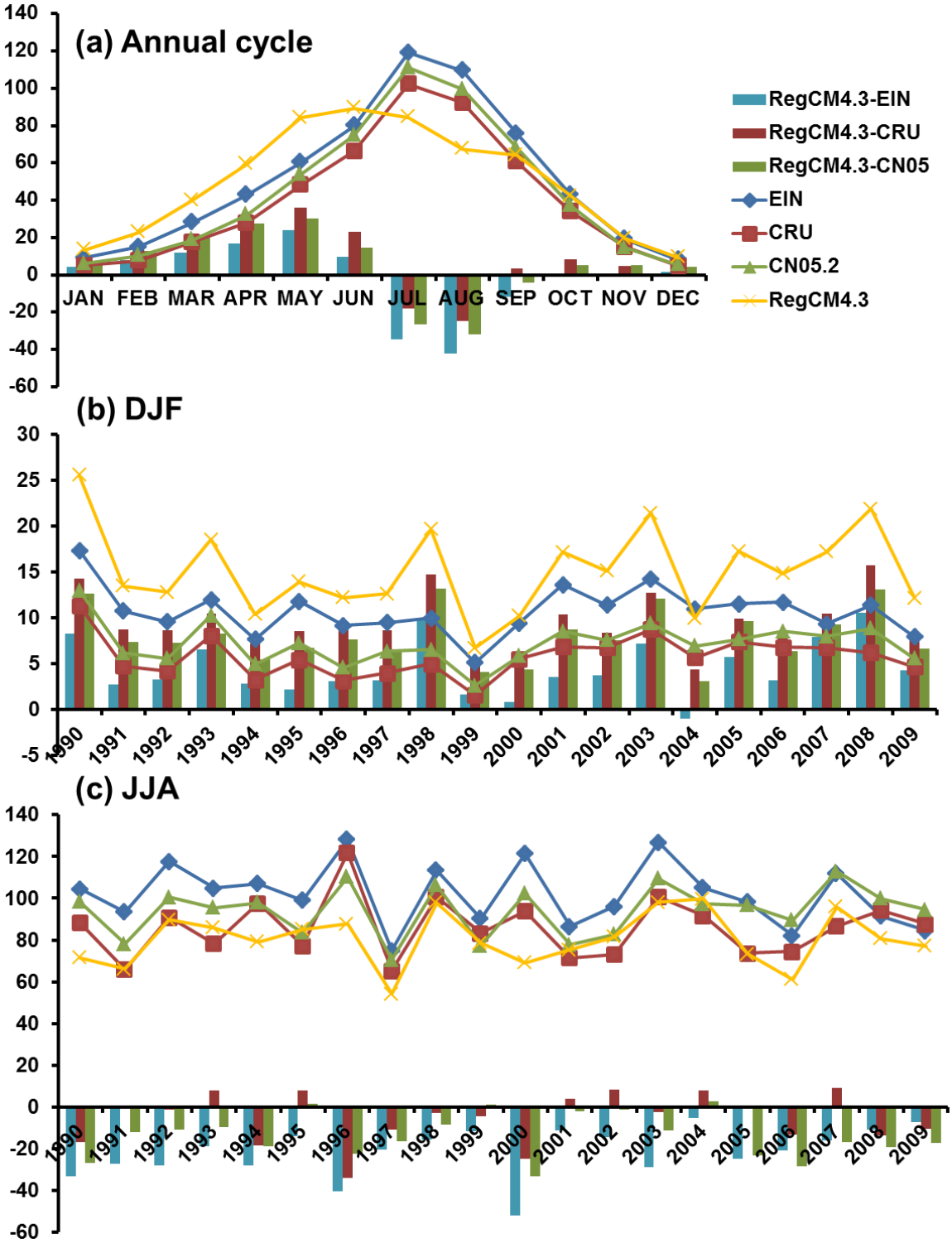

FIGURE 9 As in FIGURE 5, except for precipitation (mm month^{-1}).

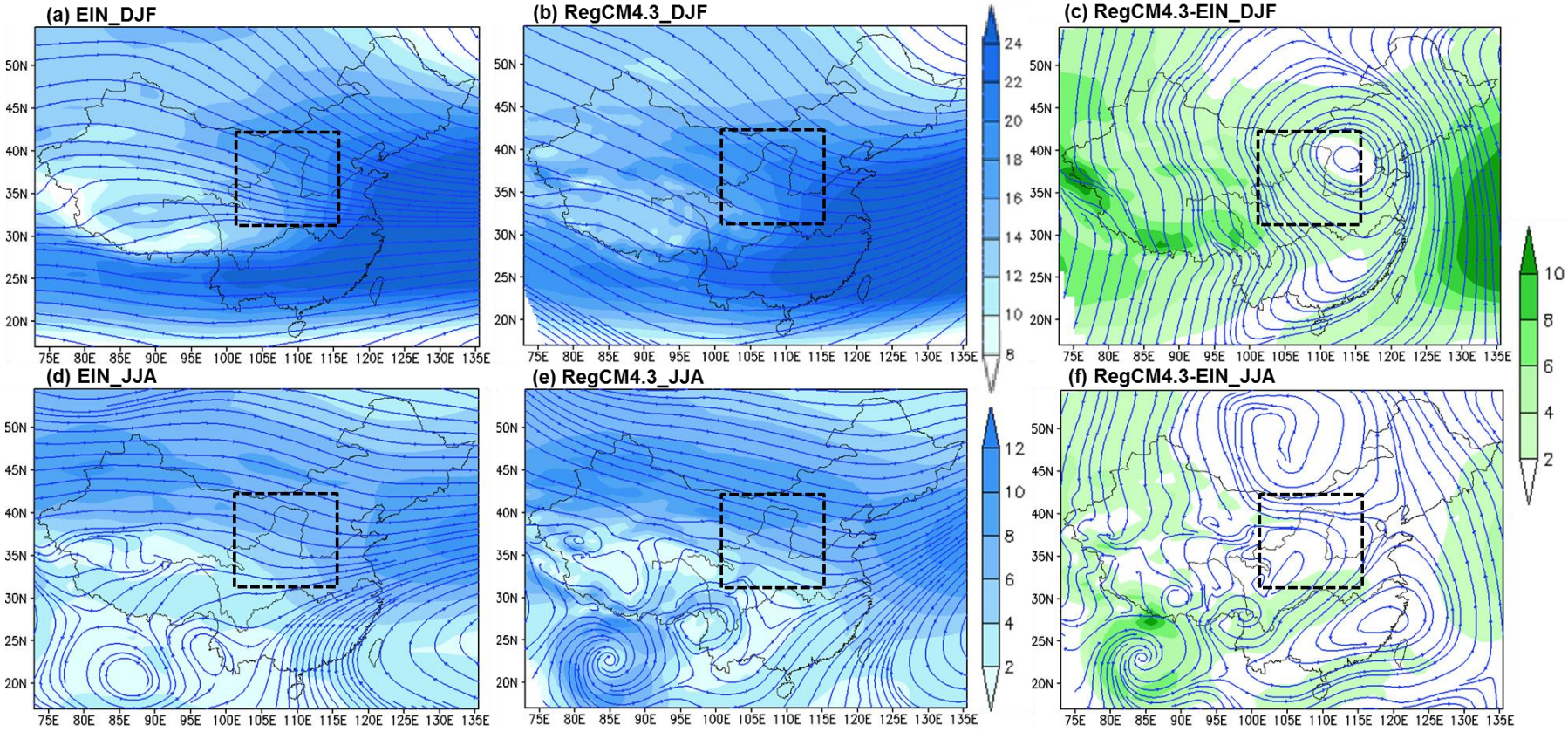

FIGURE 10 500 hPa wind (stream flow) and speed (shaded; m s^{-1}) over the entire domain with the analysis domain in the dashed box: (a) EIN reanalysis in DJF, (b) RegCM4.3 simulated in DJF, (c) differences of RegCM4.3 from EIN in DJF, (d) EIN reanalysis in JJA, (e) RegCM4.3 simulated in JJA, (f) differences of RegCM4.3 from EIN in JJA.

List of Tables

TABLE 1 Observational datasets used in this study.

Datasets	Temperature (˚C)			Precipitation (mm month^{-1})			Cloud Fraction (%)	Wind Field 500 hPa (m s^{-1})	Energy Budget (W m^{-2})				Spatial and temporal scale	References
	Mean	Tmin[a]	Tmax[b]	Total	Con[c]	Stra[d]			SWR[e]	LWR[f]	SH[g]	LH[h]		
CRU	√	√	√	√			√						0.5˚ global, 1989–2009	(New, et al., 2000)
CN05	√	√	√	√									0.5˚ China, 1989–2009	(Xu, et al., 2009)
EIN	√			√	√	√	√	√	√	√	√	√	1.5˚ global, 1989–2009	(Uppala, et al., 2008; Dee et al. 2011)
SRB							√		√	√			1.0˚ global, 1989–2007	(Stackhouse, et al., 2004)

[a] Minimum surface air temperature (Tmin); [b] Maximum surface air temperature (Tmax); [c] Convective precipitation (Con); [d] Stratiform precipitation (Stra); [e] Shortwave radiation (SWR); [f] Long-wave radiation (LWR); [g] Sensible heat flux (SH); [h] Latent heat flux (LH)

TABLE 2 Evaluation of simulated (REG) temperature and precipitation by the CRU and CN05 observations, and EIN reanalysis.

	Datasets	Temperature (˚C)							Precipitation (mm month^{-1})						
		Mean[a]	MB[b]	RMSE[c]	PCC[d]	TCC[e]	Tmin[f]	Tmax[g]	Mean	MB	RMSE	PCC	TCC	Con[h]	Stra[i]
[j]DJF	REG	-6.42					-11.76	-0.18	15.20					0.19 (1.25%)	15.01 (98.75%)
	CRU	-3.26	-3.16	3.65	0.94	0.49*	-9.01	2.48	5.80	9.40	11.06	0.72	0.83**		
	CN05	-4.55	-1.87	2.45	0.96	0.63**	-9.69	2.24	7.17	8.03	9.64	0.76	0.87**		
	EIN	-3.91	-2.51	3.07	0.96	0.65**			10.63	4.57	6.86	0.87	0.80**	1.98 (17.98%)	9.03 (82.02%)
[k]JJA	REG	21.75					15.99	28.57	80.37					49.63 (61.75%)	30.74 (38.25%)
	CRU	20.99	0.76	2.02	0.91	0.79**	15.49	26.55	86.92	-6.55	36.63	0.65	0.58**		
	CN05	20.49	1.26	1.98	0.95	0.78**	15.15	26.48	95.07	-14.70	37.55	0.73	0.64**		
	EIN	21.36	0.39	1.27	0.97	0.78**			102.79	-22.42	47.71	0.81	0.66**	53.41 (51.96%)	49.38 (48.04%)

[a] Spatial mean climatology (Mean); [b] Mean bias (MB) using the simulations minus the observations; [c] Root mean square Error (RMSE); [d] Pattern correlation coefficient (PCC); [e] Temporal correlation coefficient (TCC); [f] Minimum surface air temperature (Tmin); [g] Maximum surface air temperature (Tmax); [h] Convective precipitation (Con); [i] Stratiform precipitation (Stra); [j] Winter season months: December, January and February (DJF); [k] Summer season months: June, July and August (JJA); * Statistically significant at the 95% confidence limit; ** Statistically significant at the 99% confidence limit

TABLE 3 Observed SRB, EIN reanalysis and simulated (REG) surface energy budget.

	Unit: W m^{-2}	NS[a]	NL[b]	DL[c]	SH[d]	LH[e]
DFJ	EIN	93.22	76.64	214.04	18.89	10.31
	SRB	102.26	66.16	226.51	-	-
	REG	104.44	77.05	209.59	17.15	14.01
	Bias (REG minus EIN)	11.22	0.41	-4.45	-1.74	3.70
	Bias (REG minus SRB)	2.18	10.89	-16.92	-	-
JJA	EIN	198.59	76.45	347.85	45.85	69.74
	SRB	181.33	78.73	360.55	-	-
	REG	223.02	83.01	353.01	66.33	73.07
	Bias (REG minus EIN)	24.43	6.56	5.16	20.48	3.33
	Bias (REG minus SRB)	41.69	4.28	-7.54	-	-

[a] Surface Net Downward Shortwave Radiation (NS); [b] Surface Net Upward Longwave Radiation (NL); [c] Surface Downward Longwave (DL); [d] Sensible Heat Fluxes (SH)

TABLE 4 Observed (SRB), EIN reanalysis and simulated (REG) diabatic heating rate, temperature advection (10^{-3} °C s^{-1}).

	Unit: 10^{-3} ˚C s^{-1}	Total diabatic heating rate	Shortwave radiation heating rate	Long-wave radiation cooling rate	Sensible flux cooling rate	Latent flux cooling rate	Temperature Advection
DJF	REG	-1.45	40.27	29.70	6.62	5.40	-3.36
	EIN/SRB	-4.86/-	35.94/39.42	29.55/25.51	7.28/-	3.97/-	-0.51
JJA	REG	0.24	86.08	32.01	25.62	28.20	1.83
	EIN/SRB	2.52/-	76.56/69.91	29.47/30.35	17.68/-	26.89/-	0.52

TABLE 5 Observed (CRU and SRB), EIN reanalysis and simulated (REG) cloud fraction, specific humidity and moisture advection.

	Experiments	Cloud Fraction (%)	Specific humidity (500 hPa, g kg^{-1})	Moisture Advection (10^{-2} g kg^{-1} s^{-1})
DJF	REG	43.69	1.96	5.98
	CRU	42.88		
	EIN	40.83	2.49	2.25
	SRB	50.92		
	Bias	-7.23	-0.53	3.73
JJA	REG	45.44	10.73	34.24
	CRU	60.26		
	EIN	53.76	11.98	39.91
	SRB	65.45		
	Bias	-20.01	-1.25	-5.67

Chapter 3. A Regional Climate Modelling Study over the Loess Plateau, China. Part II: Sensitivity Tests

The aim of the work presented in this chapter was to further evaluate the performance of the RegCM over the Loess Plateau, and characterise the key parameterizations that influenced the model simulation. A further aim was to provide a model configuration that was able to reproduce the local climate more appropriately for further application of simulating the potential effects of land surface changes on the climate over the plateau. With these considerations, a series of experiments using different parameterizations were designed through applying alternative convective schemes, horizontal resolutions, and domain locations. The work in this chapter assessed the level of accuracy that the RegCM could reach over the Loess Plateau and provided general guidance for simulations over areas in a mid-latitude zone with complex topography.

Candidate's contribution to this paper

The simulations in this paper were designed and carried out by the candidate. The candidate also performs all the figure preparation and manuscript drafting. All the work was under supervision of Dr Cheung, who led the main direction of the work and guided the candidate to carry out the research.

A Regional Climate Modelling Study over the Loess Plateau, China.

Part II: Sensitivity Tests

Lang Wang and Kevin K. W. Cheung

Department of Environmental Sciences, Macquarie University, Sydney, Australia

Prepared for Journal of Climate

Submitted March 2015

* Author for Correspondence: Kevin Cheung, Department of Environmental Sciences, Macquarie University, North Ryde, NSW 2109, Australia. Email: kevin.cheung@mq.edu.au

Abstract

This paper examines the sensitivity of the Regional Climate Model version 4.3 (RegCM4.3) to a series of model parameterizations over the Loess Plateau in China. Seven sensitivity experiments spanning from 1990 to 2009 have been performed to analyse the importance of convective scheme, horizontal resolution and domain size. All the experiments generally reproduce the observed surface air temperature and precipitation climatology, although several common biases are present such as underestimation of temperature and overestimation of precipitation during the winter season, and pronounced biases over topographically diverse areas. These biases persist regardless of the changes made in the parameters above. However, there are substantial differences among the experiments.

Firstly, the simulated precipitation during summer is strongly dependent on the choice of convection scheme. The Grell convection scheme with Fritsch-Chappell closure generates the most accurate simulation among the three convective schemes analysed. The simulation that used the Emanuel convective scheme exhibits excessive convective and total precipitation, however, it represents the annual precipitation cycle better. The Emanuel scheme simulation also closely reproduces the observed precipitation spatial distribution. Secondly, using higher horizontal resolution effectively improves the spatial distribution of the surface variables, although the large-scale structure remains unchanged. The improvement is related to the improvement in representation of the terrain heterogeneity. Thirdly, the present study shows that the RegCM4.3 simulation is not particularly sensitive to domain size except when the domain does not include areas of the eastern Tibetan Plateau. The latter leads to a dramatic decrease in the model performance.

Keywords:

Regional climate model; Loess Plateau; model sensitivities; convective parameterization scheme; horizontal resolution; domain choice

1. Introduction

Regional Climate Models (RCMs) have been extensively applied in recent years to investigate climate features at the regional scales (e.g., Takle et al. 1999; Christensen et al. 2002; Linda et al. 2012; Fu et al. 2005). The Regional Climate Model (RegCM) is one of the most advanced RCMs and has performed well in capturing key characteristics of local climate regimes over most parts of the world (e.g., Gu et al. 2012; Gao et al. 2006; Im et al. 2006; Wu et al. 2012; Fu et al. 2005; Sen et al. 2004). However, deficiencies remain the RegCM especially over complex orography and climate transition zones. These deficiencies have led to difficulties in accurately simulating the climate over such areas; previous studies have exhibited large model biases and a high variability of model performance. For example, Afiesimama et al. (2006) applied the RegCM over West Africa and found the model over-predicted rainfall in the monsoon region that has a complex terrain, but under-predicted rainfall over the arid Sahel region. Simulations over the Arabian Peninsula with the RegCM overestimated both rainfall (by approximately 65 mm $month^{-1}$) and temperature (4˚C higher) over the south mountainous areas and north semi-arid plain, respectively, compared to observations (Almazroui 2012). Part I of this study using the RegCM over the Loess Plateau in China systematically exhibited a temperature deficit of approximately 2.5˚C and excessive precipitation of 8.0 mm $month^{-1}$ compared to observations during the winter months (Wang and Cheung 2015a). The biases described demonstrate that improvements in the model performance, including the identification of sources and alleviation of simulated deficiencies, are necessary to provide accurate climate simulations over complex regions.

The Loess Plateau, China, is an excellent case study to evaluate and analyse the sensitivity of the RegCM. The area is located in a semi-arid transition zone and is characterized by marked topographic gradients (Huang et al. 2008). The local topography

includes the eastern low hills at an altitude of 500 m and the western Tibetan Plateau at 3000 m, as well as widespread gullies and fragmented landscapes. The complex orography tends to regulate mesoscale circulation in the region, enhance localized convection processes and cause strong disturbance of the inflow from the boundary, resulting in a highly complex climate (Dickinson 1995; Pielke and Avissar 1990). The semi-arid transition zone over the Loess Plateau is predominantly controlled by the southeast Asian summer monsoon and northwest continental climate system (Li et al. 2010; Zhou et al. 2010). Interactions between these two systems through powerful exchanges in heat and moisture can lead to distinct climatic gradients of precipitation and temperature, especially for summer precipitation that is strongly influenced by the migration of the Asian summer monsoon (Liu and Zeng 2004; Liu et al. 2008b).

More extensive studies over the Loess Plateau are important because the local climate is essential for managing socioecological resources in the region, especially the natural habitats and rain-fed agriculture, which are highly dependent on precipitation in this semi-arid region. Therefore, systematic studies of the RegCM and an understanding of its sensitivity to key processes and major parameters over the Loess Plateau are required.

Recent research has suggested that RegCM's performance is highly sensitive to diverse physical parameterizations such as lateral boundary conditions, simulation periods and integration areas (Giorgi et al. 2012; Zanis et al. 2009; Im et al. 2008; Gao et al. 2006; Steiner et al. 2005). A systematic assessment of each factor' effects on the model processes and comparison of the relative importance of each factor are necessary to optimize the simulation. In this study, three parameterizations that critically influence the characteristics of the climate simulation over the Loess Plateau are considered: the convective scheme, horizontal resolution and integration area.

In Section 2, a description of the RegCM modelling system is presented and Section 3 details the experimental design and observational datasets used for validation. In Sections 4 and 5 the sensitivity results are presented and discussed. This study is concluded in Section 6.

2. The RegCM model

Convection processes are significantly affected by complex terrain, such as that across the Loess Plateau, which promotes the development of more localized convection due to a strong elevated heat source during the summer (Giorgi 1991; Xiao et al. 2002). Thus, the choice of different convective parameters can significantly influence the model simulation and their optimization may improve model performance (Seth et al. 2007; Pal et al. 2007; Singh et al. 2006).

The model used in the present study was version 4.3 of the Regional Climate model (RegCM4.3) developed by the International Centre for Theoretical Physics (ICTP) (Giorgi et al. 2012) from RegCM version 3 (Pal et al. 2007). RegCM4.3 has a dynamical core of the Mesoscale Model (MM5) from the National Centre for Atmospheric Research (NCAR) and Pennsylvania State University (Grell et al. 1994). The radiation scheme adopted by the RegCM4.3 is from the NCAR Community Climate Model 3 (CCM3) (Kiehl et al. 1996), the modified planetary boundary layer scheme was developed by Holtslag et al. (1990), and the land surface process used the second generation of the Biosphere-atmosphere transfer scheme (BATS) (Dickinson et al. 1993).

Precipitation in the RegCM4.3 is generated by both resolvable-scale (stratiform) precipitation and convective precipitation. The former uses the explicit moisture scheme (SUBEX) (Pal et al. 2000), which takes the variability of sub-grid clouds into account, following the work of Sundqvist et al. (1989), and links the average grid relative humidity

to cloud fraction, cloud water, cloud water accretion and evaporation of falling raindrops. The convective precipitation process is parameterized by convective schemes with sub-scale convective clouds and cumulus convection. The RegCM4.3 has been equipped with four convective schemes; three of them are examined in this study except the Kuo scheme (Anthes 1977) due to its relatively simplistic moisture convergence processes.

The first convective scheme examined in the present study is the Grell formulation (Grell 1993; Grell et al. 1994), which uses a mass flux scheme that incorporates moistening and heating effects via the formation of deep convective clouds between two steady-state circulations of an updraft and downdraft. Mixing between cloudy air and environmental air only occurs at the top and base of the circulations as a compensating motion, which in turn provides feedback to the large-scale latent heat release or absorption. The scheme is activated when a lifted parcel attains moist convection.

The Grell scheme is composed of two convective closure assumptions, the Arakawa-Schubert closure (hereafter referred to as AS) (Arakawa and Schubert 1974) and Fritsch-Chappell closure (hereafter referred to as FC) (Fritsch and Chappell 1980). The AS assumption is a quasi-equilibrium condition that assumes convective processes turn into a stable state as soon as large-scale processes destabilize them. As a result, the buoyant energy available for convection continuously changes at each time step, following a rate according to the total buoyant energy. In contrast, under the FC assumption the buoyant energy available for convection is only released during a specified timescale (between 30 min and 1 hour). This infrequent release tends to result in a relatively weak convection in FC compared to AS. This indicates that FC is more suitable to simulate fine resolutions from 10 km to 30 km and drier regions where a balance needs to be maintained between the amounts of convective and stratiform precipitation (Fritsch and Chappell 1980, Otte 1999). Conversely, AS is likely to be more appropriate for coarse horizontal resolutions

that are greater than 30 km and humid regions, to simulate the proportional increase in convective rainfall (Arakawa and Schubert 1974, Otte 1999). The influence of each closure assumption within the Grell scheme is assessed within the present study.

The Emanuel (EM) scheme has recently been implemented within the RegCM system and, as a result, its performance has not been extensively tested to date. It also consists of updrafts and downdrafts and applies the mass flux schemes and quasi-equilibrium assumption. However, in addition it allows within clouds mixing, which is highly episodic and inhomogeneous on the sub-cloud scale (Emanuel 1991; Emanuel and Zivkovic-Rothman 1999) in contrast to the continuous entraining plume model in the AS scheme. As air entrains into the cloud from its surroundings, mixing parcels are formed that can ascend or descend, depending on the mixing rate which is determined by the vertical gradients of buoyancy in the clouds. Precipitation is formed via auto-conversion of cloud water into rain water and accounts for simplified ice processes. The EM scheme is the most sophisticated among the three convective parameterizations that are investigated.

3. Experimental design

A total of seven experiments were designed to investigate the model sensitivities to the convective scheme, horizontal resolution and domain size (Table 1). The experiments spanned 21 continuous years from 1 January 1989 to 31 December 2009, with the first year of 1989 assigned as the spin-up period. The simulation period provided sufficient information to study the sensitivities of the model, annual cycle, interannual variability and spatial structures of the regional climatology. In all the experiments, 12 grid points were used as the buffer zone. A square covering the Loess Plateau with small dotted boundary (31˚N to 42˚N, 101˚E to 115˚E) is assigned as the analysis domain (Fig. 1), within which all the statistics of relevant features were calculated.

a. Convective schemes

Three experiments were designed to assess the sensitivity of the model to the convection schemes. They were driven by the reanalysis dataset of the European Centre for Medium-Range Weather Forecasts (ECMWF) Interim reanalysis (EC_In), which has a 1.5˚ grid size and 6-hourly time interval. Sea surface temperature (SST) was defined by the National Oceanic and Atmospheric Administration (NOAA) Optimum Interpolation (OI) SST dataset, on a 1˚ grid, with intervals of one week. A horizontal resolution of 50 km with 18 vertical sigma levels was used covering the entirety of China and its surrounding regions (Fig. 1a). This domain was similar to the standard domain recommended by the COordinated Regional climate Downscaling EXperiment (CORDEX), capturing basic topographic features of China such as the Tibetan Plateau and the Mongolian Plateau. The only difference between settings in these experiments was the convective scheme; the control experiment (CTL) used the FC scheme (Wang and Cheung 2015a) and the other two experiments used the AS and EM schemes respectively. Outputs from the CTL experiment with 6-hourly time intervals were used as the lateral boundary conditions for nested simulations.

b. Horizontal resolution

Simulations with finer resolution allow more adequate description of the physiographical features within an area, which in turn improves the representation of surface-atmosphere processes and the lower boundary conditions, and provides more realistic spatial and temporal variability of the local climate especially in regions with high topographic heterogeneity like the Loess Plateau (Giorgi and Marinucci 1996; Mass et al. 2002). To investigate the effect of model resolution, experiments with two resolution gradients were performed. The CTL for this experiment used a 50 km horizontal resolution

(as described above) and the nested simulation comprised of a finer horizontal resolution of 20 km (named NEST20). The NEST20 experiment used a one-way nest technique, driven by the lateral boundary conditions from the CTL outputs. It covered a limited domain across the Loess Plateau and its surroundings (Fig. 1b); this domain included the relevant regional forcings of the Mongolian Plateau and the eastern part of the Tibetan Plateau. Significant finer-scale topographic details were captured by the NEST20 experiment with more sharply defined mountain peaks and valleys compared to the CTL experiment.

c. Domain size

The final factor that the present study considers is the model sensitivity to the area extent chosen for the simulated domain. The simulation domain is likely to affect the balance between the boundary and internal model forcings in climate simulations (Giorgi and Mearns 1999; Gao et al. 2006). In particular, domain choice could greatly influence the strength of regional sources of forcing over topography (Seth and Giorgi 1998; Giorgi et al. 1997). Four experiments were designed to investigate the model sensitivity to the domain location and identify the most appropriate simulation area to simulate climate over the Loess Plateau (Figs. 1c-e). The extents of the domains analysed are described in detail in Table 1; they each used a 20 km horizontal resolution with different extents of the surrounding area. The NEST20 experiment, as described above, covered the largest nested domain among the four experiments in order to include all the relevant regional forcing. NEST20_noTB was designed to reduce the forcing from the Tibetan Plateau by narrowing the longitude extent to the west, but maintaining the same latitude extent as the NEST20 experiment. NEST20_noMG was designed to consider the influence of the Mongolian Plateau on the climate simulation, so comprising a domain area with a smaller latitude

extent (excluding the terrain in north) but had the same longitude extent as NEST20. NEST20_noMGTB was the smallest domain; it excluded both the Mongolian Plateau and a part of the Tibetan Plateau with the same latitude extent as NEST20_noMG and the same longitude extent as NEST20_noTB.

d. Observational data

Two observational data sets were used for the model evaluation: the Climate Research Unit (CRU) dataset (Mitchell and Jones 2005) and the China Meteorological Administration Meteorological Information Centre dataset version 5.2 (CN05.2) (Xu et al. 2009). The CRU dataset (0.5˚ grid size) provided monthly surface air temperature and precipitation for the entire simulation period. The CN05.2 dataset included the temperature and precipitation records analyzed using the same spatial resolution and spatial interpolation method as the CRU dataset. However, the CN05.2 dataset had a larger number of contributing stations over the simulated area and thus is likely to represent a more realistic local climate than the data outputs from the CRU dataset (Xu et al. 2009; Sun et al. 2014). Detailed differences between the CN05.2 and CRU datasets over the Loess Plateau has been investigated in Part I of this study (Wang and Cheung 2015a). Resulting from this research, CN05.2 was used in the present study as the major observational dataset. In addition, the EC_In reanalysis dataset was used to supplement observations to include convective and stratiform precipitation.

The statistical analyses used to quantify the differences among the model simulations and observations included spatial and temporal mean bias (MB), root mean square error (RMSE), as well as the pattern correlation coefficient (PCC) and temporal correlation coefficient (TCC).

4. Results

a. The control simulation

The climatology of the CTL experiment over 20 years provides a benchmark for the sensitivity analyses. The CTL experiment qualitatively reproduces the climatology over the Loess Plateau, as it simulates cold, dry winters and warm, wet summers that are controlled by the continental climate system and Asian summer monsoon, respectively (Wang and Cheung 2015a). During the winter season, the CTL experiment represents the observed spatial patterns in climate particularly well, showing cold centres over the northern (high latitude) and western (high altitude) areas (Figs. 2a, b), and high precipitation over the southeastern region (Figs. 2c, d). In the summer season, the CTL experiment also captures the observed patterns in both temperature and precipitation; the temperature maximums are located over the southeastern and northwestern regions, medium temperatures are over the central area and the minimum is over the southwestern mountains (Figs. 3a,b), while precipitation increasing gradually from the northwest towards the southeast (Figs. 3c, d). The similarity between the CTL simulation and observations is reflected in the high spatial PCCs, which are greater than 0.95 for temperature (Table 2) and over 0.73 for precipitation in both seasons (Table 3-4).

Despite the high spatial PCC, several discrepancies still exist between the CTL experiment and observations. The main differences include a systematic cold bias of -1.87˚C and over-predicted rainfall of 8.03 mm month^{-1} during the winter season, and 14.70 mm month^{-1} under-predicted precipitation during the summer (Tables 2-4). The rainfall peak in the CTL experiment is also one month ahead of observations in the annual cycle (Fig. 4a). These model biases were also observed in previous studies with similar parameterizations over East Asia (e.g., Im et al. 2008; Gao et al. 2011).

b. Comparison among the convective schemes

1) SPATIAL PATTERNS

The temperature outputs in the model simulation only vary slightly in response to different convective schemes during the winter, but differences are more pronounced in the summer. During the winter season, each experiment exhibits a similar cold bias pattern to the CTL experiment (using the FC scheme), in which there is a large bias located primarily over the eastern and southern regions in comparison with the CN05.2 observational data (Figs. 5a-c). The EM scheme slightly alleviates the cold bias magnitude over these regions (Fig. 5c). The similarity in the winter climate between the different simulations is validated through the statistical analyses, which show a small range of temperature MB from -1.83˚C in the EM to -2.36˚C in the AS schemes and a similar RMSE from 2.19˚C to 2.68˚C, respectively, along with nearly the same PCCs of 0.96 (Table 2).

During the summer, all three simulations generally exhibit warm conditions in comparison to the CN05.2 observation dataset, with large biases over the central area (Figs. 5d-f). More specifically, the simulation with the EM convective scheme shows overall warm conditions, while those with the FC (CTL) and AS schemes generate a small area of cold bias over the southeast regions. In addition, use of the AS scheme leads to cold biases over the northwest. The highest positive bias, of 1.99˚C, is observed using the EM convective scheme, compared to the FC (1.26˚C) and AS schemes (0.02˚C); the highest RMSE is also seen using the EM scheme, of 2.33˚C. Nevertheless, PCCs are high in all three experiments with values over 0.95 (Table 2).

During the winter season, the spatial bias patterns of precipitation generated by using the AS and EM schemes are similar to those in the CTL (Figs. 6a-c); the simulations consistently overestimate precipitation by up to 40 mm month^{-1} over the southwest area, with the EM convective scheme exhibiting slightly higher precipitation levels compared to

the AS and FC (CTL) schemes. The higher precipitation rates exhibited by the three experiments is reflected in the average MBs across the domain, which range from 8.03 mm $month^{-1}$ for the CTL experiment to 11.27 mm $month^{-1}$ for the EM scheme. Nevertheless, during winter the PCCs were generally high: 0.76 for the FC (CTL) scheme down to 0.69 for the EM scheme (Table 3).

During the summer season, more significant differences in the precipitation spatial bias pattern are seen among the three convective experiments compared to those in winter. In particular, the spatial bias patterns are quite distinct over the central area in comparison with the CN05.2 observations. The CTL experiment generates negative biases greater than -20 mm $month^{-1}$ in the central area, while the EM and AS schemes generate positive biases of precipitation between 10 to 40 mm $month^{-1}$ (Figs. 6d-f). The central area is the centre of the climate transition zone, where there is an intensive interaction due to the dense exchange of water, energy and momentum between the Asian summer monsoon (that carries abundant water vapour from the southeast) and the continental climate (with hot and dry conditions over the northwest). These interactions probably trigger the significantly different responses in the model simulations generated by each convective process over the central area.

Beyond the central area, the three experiments lead to an underestimate of precipitation over the southern and southeastern regions during the summer season, but with substantial differences amongst them. As shown in Figs. 6d-f, the CTL experiment generates the largest negative bias, while the other two experiments create smaller negative biases especially for the EM scheme. The insufficient rainfall simulated is likely to be predominantly affected by the shift of the southerly monsoon migration, which carries the monsoon moisture and provides water vapour to this interior area (Wang and Cheung 2015a). The relatively higher precipitation rates produced by the AS and EM schemes, in

comparison to the CTL, is largely attributed to their convective processes that lead to frequent and intensive convective precipitation.

The three model simulations also exhibit a (similar) consistent overestimation of precipitation over the southwestern and northeastern regions that occur in response to the sharp elevation changes. The largest bias is seen in the simulation with the EM scheme, in which precipitation is overestimated by 80 mm month^{-1}. This common spatial bias pattern is likely to reflect the influence of the topography on the model simulations, which is stronger than the effects of convective processes.

2) INTERANNUAL VARIABILITY

In terms of the seasonal cycle of precipitation, it is noticeable that the FC (CTL) and AS convective schemes tend to result in a peak in precipitation approximately one month ahead of the observed peak, along with their over-prediction of precipitation during the first half of the year (Fig. 4a). While the EM convective scheme simulates the peak in precipitation at the right time of year, however, it also appears to overestimate precipitation throughout the year. Similar results to these were also captured by RCM experiments over Europe (Deque et al. 2005) and Africa (Pal et al. 2007).

The three schemes simulated the annual cycle of temperature reasonably close to the observed pattern, with peak and minimum values in July and January, respectively (Fig. 7a). The temperature interannual variability is reasonably consistent among the three experiments during winter, but varies significantly during the summer season. In winter, the simulated temperature time series are consistent with each other and the observations, in spite of a systematic underestimation of around 2˚C in all three experiments (Fig. 7b); this is evident in the TCCs, which are between 0.54 (for the EM scheme) to 0.68 (for the AS scheme) (Table 2). In contrast, during the summer season the CTL experiment shows

the closest temporal pattern to the observations (Fig. 7c), demonstrated by the highest TCC of 0.78. The smallest TCC of 0.58 is seen in the simulation with the EM scheme (Table 2).

The interannual variability in precipitation is more different among the three sensitivity experiments during the summer than in winter. During the winter season, the simulated precipitation across the three experiments changes relatively consistently with the observations (Fig. 4b), demonstrated by the TCCs ranging from 0.84 for the EM scheme simulation to 0.87 for the CTL experiment. However, the precipitation simulated with the EM scheme is systematically overestimated by up to 15 mm month^{-1}. In summer, significant differences are captured among the three experiments (Fig. 4c). The CTL experiment captures more of the highs and lows of precipitation over the 20 year period than the other two experiments, validated by the highest TCC of 0.64. The simulation generated with the EM scheme also exhibits good phase coherence of the observed interannual variation in precipitation, with a TCC of 0.52 in spite of its consistent excessive precipitation. The least accurate simulation was that with the AS scheme, which had a TCC of 0.41.

3) CONVECTIVE VS. STRATIFORM PRECIPITATION

During the winter season, the dominant form of precipitation observed is stratiform precipitation, while convective precipitation is negligible, with 9.03 mm month^{-1} (82.02% of the total precipitation) and only 1.98 mm month^{-1} (17.98%) respectively observed in the EC_In reanalysis. This division in precipitation types is generally seen in the three model simulations, but there are some slight differences. The simulation using the EM scheme generates 3.74 mm month^{-1} of convective rainfall, higher than both the FC (CTL) and AS schemes, which both exhibit 0.19 mm month^{-1}. However, the three experiments consistently capture the intensive stratiform precipitation, with simulated values ranging

from 14.70 mm month^{-1} using the EM scheme to 15.15 mm month^{-1} in the simulation with the AS scheme, which primarily results in their humid tendency in winter (Table 3).

During the summer season, both convective and stratiform precipitation are dominant components of the total rainfall, with generally balanced portions of 57.02 mm month^{-1} (52.12% of the total precipitation) convective and 52.39 mm month^{-1} (47.88%) stratiform precipitation in observations. Again, similar proportions of precipitation are reproduced by the three convective schemes but there are considerable discrepancies in the magnitude of each portion. The AS and EM schemes lead to the simulation of excessive convection precipitation of 10.25 and 28.89 mm month^{-1} respectively, whereas the CTL experiment exhibits a negative bias of -7.64 mm month^{-1}. For the stratiform precipitation, the three parameterizations all exhibit negative bias compared to the EC_In reanalysis, with the smallest bias simulated with the EM scheme, of -11.25 mm month^{-1}, and the largest seen in the CTL experiment, of -21.65 mm month^{-1}.

Comparisons among the three experiments indicate that different convective parameterizations can lead to a variation in convective precipitation by up to 50% over the Loess Plateau during the summer season. These variations further account for the large differences simulated in the total precipitation. In particular, the CTL experiment exhibits the least active convective precipitation, which induces the driest conditions, whereas the EM scheme simulation is the most humid and consequently results in the most active convective precipitation. These patterns were also reported in previous studies (e.g., Chow et al. 2006; Im et al. 2008; Gianoti et al. 2012).

c. Sensitivity experiments on horizontal resolution

Generally, NEST20 retains the basic pattern of the simulated temperature in the CTL experiment but the much finer resolution results in a better understanding within the

simulation of the response to orographic-induced signals. As a result, the large bias in the CTL experiment over the area in the domain where the elevation changes sharply is effectively alleviated by using NEST20 due to the better defined terrain (Fig. 8). Comparisons between Fig. 5 and Fig. 8 illustrate that the alleviated temperature biases concentrate over the south-western and north-eastern regions by NEST20 during both winter and summer seasons. Statistically, the averaged MB and RMSE are quite similar in the NEST20 and CTL experiments, but the PCCs are slightly higher in the NEST20 experiment at 0.97 and 0.98 for winter and summer, respectively (Table 2). Further, the temporal changes in temperature captured within the NEST20 experiment follow the observations more closely (Fig. 9), which is reflected by the higher TCCs of 0.70 and 0.81 for winter and summer, respectively.

A similar broad precipitation pattern to the CTL experiment is also captured by the NEST20 experiment, but finer spatial details can again be seen especially over the orographic area (Fig. 10). In particular, during the summer season large areas of negative biases in the CTL are reduced within the NEST20 experiment over the central and northern areas (Fig. 10b). The excessively high values in the CTL experiment over the topographically complex regions, such as the northeast and southwest, have also been reduced in the NEST20 experiment. Statistically the improvement in the simulation during the summer season in the NEST20 experiment is demonstrated by smaller MB and RMSE compared to the CTL experiment by up to 3.25 mm month^{-1}, along with a higher PCC of 0.79, although TCC remains the same value of 0.64 with the CTL (Table 4).

Although the NEST20 improves the simulation in summer, the humid tendency of the simulation using NEST20 increases the overestimated precipitation bias slightly in the winter season compared to the CTL experiment. The use of NEST20 simulates wetter

conditions over the southern and eastern areas, validated by higher MB and RMSE from the NEST20 simulation and lower PCC than the CTL experiment (Table 3).

The annual cycle of precipitation in NEST20 closely follows the pattern in the CTL experiment and as such the precipitation peak one-month ahead of observations is still exhibited (Fig. 11a). Furthermore, using alternative convective schemes in conjunction with a finer horizontal resolution still generates a similar annual precipitation cycle with corresponding simulations in 50 km horizontal resolution (not shown). Such similarities in temporal pattern, along with aforementioned deficiencies of NEST20 indicate that improvements in the model simulation as a result of increasing the horizontal resolution are limited. However, the highlighted improvement of using finer resolution in RegCM4.3 is the definition of local terrains and simulations over such terrain complex regions. These results appear to be in line with those found in experiments conducted over other regions (e.g., Giorgi 1991; Giorgi et al. 1994).

d. Sensitivity experiments on domain choice

The four experiments with different domain sizes demonstrate similar differences in the patterns simulated during both seasons (Fig. 12 for NEST20_noMGTB) as reflected by the MB, RMSE and PCC, which are all similar (Table 2). It is interesting to note that the TCCs in the NEST20_noTB experiment are relatively low compared to the other experiments: 0.64 and 0.74 for winter and summer, respectively, compared to around 0.70 and 0.81. The lower TCCs are also reflected in the inter-annual variability patterns (Figs. 9b, c), which show an inadequate representation of certain phases in the temporal variability simulated within the NEST20_noTB experiment. For example, there are minimum temperatures in the 1992 winter and 2004 summer, and peaks in the 2001 winter

and 2006 summer, which are different to the other three simulations with same resolution and observations.

Similar to the simulated temperature, all the simulations exhibit similar precipitation patterns to each other in both seasons (Fig. 13 for NEST20_noMGTB). More specifically, the experiments that use a smaller domain size tend to produce slightly drier conditions in comparison to the NEST20 experiment, exhibiting lower spatially averaged values by up to 1.93 mm $month^{-1}$ during the winter and 4.32 mm $month^{-1}$ during the summer (Table 3 and Table 4). The drier conditions of the three smaller domains slightly reduces the wet condition bias generated in the NEST20 experiment during the winter season, but increases the underestimation of precipitation in the NEST20 experiment during the summer.

It is interesting to note that the TCCs between precipitation generated by the NEST20_noTB simulation and the observations are still lower than the other experiments, due to the distinct interannual precipitation pattern in Figs. 11b and c. Combined with the simulated temperature pattern, the NEST20_noTB experiment has the largest overall deviations from observations among the four domain experiments. This indicates that the Tibetan Plateau has strong effects on the simulations in the study area.

e. Comparison among all experiments

Among all the experiments the simulated surface air temperatures correlate much more strongly with observations than the simulated precipitation, as demonstrated in the Taylor diagrams (Taylor 2001), which compare the corresponding correlation coefficient, standard deviation and RMSE (Fig. 14). More specifically, during the winter season, each simulated variable is divided into two groups (Fig. 14a). For the simulated temperature, the four 20 km horizontal resolution experiments comprise one group, in which there are slightly higher correlation coefficients and smaller RMSE than those in the three 50 km

experiments, which are also grouped together. The diagram also shows that the normalized standard deviation in the 20 km horizontal resolution simulations is closer to the observations than the other three experiments, indicating that the simulated spatiotemporal variability is also better. For precipitation, two groups demonstrate similar correlation coefficients. The FC (CTL) and AS convective schemes with lower RMSE and closer spatiotemporal variability to observations constitute the better group. For the other group, the EM scheme and NEST20 perform relatively better than the rest of the experiments with a lower RMSE and higher spatiotemporal variability compared to the other experiments.

During the summer season, simulated temperatures are again divided into two groups while simulated precipitation varying widely among the experiments (Fig. 14b). Specifically, the simulated temperature is again better within experiments that used a finer resolution, which is demonstrated by a higher correlation coefficient, lower RMSE and closer standard variation to the observations. In terms of the simulated precipitation, the four experiments that used a 20 km horizontal resolution, followed by the CTL experiment, correlate more strongly with observations and have the smallest RMSE. In contrast, the simulation that used the AS convective scheme has the lowest correlation coefficient and the worst spatiotemporal variability in comparison to observations. It is noticeable that the EM scheme simulation displays better spatiotemporal variability in precipitation than all other six experiments, but also has the highest RMSE.

5. Discussion

Certain model biases are common to all configurations that have been explored, indicating that these biases are not particularly sensitive to the factors analysed in the present study. Possible reasons for the most common biases have been investigated previously in Part I of this study (Wang and Cheung 2015a). For example, temperature in

the winter season is consistently under-predicted, and precipitation is over-predicted by all experiments. The source of the consistent cold biases during the winter season is related to the negative energy budget and strong northwesterly wind flow in model domain. The over-predicted precipitation, on the one hand, is likely caused by the high percentage of stratiform precipitation generated by the large-scale precipitation scheme of SUBEX in RegCM4.3.

During summer, warm biases are shown over the central region of the Loess Plateau, which is generally caused by the excessive absorbed shortwave radiation associated with insufficient total cloud and stratiform cloud generation. Less stratiform cloud also leads to relatively weaker stratiform precipitation in SUBEX. These deficiencies are more related to the shift of the southerly monsoon fluxes that carry water vapour for the semi-arid region.

It is also important to note the pronounced biases of both temperature and precipitation over the orographically variable regions. There are several possible reasons for these biases. The first reason appears to be the large uncertainties in observations that contain insufficient numbers of high-elevation stations and thus smoothed the original dataset excessively in those regions (Wang and Cheung 2015a). A better-defined topography could significantly reduce the large biases over such areas and could be another critical factor for the pronounced bias, which has been demonstrated both in the finer resolution experiments and other studies (e.g., Giorgi 1991; Giorgi et al. 1994; Mass et al. 2002).

The RegCM4.3 simulation of precipitation is not particularly sensitive to alternative convective schemes during the winter season, revealed by the similar spatial and temporal precipitation patterns among experiments over the Loess Plateau. This could primarily be attributed to the weak convection processes; these processes are triggered by large-scale

buoyancy, which in turn is produced by lower-level heating and destabilization, and is negligible during winter but strong during summer (Giorgi and Marinucci 1996). Thus, during the winter season, insufficient available buoyancy leads to less active convection processes and weaker atmosphere perturbation than in summer.

The EM scheme has recently been implemented within the RegCM system and has the most sophisticated dynamics among the three convective schemes. Compared with the other schemes, the EM scheme tends to remove water from the atmosphere more effectively and thus results in less low-level clouds, more absorbed solar radiation from the ground and higher local precipitation. Previously, the EM scheme was found to constantly overestimate total rainfall over land areas including Europe (Zanis et al. 2009), Africa (Pal et al. 2007; Davis et al. 2009) and East Asia (Im et al. 2008), but not in humid areas like the Amazon region in South America (Seth et al. 2007). The present study also shows noticeable high total and convective precipitation when the EM convective scheme is used, in comparison to the other two schemes.

Although it has a tendency to overestimate total rainfall, use of the EM convective scheme allows a good representation of realistic spatial and temporal precipitation patterns to be simulated, due to its sophisticated treatment of mixing and entrainment processes. Singh et al. (2006) and Im et al. (2008) have both reported that simulations with the EM scheme perform better in monsoon circulations and precipitation timing over East Asia than other schemes implemented in RegCM. In the present study, using the EM scheme resulted in the simulation of the rainfall peak at the correct time in the annual cycle, which occurs one month ahead of time in analogous simulations using the other schemes. The EM scheme also displays consistent spatial and interannual temporal precipitation patterns compared with observations, reflected by high PCC and TCC values.

Considering the good performance of the model simulation when the EM scheme is used, in terms of the spatiotemporal pattern of precipitation, it is worthwhile to further modify the EM scheme to limit the overestimation of precipitation that occurs. Several previous studies (e.g., Chow et al. 2006; Peng et al. 2004) focused on a series of internal parameterizations of the EM scheme that are influential in producing convective rainfall and realising energy, such as moisture convergence and cloud mass flux mixing. However, this kind of method needs to be configured systematically before applying over specific regions, since its related water and energy balance would be changed with the modifications in model parameters.

The performance of the RegCM4.3 simulation with the EM convective scheme can be further modified by coupling it with different land surface models. Preliminary results over the Loess Plateau (not shown) based on the use of a more advanced land surface model, the Community Land Model (CLM) (Oleson et al. 2004b; Oleson et al. 2008) have been promising. These preliminary findings indicate that the over-effective convection which occurs using EM-BATS is shut down by EM-CLM when the low-level boundary is more realistically defined. Corresponding to this, the EM-CLM simulation exhibits a better match of convective and total rainfall with observations. A follow-up study has been designed using EM-CLM for potential model improvement and investigating interactions between the convective scheme and land surface characters over the Loess Plateau.

In the present study, the FC convective scheme generally performs the best among the three convective experiments, although it appears to generate slightly less total precipitation during the summer season. The dry bias of the FC scheme is more likely to be due to the discontinuous mechanism of releasing available buoyancy energy for triggering convective activity at 30 min and 1 hr timescales (Gochis et al. 2002; Ratnam and Kumar 2005; Im et al. 2006), and decrease the timescale tends to produce more precipitation (Da

Rocha et al. 2012). In contrast, the AS convective scheme applies continuously available energy for convection changes and produces excessive convective rainfalls as a result. Considering the semi-arid climate over the Loess Plateau, where the atmospheric conditions are less favourable for continuously activating convection, the FC scheme is more appropriate than the AS one in this interior region.

The AS convective scheme configuration represents the local precipitation in general, but the simulation generated is the least accurate among the three convective experiments. In addition to the continuous release of convection energy, the AS scheme does not have parameters that deal with the fall and evaporation of rain and, as a result, unsaturated, precipitation-driven downdrafts are not represented. These deficiencies tend to omit a major contribution to convective transport and, further, cause the excessive proportion of convection precipitation particular over arid regions and other simulation biases seen in the present study (Emanuel and Pierrehumber 1996). Moreover, Zhang (2002) reported that the AS assumption may not be suitable for mid-latitude continental convection, since it was largely developed based on tropical maritime observations. In agreement with this, Huang el al. (2013) and Singh et al. (2006) found that the AS scheme performed well over southeast China and the Korea Peninsula, respectively, which both have a tropical maritime climate, in contrast to the Loess Plateau.

More realistic mesoscale structures, leading to the development of more accurate simulated temperatures and precipitation, are generated when the horizontal resolution is increased from 50 km to 20 km, which is in agreement with other research (Seth et al. 1998; Im et al. 2010; Torma et al. 2011). The 20 km grid spacing especially enhances the simulation of pattern variations, primarily because it allows for the better definition of major topographic features and heterogeneities within the region, which in turn impact on the atmospheric circulations at a finer scale. Simulations with the 20 km resolution do

slightly amplify the total precipitation magnitude. This wet tendency can primarily be attributed to the parameters that control precipitation, which are more effective with smaller grids via cumulus convection and resolvable-scale precipitation processes. This increase in precipitation can also be seen when the other two convective schemes are used and the resolution is downscale from 50 km to 20 km (not shown).

This study indicates that the RegCM4.3 is less sensitive to domain size than convective scheme type and horizontal resolution, according to the similar spatial distributions of surface variables when simulated using different domain sizes. However, it is noted that when the simulation domain includes a large portion of the Tibetan Plateau, the model temporal pattern is most similar to the observations (such as NEST20); this indicates the aggregated domain must be carefully selected before model simulation.

It was also noticed that the land surface scheme could impact on the model performance (Giorgi and Avissar 1997; Pielke 2001; Seneviratne et al. 2006; Betts et al. 2007). Particularly, the BATS scheme, used as the default land surface scheme, was found with several deficiencies, and revisions of such deficiencies could positively improve the model performance. For example, the soil moisture content of the irrigated crop was assigned as field capacity at each time step in BATS which was unreasonably high over the semi-arid Loess Plateau (Dickinson et al. 1993). Furthermore, the irrigation density and extent were potentially overestimated over the plateau, and most of irrigated crops should be assigned as rain-fed crops in reality (Loveland et al. 2000; Siebert and Döll 2001; Siebert et al. 2005).

Sensitivity tests of RegCM4.3 focusing on these deficiencies of BATS were approached in our study (not shown here). The first group of the sensitivity tests used a simply revised BATS compared with the CTL, aiming at detecting impacts of the unreasonably high soil water content of the irrigated crop on the model simulation. The

revised BATS replaced all irrigated crops by rain-fed crops over the Loess Plateau. Soil water content of the rain-fed crop was decided by the local surface water budget (Dickinson et al. 1993) and was considered closer to the real situation in this semi-arid region compared with the irrigated crop.

Instead of revising deficiencies in BATS, applying a more advanced land surface model in RegCM4.3 could be another approach for model improvement. In particularly, the Community Land Model (CLM) version 3.5 (Oleson et al. 2004b; Oleson et al. 2008) was used to replace BATS for model sensitivity tests. The CLM achieved a better description of the land surface compared with BATS, particularly in representing the crop land distribution and its corresponding parameterizations over the Loess Plateau (Wang and Cheung 2015c).

Primary results of the two groups of sensitivity tests showed that the revised BATS and the CLM coupled model could alleviate cold biases during winter as well as the overestimation of precipitation compared with the CTL. Meanwhile, during summer, the temperature and precipitation biases over several areas were deteriorated by both revised models compared with the CTL. Such differences from these sensitivity tests indicated that revising parameterization of land surface scheme in a comprehensive way according to local reality was highly needed for a better model simulation (e.g. Evans and Zaitchik 2008; Lawston et al. 2015), although it is rather complex to be fully parameterized.

6. Conclusion

In the present study, we have identified major sensitivities of RegCM4.3 in simulating the regional climate over the Loess Plateau, a topographically diverse region in a semi-arid transition zone. The model sensitivity to convective parameterization,

horizontal resolution and domain choice has been investigated under different configurations in seven experiments.

Firstly, the surface air temperature and precipitation simulated by the RegCM4.3 is very sensitive to the choice of convective parameterization. This is particularly so for the simulated precipitation in the summer season, where differences up to 50% are seen when the three convective schemes are compared. Generally, the Grell scheme with the Fritsch-Chappell closure assumption is the best suited scheme for use over the Loess Plateau, since it presents the smallest bias in surface air temperature and precipitation amongst the three convective experiments. However, the Emanuel convective scheme has outstanding advantages in representing the observed temporal and spatial pattern of simulated precipitation, although it does produce significant positive biases of precipitation. These characteristics of the simulation using the Emanuel convective scheme are in agreement with previous studies. We suggest that there is the potential to substantially improve the RegCM4.3 simulation when it is configured with the Emanuel convective scheme coupled with the new land surface model of CLM.

Secondly, results from this study show that the model simulation is sensitive to horizontal resolution. A comparison of simulations at resolutions of 20 km and 50 km reveal that with finer resolution the model simulates the climate better, with an improvement in the resolved climate spatial pattern and lower biases over the orographically diverse areas. These improvements are attributed to the properly defined terrain features in the fine-resolution experiment that are critical in determining surface contrasts and the local climate. However, downscaling via model nesting has limitations in improving certain biases such as the temporal pattern of precipitation. Generally, the 20 km grid using the Grell scheme with Fritsch-Chappell closure assumption shows the most

outstanding configuration among all experiments, which has important implications for surface climate simulations over the Loess Plateau.

Thirdly, our results reveal that the RegCM4.3 simulations are relatively less sensitive to domain size in comparison to the convective scheme and horizontal resolution. However, excluding the Tibetan Plateau from the domain degrades the model simulation. This indicates that the Tibetan Plateau has an important effect on the local climate than other surrounding terrain in spatially redistributing temperature and precipitation and should be retained in the simulation domain.

Last but not least, the study has presented a series of consistent biases in the RegCM4.3 simulation over the Loess Plateau. These biases, including a consistent low temperature and excessive precipitation during the winter season, persist to varying degrees with changing convective schemes, horizontal resolution and domain size. They are thought to be the result of a fundamental issue in the RegCM4.3 over semi-arid regions such as the Loess Plateau. Although the results presented here are only applicable to the Loess Plateau, they may provide general guidance regarding the performance of model simulations in a mid-latitude zone with complex topography.

Acknowledgement. The first author (LW) is supported by the China Scholarship Council, the International Macquarie Research Excellence Scholarship, and Higher Degree Research support fund from Macquarie University. Computational facilities are provided by Intersect Inc., NSW and the National Computational Infrastructure of Australia. We would like to thank Prof. C.-P. Chang of the US Naval Postgraduate School and the National Taiwan University for co-supervising LW and his many valuable comments on this work.

List of Tables

TABLE 1 Experiments performed in this study.

Simulation	**Domain Size**	**Grid**	**Resolution**	**Convective Scheme**	**Forcing data**
CTL (Wang et al. 2014)	China terrain and surroundings	110*144	50 km	Grell Fritsch-Chapell	EC_In 1.5˚
AS	Same as CTL	110*144	50 km	Grell Arakawa-Schubert	EC_In 1.5˚
EM	Same as CTL	110*144	50 km	Emanuel	EC_In 1.5˚
NEST20	The entire Loess Plateau, most of the Mongolian Plateau and the eastern Tibetan Plateau	144*112	20 km	Grell Fritsch-Chapell	CTL Output 0.5˚
NEST20_noMG	The entire Loess Plateau, a smaller area of the Mongolian Plateau, and the eastern Tibetan Plateau.	106*112	20 km	Grell Fritsch-Chapell	CTL Output 0.5˚
NEST20_noTB	The entire Loess Plateau, most of the Mongolian Plateau and a smaller area of the eastern Tibetan Plateau.	144*96	20 km	Grell Fritsch-Chapell	CTL Output 0.5˚
NEST20_noMGTB	The entire Loess Plateau, a smaller area of both the Mongolian Plateau and the eastern Tibetan Plateau	106*96	20 km	Grell-Fritsch-Chapell	CTL Output 0.5˚

TABLE 2 Simulated (CTL, AS, EM, NEST20, NEST20_noMG, NEST20_noTB, NEST20_noMGTB), observed (CRU, CN05.2) and reanalysis (EC_In) surface air temperature during the winter and summer seasons.

	Experiments	**DJF**					**JJA**				
		Mean	**MB**	**RMSE**	**PCC**	**TCC**	**Mean**	**MB**	**RMSE**	**PCC**	**TCC**
			(˚C)					**(˚C)**			
Observation	CRU	-3.26					20.99				
	CN05.2	**-4.55**					**20.49**				
50 km	CTL (Wang et al. 2014)	-6.42	-1.87	2.45	0.96	0.63**	21.75	1.26	1.98	0.95	0.78**
	AS	-6.91	-2.36	2.68	0.96	0.68**	20.51	0.02	1.54	0.97	0.60**
	EM	-6.38	-1.83	2.19	0.96	0.54*	22.48	1.99	2.33	0.97	0.58**
20 km	NEST20	-6.40	-1.85	2.41	0.97	0.70**	21.79	1.30	2.12	0.98	0.81**
	NEST20_noMG	-6.50	-1.95	2.41	0.97	0.70**	21.77	1.28	2.10	0.98	0.82**
	NEST20_noTB	-6.49	-1.94	2.36	0.97	0.64**	21.84	1.35	2.15	0.98	0.74**
	NEST20_noMGTB	-6.51	-1.96	2.40	0.97	0.69**	21.79	1.30	2.18	0.98	0.81**

* stastistically significant at the 95% confidence limit and ** statistically significant at the 99% confidence limit.
Bold values indicate the observation used in the comparison.

TABLE 3 Simulated (CTL, AS, EM, NEST20, NEST20_noMG, NEST20_noTB, NEST20_noMGTB), observed (CRU, CN05.2) and reanalysis (EC_In) precipitation during the winter season.

DJF	Experiments	Mean	MB	RMSE	PCC	TCC	Convective		Stratiform	
		(mm month^{-1})					Mean	MB	Mean	MB
							(mm month^{-1}) / Percentage			
Observation	CRU	5.80								
	CN05.2	**7.17**								
Reanalysis	**EC_In**	11.01					**1.98**		**9.03**	
							17.98%		**82.02%**	
50 km	CTL (Wang et al. 2014)	15.20	8.03	9.64	0.76	0.87**	0.19	-1.79	15.01	5.98
							1.25%	-16.73%	98.75%	16.73%
	AS	15.34	8.17	9.88	0.74	0.86**	0.19	-1.79	15.15	6.12
							1.24%	-16.74%	98.76%	16.74%
	EM	18.44	11.27	13.36	0.69	0.84**	3.74	1.76	14.70	5.67
							20.28%	2.30%	79.72%	-2.30%
20 km	NEST20	16.87	9.70	11.81	0.72	0.87**	0.18	-1.80	16.69	7.66
							1.07%	-16.91%	98.93%	16.91%
	NEST20_noMG	16.43	9.26	11.57	0.71	0.86**	0.17	-1.81	16.26	7.23
							1.03%	-16.95%	98.96%	16.94%
	NEST20_noTB	15.43	8.26	11.07	0.68	0.58*	0.15	-1.83	15.28	6.25
							0.97%	-17.01%	99.03%	17.01%
	NEST20_noMGTB	14.94	7.77	10.63	0.69	0.88**	0.15	-1.83	14.79	5.76
							1.00%	-16.98%	99.00%	16.98%

Bold values indicate the observation used in the comparison.

TABLE 4 Simulated (CTL, AS, EM, NEST20, NEST20_noMG, NEST20_noTB, NEST20_noMGTB), observed (CRU, CN05.2) and reanalysis (EC_In) precipitation during the summer season.

JJA	**Experiments**	**Mean**	**MB**	**RMSE**	**PCC**	**TCC**	**Convective**		**Stratiform**	
		(mm month^{-1})					**Mean**	**MB**	**Mean**	**MB**
							(mm month^{-1}) / Percentage			
Observation	CRU	86.92								
	CN05.2	**95.07**								
Reanalysis	**EC_In**	109.41					**57.02**		**52.39**	
							52.12%		**47.88%**	
50 km	CTL	80.37	-14.70	37.55	0.73	0.64**	49.63	-7.39	30.74	-21.65
	(Wang et al. 2014)						61.75%	-9.63%	38.25%	-9.63%
	AS	103.50	8.43	41.79	0.62	0.41	67.27	10.25	36.23	-16.16
							65.00%	12.88%	35.00%	-12.88%
	EM	127.05	31.98	54.62	0.75	0.52*	85.91	28.89	41.14	-11.25
							67.62%	15.50%	32.38%	-15.50%
20 km	NEST20	82.35	-12.72	34.30	0.79	0.64**	51.93	-5.09	30.42	-21.97
							63.06%	10.94%	36.94%	-10.94%
	NEST20_noMG	81.04	-14.03	35.30	0.80	0.67**	50.51	-6.51	30.53	-21.86
							62.33%	10.21%	37.67%	-10.21%
	NEST20_noTB	78.89	-16.18	37.55	0.82	0.34	50.89	-6.13	28.00	-24.39
							64.51%	12.39%	35.49%	-12.39%
	NEST20_noMGTB	78.03	-17.04	41.79	0.83	0.64**	49.72	-7.30	28.31	-24.08
							63.72%	11.60%	36.28%	-11.60%

Bold values indicate the observation used in the comparison

List of Figures

FIGURE 12 Spatial differences of surface air temperature (˚C) of the NEST20_noMGTB experiment from CN05.2 during (a) DJF and (b) JJA with the analysis domain in the black dashed box.

FIGURE 13 As in FIGURE 12, except for precipitation (mm $month^{-1}$).

FIGURE 14 Taylor diagram evaluating simulations of surface air temperature (red) and precipitation (blue) during (a) DJF and (b) JJA. The angular coordinate is the correlation coefficient between the model simulations and observations. The radial coordinate is the standard deviation of the model simulations divided by the standard deviation of the observations (REF). The light grey contours indicate the model simulation's RMSE values. Statistics were calculated based on multiyear averages of monthly mean values over the analysis domain. Results of a perfect model would be plotted on the horizontal axis at a radial coordinate value of one.

.

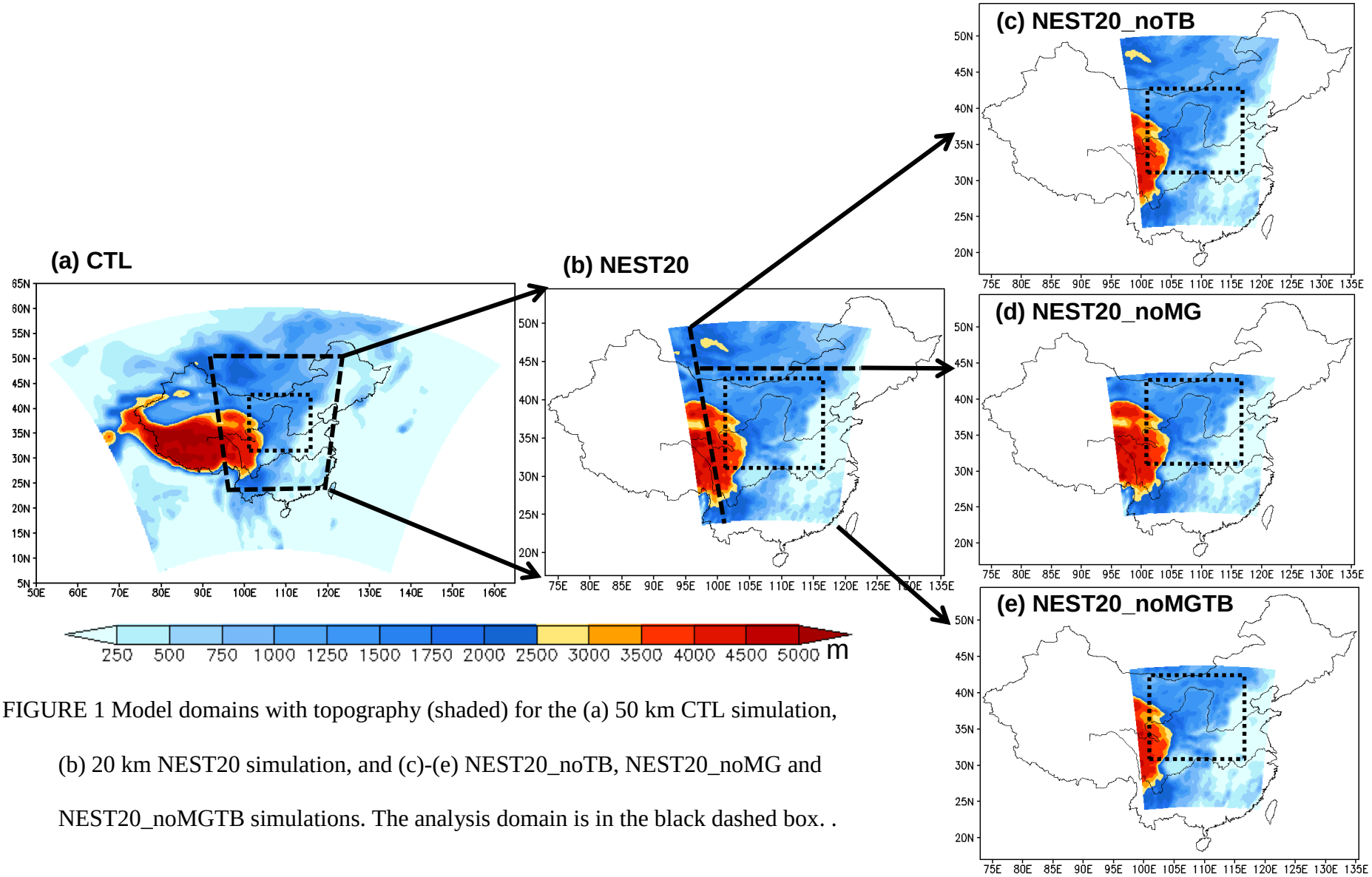

FIGURE 1 Model domains with topography (shaded) for the (a) 50 km CTL simulation, (b) 20 km NEST20 simulation, and (c)-(e) NEST20_noTB, NEST20_noMG and NEST20_noMGTB simulations. The analysis domain is in the black dashed box. .

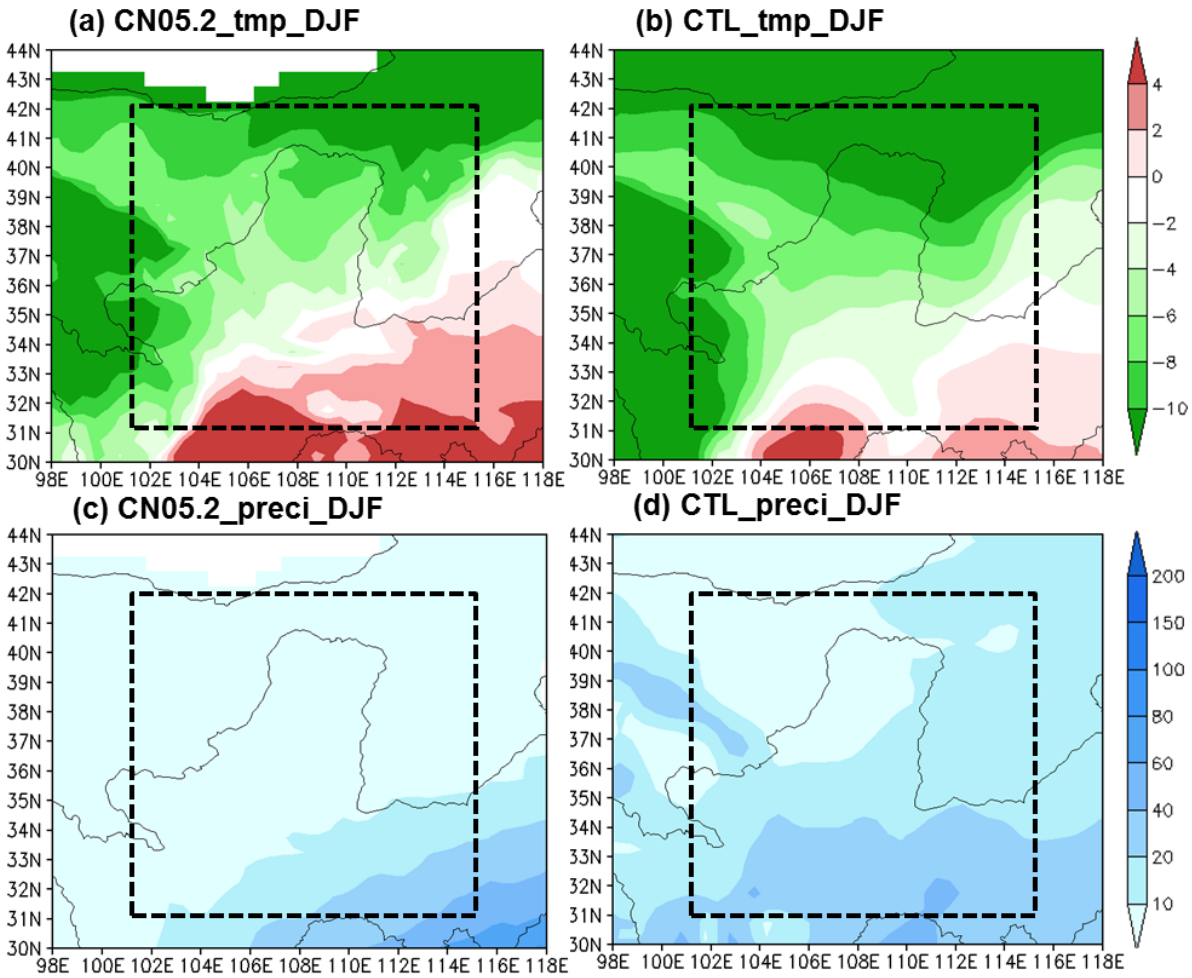

FIGURE 2 (a) Observed (CN05.2) and (b) simulated (CTL) spatial distribution of surface air temperature (˚C) and precipitation (mm month^{-1}) for DJF with the analysis domain in the black dashed box. (c) and (d) As in (a) and (b) except for monthly precipitation.

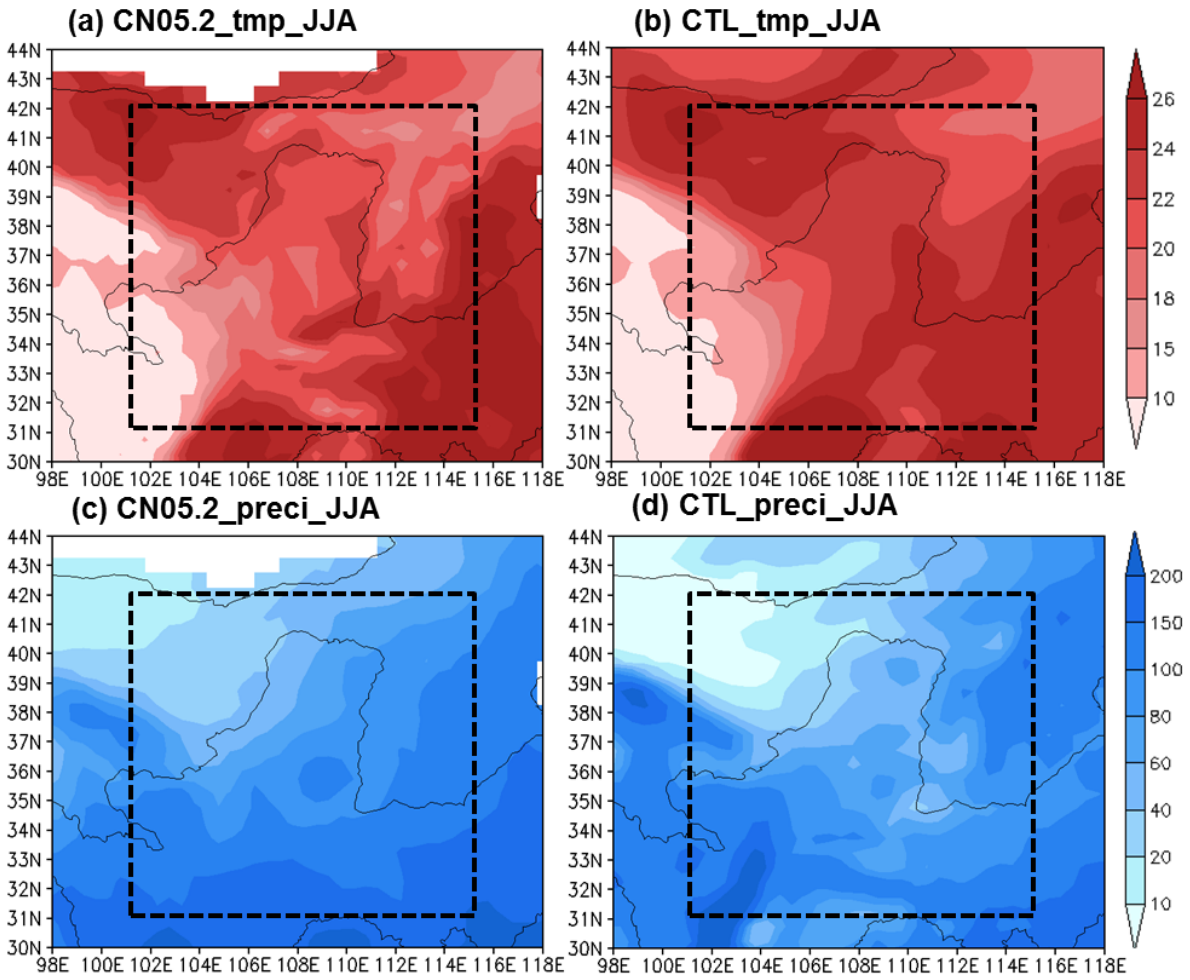

FIGURE 3 As in FIGURE 2, except for JJA.

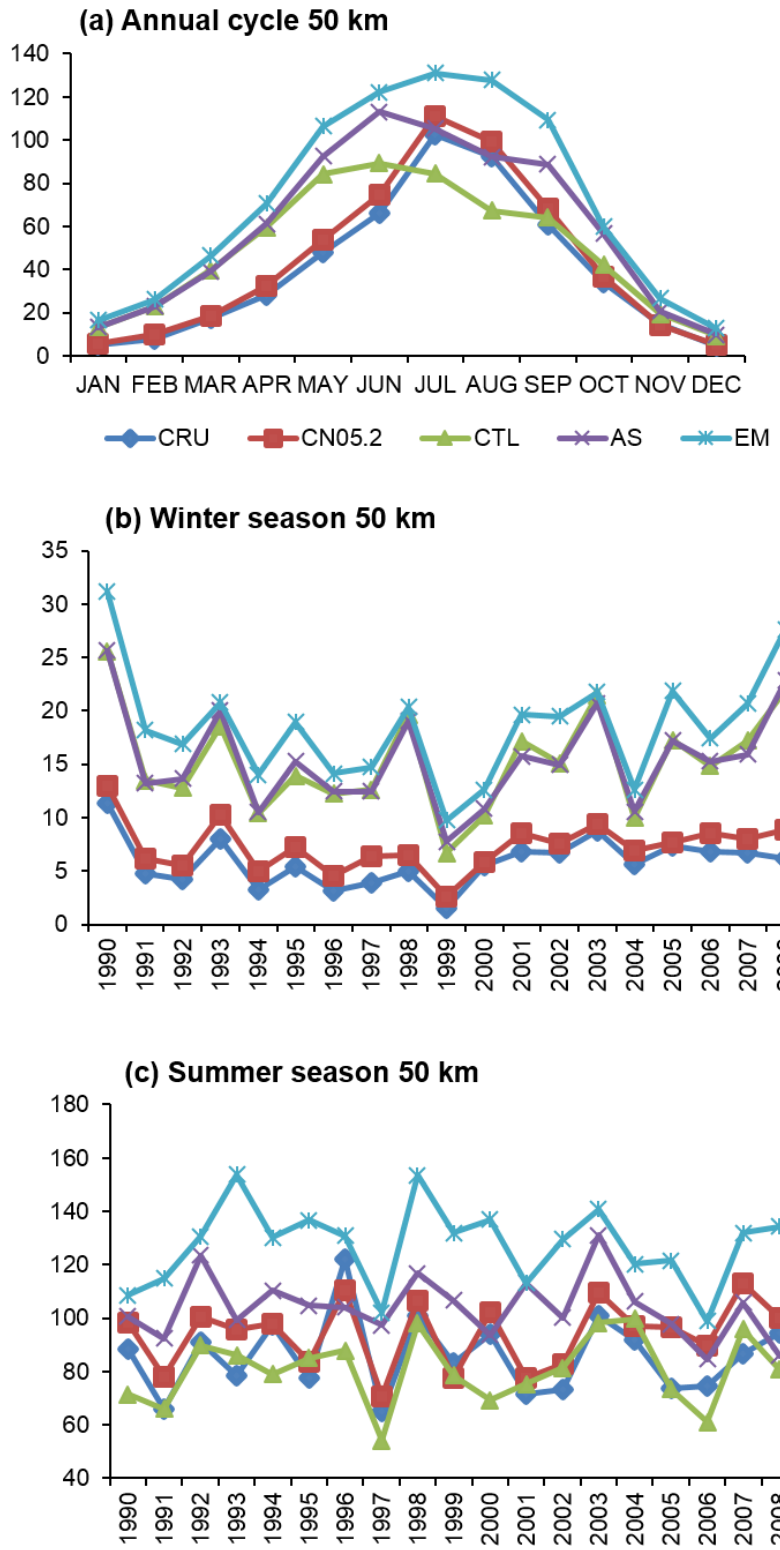

FIGURE 4 (a) annual cycle and time series of (b) DJF and (c) JJA precipitation (mm month^{-1}) for the CRU, CN05.2 observation and the three experiments with 50 km resolution.

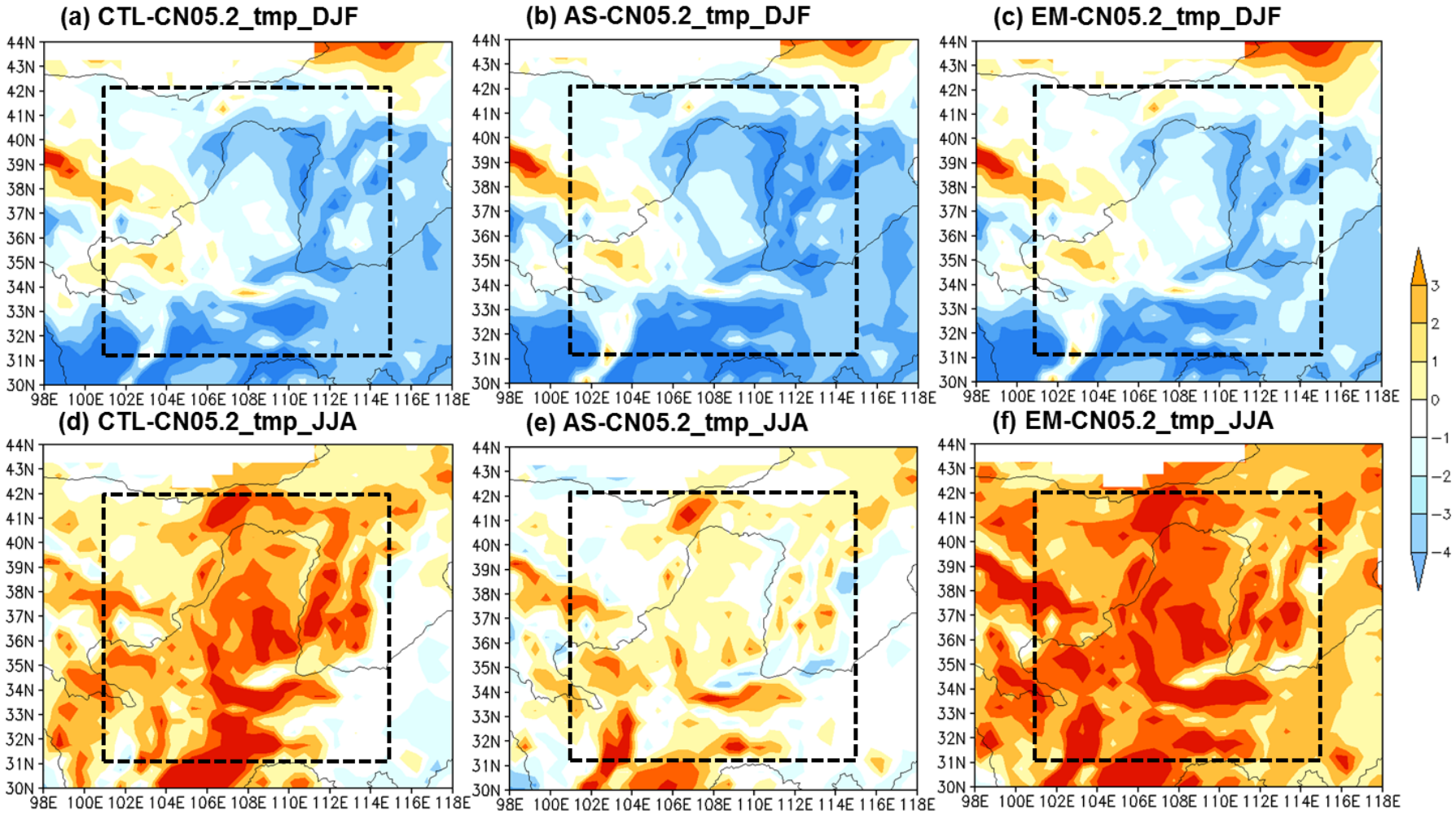

FIGURE 5 Spatial distributions of surface air temperature (˚C) differences of (a) CTL, (b) AS and (c) EM from the CN05.2 observations for DJF.

(d)-(f) As in (a)-(c) respectively except for JJA. The black dashed box is the analysis domain.

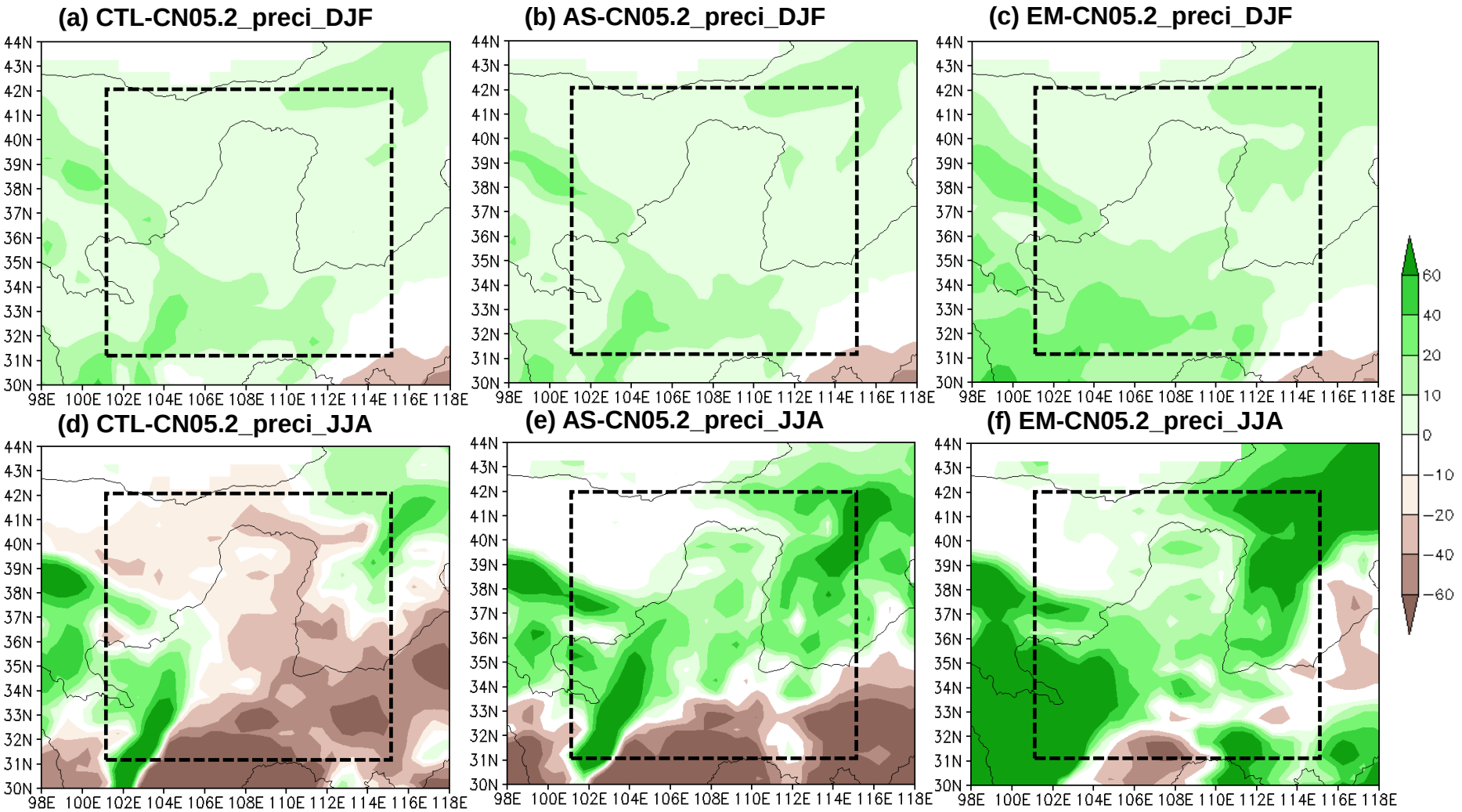

FIGURE 6 As in FIGURE 5, except for precipitation (mm month^{-1}).

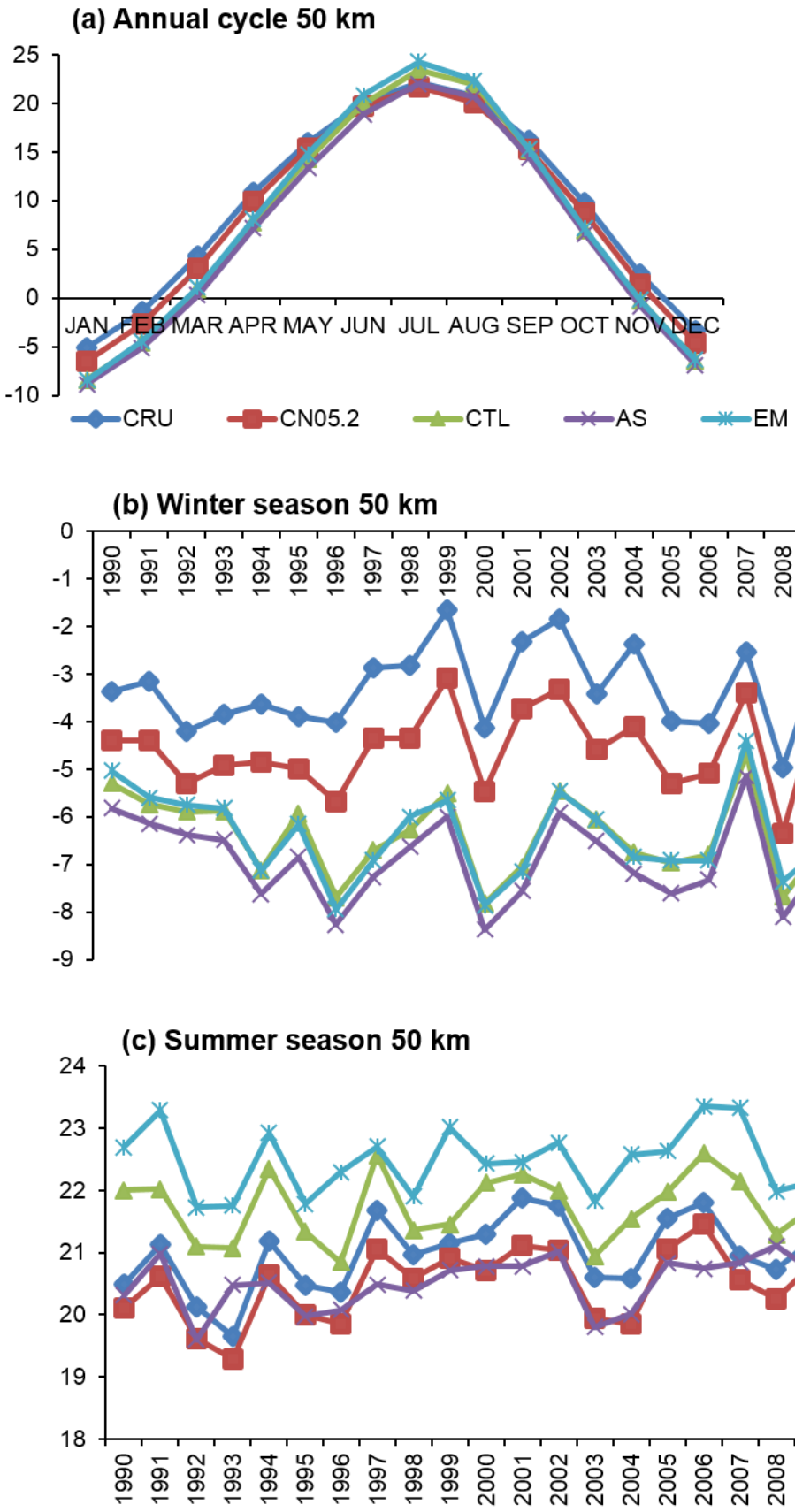

FIGURE 7 Same as FIGURE 4, except for surface temperature (˚C).

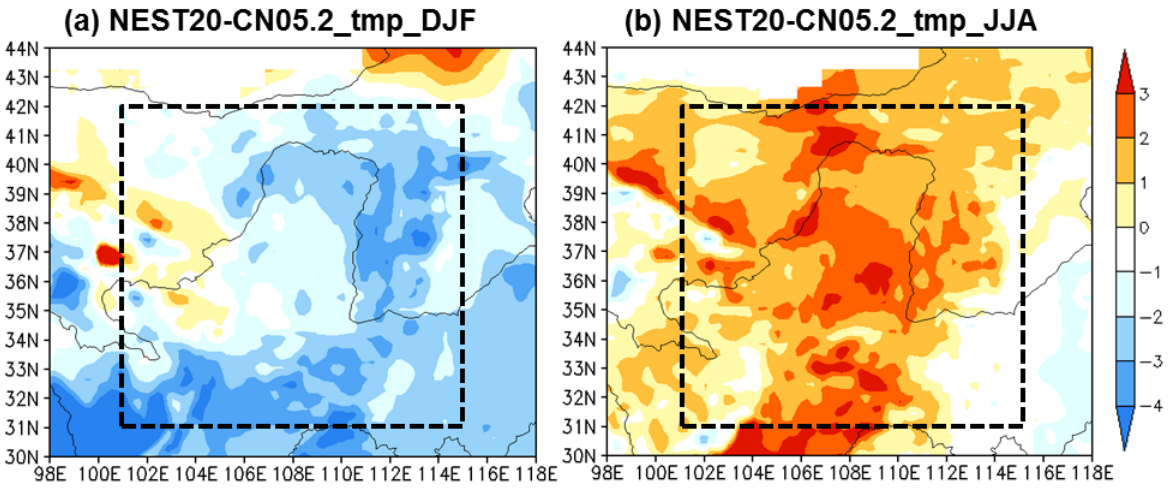

FIGURE 8 Spatial differences of surface air temperature (˚C) of NEST20 from CN05.2 for (a) DJF and (b) JJA with the analysis domain in the black dashed box.

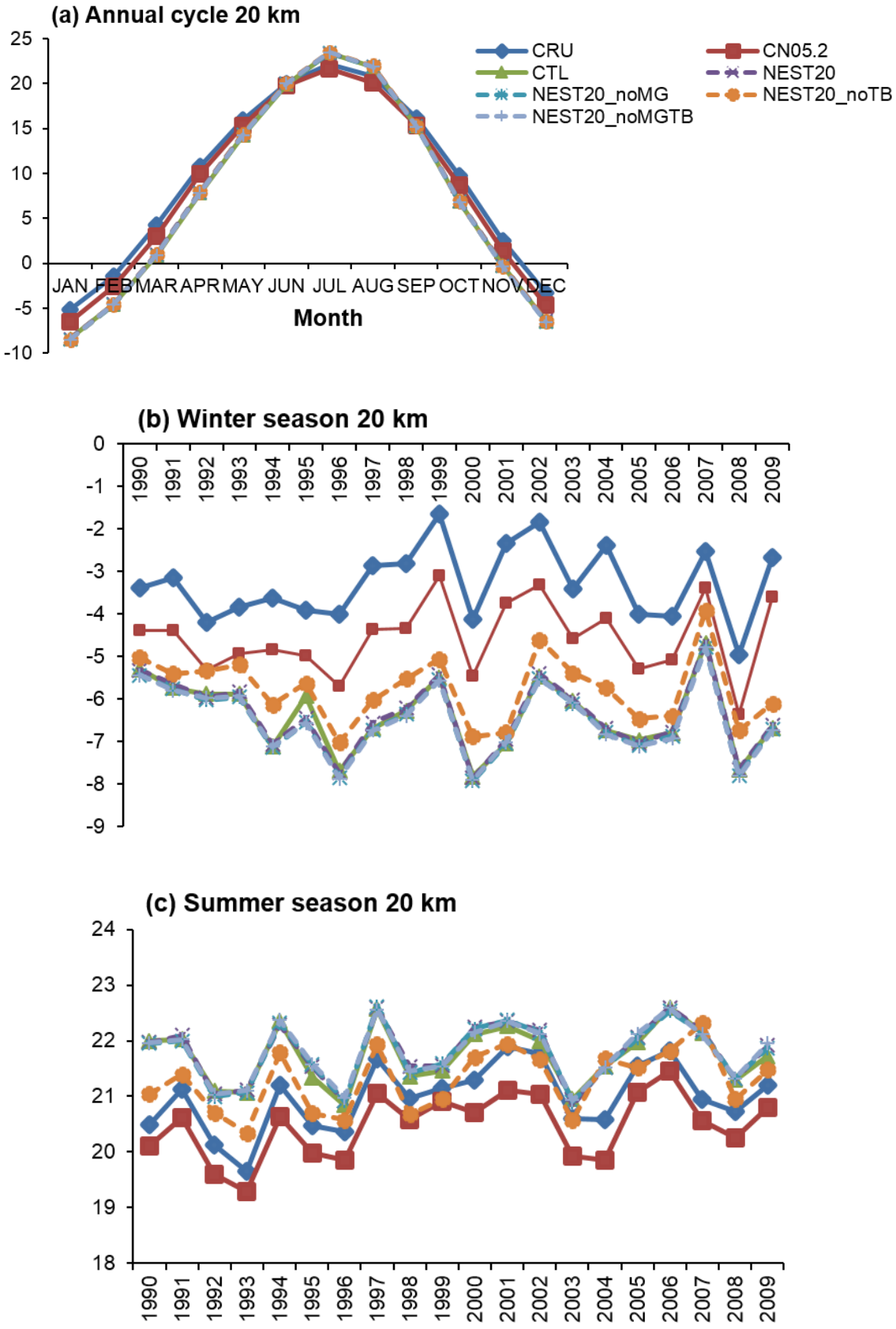

FIGURE 9 As in FIGURE 7, except for the CRU and CN05.2 observation, CTL and the four experiments with 20 km horizontal resolution.

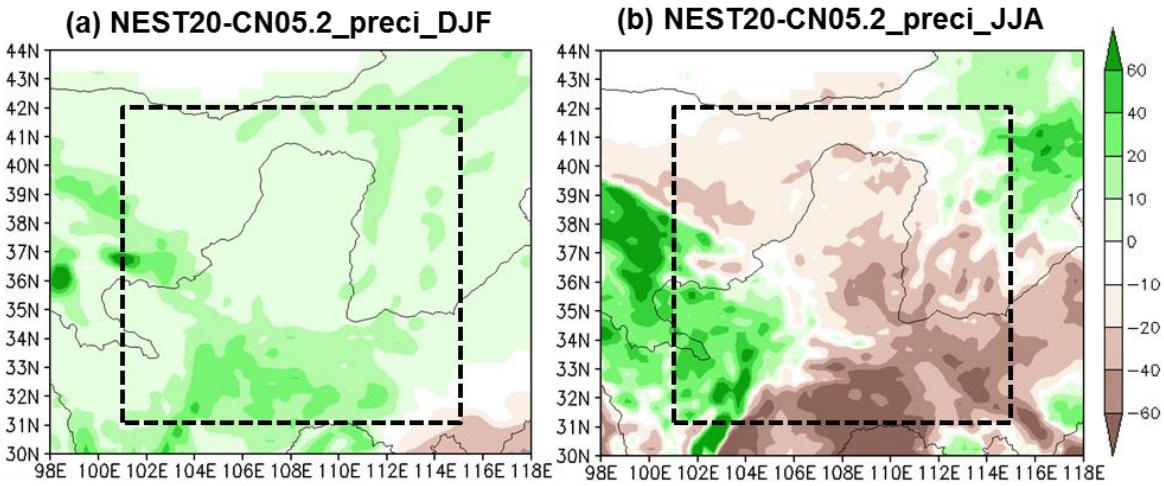

FIGURE 10 As in FIGURE 8, except for precipitation (mm month^{-1}).

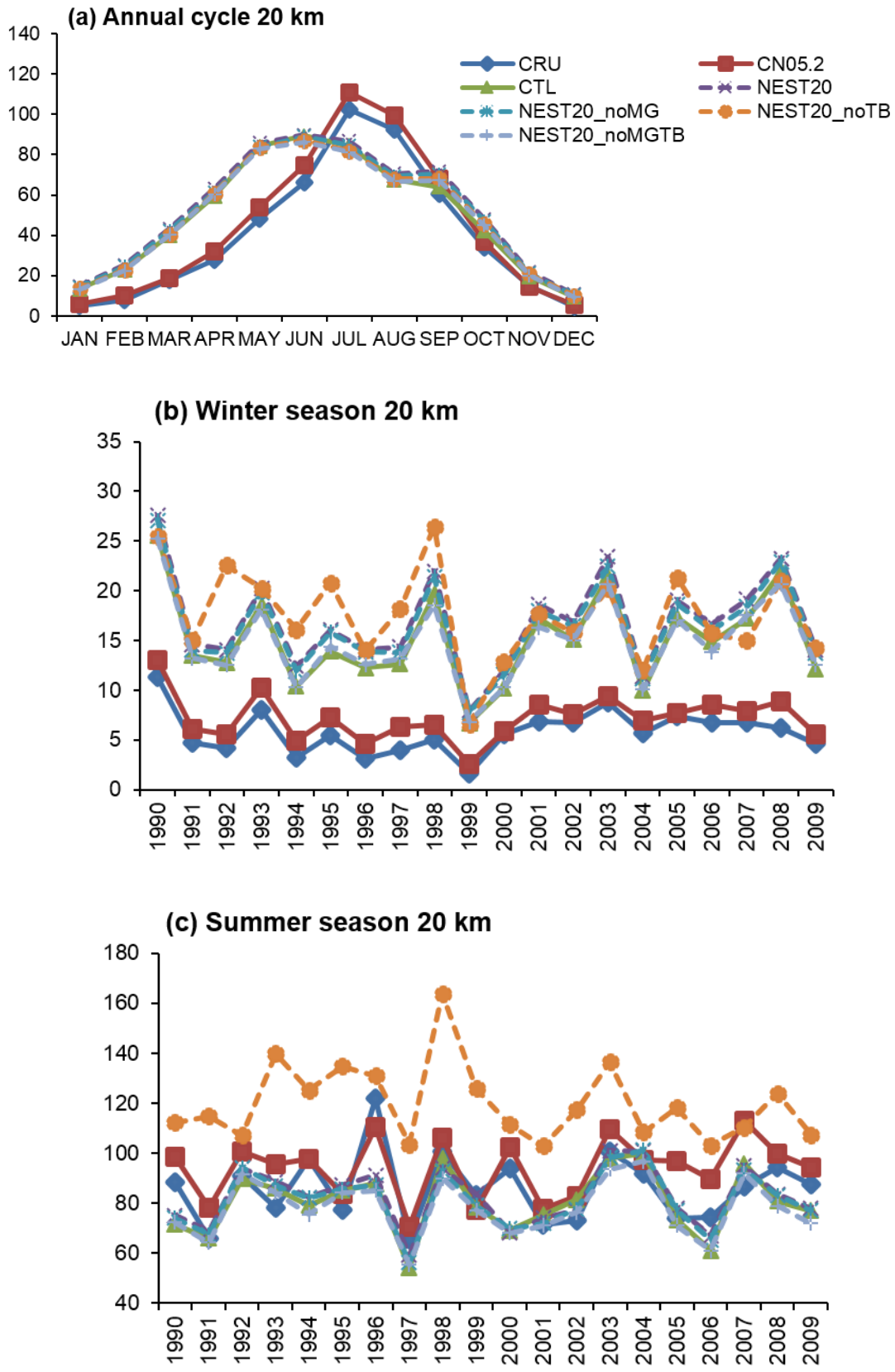

FIGURE 11 As in FIGURE 9, except for precipitation (mm month^{-1}).

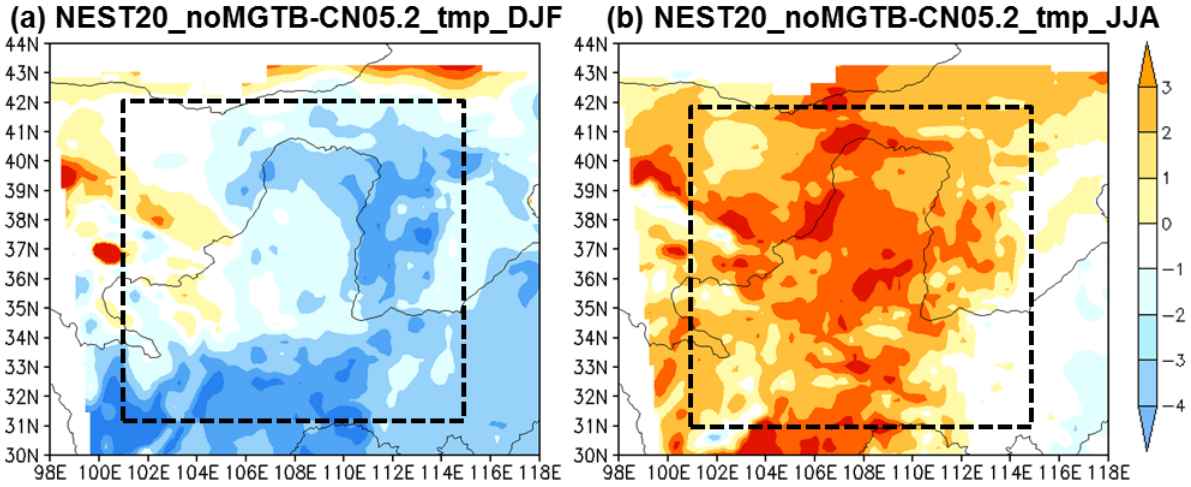

FIGURE 12 Spatial differences of surface air temperature (˚C) of the NEST20_noMGTB experiment from CN05.2 during (a) DJF and (b) JJA with the analysis domain in the black dashed box.

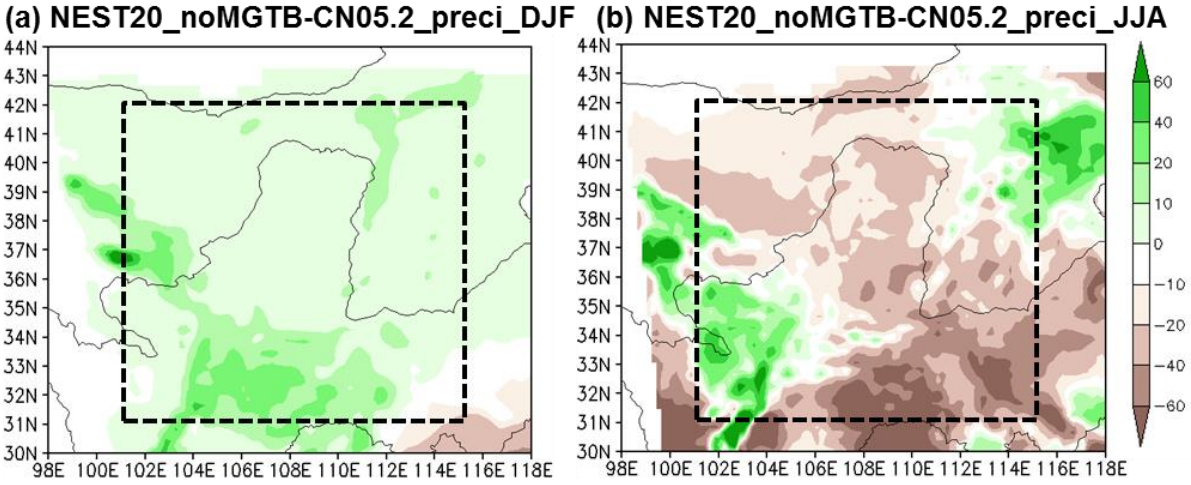

FIGURE 13 As in FIGURE 12, except for precipitation (mm month^{-1}).

FIGURE 14 Taylor diagram evaluating simulations of surface air temperature (red) and precipitation (blue) during (a) DJF and (b) JJA. The angular coordinate is the correlation coefficient between the model simulations and observations. The radial coordinate is the standard deviation of the model simulations divided by the standard deviation of the observations (REF). The light grey contours indicate the model simulation's RMSE values. Statistics were calculated based on multiyear averages of monthly mean values over the analysis domain. Results of a perfect model would be plotted on the horizontal axis at a radial coordinate value of one.

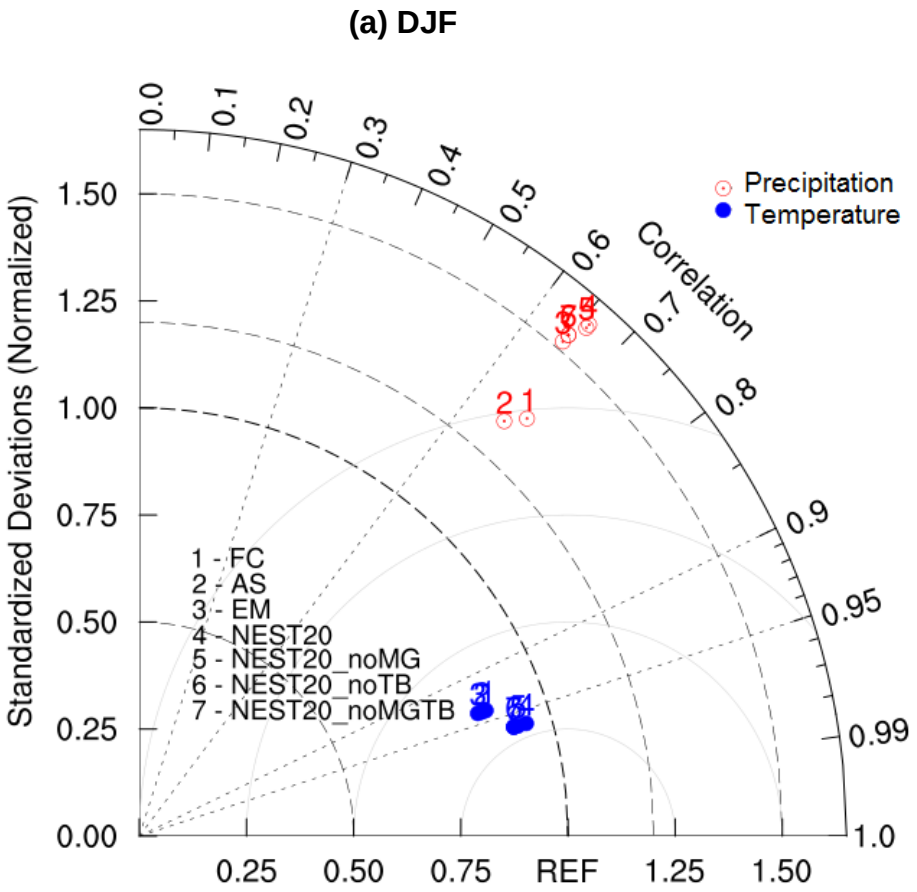

FIGURE 14 (continued).

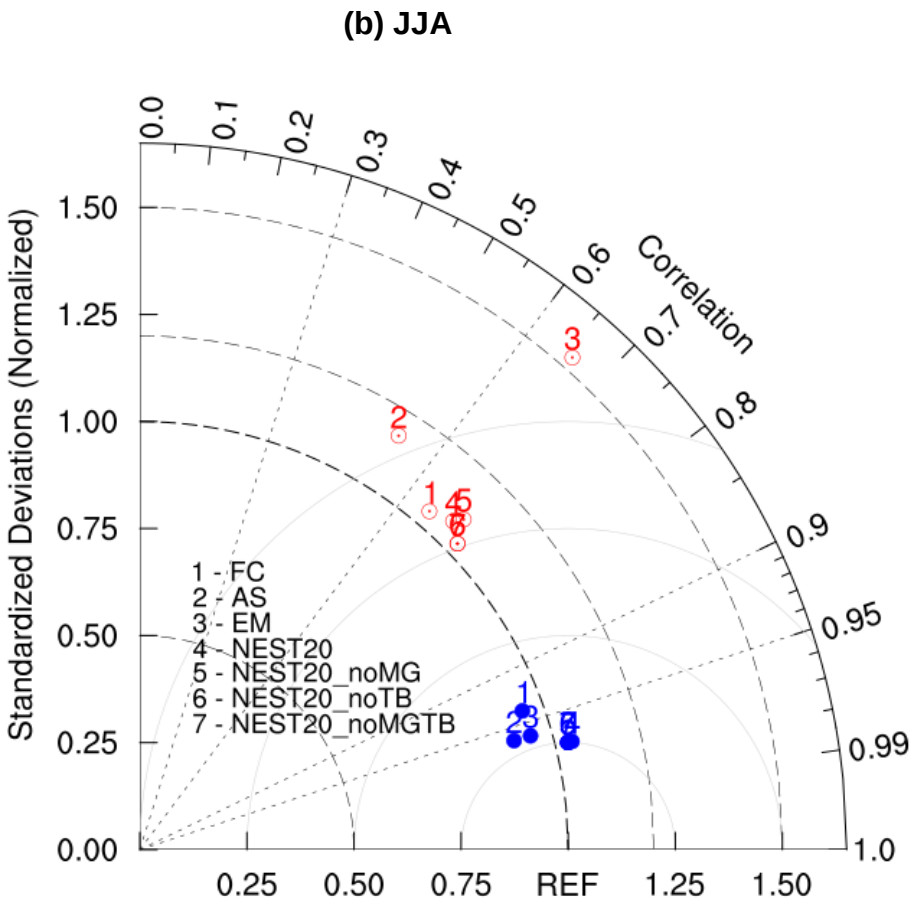

Chapter 4. A Regional Climate Modelling Study over the Loess Plateau, China. Part III: Impacts from the Community Land Model

The aim of the work presented in this chapter was to investigate the model sensitivity to the land surface model (LSM) in the RegCM system over the Loess Plateau. Generally, the LSM is applied to represent the land surface conditions and provide biophysical feedbacks to the atmosphere; therefore, it plays a critical role in simulating the effects of reforestation on the local climate. The work presented in this chapter evaluated the performance of the RegCM configured with the two LSMs over the study area, and investigated the key processes and mechanisms that led to the differences between the simulations generated by the RegCM. Based on these analyses, an optimized configuration of the RegCM over the Loess Plateau was achieved, which could then be applied to model the potential climate impacts of the reforestation programme.

Candidate's contribution to this paper

The simulations in this paper were designed and carried out by the candidate. The candidate also performs all the figure preparation and manuscript drafting. All the work was under supervision of Dr Cheung, who led the main direction of the work and guided the candidate to carry out the research.

A Regional Climate Modelling Study over the Loess Plateau, China.

Part III: Impacts from the Community Land Model

Lang Wang and Kevin K. W. Cheung

Department of Environmental Sciences, Macquarie University, Sydney, Australia

Prepared for Journal of Climate

March 2015

* Author for Correspondence: Kevin Cheung, Department of Environmental Sciences, Macquarie University, North Ryde, NSW 2109, Australia. Email: kevin.cheung@mq.edu.au

Abstract

This paper describes an assessment of the capability of the Regional Climate Model version 4.3 (RegCM4.3) using the Community Land Model version 3.5 (CLM) over the Loess Plateau in China. The Loess Plateau is located in a semi-arid transition zone characterized by a pronounced heterogeneity in topography and vegetation cover. Three simulations applying the CLM with three different convective schemes spanning a period from 1990 to 2009 with a 50 km horizontal resolution are performed. Based on previous RegCM4.3 simulations that applied the Biosphere-Atmosphere Transfer Scheme (BATS), this study analyzes the impact of land surface model and convection scheme on model performance in this region.

The results demonstrate that the three CLM simulations generally reproduce the observed climatology of surface temperature and precipitation, although there are several aspects of biases. When compared with the corresponding BATS simulations, two significant differences are seen: 1) the CLM simulations tend to reduce precipitation during both the winter and summer seasons, and 2) the CLM simulations increase the temperature during the winter season but decrease it during the summer. These differences persist for each corresponding convective scheme and are mostly related to differences in the water and energy budgets between the two LSMs. In particular, the higher cloud coverage, pronounced lower evapotranspiration and excessive runoff in the CLM primarily account for the temperature and precipitation differences. The present study indicates that the CLM agrees better with observations during the winter season, and improve the model performance when the Emanuel convective scheme is used during summer as compared with the BATS.

Keywords:

Regional climate model; Loess Plateau; Community Land Model; convective scheme; net radiative energy balance; water budget

1. Introduction

One of the strongest forcings that influence regional climate systems is the land surface (Dickinson 1995; Pielke and Avissar 1990; Pitman et al. 2011). It provides a lower boundary condition to the atmosphere as a key source of heat, water and momentum, thereby impacting on the local climate significantly (Pielke 2001; Seneviratne et al. 2006; Betts et al. 2007; Giorgi and Avissar 1997). Land surface models (LSMs) are designed to represent land surface characteristics and are coupled with climate models to simulate land-atmosphere interactions (Henderson-Sellers et al. 1996; Pitman 1999). A well-established LSM is critical to perform realistic climate model simulation.

The Regional Climate Model (RegCM) has been extensively applied during recent years and is considered one of the most effective climate models at the local scale (e.g., Giorgi et al. 2012; Gu et al. 2012; Gao et al. 2007; Im et al. 2006; Fu et al. 2005). Since establishment, the model has been utilizing the Biosphere Atmosphere Transfer Scheme (BATS, Dickinson et al. 1993) to represent land surface characteristics and land-atmosphere exchanges. However, BATS utilises a relatively simple process that introduces deficiencies in certain aspects of the simulated climate, especially over complex topographic regions and climate transition zones (e.g., Afiesimama et al. 2006; Almazroui 2012; Wang and Cheung 2015a). Therefore, incorporating a more comprehensive LSM than BATS is likely to improve model simulations using the RegCM, especially over complex areas, by generating more realistic land surface forcings.

The Loess Plateau in China is a good study area to examine the performance of the RegCM coupled with alternative LSMs to the BATS. It is characterized by a diverse geographic topography, which contains thousands of gullies and heterogeneous land patches, as well as a substantial increase in elevation from the eastern lower hills up to the western Tibetan Plateau. Furthermore, the plateau is located in a semi-arid transition zone

that is strongly influenced by the East Asian monsoon system. The monsoon migration leads to intensive heat and moisture exchanges between the land and atmosphere and causes distinct climate gradients from the eastern, humid, to the western, continental, regions (Li et al. 2010; Zhou et al. 2010; Liu and Zeng 2004). Due to these complex characteristics, previous studies that used the BATS in the RegCM poorly captured key climate features over this region (Wang and Cheung 2015a). The need to use a more comprehensive LSM that better describes the land surface and improves the model's simulation over the Loess Plateau was thus identified.

A series of recent RegCM simulations using more comprehensive LSMs have better performance in certain climate aspects compared to simulations using BATS (e.g., Steiner et al. 2005, 2009; Winter et al. 2009; Gianoti et al. 2012; Im et al. 2014). In particular, the RegCM coupled with the Community Land Model (CLM, Oleson et al. 2004b, 2008) has been extensively applied (e.g. Steiner et al. 2005, 2009; Diro et al. 2012; Mei et al. 2013; Reboita et al. 2014). For example, Steiner et al. (2009) configured the RegCM with the CLM over West Africa and found that the seasonal timing and quantity of precipitation was substantially improved compared to that using the BATS. Steiner et al. (2005) applied the RegCM coupled with the CLM over East Asia and achieved a warmer winter temperature that was more consistent with observations than the BATS configuration. Diro et al. (2012) found that the RegCM coupled with the CLM resulted in a better simulation of the seasonal average spatial pattern of precipitation over Central America. These improved simulations likely resulted from the CLM's sophisticated physical representation of surface water and energy budgets, as well as its bio-geophysical parameterizations describing the heterogeneous land surface (Steiner et al. 2009; Reboita et al. 2014; Oleson et al. 2004b, 2008).

Another important factor that significantly impacts the RegCM simulations is the convective scheme utilized. It controls the water and energy distribution between the land surface and atmosphere through convective processes, and is the dominant factor that determines the amount of convective precipitation (Dash et al. 2006; Hong and Choi 2006; Im et al. 2008; Pal et al. 2007). Several recent studies of the RegCM identified that the convective scheme used strongly influenced the model performance when coupled with comprehensive LSMs (e.g., Gianoti et al. 2012; Im et al. 2014; Reboita et al. 2014). For example, Reboita et al. (2014) implemented a series of sensitivity simulations of the RegCM over South America and found that a configuration using the CLM together with the Emanuel convective scheme reproduced the best simulation of air temperature. In contrast, a configuration of the RegCM using the Grell convective scheme coupled with the Integrated Biosphere Simulator (IBIS) LSM produced the most accurate simulation of local precipitation, surface energy and evapotranspiration over the Maritime Continent (Gianoti et al. 2012). Therefore, an investigation of the appropriate LSM to use when simulating the climate using the RegCM over a particular region must also consider different convective schemes for generating the most realistic model simulation.

In this study, we perform RegCM simulations with the CLM to (1) investigate the impact of the LSM on climate simulation over the Loess Plateau in China, (2) determine the key processes and mechanisms that lead to the differences between the simulations produced by the RegCM coupled with the BATS versus the CLM, and (3) evaluate the model configuration that achieves the best simulation of climate over the study area. The RegCM using the BATS has been validated over the Loess Plateau and the model simulation has been improved substantially through investigating various configurations of convective scheme, horizontal resolution and domain choice in Wang and Cheung (2015a, b); however, most simulation results still exhibited systematic deficiencies and there is

significant room for improvement. In the present study, we build on this previous work by evaluating the performance of the RegCM over this complex region in respect of both the LSM and convective scheme used. Specifically, we evaluate how the use of the CLM affects the surface air temperature and precipitation simulated with each convective scheme (Section 3) and how it affects the surface water and energy budgets, the atmospheric circulation and cloud coverage. Based on these analyses, the best configuration of the RegCM over the Loess Plateau is described in Section 4; final conclusions are presented in Section 5.

2. Methods

a. Description of the RegCM4.3

The model used in the present study is the RegCM version 4.3 (RegCM4.3) (Giorgi et al. 2012) developed by the International Centre for Theoretical Physics (ICTP). It has a dynamical core of the Mesoscale Model (MM5) from the National Centre for Atmospheric Research (NCAR) of Pennsylvania State University (Grell et al. 1994). The radiation scheme adopted by the RegCM4.3 is from the NCAR Community Climate Model 3 (CCM3) (Kiehl et al. 1996) and the modified planetary boundary layer scheme was developed by Holtslag et al. (1990).

Within the RegCM4.3, precipitation is derived as both resolvable scale (stratiform) precipitation and convective precipitation. The resolvable process uses the sub-grid explicit moisture scheme (SUBEX) (Pal et al. 2000), which takes the variability of sub-grid clouds into account and links the average grid relative humidity to cloud fraction, cloud water, cloud water accretion and evaporation of falling raindrops. Convective precipitation is produced by the convective schemes, with sub-scale convective clouds and cumulus convection. The three convective schemes applied in this study consist of the Grell

formulation (Grell 1993; Grell et al. 1994) with the Arakawa-Schubert closure assumption (AS) (Arakawa and Schubert 1974), the Grell formulation with the Fritsch-Chappell closure assumption (FC) (Fritsch and Chappell 1980), and the Emanuel scheme (EM) (Emanuel, 1991; Emanuel and Zivkovic-Rothman, 1999).

The two Grell schemes include moistening and heating effects via deep convective clouds between two steady-state circulations of an updraft and downdraft. Mixing between cloudy air and environmental air only occurs at the top and base of the circulations. The AS assumption is a quasi-equilibrium condition that assumes convective processes turn into a stable state as soon as large-scale processes destabilize them, in contrast, for the FC assumption, buoyant energy is only released during a specified timescale (between 30 min and 1 hour). The EM scheme is a more advanced scheme (Giorgi et al. 2012) that allows mixing within clouds, it is highly episodic and inhomogeneous on the sub-cloud scale; the mixing rates are determined by the vertical gradients of buoyancy within the clouds.

b. Comparison between the two LSMs

1) THE BATS LAND SURFACE SCHEME

The BATS scheme, which is the default LSM, has been used for many years in the RegCM. It contains a single vegetation canopy layer, one snow layer, a simple surface runoff model and three soil layers and calculates land surface variables within these layers (Dickinson et al. 1993). The scheme also includes 20 surface categories and 12 soil colour and texture types, which are derived from the Global Land Cover Characterization (GLCC) dataset (Loveland et al. 2000), with horizontal spacing of 0.5˚ based on one year (from April 1992 to March 1993) of Advanced Very High Resolution Radiometer (AVHRR) land cover data. A vegetation class at each model grid is assigned that depends on seasonal parameters including roughness length, maximum and minimum leaf area index (LAI),

stem area index (SAI), vegetation albedo and minimum stomatal resistance (Dickinson et al. 1993).

Sensible heat, water vapour and momentum fluxes at the surface are computed based on a surface layer similarity theory. Surface evapotranspiration accounts for evaporation from the soil and the wet portion of the canopy, as well as transpiration from the dry portion of the canopy. Ground evaporation and transpiration rates depend on the availability of soil water, which is a prognostic variable (Elguindi et al. 2011). The soil hydrology calculations include predictive equations of the water content of the surface soil layer, the root zone, and a deep soil layer characterized by depths of 10 cm, 1–2 m and 3 m, respectively. Soil temperature is computed by a generalization of the 'force-restore' approach of Deardoff (1978). The surface runoff rate is proportional to the precipitation, snowmelt rates and the soil water content relative to saturation.

2) THE CLM LAND SURFACE MODEL

The additional LSM that had been recently coupled with the RegCM is the CLM version 3.5 (Tawfik and Steiner 2011). The CLM possesses several advantages over the BATS, described in detail by Oleson et al. (2004b; 2008). It represents the land surface heterogeneity using a "mosaic" approach, so that each CLM grid cell contains up to four sub-grid land types (glacier, wetland, lake and vegetated); the vegetated unit is further divided into 17 different plant function types (PFTs; Oleson et al. 2004b). Hydrological and energy balance equations are calculated for each sub-grid land type and returned to create the grid-aggregated value to the atmosphere. A series of bio-geophysical processes are adopted in the CLM to describe the land-atmosphere exchanges of energy, momentum and water (Oleson et al. 2004b, 2008). Soil temperature and moisture are determined via explicit treatment of liquid water and ice among ten unevenly spaced soil layers and five snow layers (Dai and Zeng 1996). Surface runoff is derived from surface and base flow,

which are both computed over saturated and unsaturated areas separately based on the Simple TOPMODEL (Stieglitz et al. 1997) (SIMTOP, Niu et al. 2005).

Compared with the BATS that uses the GLCC dataset for vegetation and land cover type, the CLM additionally applies multi-year Moderate Resolution Imaging Spectroradiometer (MODIS) products (Lawrence and Chase 2007) to reproduce the land physical properties. Furthermore, a sophisticated surface albedo was adopted in the CLM to improve the simulations of surface energy balance (Lawrence and Chase 2007). Descriptions of the physical similarities and differences between the BATS and CLM LSMs are summarized in Table 1. Although the CLM uses PFT percentages in each vegetation sub-grid and the BATS uses GLCC land use types in each grid, the primary land use distribution over the Loess Plateau and surrounding region is similar between the two LSMs (Fig. 1).

c. Experimental design

A total of three simulations were run in this study using the CLM coupled with the RegCM. They were configured with the three different convection schemes included in the model: FCCLM, ASCLM and EMCLM. The model domain covered the entirety of China and its surrounding regions, with the Lambert conformal projected grid centred at 107˚E and 35˚N and 50 km grid spacing (Fig. 1a). This domain is similar to the standard domain recommended by the COordinated Regional climate Downscaling Experiment (CORDEX) and captures basic topographic features of China. The analysis domain was an immediate square covering the Loess Plateau (31–42˚N and 101–115˚E), within which statistics of the relevant features were calculated for all experiments (Fig. 1a). The statistics include spatial mean climatology (Mean), spatial mean bias (MB), root mean square error (RMSE), spatial pattern correlations (PCCs) and temporal patterns correlations (TCCs) of inter-annual

variability between two climatic variables. The simulations spanned a period of 20 years from January 1989 to December 2009, in which the first year was the spin-up time. The resulting simulations (1990–2009) were used to evaluate the model performance in terms of the interannual variability, annual cycles and the spatial structure of the long-term climatology. The simulation applied 18 vertical atmospheric model layers in sigma coordinates from the surface to 100 mbar.

Initial and lateral boundary conditions (consisting of 17 pressure levels every 6 hours) were sourced from the European Centre for Medium-Range Weather Forecasts (ECMWF) Reanalysis Interim dataset (EC_In) with horizontal resolution of 1.5˚ latitude/longitude. Weekly sea surface temperatures (SST) were incorporated from the National Oceanic and Atmospheric Administration (NOAA) Optimum Interpolation (OI) SST dataset with 1˚ latitude/longitude grid spacing. Table 2 summarizes the different settings of the simulations in this part of study and those in Wang and Cheung (2015a, b) that applied the BATS.

d. Observational datasets

Both observations and reanalysis data were used for the model evaluation: the China Meteorological Administration Meteorological Information Centre dataset version 5.2 (CN05.2) (Xu et al. 2009) and the EC_In reanalysis dataset. The CN05.2 dataset (0.5˚ grid size) provides monthly mean, maximum and minimum surface air temperatures, as well as monthly mean precipitation for the entire simulation period. The CN05.2 dataset uses the same spatial resolution and spatial interpolation method as the widely applied Climate Research Unit (CRU) dataset (Mitchell and Jones 2005), but the CN05.2 dataset has a higher number of contributing stations over the simulated study area and thus is likely to represent a more realistic local climate than the data outputs from the CRU (Xu et al. 2009;

Sun et al. 2014). Detailed differences between the CN05.2 and CRU datasets over the Loess Plateau has been investigated in Wang and Cheung (2015a), which showed that the CN05.2 dataset to be more accurate. The EC_In reanalysis dataset (1.5˚ grid size) was used to supply observational data of convective and stratiform precipitation, surface energy budget components (radiation fluxes, sensible and latent heat fluxes) and surface water budget components (evapotranspiration, runoff and soil moisture).

3. Results

a. Impact of the LSM on surface temperature

1) SPATIAL VARIABILITY

During the winter season, the CN05.2 observations over the Loess Plateau represent the cold centres over the northern and western plateau well, along with the warm centre over the south-eastern region (Fig. 2a). All the RegCM4.3 simulations that coupled with CLM exhibit a similar temperature pattern to CN05.2. However, a primary cold bias pattern is captured by each experiment in comparison with the CN05.2 observations (Figs. 3a–c). The magnitude of cold biases is particularly high over the northeastern and southern regions in the FCCLM and ASCLM simulations (up to 4˚C), whereas the EMCLM simulation exhibits a narrower cold area with a smaller bias magnitude compared to the former two simulations (Fig. 3c). The cold tendency and variations within the three simulations are quantified through the statistics: the temperature MB is least in EMCLM at -1.33˚C, and largest in ASCLM at -1.75˚C, while the RMSE ranges from 1.83˚C (EMCLM) to 2.20˚C (ASCLM) (Table 3). The similar spatial pattern in the three runs is demonstrated by the PCCs, which are all 0.96. When compared with the BATS, the CLM simulations generate slightly warmer winter temperatures for each corresponding convective scheme configuration over the majority of the Loess Plateau (Figs. 3d–f). The warmer temperatures

simulated by the CLM better agree with observations compared to the BATS; the MB and RMSE are on average 0.46˚C and 0.37˚C less, respectively, in the CLM simulations.

During the summer season, the observed spatial temperature pattern shows maximum values over the north-western and south-eastern plateau and minimum values over the south-western region (Fig. 2b). The general pattern is reproduced by the three CLM simulations. However, temperature biases are still captured, with significantly different bias patterns among the three CLM runs (Figs. 4a–c). The FCCLM and ASCLM simulations tend to produce cold biases over most of the plateau especially over the central and eastern regions, where the ASCLM simulation underestimates temperatures over large areas by larger than -3˚C. In contrast, the EMCLM simulation captures some areas of warm bias over central and southwest regions, as well as areas of slightly cold bias over the eastern region. The biases in the EMCLM simulation are within the range of -2–1˚C, agreeing better with observations than the other CLM simulations. Statistically, the general cold tendency of the CLM simulations and better performance of the EMCLM simulation are validated, whereby the smallest MB of -0.26˚C is seen in the EMCLM simulation, compared to -1.95 and -2.83˚C, respectively, in the FCCLM and ASCLM simulations. The RMSE is smallest in the EMCLM simulation at 1.25˚C, and highest in the ASCLM simulation at 3.05˚C. The PCCs are similar among the three experiments ranging from 0.96 to 0.97 (Table 3).

Compared to the BATS, the CLM simulations generate lower temperatures for each convective scheme during the summer, particularly over the central band of the plateau (Figs. 4d–f). This difference is most obvious between the FCCLM and FCBATS simulations, the former generates over 4˚C lower temperatures over the central plateau. In contrast, the difference is relatively weaker in the simulations using the EM convective scheme. These results are validated by statistics, the largest MBs are captured between the

FC convective scheme experiments (-3.21˚C), and the lowest observed using the EM scheme (-2.25˚C). The RMSE of the EMCLM run is 1.08˚C less than that of the EMBATS simulation whilst for the other two convective schemes the RMSE is higher when the CLM is used. The PCCs of the all simulations, with the observed data are with similar values (Table 3).

From point of view of the model performance, using the CLM tends to simulate colder temperatures than BATS. This in particular improves upon the performance of the RegCM when the EM convective scheme is used as it reduces the large warm bias generated by the EMBATS configuration. However, for the FC and AS convective schemes, coupling with the CLM simulates excessively lower temperatures and the corresponding results are worse than the BATS simulations.

2) SEASONAL AND INTERANNUAL VARIABILITY

To further assess the capability of the CLM in reproducing surface features, the temporal variation of the simulated temperature is compared with observations. In general, the CLM simulations capture the inter-annual variability of temperature well during both seasons (Figs. 5a, b). The TCCs of the CLM simulations with observations are high during winter, which range from 0.74 (EMCLM) to 0.81 (FCCLM). These values are improvements over the BATS simulations that range from 0.12 (ASBATS) to 0.20 (EMBATS) (Table 3). During the summer season, the TCCs of the CLM simulations are highest in FCCLM (0.73) and the lowest in ASCLM (0.34), which have been slightly degraded compared to the BATS simulations by 0.05 and 0.26, respectively. The annual cycle of temperature simulated using the CLM also reproduces the general shape and timing of observations well, although the underestimation from January to September under the FCCLM and ASCLM configurations are evident (Fig. 5c). These results are similar to those generated by the BATS simulations in Wang and Cheung (2015b). Overall,

the EMCLM configuration performs the best amongst the three CLM experiments in terms of both the spatial and temporal distribution of surface temperature during the two seasons over the Loess Plateau.

b. Impact of the LSM on precipitation

1) SPATIAL VARIABILITY

The spatial distribution of precipitation in CN05.2 shows a generally dry condition during the winter season. Minimum precipitation values (up to 10 mm month^{-1}) are observed over the northern and central plateau, with the relatively humid regions over the southeast up to 60 mm month^{-1} (Fig. 2c). This pattern is reproduced well by the three CLM simulations with only slight overestimations (Figs. 6a–c). This slight overestimation is seen in the spatial MB values, which range from 5.51 mm month^{-1} (ASCLM) to 7.01 mm month^{-1} (EMCLM). Correspondingly, the RMSE ranges from 7.13 to 8.71 mm month^{-1} for ASCLM and EMCLM, respectively. The PCCs are generally high: the FCCLM configuration produces the highest PCC of 0.79 among all three runs (Table 4).

Compared with the BATS, the CLM simulations exhibit relatively drier conditions, which are more consistent with observations. The CLM simulations reduced the winter precipitation by up to 10 mm month^{-1} over most of the domain in comparison to the BATS simulations (Figs. 6d–f). The spatially averaged differences between the two LSMs simulations confirm the drier tendency generated by the CLM with 2.05 and 4.26 mm month^{-1} less precipitation in the FCCLM and EMCLM configurations, respectively. Applying the CLM also decreases the RMSE by up to 4.61 mm month^{-1} and increases PCC by averagely 0.04, compared to using the BATS (Table 4).

During the summer season, the CLM simulations with the different convective schemes exhibit have larger discrepancies in precipitation pattern than in winter. On the

one hand, each experiment generally reproduces the observed spatial pattern that exhibits wet centers over the southern and eastern plateau, and dry centers over the northwest region (Fig. 2d). On the other hand, the spatial bias of summer precipitation is significantly different among the three simulations using CLM (Figs. 7a–c). Specifically, the EMCLM simulation has an overestimation over a wide extent of the plateau ranging between 10–80 mm month^{-1} along with certain areas of under-prediction of over 20 mm month^{-1} across the southern and northwestern areas (Fig. 7c). In contrast, large areas of underestimation are simulated in the FCCLM and ASCLM over the southern and southeastern regions with biases of over 60 mm month^{-1} compared to observations (Figs. 7a–b).

The large variability in the simulated precipitation of the three experiments is seen in the statistics, which show humid conditions in the EMCLM simulation with a positive MB of 18.46 mm month^{-1}, but dry conditions in the FCCLM and ASCLM simulations with negative MB of -18.69 and -14.77 mm month^{-1}, respectively. The RMSE is lowest at 33.99 mm month^{-1} in the FCCLM simulation, followed by the EMCLM and ASCLM simulations with 35.57 and 40.09 mm month^{-1}, respectively. The PCCs between the simulations and observations is highest in the EMCLM simulation (0.82) compared to the FCCLM (0.79) and ASCLM (0.57) simulations (Table 4). These statistics demonstrate the better ability of the FCCLM and EMCLM configurations, compared with the ASCLM configuration, in reproducing the observed summer precipitation over the Loess Plateau.

Compared with the series of simulations using the BATS, summer precipitation is generally lower by using the CLM over the northeast, southeast and southwest regions (Figs. 7d–f). Excessive humid conditions are also captured using the CLM over the northwest region compared to BATS. The largest differences among the convective schemes are over the central area with excessive precipitation of 0–40 mm month^{-1} from the CLM compared to the BATS simulations when coupled with the FC and EM

convective schemes. With the AS scheme, using the CLM results in a decrease in simulated rainfall of over 20 mm month^{-1} compared to the BATS. The statistics reveal the overall drier tendency in the CLM simulations compared to the BATS, with the largest reduction in ASCLM of 23.20 mm month^{-1} followed by EMCLM of 13.52 mm month^{-1} and FCCLM of only 3.99 mm month^{-1} (Table 4).

Furthermore, over the southwest mountainous regions, the CLM simulations significantly mitigate the large positive bias generated by the BATS. This area has intensive interactions between the orographic surface and the atmosphere. The interactions are likely more reasonably simulated by the CLM due to its more sophisticated land surface physical processes and subsequently generating better precipitation results. These spatial improvements particularly result in higher PCCs in the CLM compared to the BATS simulations when coupled with the FC and EM schemes, with an increase of 0.06 and 0.07, respectively (Table 4).

2) SEASONAL AND INTERANNUAL VARIABILITY

In general, the time series of CLM simulations capture the observed interannual variability of precipitation well during the winter season, but perform more distinctively during summer (Figs. 8a, b). During the summer season, the ASCLM simulates unreasonably high level of precipitation compared to observations and also does not capture the maxima and minima in precipitation well. In contrast, the FCCLM and EMCLM configurations capture the observed temporal patterns more consistently. These variations are validated by the TCCs; the ASCLM simulation has the lowest TCC of only 0.13 with observations, in contrast to the higher TCCs of the FCCLM and EMCLM, which are 0.42 and 0.40 respectively. Moreover, the TCCs of the CLM simulations with observations are generally lower than those of the BATS simulations, with the smallest reduction of 0.12 seen in the EM convective scheme experiments. During winter, the TCCs

are generally high between the CLM simulations and observations. The values range from 0.87 (FCCLM) to 0.93 (ASCLM), which are equal to or higher than those between the BATS simulations and observations (Table 4).

The annual cycle in precipitation is reproduced well by the EMCLM configuration with maximum precipitation in July and minimum in January and December (Fig. 8c). However, the precipitation among is systematically overestimated by 5–10 mm month^{-1} throughout the first half of the year. In contrast, the FCCLM and ASCLM configurations both simulate the annual peak in rainfall one month earlier compared to observations and significantly underestimate the magnitude of precipitation from July to September. The erroneous early rainfall peak simulated using the FC and AS convective schemes coupled with the CLM is similar to that using the BATS, and both LSMs simulate the correct annual peak when coupled with the EM convective scheme.

4. Discussion

The simulations presented here have demonstrated two significant differences between configuring the RegCM with the two LSMs: 1) the CLM tends to reduce the amount of precipitation during winter and summer seasons compared to the BATS, and 2) the CLM increases the temperature during the winter season but decreases it during summer. These differences persist, to a greater or lesser degree, regardless of the choice of convective parameterization and are more related to the differences in water and energy budgets between the two LSMs. These budget differences and the differences in related variables are further investigated in this section.

a. Impact of LSM on surface water budget

An investigation into the components of the surface water budget can obtain insights into the reasons for the differences in precipitation simulated by the two LSMs. These components include inputs to the water budget (convective and stratiform precipitation), storage within the system (as soil water) and outgoings (evapotranspiration and runoff).

1) CONVECTIVE AND STRATIFORM PRECIPITATION

Precipitation is the primary input of the water budget especially during the summer season. This variation in precipitation may result from differences in the partitioning of convective and stratiform precipitation between the experiments that coupled one of the convective schemes with a LSM. During winter, the CLM and BATS simulations show that the dominant precipitation type is stratiform precipitation and there is negligible convective precipitation. However, the series of CLM simulations exhibit slightly lower quantities of stratiform precipitation with an average difference of -2.58 mm month^{-1}. The negative difference accounts for the lower total precipitation in the CLM simulations to a certain degree (Table 5).

During the summer season, both convective and stratiform precipitation are noticeable components of the total rainfall according to the CLM and BATS simulations (Table 5), which were consistent with EC_In reanalysis in spite of the scale dependence. Nevertheless, considerable discrepancies are generated among the simulations resulting from the two LSMs. In general, the CLM simulations generate lower amounts of convective precipitation, but increase the stratiform precipitation compared with the BATS simulations.

In terms of summer convective precipitation, the three CLM simulations exhibit considerable discrepancies over the southwest, northeast and southeast regions (Figs. 9a–c). These spatial distributions of lower convective precipitation in the CLM appear to correlate

well to the discrepancies in the spatial patterns of total rainfall as compared with the BATS (Figs. 7d–f). This is also validated through PCCs matrices, in which the spatial differences in patterns of precipitation, temperature and their related variables are analysed (Fig. 10). In the CLM simulations with the three convective schemes, the patterns of convective precipitation correlate well with total precipitation with PCCs over 0.63.

There are also differences in stratiform precipitation between the simulations generated by the two LSMs. In general, higher stratiform precipitation is simulated in the CLM simulations over the central area compared to the BATS (Figs. 9d–f). In the same area, total precipitation is also stronger in the CLM simulations when coupled with the FC and EM convective schemes (Figs. 7d–f), which is found with high PCCs between stratiform and total precipitation of 0.82 for both configurations. The ASCLM configuration has a lower PCC between stratiform and total precipitation of 0.50 (Fig. 10).

2) EVAPOTRANSPIRATION

Evapotranspiration (ET) is the major outgoing of the water budget during both seasons according to the EC_In reanalysis, which has been reproduced in both the CLM and BATS simulations. However, ET is lower in the CLM simulations compared with those using the BATS. During winter, the CLM simulations have slightly lower rates of ET by up to -3.98 mm month^{-1} compared to the BATS simulations and agree better with the EC_In reanalysis. However, there are noticeable deficiencies in ET within the CLM simulations compared with those generated using the BATS during summer, which range from -16.04 mm month^{-1} to -29.54 mm month^{-1} (Table 6).

The discrepancy in ET between the CLM and BATS simulations is likely caused by different parameterizations in the two LSMs that describe the land surface and land-atmosphere interaction processes. For example, in the BATS system cultivated land is further divided into crop land and irrigated crop land, and large area is considered as

irrigated crop land over the southeast region of the Loess Plateau (Fig. 1b). However, the CLM only includes one type of crop land and its characteristics are similar to the non-irrigated crop land in the BATS (Fig. 1c). Primary difference between the two crop types is the soil water content. Irrigated crop in the BATS is assigned to the field capacity during the year, whilst crop land in the BATS and the CLM depends on variability of the surface water budget (Pal et al. 2007). In particular, available soil water over semi-arid areas is the key factor for maximum rates of ET (Dickinson et al. 1993). Thus, supported by sufficient soil water irrigated crop in the BATS tends to produce excessively high ET over the southeast plateau, but ET of crop in the CLM is restrained by the limited soil water and results in deficiencies compared with BATS simulations.

The tendency of less ET resulting from the CLM simulations may account for the convective precipitation discrepancy compared to the BATS simulations during summer (Figs. 11a–c; Figs. 9a–c), which is consistent with the generally high PCCs between patterns of ET and convective precipitation of 0.60 and 0.70 for the FC and AS convective schemes, respectively, and 0.41 for the EM scheme (Fig. 10). One mechanism that may explain this relationship is ET-rainfall feedback at the local scale: lower ET in the CLM simulations supplies less water vapour to the atmosphere from the land surface and this in turn results in drier boundary conditions, which consequently reduces the potential water sources for convection and the total rainfall.

3) RUNOFF

Runoff in the CLM simulations is much higher than the BATS simulations during both seasons. In particular, during the summer the excessive rates of runoff in the CLM simulations range from 20.08 (ASCLM) to 35.39 mm month^{-1} (EMCLM) compared with the corresponding BATS simulations. The high runoff rates in the CLM simulation are mostly associated with the incorporated runoff scheme SIMTOP developed from the

TOPMODEL (Oleson et al. 2007), which considers surface and base flow for saturated and unsaturated zones. The surface flow corresponds to both the BATS surface runoff and the saturation excess runoff, while the base flow is proportional to the surface soil moisture conditions (Dai et al. 2003). As a result, the total runoff generated by using the CLM appears to be larger in comparison to the BATS. In addition, SIMTOP takes topographic characteristics into account (Niu et al. 2005), and thus tends to produce excessive runoff over the Loess Plateau with very steep slopes. The excessive runoff in the CLM can remove water from the surface over-effectively and substantially reduce water stored in the soil layer, and is considered another reason for the decreased ET.

4) SOIL WATER STORAGE

Soil water storage is defined as the sum of the surface inflow (total precipitation minus ET and runoff) and indicates the net ground water budget. Compared with the BATS, the CLM simulations tend to store less water in the soil, with deficit ranging from -3.16 (FCCLM) to -7.78 mm $month^{-1}$ (EMCLM) during winter and -8.81 to -22.85 mm $month^{-1}$ during summer. This deficiency in the soil water storage in the CLM is likely attributed to the excessive runoff outgoings and the deficiency of precipitation input (Table 6).

In addition, the relatively low soil water storage in CLM compared with BATS may be related to different parameterizations of the irrigated crop. The irrigated crop in BATS is assigned with soil water content as field capacity at every time step. This approach adds external water into soil, and remains soil water storage at a high level over the irrigated area. On the contrary, CLM does not include irrigated crop but assigns corresponding cells as the sum of the surface inflow in the soil water storage.

The deficiencies in the soil water storage are related to the drier soil moisture in the CLM compared to the BATS that substantially accounts for decreases of the total ET. It is

also found with high spatial PCCs between the soil moisture and the ET (from 0.53 in the EM convective scheme to 0.74 in the FC convective scheme) (Fig. 10). Such impacts of soil moisture on the local climate have previously been found in studies using the RegCM and other climate models (e.g., Zhang et al. 2011; Koster et al. 2004; Pielke 2001).

b. Low-level winds and cloud coverage

With feedbacks from the LSM and convective scheme, the simulated circulation would further change the pattern of moisture advection, which in return has impact on precipitation. Fig. 12 displays the spatial differences in the 850-hPa wind field and geopotential height between the two LSMs during summer over the entire simulation domain. The CLM enhances the southerly flow in central China compared to the BATS as part of the anomalous anticyclone. This brings in excessive moisture from the humid area to the Loess Plateau, consequently increasing the local water vapour and mitigating against the drier conditions in the CLM. This relationship is also validated by PCCs between the spatial differences of precipitation and the meridional component of the 850-hPa wind, which are all over 0.62 (Fig. 10). The stronger southerly flows in the series of CLM simulations are primarily driven by the intensive geopotential height gradient, with the highest pressure difference to the southeast of the plateau. These processes reflect that a change in the LSM can substantially influence the overlying atmospheric pressure and circulation, which further modifies the surface precipitation through advection.

The stronger southerlies simulated using the CLM may also be related to the increase in cloud coverage over the Loess Plateau during summer (Figs. 11d–f). The stronger southerlies associated with positive moisture advection in the CLM is supportive to trigger more cloud development in the RegCM. This is validated by the high PCCs between the spatial differences in cloud coverage and the meridional component of the 850-hPa wind,

which ranges from 0.61 to 0.67 (Fig. 10). The higher cloud coverage is attributed to the production of excessive stratiform precipitation simulated by SUBEX when the PCC between the spatial patterns is high (0.77, Fig. 10).

c. Impact of LSM on surface energy budget

The differences in temperature simulated by the CLM and BATS LSMs may be caused by the various components of the surface energy budget. The surface net shortwave radiation (NSR) (incoming minus reflected) and net long-wave radiation (NLR) result in the radiation energy budget, and the turbulent energy includes the latent heat flux (LH) and the sensible heat flux (SH). The partitioning in turbulent energy is also evaluated in this section by assessing the Bowen Ratio (β; Bowen, 1926), defined as the ratio between SH and LH fluxes.

1) WINTER SEASON

During the winter season, the CLM and BATS simulations reproduce the patterns of the energy budget well according to the EC_In reanalysis. However, major differences of the energy budget between the simulations by the two LSMs are seen in the NSR and LH flux. Compared with the BATS simulations, the NSR is higher in the CLM simulations by 4.57 Wm^{-2} on average, but LH fluxes are lower by -3.18 W m^{-2} (Table 7). The excessive NSR in the CLM simulations accounts for the warmer simulated temperature compared to that by BATS. The high PCC values between the patterns of NSR and temperature (not shown) also support this potential mechanism. Furthermore, the lower LH flux accounts for the higher β in the CLM simulations (but with the larger downward SH contributing to the warmer temperature) compared with the BATS.

2) SUMMER SEASON

The radiation budget of EC_In reanalysis is reproduced well by both the CLM and BATS series of simulations, but the CLM simulations capture lower NSR and NLR fluxes compared to the BATS simulations by -3.40 W m^{-2} and -6.34 W m^{-2} on average, respectively (Table 7). The lower NLR in the CLM simulations is primarily caused by the lower temperature, which emits less outgoing energy to the atmosphere. However, the NLR is affected by the larger cloud coverage that reflects the radiation back to the earth's surface. In contrast, the NSR deficiencies in the CLM simulations indicate energy absorbed by the higher cloud coverage. The CLM simulations show excessive cloud coverage over the central band of the plateau (Figs. 11d–f), which is found where the NSR is low (Figs. 13a–c). The corresponding negative PCCs also have large magnitude (Fig. 10). Moreover, the PCC between cloud coverage and mean temperature is also large in magnitude (-0.62), which is consistent with previous studies (e.g., Pal et al. 2000; Sylla et al. 2010; Coppola and Giorgi 2010).

The NSR is spatially correlated with the colder condition in the CLM simulation of the mean temperature and the daily maximum temperature (Tmax). The pattern of the Tmax difference between the CLM and BATS simulations show apparently lower values over the central band of the plateau in the CLM (Figs. 13d–f). This pattern (similarly for the pattern of the mean temperature difference) is correlated to the spatial difference pattern of the NSR (PCCs over 0.70 especially for the FC and AS convective schemes, Fig. 10). However, in the simulation with the EM convective scheme the NSR does not affect either mean temperature or Tmax much (PCC of 0.38 and 0.40, respectively), but is more related to the total incoming solar radiation (not shown here). In general, the summer cold tendency simulated using the CLM over the Loess Plateau is in line with results from a study over Europe that compared a series of regional climate models (Daniela et al. 2007).

In terms of turbulent fluxes the EC_In reanalysis shows higher LH than SH fluxes during the warm and humid summer season; this structure is reproduced in the simulations using the two LSMs. When the CLM simulations are compared with the BATS, significantly lower turbulent fluxes are captured with the SH fluxes being lower by -12.60 to -22.22 W m^{-2} and the LH fluxes by -15.54 to -28.61 W m^{-2} (Table 7). These lower SH and LH fluxes lead to a higher net energy budget in the CLM with excess over 40 W m^{-2}. This large energy residual is an inconsistency in the energy budget between the land surface model and the overlying atmospheric processes and an in-depth review of the corresponding parameters in the CLM and RegCM is thus needed. Li et al. (2014) applied a revised coupling system of the CLM and RegCM over East Asia and achieved better agreement with observations including the energy budget.

The weaker turbulent fluxes in the CLM compared to those in BATS may be attributed to the drier conditions of soil moisture resulting from the increase in runoff and decrease in precipitation. This drier soil moisture can decrease the soil heat capacity, which is associated with the energy available to heat the air at the surface, and consequently reduces the SH fluxes in the CLM simulations. The drier soil moisture also triggers a decrease in soil evaporation, thereby reducing the soil and the total LH flux (Lawrence and Chase 2007). Although there are significant decreases in the SH and LH fluxes, the β in the CLM simulations remains similar to that in the BATS simulations. Thus, the differences in SH and LH fluxes may not account for the significantly lower temperature in the CLM simulations.

5. Conclusion

The present study analysed regional climate simulations over the Loess Plateau in China using the RegCM version 4.3 coupled with the new LSM: the CLM version 3.5. As

a semi-arid transitional zone, the Loess Plateau is characterized by its orographic topography and distinct climate gradient and provides a good study area to examine the performance of the new CLM. We carried out three simulations applying the CLM with three convective schemes in the RegCM. Simulations covered the entire China domain with a 50 km horizontal resolution over 20 years from 1990 to 2009. The model's performance in simulating the local climate over the Loess Plateau was evaluated against the CN05.2 observational dataset and the EC_In reanalysis. Combined with previous simulations in Wang and Cheung (2015a, b) using the default BATS land surface scheme, this work identifies the best configuration of the RegCM in simulating the local climate features over the Loess Plateau with a particular emphasis on the impact of the choice of LSM and convection scheme.

First, simulations using the CLM generate consistently less precipitation compared to the BATS during both seasons, however, the amount of precipitation varies significantly within each LSM series, depending on which convective scheme is applied. Lower precipitation levels in the CLM simulation can primarily be attributed to lower evapotranspiration fluxes, associated with drier boundary conditions in comparison to the BATS. The lower evapotranspiration levels are partially constrained by the drier soil moisture in this semi-arid region, because excessively high runoff rates remove large portions of the surface water, as well as the lack of the irrigated crop PFT in the CLM.

Considering the model performance, the drier tendency in the CLM helps to reduce the bias of winter precipitation generated by the BATS, and during summer results in a better performance when the EM convective scheme is used. In contrast, the FC and AS convective schemes coupled with the CLM significantly deteriorates the model performance using the BATS. Furthermore, EMCLM can accurately reproduce the precipitation annual cycle， although it also systematically overestimates precipitation

during summer. In contrast, configurations using the FC and AS convective schemes simulate the annual peak in precipitation occurring one month too early.

The CLM simulates consistently warmer temperatures than the BATS simulations during winter, but significantly colder temperatures during summer. These differences between the two LSMs can primarily be explained by the positive correlation between the absorbed solar radiation and the surface air temperature. In particular, the warmer temperature during winter is related to the higher net solar radiation in the model with CLM as well as the larger downward SH. During the summer, colder temperatures in the CLM experiments primarily occur over the central band of the Loess Plateau, corresponding spatially to the low levels of net solar radiation and excessive cloud coverage. The excessive cloud coverage is likely triggered by the moisture advection carried by the anomalous southerly monsoon flow and decreases in the net solar radiation at the surface. This indicates that changes of the land surface processes can substantially alter the overlying atmospheric circulation.

In terms of the model performance, the warmer winter temperature in the CLM can decrease the cold bias generated by the BATS in simulations, but the colder summer temperatures only contribute to an improvement in model performance when coupled with the EM convective scheme, for configurations with the FC and AS convective schemes large cold biases are captured in the CLM.

It is difficult to unambiguously determine the best model simulation, since each configuration has its own pros and cons. In general, using the CLM systematically improves simulations during the winter season when compared with the BATS. The simulated temperature and precipitation match with observations better and the components of the water and energy budgets are more realistic. This improvement achieved by the RegCM coupled with the CLM in winter was also shown by Steiner et al.

(2005) over East Asia. In contrast, the CLM simulations during the summer season vary substantially amongst the three convective schemes. The CLM coupled with the EM convective scheme can generate encouraging simulations (except for the overestimation of the summer precipitation), which agrees with previous studies (e.g., Chow et al. 2006; Im et al. 2008; Reboita et al. 2014). However, the CLM coupled with the FC and AS schemes leads to dramatic model biases of surface temperature and precipitation. Combined with our previous study that investigated the BATS configurations (Wang and Cheung 2015a, b), FCBATS and EMCLM give more satisfactory performances over the Loess Plateau amongst all the configurations tested. The results presented here also provide general guidance regarding the performance of regional model simulations in climate transitional zones that have a complex topography. Finally, over-effective runoff in the surface water budget and large amounts of energy residual in the surface energy budget are the key inconsistences of the CLM simulations with the RegCM, which require further investigation. Irrigated crop as an important land surface type may need to be parameterized as an independent land-type category of CLM in the future. This last issue will be discussed in our next part of study that simulates realistic reforestation programs in the Loess Plateau.

Acknowledgement. The first author (LW) is supported by the China Scholarship Council, the International Macquarie Research Excellence Scholarship, and Higher Degree Research support fund from Macquarie University. Computational facilities are provided by Intersect Inc., NSW and the National Computational Infrastructure of Australia. We would like to thank Prof. C.-P. Chang of the US Naval Postgraduate School and the National Taiwan University for co-supervising LW and his many valuable comments on this work.

List of Tables

TABLE 1 Summary of the major differences between the BATS[a] and CLM[b] LSMs [c].

Characteristics	BATS	CLM
Grid	1 grid (sub-grid is available, but not used in this paper)	4 sub-grid land units (glacier, wetland, lake, and vegetated) (Oleson et al. 2004b)
Model layers	Snow layers: 1	Snow layers: 5
	Soil layers: 3 (groups of soil and snow layers used for temperature and soil moisture calculations (Yang and Dickinson 1997)	Soil layers: 10 (calculates temperature and moisture explicit for each snow and soil layer (Dai and Zeng 1996), here this was aggregated back to 3 soil layers and 1 snow layer to enable comparison to the BATS)
	Vegetation layers: 1	Vegetation layers: 1
	Runoff layers: 1 (simple rate to surface water saturate)	Runoff layers: 1 (calculated according to SIMTOP, with both saturated and unsaturated areas)
Surface type	20 surface categories based on GLCC[d]	4 sub-grid land units and 17 PFTs[e] in the vegetation unit, based on GLCC and MODIS[f]
	8 soil colors and 12 soil texture types (based on the Global Soil Types data, 0.5˚ horizontal resolution (Zobler 1999)	20 soil colors, soil texture is based on the percentage of sand, clay and silt from IGBP[g] soil dataset (Global Soil Data Task 2000; Bonan et al. 2002)
Canopy radiation	All vegetation receives the same amount of radiation	Leaves are divided into sunlit and shaded (Bonan 1996)
Stomatal conductance	Simple stomatal conductance model using light, moisture and vapor pressure deficit factors (Jarvis 1976)	Photosynthesis-stomatal conductance scheme, using photosynthetic rates, CO2 leaf-surface concentration and the gradient of water vapor pressure over the leaf surface
Surface fluxes	Standard surface drag coefficient formulation based on Monin-Obukhov similarity theory	Monin-Obukhov similarity theory adjusted for free convection (Zeng et al. 1998)
Soil moisture	Predictive equations using diffusive/gravitational method (accounts for liquid water only)	Explicit treatment of liquid water and ice between each soil and snow layer (SIMGM[h] is used for the ground water component)
Soil temperature	2 layer force-restore model for temperature (Dickinson 1988)	Explicit treatment of heat transfer between each soil and snow layer
Albedo	Vegetation albedo is generally larger than CLM (Zeng et al. 1998)	Two stream approach (equal to the underlying ground when LAI is zero, changes to the covered vegetation albedo when LAI reaches a seasonal maximum)
Same	Soil color is based on the land cover, canopy temperature follows the canopy energy balance (Steiner et al. 2005), initialization of the prescribed soil water content is relative to saturation as a function of land cover type (Giorgi and Bates 1989), initialization of LAI, snow albedo the same	

[a] The Biosphere-Atmosphere Transfer Scheme (BATS) (Dickinson et al. 1993); [b] The Community Land Model version 3.5 (CLM) (Oleson et al. 2004b, 2007); [c] Land surface models (LSMs); [d] The Global Land Cover Characterization (GLCC) dataset (Loveland et al. 2000); [e] Plant function types (PFTs); [f] Moderate Resolution Imaging Spectroradiometer (MODIS) products (Lawrence and Chase 2007); [g] International Geosphere-Biosphere Programme (IGBP) (Loveland et al. 2000); [h] Simple Ground Water Model (SIMGM).

TABLE 2 Experimental design.

	Experiment	**Convective Scheme**
CLM Simulations	FCCLM	Grell Fritsch-Chapell (Grell 1993)
	ASCLM	Grell AS (Grell 1993)
	EMCLM	Emanuel (Emanuel 1991; Emanuel and Zivkovic-Rothman 1999)
BATS simulations (Wang and Cheung 2015a, b)	FCBATS	Same as FCCLM
	ASBATS	Same as ASCLM
	EMBATS	Same as EMCLM

TABLE 3 Simulated and observed surface air temperature during the winter and summer seasons.

	Experiments	DJF[a]					JJA[b]				
		Mean[c]	MB[d]	RMSE[e]	PCC[f]	TCC[g]	Mean	MB	RMSE	PCC	TCC
		(˚C)					(˚C)				
Observation	**CN05.2**	**-4.55**					**20.49**				
Simulations	FCCLM	-6.15	-1.60	2.17	0.96	0.81**	18.54	-1.95	2.33	0.97	0.73**
	ASCLM	-6.30	-1.75	2.20	0.96	0.80**	17.66	-2.83	3.05	0.96	0.34
	EMCLM	-5.88	-1.33	1.83	0.96	0.74**	20.23	-0.26	1.25	0.97	0.52*
Difference from BATS	FCCLM-FCBATS		0.27	-0.28	0.00	0.18		-3.21	0.35	0.02	-0.05
	ASCLM-ASBATS		0.61	-0.48	0.00	0.12		-2.85	1.51	-0.01	-0.26
	EMCLM-ASBATS		0.50	-0.36	0.00	0.20		-2.25	-1.08	0.00	-0.06
LSM average results	CLM	-6.11	-1.56	2.07	0.96	0.78	18.81	-1.68	2.21	0.97	0.53
	BATS	-6.57	-2.02	2.44	0.96	0.62	21.58	1.09	1.95	0.96	0.65
	CLM-BATS		0.46	-0.37	0.00	0.16		-2.77	0.26	0.01	-0.12

[a] Winter season months: December, January and February (DJF); [b] Summer season months: June, July and August (JJA); [c] Spatial mean climatology (Mean); [d] Spatial mean bias (MB); [e] Root mean square error (RMSE); [f] Pattern correlation coefficient (PCC); [g] Temporal correlation coefficient (TCC); * Statistically significant at the 95% confidence limit; ** Statistically significant at the 99% confidence limit.

TABLE 4 Simulated and observed precipitation during the winter and summer seasons.

	Experiments	DJF					JJA				
		Mean	MB	RMSE	PCC	TCC	Mean	MB	RMSE	PCC	TCC
		(mm month^{-1})					(mm month^{-1})				
Observation	**CN05.2**	**7.17**					**95.07**				
Simulations	FCCLM	13.15	5.98	7.33	0.79	0.87**	76.38	-18.69	33.99	0.79	0.42
	ASCLM	12.68	5.51	7.13	0.78	0.93**	80.30	-14.77	40.09	0.57	0.13
	EMCLM	14.18	7.01	8.71	0.73	0.90**	113.53	18.46	35.57	0.82	0.40
Difference from BATS	FCCLM-FCBATS		-2.05	-2.31	0.03	0.00		-3.99	-3.56	0.06	-0.22
	ASCLM-ASBATS		-2.66	-2.73	0.04	0.07		-23.20	-1.70	-0.05	-0.28
	EMCLM-EMBATS		-4.26	-4.61	0.04	0.06		-13.52	-19.05	0.07	-0.12
LSM average results	CLM	13.34	6.17	7.72	0.77	0.90	90.07	-5.00	36.55	0.73	0.32
	BATS	16.33	9.16	10.94	0.73	0.86	103.64	8.57	44.65	0.70	0.52
	CLM-BATS		-2.99	-3.22	0.04	0.04		-13.57	-8.10	0.03	-0.20

TABLE 5 Simulated and EC_In reanalysis estimated convective and stratiform precipitation.

	Experiments	DJF				JJA			
		Convective		Stratiform		Convective		Stratiform	
		Mean	MB	Mean	MB	Mean	MB	Mean	MB
		(mm month^{-1}) / Percentage							
Reanalysis	**EC_In**	**1.98**		**9.03**		**57.02**		**52.39**	
		17.98%		**82.02%**		**52.12%**		**47.88%**	
Simulations	FCCLM	0.16	-1.82	12.99	3.96	41.07	-15.95	35.31	-17.08
		1.22%	-16.76%	98.78%	16.76%	53.77%	1.65%	46.23%	-1.65%
	ASCLM	0.19	-1.79	12.49	3.46	39.03	-17.99	41.27	-11.12
		1.50%	-16.48%	98.50%	16.48%	48.60%	-3.52%	51.39%	3.51%
	EMCLM	2.56	0.58	11.62	2.59	70.43	13.41	43.10	-9.29
		18.05%	0.07%	81.95%	-0.07%	62.04%	9.92%	37.96%	-9.92%
Difference from BATS	FCCLM-FCBATS		-0.03		-2.02		-8.56		4.57
			-0.03%		0.03%		-7.98%		7.98%
	ASCLM-ASBATS		0		-2.66		-28.24		5.04
			0.26%		-0.26%		-16.40%		16.40%
	EMCLM-EMBATS		-1.18		-3.08		-15.48		1.96
			-2.23%		2.23%		-5.58%		5.58%
LSM average results	CLM	0.97	-1.01	12.37	3.34	50.18	-6.84	39.89	-12.50
		6.92%	-11.06%	93.08%	11.06%	54.80%	2.69%	45.19%	-2.69%
	BATS	1.37	-0.61	14.95	5.92	67.60	10.58	36.04	-16.35
		7.59%	-10.39%	92.41%	10.39%	64.79%	12.67%	35.21%	-12.67%
	CLM-BATS		-0.40		-2.58		-17.42		3.85
			-0.67%		0.67%		-9.98%		9.98%

TABLE 6 Simulated and EC_In reanalysis estimated surface water budget, top and root layer soil moisture, and total cloud coverage.

Water Budget		DJF						JJA					
		ET[a]	**Runoff**	**Stor**[b]	**Soil Moisture**		**Cloud**	**ET**	**Runoff**	**Stor**	**Soil Moisture**		**Cloud**
		mm month^{-1}			**Top**	**Root**	%	mm month^{-1}			**Top**	**Root**	%
					mm^3 mm^{-3}						mm^3 mm^{-3}		
Reanalysis	**EC_In**	**10.62**	**5.10**	**-5.09**	**0.23**	**0.25**	**40.92**	**71.63**	**19.10**	**12.06**	**0.24**	**0.25**	**53.70**
Simulations MB	FCCLM	0.24	3.30	-1.02	-0.12	-0.11	1.24	-11.88	7.83	-22.36	-0.06	-0.08	-4.66
	ASCLM	0.35	5.73	-4.03	-0.12	-0.10	1.67	-16.20	17.69	-23.98	-0.05	-0.08	-0.13
	EMCLM	1.34	7.88	-5.67	-0.12	-0.10	3.26	4.12	37.88	-31.26	-0.05	-0.08	-8.82
Difference from BATS	FCCLM-FCBATS	-2.51	3.62	-3.16	-0.07	-0.14	-1.59	-16.04	20.86	-8.81	-0.03	-0.11	3.60
	ASCLM-ASBATS	-2.66	5.72	-5.72	-0.06	-0.14	-1.60	-29.54	20.08	-13.74	-0.03	-0.13	4.04
	EMCLM-EMBATS	-3.98	7.50	-7.78	-0.07	-0.14	-2.10	-26.06	35.39	-22.85	-0.03	-0.13	2.05
LSM average results	CLM	0.64	5.64	-3.57	-0.12	-0.10	2.06	-7.99	21.13	-25.86	-0.05	-0.08	-4.54
	BATS	3.69	0.02	1.99	-0.05	0.04	3.82	15.89	-4.31	-10.73	-0.02	0.04	-7.77
	CLM-BATS	-3.05	5.62	-5.56	-0.07	-0.14	-1.76	-23.88	25.44	-15.13	-0.03	-0.12	3.23

[a] Evapotranspiration (ET); [b] Net soil water storage (Stor)

TABLE 7 Simulated and EC_In reanalysis estimated energy budget parameters during the winter and summer.

Energy Budget		DJF							JJA						
		Energy Balance (W m^{-2})						β[g]	Energy Balance (W m^{-2})						β
		NSR[a]	NLR[b]	NR[c]	SH[d]	LH[e]	NE[f]		NSR	NLR	NR	SH	LH	NE	
Reanalysis	**EC_In**	**92.72**	**76.57**	**16.15**	**18.81**	**10.36**	**-13.02**	**1.82**	**198.88**	**76.93**	**121.95**	**46.35**	**69.11**	**6.49**	**0.67**
Simulations MB	FCCLM	15.42	3.37	12.05	-3.02	1.35	13.72	-0.47	20.25	-2.65	22.90	-2.56	-11.24	36.70	0.09
	ASCLM	15.31	3.04	12.27	-2.78	1.69	13.36	-0.49	9.44	-9.08	18.52	-6.27	-15.42	40.21	0.08
	EMCLM	15.39	3.38	12.01	-4.20	2.76	13.45	-0.71	34.67	3.28	31.39	-7.82	4.25	34.96	-0.14
Difference from BATS	FCCLM-FCBATS	3.98	3.09	0.89	-1.42	-2.47	4.78	0.14	-3.78	-8.65	4.87	-22.22	-15.54	42.63	-0.14
	ASCLM-ASBATS	4.53	3.24	1.29	-0.93	-2.85	5.07	0.19	-5.45	-6.06	0.61	-16.84	-28.61	46.06	0.06
	EMCLM-EMBATS	5.20	3.95	1.25	0.62	-4.21	4.84	0.30	-0.97	-4.29	3.32	-12.60	-25.24	41.16	0.01
LSM average results	CLM Series	15.37	3.26	12.11	-3.33	1.93	13.51	-0.56	21.45	-2.82	24.27	-5.55	-7.47	37.29	-0.68
	BATS Series	10.80	-0.16	10.96	-2.76	5.11	8.61	-0.78	24.85	3.52	21.33	11.67	15.66	-5.99	-0.66
	CLM-BATS	4.57	3.42	1.15	-0.57	-3.18	4.90	0.22	-3.40	-6.34	2.94	-17.22	-23.13	43.28	-0.02

[a] Net shortwave radiation (NSR); [b] Net long-wave radiation (NLR); [c] Net radiation (NR); [d] Sensible heat flux (SH); [e] Latent heat flux (LH); [f] Net energy budget (NE); [g] Bowen ratio (β).

List of Figures

component of the 850-hPa wind, average, maximum and minimum surface temperatures, surface net solar radiation, sensible and latent heat flux and cloud coverage for the three set of experiments using the FC, AS and EM convective scheme.

FIGURE 11 As in FIGURE 9, except for evapotranspiration (ET, left panels) (mm $month^{-1}$) and cloud coverage (%, right panels).

FIGURE 12 Spatial differences of the 850-hPa wind (streamline; m s^{-1}) and geopotential height (shaded; m) between the CLM and BATS simulations during the summer season over the entire China domain for (a) FC, (b) AS and (c) EM convective scheme.

FIGURE 13 As in FIGURE 9, except for surface net solar radiation (NSR, left panels) (W m^{-2}) and maximum surface temperature (Tmax, right panels) (˚C).

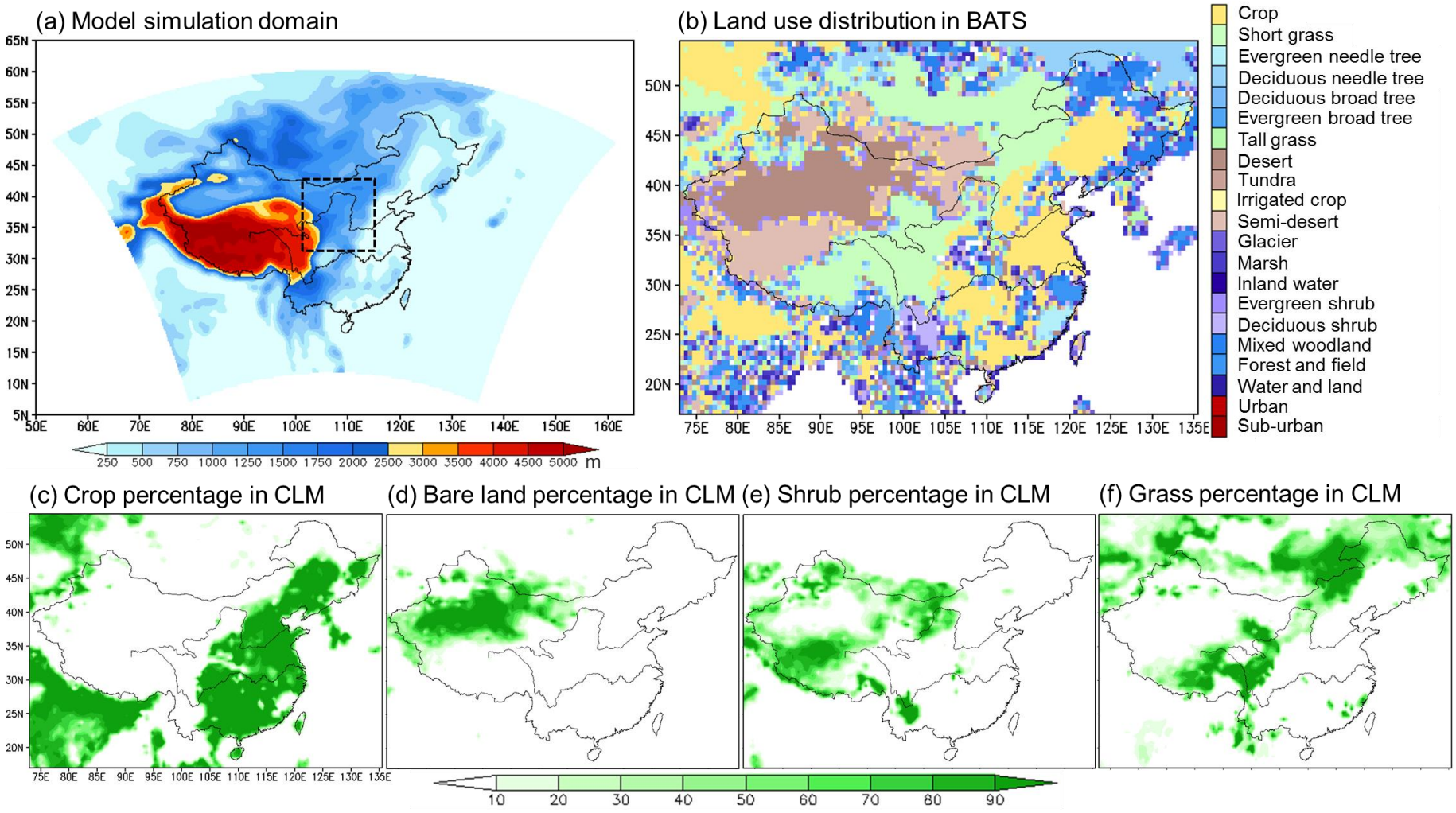

FIGURE 1 (a) Model simulation and analysis domains with elevation (shaded); (b) land use distribution in the BATS; and percentage of (c) crop land, (d) bare land, (e) shrub land, and (f) grass land in the CLM.

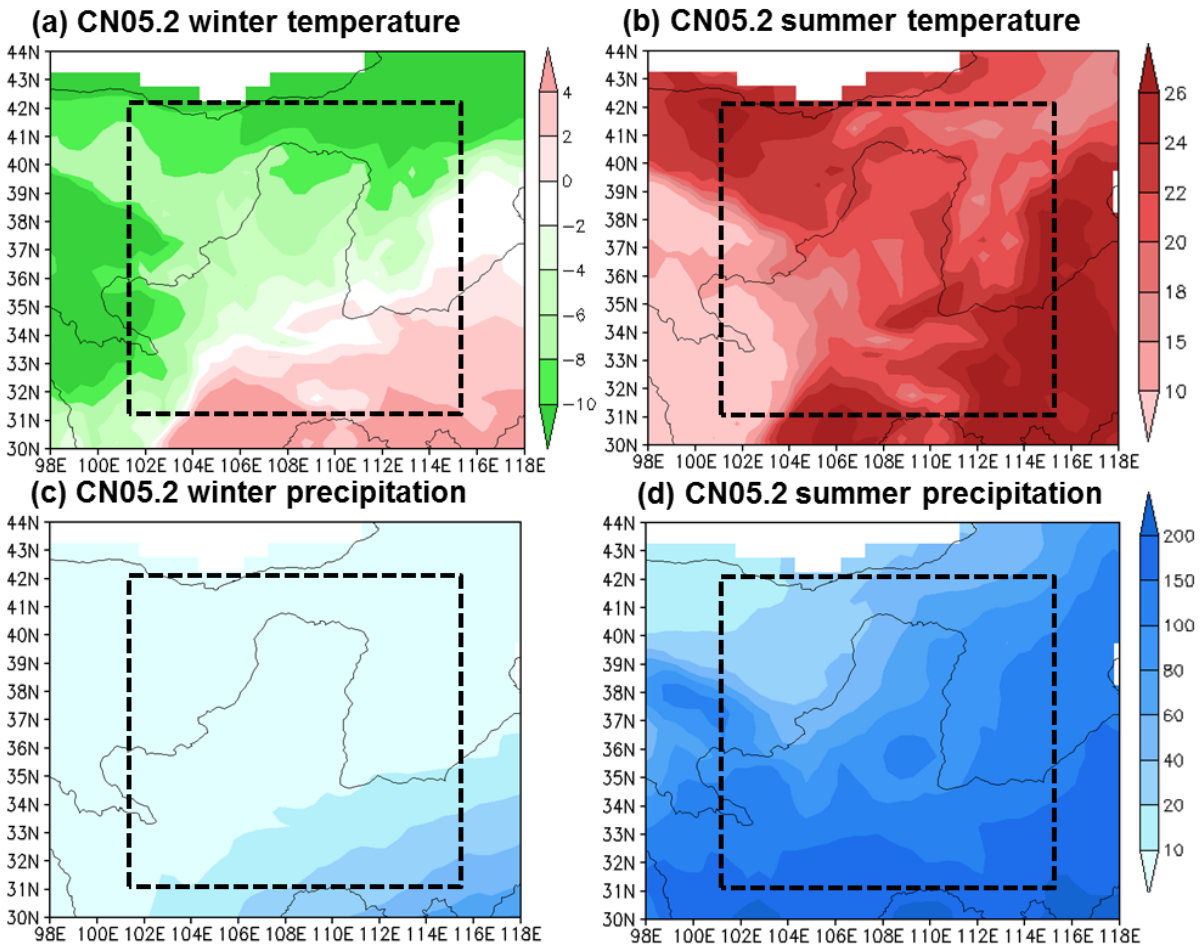

FIGURE 2 Spatial distribution of (a) winter, (b) summer surface temperature (˚C) and (c) winter, (d) summer monthly mean precipitation (mm month^{-1}) from the CN05.2 observations over the Loess Plateau domain with the analysis domain in the black dashed box.

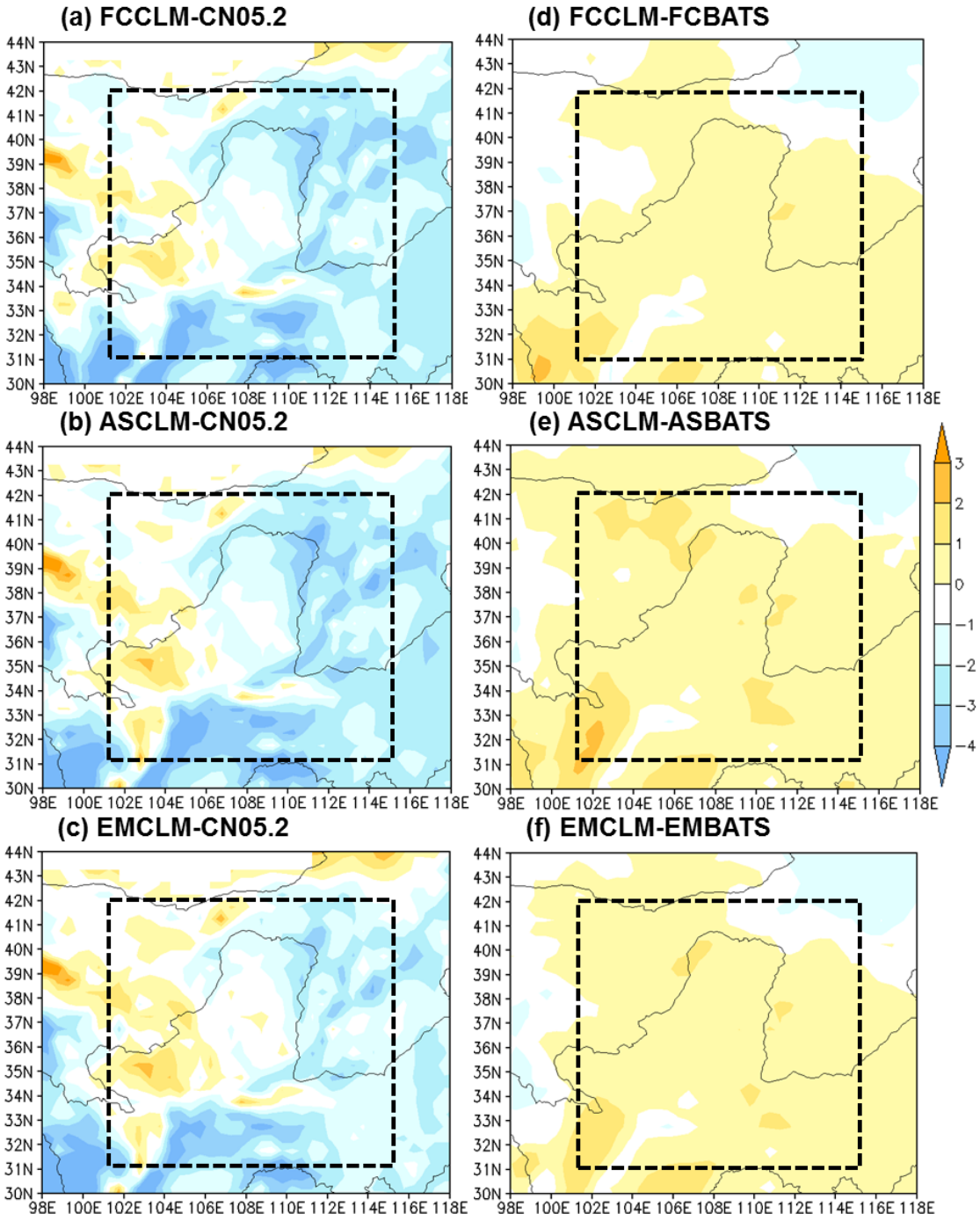

FIGURE 3 Spatial differences in winter simulated surface temperature (˚C) using the CLM from CN05.2 observations (left panels) and the BATS simulations (right panels) over the Loess Plateau domain with the analysis domain in the black dashed box for (a) and (d) FCCLM, (b) and (e) ASCLM, (c) and (f) EMCLM.

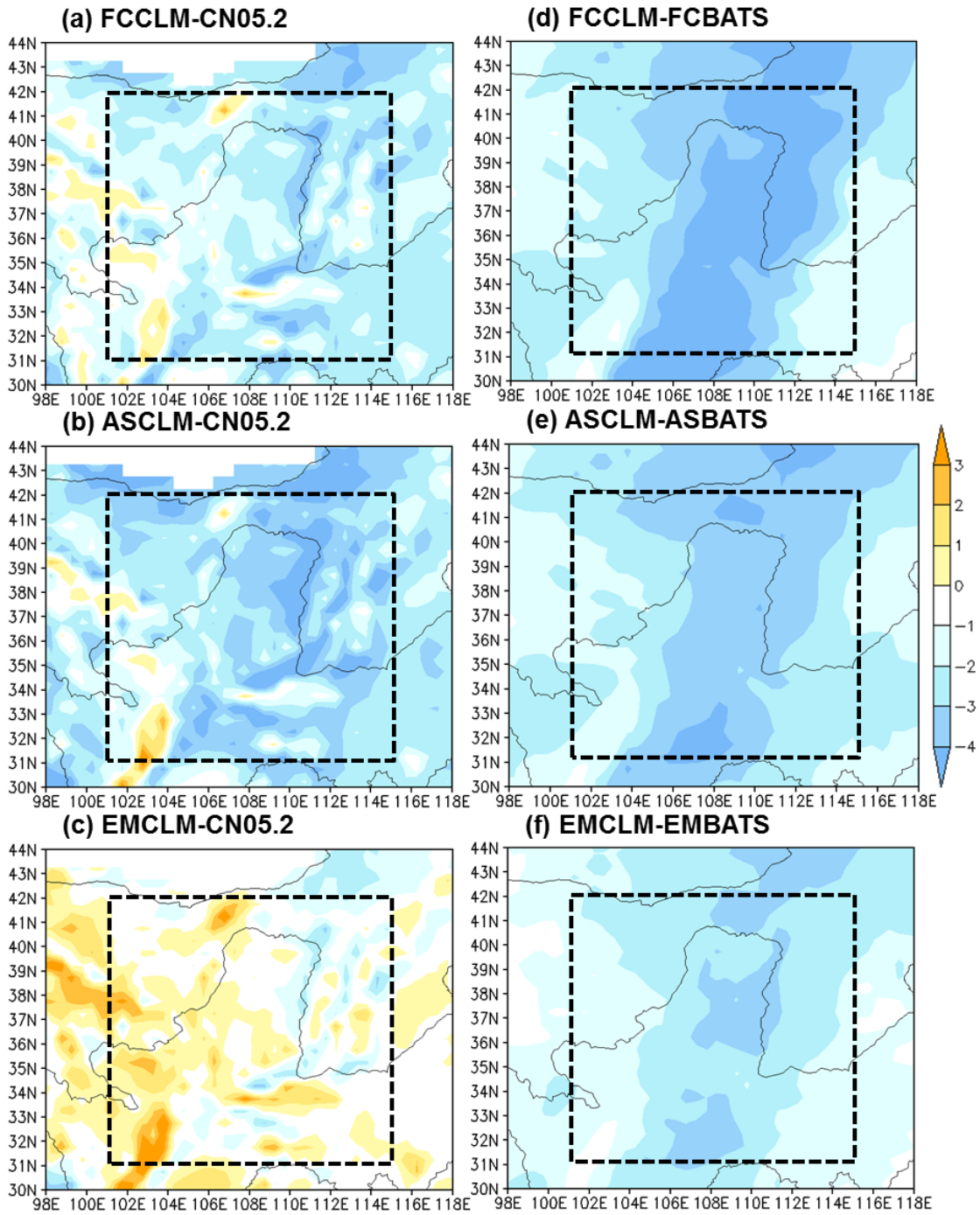

FIGURE 4 As in FIGURE 3, except for summer surface temperature (˚C).

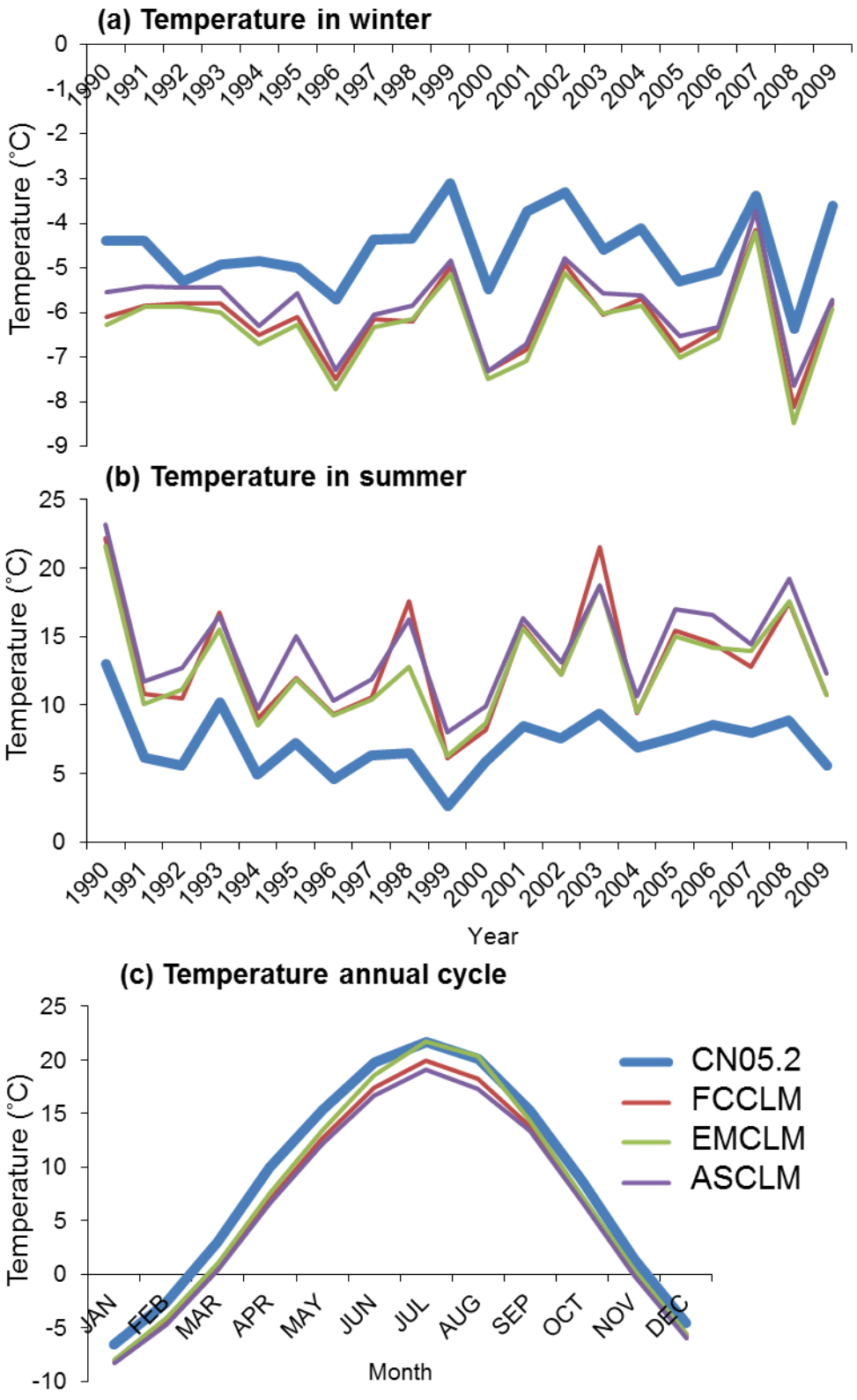

FIGURE 5 Observed and simulated (from three CLM experiments) interannual variability during (a) winter, (b) summer, and (c) annual cycle of surface temperature (˚C).

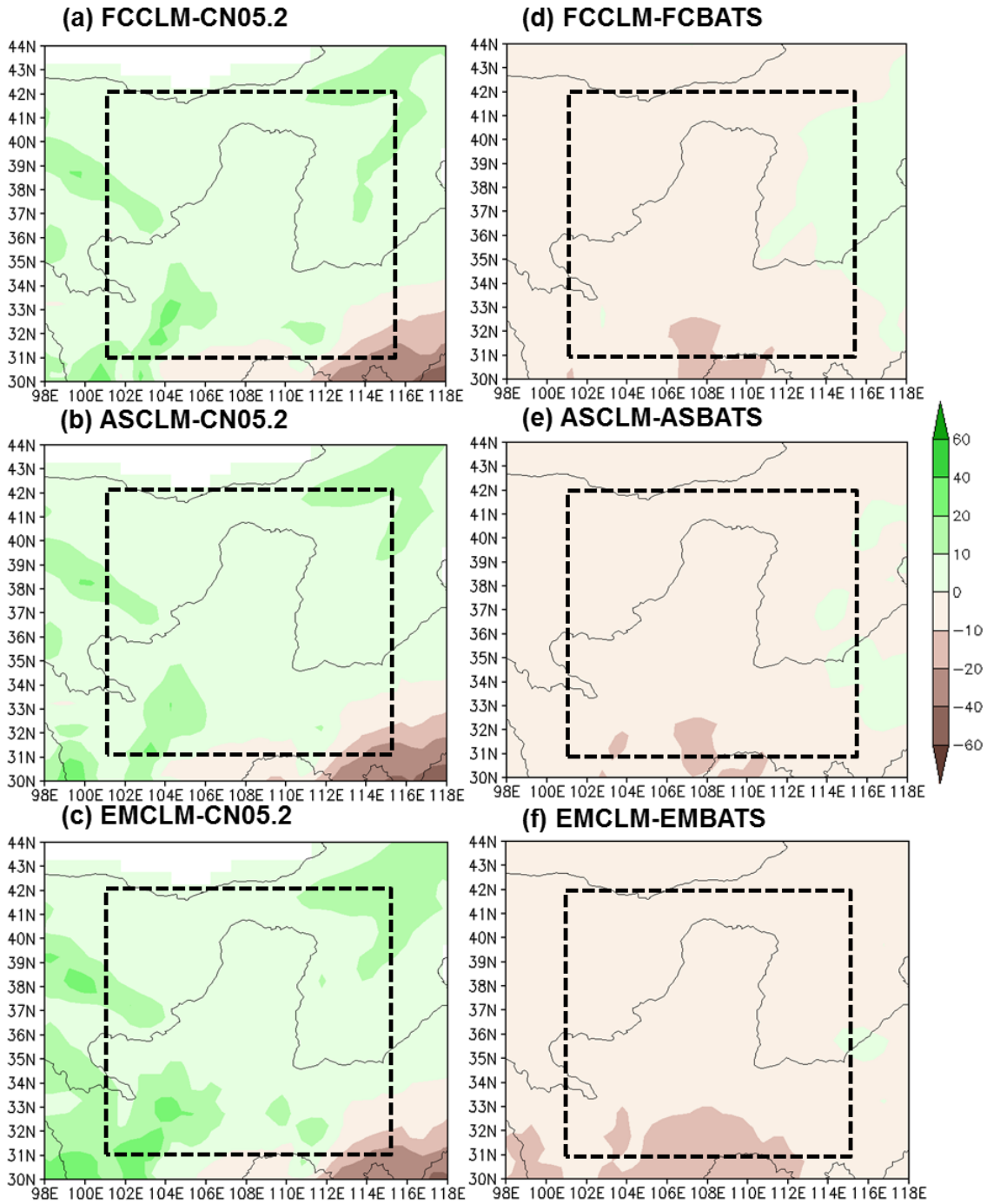

FIGURE 6 As in FIGURE 3, except for winter precipitation (mm month^{-1}).

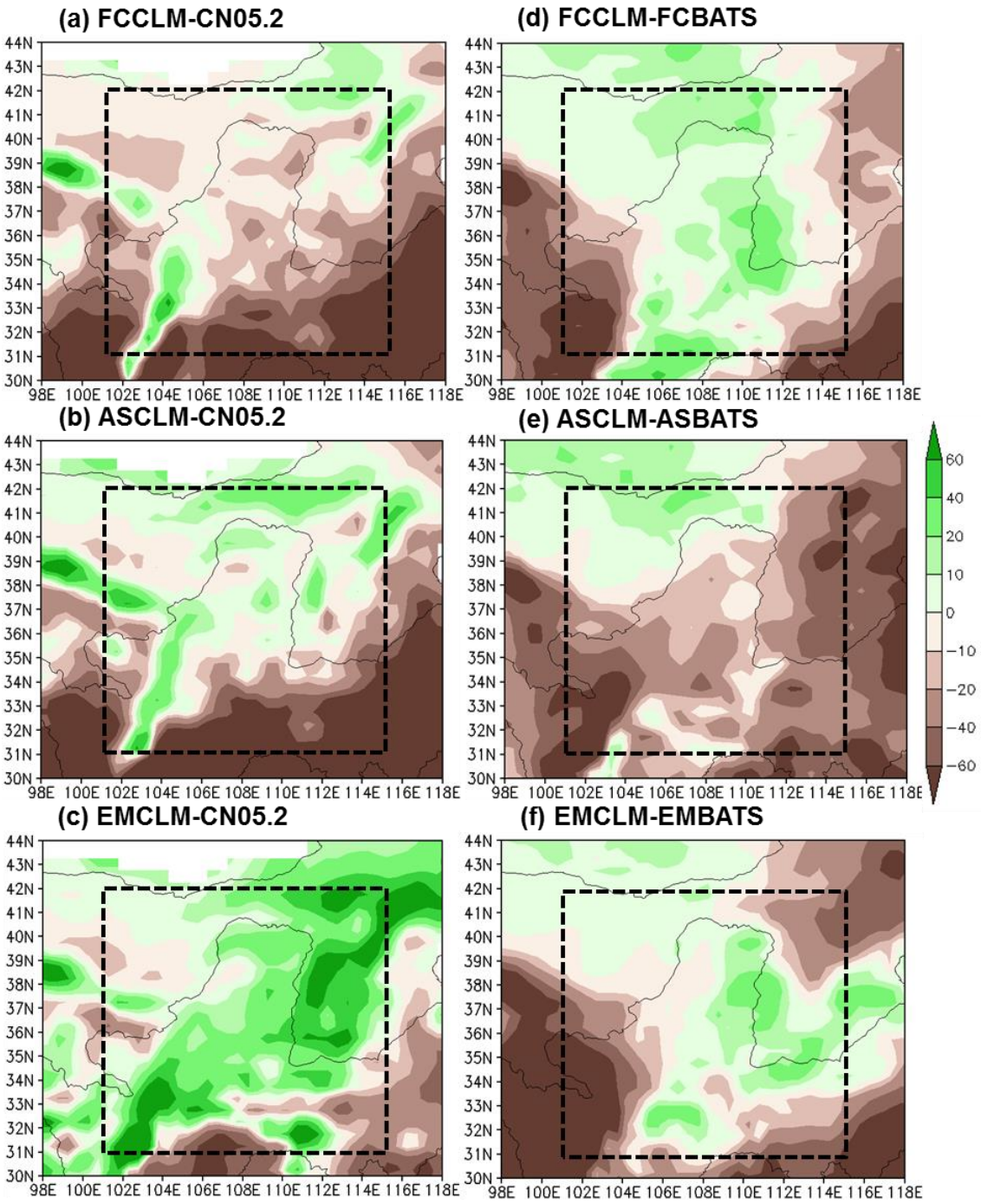

FIGURE 7 As in FIGURE 4, except for summer precipitation (mm month^{-1}).

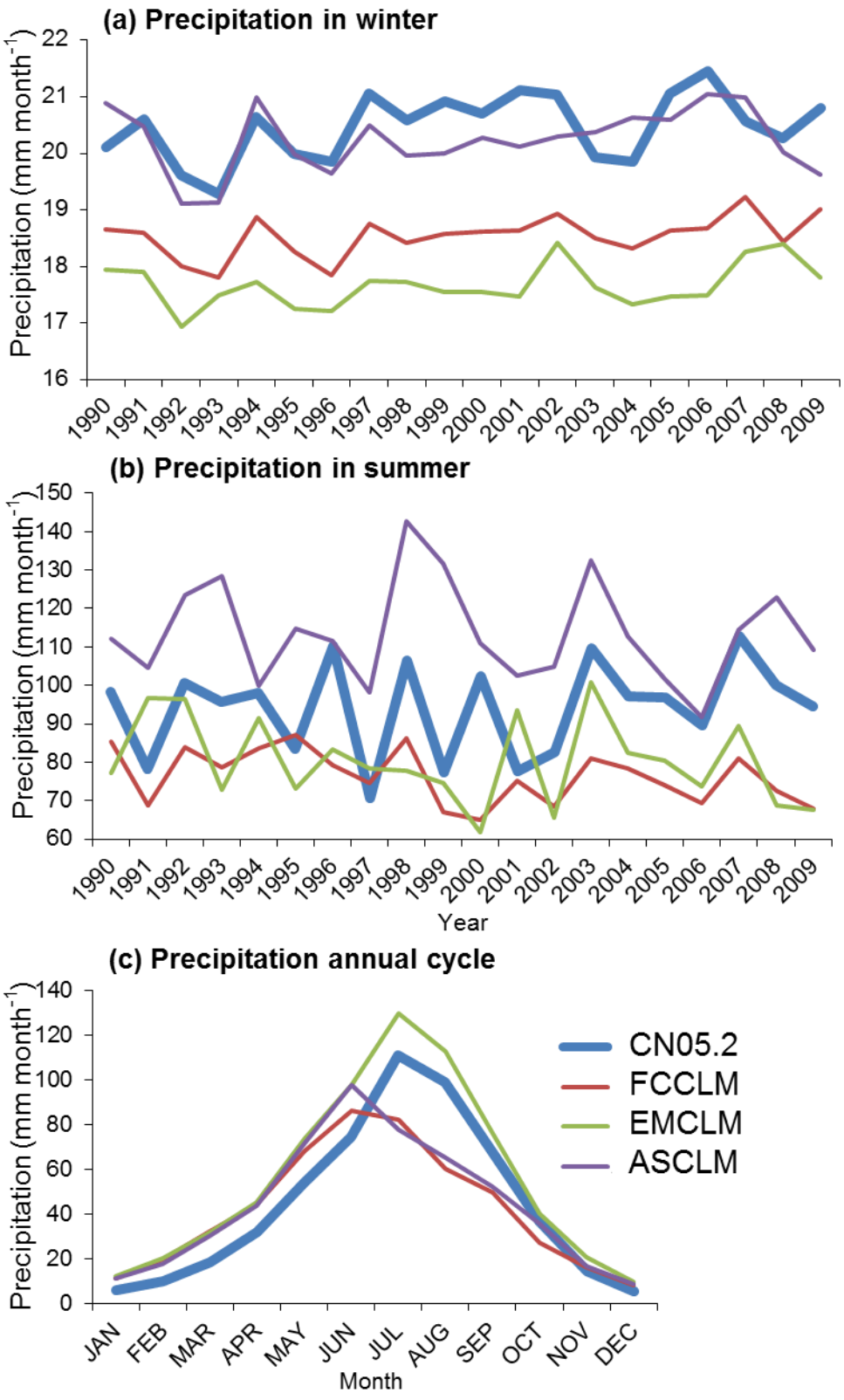

FIGURE 8 As in FIGURE 5, except for precipitation (mm month^{-1}).

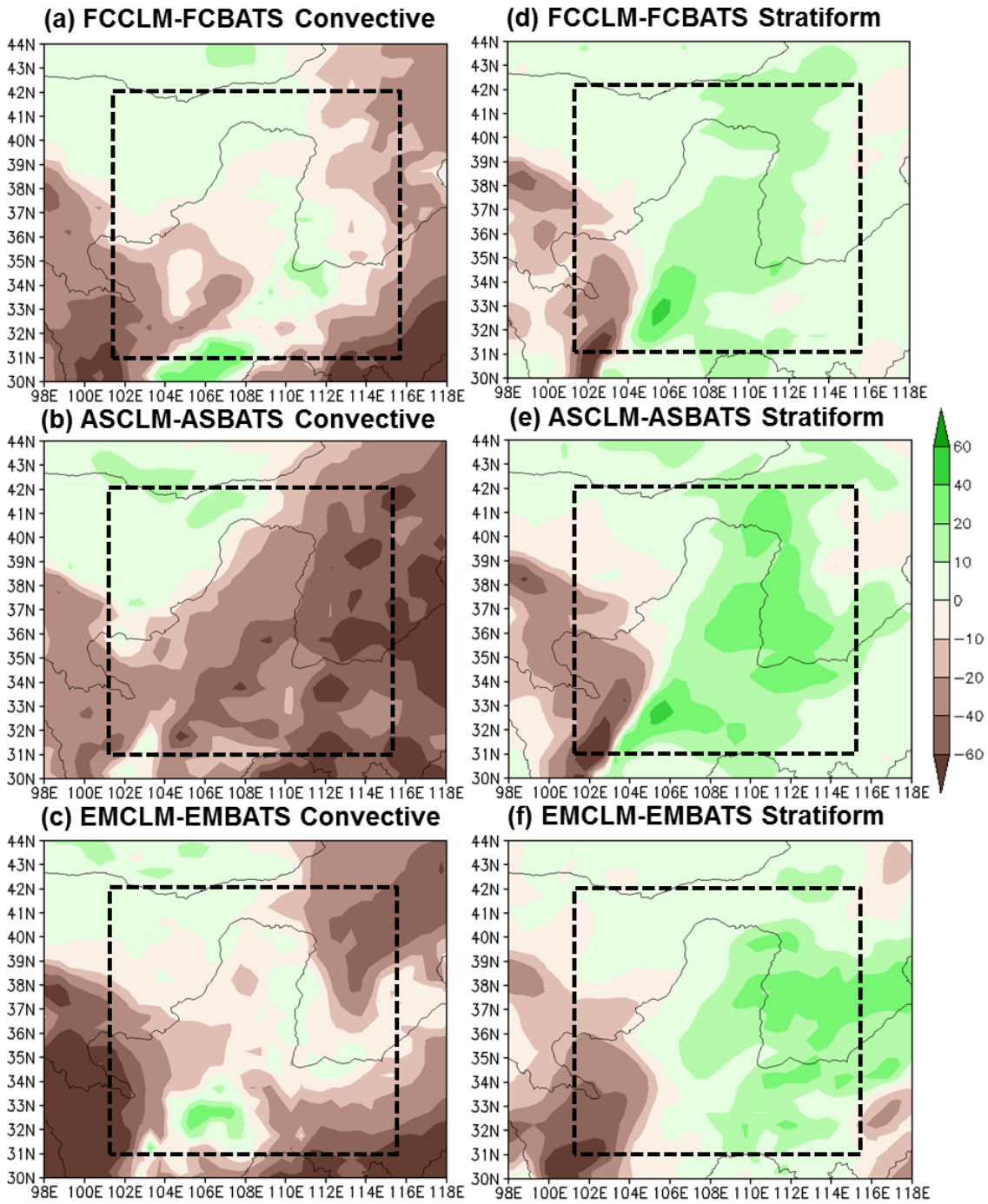

FIGURE 9 Spatial differences of summer convective (left panels) and stratiform (right panels) precipitation (mm month^{-1}) between the CLM and BATS simulations over the Loess Plateau (a) and (c) FC, (b) and (e) AS, (c) and (f) EM scheme.

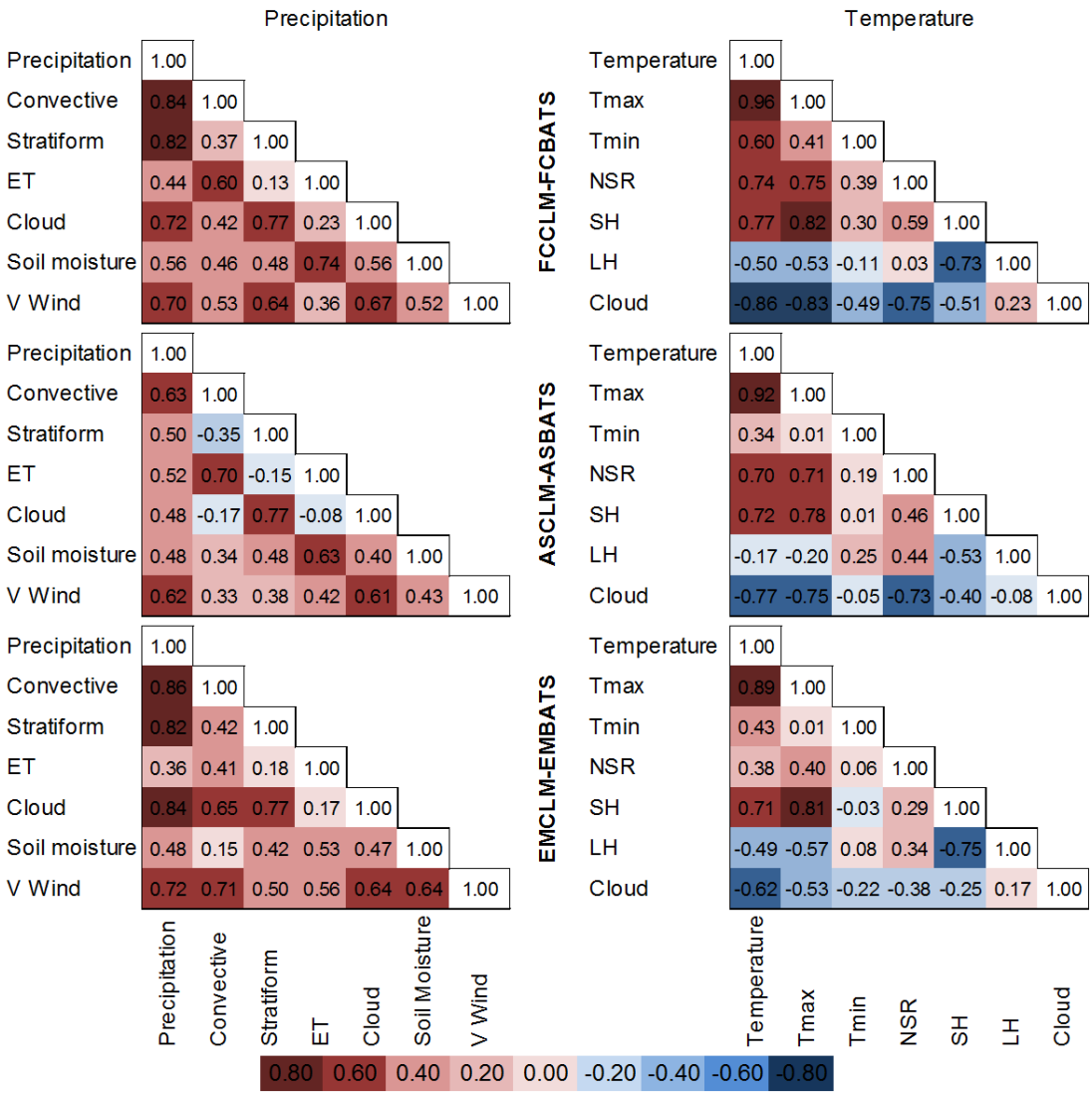

FIGURE 10 PCCs matrices of spatial precipitation (left panels) and temperature (right panels) differences between the two LSMs during the summer season over the Loess Plateau among the parameters: total, convective and stratiform precipitation, cloud coverage, evapotranspiration (ET), soil moisture of the top layer, the meridional component of the 850-hPa wind, average, maximum and minimum surface temperatures, surface net solar radiation, sensible and latent heat flux and cloud coverage for the three set of experiments using the FC, AS and EM convective scheme.

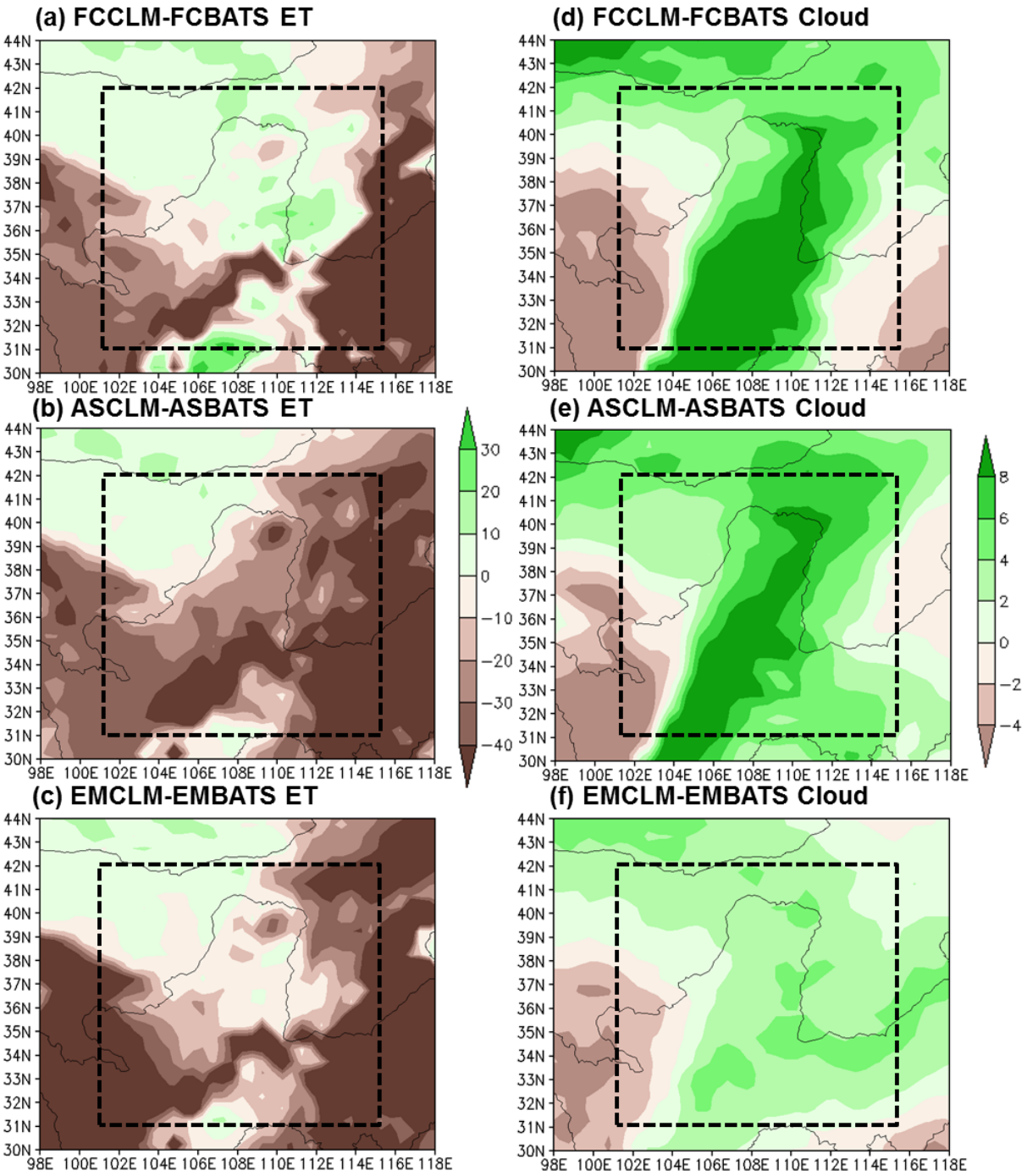

FIGURE 11 As in FIGURE 9, except for evapotranspiration (ET, left panels) (mm month^{-1}) and cloud coverage (%, right panels).

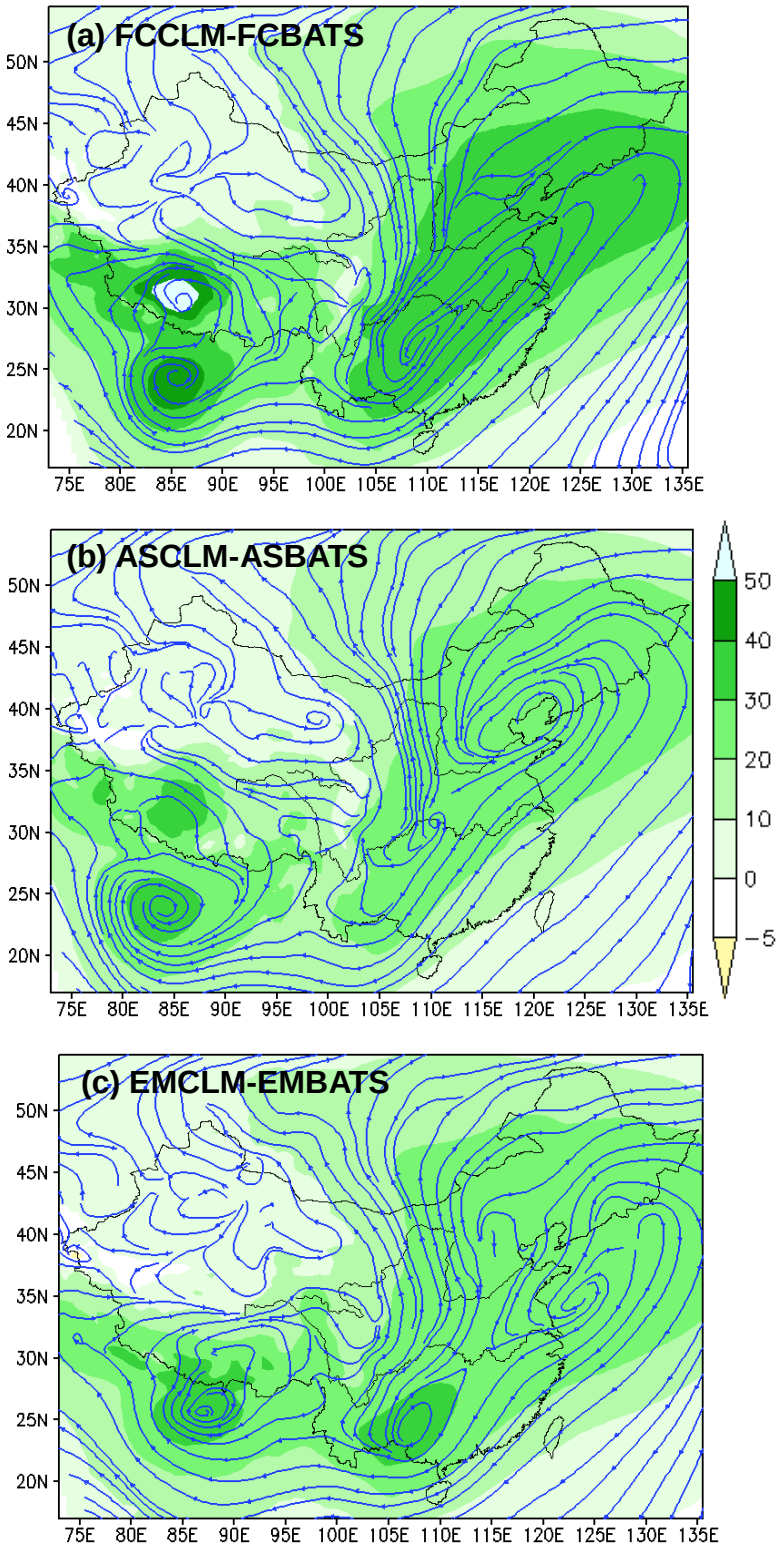

FIGURE 12 Spatial differences of the 850-hPa wind (streamline; m s^{-1}) and geopotential height (shaded; m) between the CLM and BATS simulations during the summer season over the entire China domain for (a) FC, (b) AS and (c) EM convective scheme.

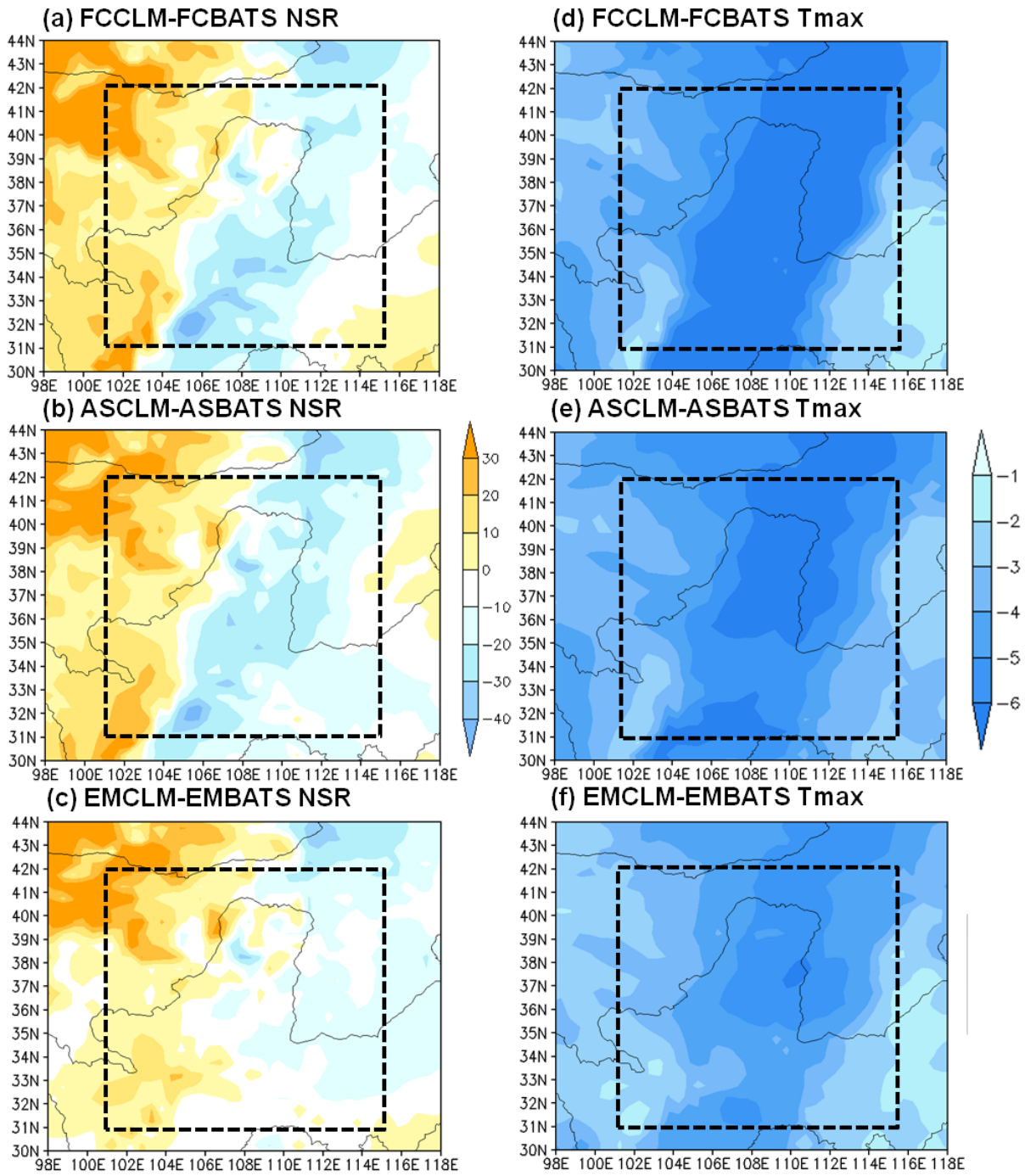

FIGURE 13 As in FIGURE 9, except for surface net solar radiation (NSR, left panels) (W m^{-2}) and maximum surface temperature (Tmax, right panels) (˚C).

Chapter 5. A Regional Climate Modelling Study over the Loess Plateau, China. Part IV: Impacts of Reforestation Programmes

The aim of the work presented in this chapter was to investigate the potential climatic effects of reforestation over the Loess Plateau region, with a focus on land-atmospheric interactions and the modulations to climate variability. The two most appropriate RegCM configurations were used in the work presented in this chapter; these configurations were identified from the evaluations in Chapters 2 to 4. We explored the dominant atmospheric dynamical processes that were responsible for the simulated impacts of reforestation on the local climate, through a series of hypothetical reforestation scenarios. These scenarios led to changes in the surface albedo, ET fluxes, roughness length and stomatal resistance, which modified the land-atmosphere interactions and further influence the regional climate features. By performing these analyses, the potential impacts of reforestation on the local climate were revealed, including its impact of mitigating climate change and improving ecosystem conditions.

Candidate's contribution to this paper

The simulations in this paper were designed and carried out by the candidate. The candidate also performs all the figure preparation and manuscript drafting. All the work was under supervision of Dr Cheung, who led the main direction of the work and guided the candidate to carry out the research.

A Regional Climate Modelling Study over the Loess Plateau, China.

Part IV: Impacts of Reforestation Programmes

Lang Wang and Kevin K. W. Cheung

Department of Environmental Sciences, Macquarie University, Sydney, Australia

Prepared for Journal of Climate

April 2015

* Author for Correspondence: Kevin Cheung, Department of Environmental Sciences, Macquarie University, North Ryde, NSW 2109, Australia. Email: kevin.cheung@mq.edu.au

Abstract

Reforestation has been considered as a strategy for alleviating diverse environmental degradation problems and mitigating anthropogenic global warming in recent years. In particular, the 'Grain for Green Project' in China is one of the key reforestation programmes that have been implemented in recent years; the primary goal of the project is to mitigate soil erosion problems across the Loess Plateau region, through converting erodible crop lands into forests. Such large changes in land cover can modify important biophysical characteristics of the land surface, potentially resulting in climate change at a variety of spatial scales. Using the Regional Climate Model (RegCM), this paper investigates the potential effects of reforestation on the regional climate over the Loess Plateau, with a focus on land-atmospheric interactions and the modulating influence of climate variability. Two land surface schemes were used here: the default Biosphere Atmosphere Transfer Scheme (BATS) and the newly coupled Community Land Model (CLM). We report on five climate simulations using a series of hypothetical reforestation scenarios from 1990 to 2009.

The conversion from agricultural land to forest led to pronounced changes in the local climate according to the BATS simulations, but medium changes in the series of CLM experiments. When the BATS was used, the surface air temperature increased and precipitation decreased significantly, during both summer and winter seasons; these patterns were particularly evident over the southeast of the plateau, where extensive areas of irrigated crop land were converted to forest. The conversion of irrigated crop lands substantially reduced the levels of evapotranspiration (ET) and this, in turn, primarily led to a diminished latent heat flux and increase in temperature, as well as the decrease in precipitation simulated. In contrast, in the CLM simulations, in which irrigated crops were not differentiated from non-irrigated ones, reforestation generally produced a warmer

winter, as well as a cooler and more humid summer. The higher temperatures in winter were largely attributed to a reduction in the albedo by the darker forest. During summer, reforestation induced a larger roughness length and increased ET rates, which favoured an increase in water vapour in the atmosphere and thus led to the increase in precipitation and reduction in temperature. Therefore, this study, suggests that coupling the RegCM with the BATS and the CLM can generate opposite climate responses to the same land use change scenario; the critical reason found for these opposite responses was the different representation of the irrigated crop land in the two land models. The study highlights the need for better descriptions of land surface characteristics in climate models, to enable the reliable prediction of climate responses to land surface change.

Keywords:

Regional climate model; Biosphere Atmosphere Transfer Scheme; Community Land Model; Loess Plateau; Reforestation

1. Introduction

The Intergovernmental Panel on Climate Change (IPCC) Special Report on Land Use, Land-Use Change and Forestry states that reforestation practices are considered to be a strategy for alleviating diverse environmental degradation problems and mitigating greenhouse gas emissions, by carbon sequestration into forest biomass (Nabuurs et al. 2007). Various reforestation projects have been implemented for such purposes around the world in recent years (e.g., Ribaudo et al. 1990; George et al. 1999; World Bank 2000; Walker et al. 2002; Foley et al. 2005; Watson 2009; Abiodun et al. 2012).

The 'Grain for Green Project' (GGP) in China is considered to be one of the key reforestation programmes implemented in recent years (Cao et al. 2011). It started in 1999 and predominantly covered the Loess Plateau region, in northern China. The primary goal of the GGP is to conserve water and soil resources that are impacted by severe soil erosion; this soil erosion is caused by a series of natural and anthropogenic factors across the Loess Plateau, including the local loose soil texture, gully and hilly terrains and summer extreme rainfalls, as well as low vegetation coverage and highly erodible cultivation practices. The GGP is primarily concerned with anthropogenic effects on soil erosion and has focussed on reducing the area of erodible cultivation practices. Crop lands and bare lands with slopes over 25˚, which are more vulnerable to erosion, have gradually been replaced by natural vegetation through the GGP (e.g., Li 2004; McVicar et al. 2007; Lü et al. 2012). As a result of the GGP, the land surface over the Loess Plateau has experienced a significant change since 1999. By the end of 2008, the area of farming land had decreased from 40.80% to less than 30%, of the total area of the plateau. Meanwhile the area of woodland (forest and bush land) had increased from 11.91% to over 16%; and grassland had increased from 38.97% to over 43% of the total plateau area (Lü et al. 2012). Over the next two decades,

the GGP proposes to convert another 17% of the erodible areas on the plateau to natural vegetation (NDRC et al. 2010).

Associated with the increase in natural habitats, positive environmental impacts of the GGP have been captured, such as reductions in the amount of erosion and flood risk (McVicar et al. 2007; Fu et al. 2011; Li et al. 2011), although certain negative effects, such as a dried soil layer and decrease in stream flow have also been shown (e.g., He et al. 2003; Sun et al. 2006; Cao 2008; Cao et al. 2011). The potential influence that the GGP has had, and will have, on global and regional climate change remain unclear. A better understanding of the climatic effects would guide policymakers on the pros and cons of creating such reforestation belts over these regions, from the point of view of climate change.

The Loess Plateau and its surrounding regions are considered one of the world's most climatic sensitive areas (Stocker et al. 2013). The plateau is located in the largest climate transition area in northern China, between the humid East Asian monsoon region and the continental semi-arid region (Huang et al. 2008). Extensive land surface modifications across the plateau could lead to changes in the complex conditions of the local climate (e.g., Chang and Krishnamurti 1987; Chang 2004). Most of the published studies, on land surface changes in China, have characterized large-scale climate responses and have not explicitly documented the climatic effects of reforestation over the Loess Plateau (e.g., Xue 1996; Fu and Yuan 2001; Zheng et al. 2002; Liu et al. 2008c, Fan et al. 2015a, Fan et al. 2015b). The local climate is critical for the rain-fed agriculture and natural vegetation, primarily through affecting the water availability, in this semi-arid area. Therefore, it is important to understand the local climate and be able to predict the potential impacts of such land surface changes on the climate.

Extensive land cover changes caused by reforestation impact the climate through their interactions with atmospheric systems on a variety of spatial scales. The interactions occur primarily through the modification of land surface biophysical properties, such as soil water content, surface albedo, evapotranspiraton (ET) and surface roughness (Pielke et al. 2002; Foley et al. 2003; Field et al. 2007; Anderson 2010). For instance, forested areas generally have a lower surface albedo, compared to agricultural land; this appears to result in an increase in the amount of energy absorbed by the surface, which in turn favours an increase in surface air temperatures and may enhance precipitation (Charney et al. 1977; Sud and Fennessy 1982; Betts 2000; Bonan 2008). Meanwhile, forests are more efficient at ET and thus are able to partition more energy into latent heat, which means that they are more likely to lead to a decrease in surface air temperatures and possibly an increase in precipitation (Shukla and Mintz 1982; Bounoua and Krishnamurti 1993; Zeng et al. 1999; Bonan 2008). The overall effects of reforestation on the climate vary significantly across regions, dependent on the relative importance of the biophysical processes, which in turn depend on the local climate background (Snyder et al. 2004; Bonan 2008; Chen et al. 2012).

In addition to the effects of reforestation on albedo, a higher roughness length of forested areas compared with crop lands, can also impact on climate systems. The higher roughness length favours the generation of more mass convergence, associated with an anomalous low-pressure system, which enhances upward moisture transport and convective clouds, thus increasing precipitation (Dickinson and Henderson-Sellers 1988; Sud et al. 1988; Bonan 1997; Pielke 2001). For instance, Xue and Shukla (1996) used a general circulation model (GCM) and found that precipitation increased by 0.8 mm day^{-1} over the reforested area in the Sahel; this was primarily caused by the changes in moisture convergence due to changes in roughness length. Higher roughness length can also reduce

near surface wind, thereby changing temperature and moisture advection (Liu et al. 2008c; Zhang and Gao 2009; Zhang et al. 2009; Liu 2011; Abiodun et al. 2012). Liu (2011) evaluated the potential climate effects of reforestation over the southeast United States using a regional climate model (RCM). They captured a decrease in precipitation during summer, mainly due to the increased surface roughness of the forest, which reduced the prevailing winds that transport the moisture.

The general influence of land surface changes on regional climate has been investigated using a wide range of GCMs, RCMs and observational studies (e.g., Pielke and Avissar 1990; Nobre et al. 1991; Chase et al. 2000; Bounoua 2002; Oleson et al. 2004a; Feddema et al. 2005; Findell et al. 2007). In particular, RCMs, with a more pronounced climate response to land changes at the local scale than GCMs, are the most appropriate for the subject of this study; they also have a finer horizontal resolution and so are able to represent land surfaces patterns adequately (e.g., Copeland et al. 1996; Gao et al. 2003; Jackson et al. 2005; Zhao and Pitman 2005; Findell et al. 2007; Liu 2011).

The primary aim of this study was to improve our knowledge on how reforestation activities over the Loess Plateau could alter the local climate. The study used the Regional Climate Model (RegCM) to examine the modelled climate response to different land surface change strategies. We also upgraded the land surface scheme from the Biosphere Atmosphere Transfer Scheme (BATS, Dickinson et al. 1993) to the newly coupled Community Land Model (CLM, Oleson et al. 2004b, 2008), and compared the two LSMs through a series of experiments. The outcomes are to (1) identify the sensitive climate features to land cover change under these two land surface schemes, (2) explore the dominant model dynamical and physical responses to land surface changes induced by reforestation, and (3) quantify the uncertainties underlying the two land surface schemes and their impacts on the model simulations. In the following, section 2 reviews the

performance of RegCM in regard to land surface changes, and depicts our experimental design. The model simulation results on temperature and precipitation are analysed in section 3. Section 4 then discusses the physical processes associated with the simulated land surface changes. Conclusion is provided in section 5.

2. Methods

a. The RegCM

The climate model used in this study is the RegCM version 4.3 (RegCM4.3), which was developed for regional climate simulations by the International Centre for Theoretical Physics (ICTP) (Giorgi et al. 2012). The model uses a dynamic core of the Mesoscale Model (MM5), from the National Centre for Atmospheric Research (NCAR) of Pennsylvania State University (Grell et al. 1994). The model applies the radiation scheme from the NCAR Community Climate Model 3 (CCM3) (Kiehl et al. 1996). The modified planetary boundary layer scheme is parameterized by Holtslag et al. (1990).

The stratiform precipitation is generally related to large-scale weather systems. The model decides the formation of stratiform precipitation when the atmosphere is saturated, based on the sub-grid explicit moisture scheme (SUBEX) (Pal et al. 2000) and the variability of sub-grid clouds (Sundqvist et al. 1989). The convective precipitation, on the other hand, is formed with intense upward motion of the air mass. There are four convective scheme options: the Kuo scheme (Anthes 1977), the Grell formulation (Grell 1993; Grell et al. 1994) with the Arakawa-Schubert closure assumption (Arakawa and Shubert 1974), the Grell formulation with the Fritsch-Chappell closure assumption (FC, Fritsch and Chappell 1980), and the Emanuel scheme (EM, Emanuel 1991; Emanuel and Zivkovic-Rothman 1999).

There are two options of land surface model in the RegCM4.3 system. The first land surface model (LSM) is the BATS (Dickinson et al. 1993), which applies one vegetation canopy layer, a single snow layer, three soil layers and a simple surface runoff model. Land surface variables are calculated within these layers. The BATS also includes 20 surface categories and 12 soil colour and texture types, which are derived from the Global Land Cover Characterization (GLCC) dataset, based on 1 km Advanced Very High Resolution Radiometer (AVHRR) land cover data, collected from April 1992 to March 1993 (Loveland et al. 2000). A land surface category at each model grid is assigned, according to seasonal parameters, such as roughness length, maximum and minimum leaf area index (LAI), stem area index (SAI), vegetation albedo and minimum stomatal resistance (Dickinson et al. 1993).

The other LSM is the CLM version 3.5 (Tawfik et al. 2011). In the CLM, the land surface in a grid cell can consist of up to 4 patches, including glacier, wetland, lake and vegetated; the vegetated portion is itself composed of one of 17 plant function types (PFTs) (Oleson et al. 2004b, 2008). In particular, the PFTs determine the plant physiology (leaf optical properties, stomatal physiology, and leaf dimensions) and structure (canopy height, roughness length, displacement height, root profile, LAI and SAI). The PFTs and other patches also use the GLCC land cover map, as well as the multi-year Moderate Resolution Imaging Spectroradiometer (MODIS) products (Lawrence et al. 2007) to determine the land physical properties. Particularly, LAI parameters in CLM were derived from the monthly MODIS LAI data of Myneni et al. (2002) that was averaged for the 2001–2003 time period to produce climatological monthly LAI.

The CLM bio-geophysical parameterisations differ significantly from the BATS. For example, the CLM applies multiple land surface types in a grid cell, while the BATS assigns only one land cover type for each grid cell. Consequently, fine-scale heterogeneity

of land cover, such as that present over the Loess Plateau region, is better represented in the CLM. Furthermore, the CLM has 10 layers for soil water and soil temperature, with explicit treatment of liquid water and ice; in contrast, the BATS only has 3 layers that account for liquid water. Both models use the Monin-Obukhov similarity theory for surface fluxes, but with different aerodynamic resistance formulations and flux gradient relations. Snow layers, surface runoff and base flow are also parameterized differently. A detailed description of the differences between the CLM and BATS can be found in Steiner et al. (2005) and Wang and Cheung (2015c).

Another difference between the two LSMs for this study, is the representation of irrigated crops, which may have important implications for the response of the climate system. The BATS includes two agricultural land categories: irrigated crop and non-irrigated crop. To mimic the effects of irrigation in the BATS, where irrigated crops are present, the RegCM4.3 assigns the soil moisture of the root zone (top 1 m) to be at field capacity during every time step (Dickinson et al. 1993). As a consequence, high ET fluxes are produced from irrigated crop areas, which could be overestimated over the Loess Plateau, because it is a semi-arid region where the soil water availability is generally low and is the primary limiting factor of ET (Dickinson et al. 1993). In contrast, the CLM only includes one category of agricultural land, called ‘crop land’; its characteristics are similar to the non-irrigated crop land category in the BATS. Accordingly, the ET fluxes of crop land in the CLM are restrained by the availability of soil water, which depends on the variability of the surface water budget (Pal et al. 2007).

b. Past performance of the RegCM

The RegCM has previously been validated and applied for investigating the impacts of land surface changes on the climate over China (e.g., Zheng et al. 2002; Gao et al. 2003;

Gao et al. 2007; Liu et al. 2008c; Wu et al. 2012). For example, Zheng et al. (2002) and Liu et al. (2008c) used version 2 of the model to simulate the climatic response to a series of land surface change scenarios; overall, they found that the conversion from bare soil and crop land to forests over northern China increased precipitation locally. Liu et al. (2008c) additionally found that land surface change led to a reduction in both the temperature and prevailing winds. Gao et al. (2007) applied version 3 of the model to compare the potential and current vegetation patterns and their impacts on the local climate. Their results showed different climate responses to the land surface changes between northern and southern China. In particular, they found that natural vegetation, with large areas of grass and bush land over the Loess Plateau region, was likely to produce more rainfall and lower temperatures during summer, compared with the current vegetation patterns which comprise extensive areas of crop land.

The RegCM results aforementioned are consistent with other RCM studies that have considered similar land use changes over China (e.g., Fu and Yuan 2001; Wang et al. 2003; Zhao and Pitman 2005); however, there have been some conflicting results of the climate responses to the same changes in land cover from other RCMs. For example, Zhang et al. (2009) studied the impact of changes from natural vegetation to the current vegetation, using the Australian Bureau of Meteorology Research Centre model, and found that natural vegetation tended to generate less summer preciptaiton over China, which is the opposite sign to that captured by Zhang and Gao (2009) using the RegCM. The major factor that explained the differences in summer precipitation between the two models appeared to be the difference in the simulated monsoon spatial pattern. Therefore, more accurate models are required to simulate changes in the climate and gain confidence in our understanding of the impact of land surface changes under current climate conditions.

Another approach to increase our confidence in the performance of RegCM is to improve the robustness of the LSM. Considering the high heterogeneity of the land surface, one possible deficiency in the RegCM, suggested by previous studies, is the relatively simple representation of the land surface characteristics and their interaction processes with the atmosphere (e.g., Steiner et al. 2005; Steiner et al. 2009; Winter et al. 2009; Gianoti et al. 2012; Im et al. 2014; Wang and Cheung 2015c). Past studies have noted that the RegCM coupled with the CLM performs better in simulating several characteristics of the climate, compared to the BATS (e.g., Steiner et al. 2005; Diro et al. 2012; Mei et al. 2013; Reboita et al. 2014). However, very few published studies have investigated the potential uncertainty in simulations using the two LSMs to force the climate, when associated with changes in the land surface (e.g., Bonan et al. 2002; Xue et al. 2004). It is thus necessary to identify the potential causes of such uncertainties, thereby enhancing our understanding of the effects of reforestation on the climate.

c. Experimental design

A set of RegCM4.3 simulations was conducted to investigate the impacts of land surface changes induced by reforestation on the local climate. Our previous study found that the BATS coupled with the FC convective scheme (BATSFC), and the CLM coupled with the EM scheme (CLMEM) were the two configurations with 50 km resolution in RegCM4.3 which represented the most realistic local climate over the Loess Plateau (Wang and Cheung 2015c). These configurations were driven by the European Centre for Medium-Range Weather Forecasts (ECMWF) Reanalysis Interim dataset, at a horizontal resolution of $1.5^{\circ} \times 1.5^{\circ}$. Their domains covered the entire of China and its surrounding regions (Wang and Cheung 2015c).

The experiments conducted in this study used the two configurations of the LSMs and convective schemes, but at a 20 km horizontal resolution. The experiments using the BATS coupled with the FC scheme (BCTL, BFOR and BCRP) were downscaled from the previous BATSFC simulation, through the one-way nesting method. Similarly, the experiments using the CLM coupled with the EM scheme (CCTL and CFOR) were downscaled from the previous CLMEM simulation (Table 1). The experiments used a domain limited to the Loess Plateau and its surroundings, centred on 37˚N and 108˚E and spanned approximately 22˚N–50˚N and 92˚E–122˚E (Fig. 1). The domain included the relevant regional forcings and was assessed using a realistic representation of the local land surface (Wang and Cheung 2015b). Weekly sea surface temperatures (SST) were incorporated from the National Oceanic and Atmospheric Administration (NOAA) Optimum Interpolation (OI) SST dataset, at 1˚ grid spacing. All model simulations were performed over 20 years, from January 1989 to December 2009 (with the year of 1989 used for the model spin-up); this covered the period of GGP programme land changes, to explore the impacts of reforestation on the modelled climate.

The simulations in this study used three land surface type scenarios, with different distributions of reforested lands and crop lands (Table 1; Fig. 1; Fig. 2). The first two configurations (BCTL and CCTL) applied the default land surface map, using the BATS and CLM LSMs, respectively, were considered as the pre-reforested, control simulations. The second two configurations (BFOR and CFOR) allowed an assessment of the potential impacts of reforestation, through the conversion of all the crop lands into forest lands (temperate broadleaf deciduous trees); in the BFOR simulation, which used the BATS, both the irrigated and non-irrigated crop lands were converted into forest. To consider the difference between the original land surface categories in the two LSMs (i.e., the erroneous parameterization of irrigated crop lands in the BATS), a third experiment using the BATS

(BCRP), was designed; in this simulation, the default irrigated crop land was converted into crop land over the plateau region, so that the land surface distribution was more similar to the original land surface distribution of the CLM (in the CCTL simulation). Therefore, simulated differences in the climate between the BFOR and BCRP experiments were only associated with the replacement of crop land by the forest and were more comparable to the climate differences simulated between the CFOR and CCTL experiments.

The vegetation pattern changes among these simulations were limited to the boundary of the Loess Plateau region of China (Fig. 1f–g, Fig. 2e–f). This region was between 31–42˚N and 101–115˚E and was also used for as the analysis domain for the statistical analyses of the entire plateau. Another analysis domain focused on the irrigated region over the southeast of the plateau in the BATS simulations, hereafter referred to as the irrigated analysis domain (between 31–35˚N and 110–115˚E; Fig. 1a). Furthermore, the changes in vegetation characteristics such as LAI, surface albedo and roughness length were slightly different between the two LSMs (Table 2).

In order to validate and compare the modelling results, both observational and reanalysis data were used: the China Meteorological Administration Meteorological Information Centre data set version 5.2 (CN05.2) (Xu et al. 2009) and the ECMWF Interim reanalysis data set. The CN05.2 data set, at a horizontal resolution of 50 km, provided monthly mean, maximum and minimum surface air temperatures, as well as monthly mean precipitation for the entire simulation period. A detailed analysis of the CN05.2 data set was performed in a separate study, which showed that it is reliable over the Loess Plateau (Wang and Cheung 2015a). The ECMWF Interim reanalysis data set, at a 1.5˚ horizontal resolution (around 1500 km), was used to provide observational data of convective and

stratiform precipitation, surface energy budget components (radiation fluxes, sensible and latent heat fluxes) and surface water budget components (ET and soil moisture).

3. Results

a. Model validation of the CCTL and CFOR

Prior to the analyses of the models' simulated changes in the climate as a result of the land surface changes, the simulated surface climate derived with the CCTL configuration, using the default vegetation data set, was validated. The BCTL configuration was validated in Wang and Cheung (2015a, b), showing that the configuration generally performed well at reproducing both the surface temperature and precipitation patterns. In this study, the CCTL configuration was also found to represent most of the climate features well. In fact, it was better than the BCTL configuration in simulating precipitation during winter, and temperature during both winter and summer. In particular, during the winter the observed cold regions over the north and the west of the plateau were captured reasonably well by the CCTL (Fig. 3a); in the summer season, the hot centres over the southeast region of the plateau were also captured (Fig. 3b). In terms of precipitation, in observations the amount of precipitation increased from the northwest to the southeast in both winter and summer seasons, but the amount of summer precipitation was much higher than that in winter. Both of these patterns were reproduced by the CCTL (Fig.4a–b). Furthermore, the inter-annual variability and annual cycle of the surface temperatures and precipitation in both seasons were mostly captured in the CCTL (Fig. 5).

The skills of the CCTL configuration, in simulating some of the more detailed local climate features were less satisfactory. For example, the winter temperatures over the northeast and southwest of the plateau were slightly underestimated, by around 2˚C (Fig.

3c), while the summer temperatures were mostly overestimated over the western region by 1˚C (Fig. 3d). The model also tends to overestimate precipitation during both seasons, especially over the northeast and southwest mountainous regions (Fig. 4c–d). The largest positive bias of precipitation was simulated during the summer season over these mountainous areas, with a few overestimations over 60 mm month^{-1}. Compared with the BCTL that applied BATS, the CCTL mitigated the temperature biases in both seasons (Fig. 3e–f), by on average 0.75˚C in winter and 1.36˚C in summer (Table 3 and 4); as well as this, the winter precipitation was slightly improved (Fig. 4e). However, the magnitude of the summer precipitation bias simulated by the CCTL configuration was larger than that by the BCTL, by on average 15.86 mm month^{-1} (Table 4).

The model deficiencies and simulated climate features from the two LSMs were mostly seen in the 50 km resolution simulations from which they were downscaled (Wang and Cheung 2015b, c). In particular, the apparently high summer precipitation levels in the CCTL, and its driving simulation (CLMEM), were mostly caused by the EM convective scheme. The EM scheme was found to generate excessive summer convection compared with the FC convective scheme, used in the BCTL and its driving simulation (BATSFC); this has also been shown in many other studies (e.g., Pal et al. 2007; Im et al. 2008; Davis et al. 2009; Zanis et al. 2009). Nevertheless, in general the model simulation produced using the CCTL configuration was more consistent with the observations, compared with the BCTL over the plateau; this outcome was related to the use of the CLM, with its detailed description of land surfaces and the more sophisticated biophysical processes.

b. Climate responses of land surface change from agricultural land to forest

In this section, we compared the experiments that used the two LSMs (the BATS and CLM) before and after the changes in the land surface patterns to quantify the impact of

reforestation on the local climate over the Loess Plateau. Specifically, we analysed the differences of each reforestation experiment after the land surface has been modified in experiments BFOR and CFOR versus the control experiments using pre-reforested maps (BCTL and CCTL, respectively). We also analysed the differences between the BFOR with the BCRP that used the revised map of the irrigated crop land in the BATS. Student's *t* tests were used to identify the statistical significance at the 90% confidence level of the differences between the simulations.

1) TEMPERATURE RESPONSES

The replacement of agricultural land by forest in the simulations using the two LSMs resulted in more pronounced temperature responses in summer, compared to winter. In the winter season, the BFOR configuration led to a slight increase in the temperatures over most of the Loess Plateau, compared with the BCTL, with some areas of statistically significant warming over the southeast of the plateau (Fig. 6a). This southeast region was mostly covered by irrigated crop lands in the BCTL simulation. The BFOR also demonstrated a slight warming effect when compared to the BCRP, although the temperature changes were not significant (Fig. 6b). In contrast, the CFOR configuration simulated a slight cooling effect over the central and northwest regions of the plateau, as well as several areas of warming over the eastern plateau, compared to the CCTL simulation (Fig. 6c). The averaged temperature differences across the plateau were less than 0.2˚C in all of the reforested experiments (Table 3).

During the summer season, the most intensive temperature changes were captured over the southeast region in the BFOR simulation, when compared with the BCTL (Fig. 6d–f). Most of these temperature overestimations were statistically significant; the spatially averaged difference was 2.42˚C over the irrigated analysis domain (Table 4). Meanwhile, some cooling effects in the BFOR simulation were also captured, over the central and

northwest regions, compared to the BCTL, although the effects were not statistically significant. Overall, an increase of 0.56˚C over the entire plateau domain was found (Table 4). When the BFOR simulation was compared with the BCRP, the temperature responses showed an opposite pattern overall, compared with that seen between the BFOR and the BCTL (Fig. 6e). Compared with the BCRP simulation, the BFOR configuration simulated a slight cooling effect over the central and east regions, but a slight warming effect over the northwest region; overall the BFOR simulated a decrease of -0.12˚C, compared with the BCRP simulation (Table 4).

The differences in temperature between the CFOR and the CCTL exhibited a similar spatial pattern to the differences between the BFOR and BCRP simulations during summer. Furthermore, the cooling effects over the central and east regions were statistically significant, along with a slight warming effect over the northwest region but not statistically significant (Fig. 6f). The averaged difference in temperatures over the entire plateau was -0.35˚C in the CFOR, compared with the CCTL simulation (Table 4).

The warming effect of the BFOR simulation, compared with the BCTL, over the southeast region was also seen in the daily maximum and minimum temperatures (Tmax and Tmin, respectively; Tables 3 and 4). During the winter, the Tmax simulated by the BFOR was 0.79˚C higher than that simulated by the BCTL, averaged over the southeast irrigated analysis domain. The corresponding Tmin slightly increased, by 0.02˚C. During summer, the Tmax and Tmin in the BFOR simulations were both significantly higher over the irrigated analysis domain (by 2.93˚C and 1.13˚C, respectively), than in the BCTL simulation. However, over the entire plateau, the simulated Tmax and Tmin by the BFOR configuration were not significantly different to those simulated by the BCTL. Furthermore, the Tmax in the BFOR and the CFOR simulations did not significantly change, in comparison with the BCRP and the CCTL simulations, respectively, over the entire plateau.

The Tmin in the CFOR simulation was significantly lower, by 0.61˚C, compared to that in the CCTL simulation.

2) PRECIPITATION RESPONSES.

The simulated precipitation responses to the conversion of vegetation from agricultural land to forest were also stronger in the summer, but relatively weak in winter, using both of the LSMs. The winter precipitation in both the BFOR and the CFOR simulations only changed by small amounts compared to that in the corresponding control simulations; a slight increase in precipitation over the eastern region, but decrease over the northwest of the plateau was simulated, in comparison to the BCTL and CCTL runs, respectively, and the BCRP run (Fig. 7a–c). The differences in winter precipitation were less than 1 mm month^{-1}, averaged both over the entire plateau and the irrigated analysis domains (Table 3).

During the summer season, the differences in precipitation among the experiments varied substantially. The BFOR configuration resulted in a significant reduction in precipitation over the southeast region, by 15.33 mm month^{-1} on average, compared with the BCTL. However, it also increased precipitation significantly over the central region and slightly increased precipitation over the northwest area (Fig. 7d; Table 4). Over the entire plateau, the BFOR configuration produced a slight increase of 2.03 mm month^{-1}, compared with the BCTL simulation (Table 4). In contrast, when the BFOR configuration was compared with the BCRP, the spatial difference in precipitation was mostly of the opposite pattern to that seen between the BFOR and the BCTL simulations. In particular, over the southeast region excessive rainfall responses were captured, along with slight deficit rainfall responses over the northwest region (Fig. 7e). Accordingly the overall difference was 8.67 mm month^{-1} higher in the BFOR compared with the BCRP over the entire plateau (Table 4).

The features of the CFOR configuration simulated precipitation, compared with the CCTL, were again more consistent with the spatial differences between the BFOR and the BCRP simulations. Nevertheless, the effects were more pronounced over the east region of the plateau, with several areas being significantly different (Fig. 7f). Several negative differences were also captured over the northwest region. The overall precipitation response was positive, with an average difference of 5.66 mm month^{-1}, in the CFOR simulation compared with the CCTL simulation (Table 4).

The convective precipitation during summer exhibited similar variations to the total precipitation in the BFOR simulation, compared with the BCTL. The largest decreases in convective precipitation occurred over the southeast region, with a magnitude of -11.43 mm month^{-1}, on average, over the southeast, irrigated analysis domain (Table 4). In accordance with this, the stratiform precipitation also exhibited an average reduction of -3.90 mm month^{-1} over the southeast region. However, when the BFOR simulation was compared with the results produced by the BCTL configuration over the entire plateau, only minor changes in both the convective and stratiform precipitation were found. These responses were similar in the comparison between the BFOR and the BCRP simulations, as well as the CFOR and the CCTL simulations, showing that the convective precipitation increased by up to 4.53 mm month^{-1} overall along with minor positive changes in the stratiform precipitation (Table 4).

Overall, the climate responses to the land surface conversions, from agricultural land to forest, were dominantly dependent on the type of agricultural land that was converted. When the BFOR was compared with the BCTL, both the irrigated and non-irrigated crops were converted to forest. This resulted in pronounced temperature and precipitation changes, especially over the southeast region of the plateau that were mostly covered by irrigated land before reforestation. In particular, the temperature in the BFOR was

significantly increased, and the precipitation was significantly decreased over the irrigated area, compared with the BCTL. However, when the BFOR (CFOR) was compared with the BCRP (CCTL), only the non-irrigated crop was converted to forest, the climate responses to the land surface changes were largely reduced, and even with several opposite responses compared to the simulations that changed the irrigated crop. In particular, during the summer, the temperature was cooler and precipitation was higher over the reforested region with conversions from non-irrigated crop to forest.

4. Discussion

a. Hydrological impacts of the land surface changes on the local climate

The reasons for the different climate responses to land surface changes across the experiments are investigated here. In particular, the conversion from irrigated crop land to forest dramatically decreased the surface ET, which then played a critical role in the pronounced temperature warming and decreases in precipitation simulated in the BFOR compared with the BCTL. The decrease in ET mainly occurred due to differences in the soil water content between the irrigated crop land and forest, which was particularly important over this semi-arid region, where the soil water content was the primary limiting factor for ET. The soil water content was assigned to be at field capacity in the irrigated regions, whereas in forests it was limited by the surface water budget and was much less than the field capacity. This was found with significantly lower soil moisture present in the top layer over the southeast irrigated analysis domain in the BFOR simulation, with average negative differences of -5.92 and -3.68 mm for winter and summer, respectively, compared with the BCTL simulation (Tables 3 and 4). In accordance with this, the relatively dry soil layer in the forests substantially decreased the surface ET, compared with that in the irrigated crop areas over the southeast of the plateau.

The differences in the ET fluxes directly influenced precipitation. Lower surface ET rates favoured the simulation of drier boundary conditions and, although the lower atmosphere was more positively buoyant, this generated a reduction in convective precipitation. This was found in this study, which showed significant decreases in the convective precipitation over the southeast of the plateau during the summer. Furthermore, the availability of water for ET can significantly influence the formation of clouds, as well as the intensity and distribution of precipitation. With the decreases in ET fluxes that occurred, the cloud coverage captured also decreased, by around 0.5% in winter and, of statistical significance, by around 6% in summer, in the BFOR simulation compared with the BCTL simulation, over the southeast of the plateau (Tables 3 and 4). Such decreases in ET and cloud coverage have also been captured in previous studies (e.g., Findell et al. 2007).

The negative differences in ET rates were also the primary reason for the significant warming over the irrigated region in the BFOR simulation, compared with the BCTL. The large decreases in surface ET substantially altered the surface energy balance by significantly reducing the latent heat flux and increasing the sensible heat flux by a similar magnitude (Tables 3 and 4). The shift away from latent, towards sensible, heat fluxes indicated that more energy was used to directly heat the air and thus led to a significant warming in the simulated Tmax and mean temperatures.

The decrease of surface ET and cloud coverage in the BFOR simulation (compared to the BCTL simulation) also favoured an increase in the net solar radiation (NSR) regionally; the NSR fluxes were up to 9.70 W m^{-2} higher over the southeast region (Tables 3 and 4). This enhancement in the NSR can also lead to increases in the Tmax during the daytime, as well as the sensible heat flux; this therefore resulted in the generally higher mean temperature in the BFOR simulation compared to the BCTL simulation.

In the BATS coupled RegCM4.3, reforestation (BFOR) favoured significant increases in temperatures over the Loess Plateau, consistent with a series of field observations. The observational data have shown a pronounced warming of the climate over the plateau during the past five decades, including the reforestation period (Li et al. 2010; Lü et al. 2012); this suggests that the implementation of reforestation strategies may introduce an overlapping effect with greenhouse gases on the climate. The strong impact of irrigation on the climate simulated here was also captured in several other modelling studies (e.g., Anthes 1984; Boucher et al. 2004; Lobell et al. 2006; Kueppers et al. 2007). For example, Kueppers et al. (2007) converted irrigated crops to natural vegetation over the California Central Valley, in the United States. Their results showed that irrigation resulted in decreased surface temperatures, increased precipitation and relative humidity, as well as large changes in the temperature profile of the troposphere compared with natural vegetation, with geographic variations in the strength of these effects. Observational analyses also suggest potential significant impacts of irrigation on local precipitation and temperature (Barnston and Schichedanz 1984).

b. Albedo and ET impacts of the land surface changes on the local climate

Coupling with the LSMs used non-irrigated crop as the only agricultural land category (i.e. comparing the CFOR with the CCTL simulation and the BFOR with the BCRP simulation), the RegCM4.3 favoured the generation of modest temperature and precipitation responses to the conversion of agricultural land to forest. Such modest changes were primarily due to the smaller differences in the land properties between non-irrigated crop lands and forests, compared to the differences between irrigated crop lands and forests.

During the winter, the conversion from crop lands to forest generally resulted in a slight warming effect over the reforested area, captured in the CFOR and BFOR simulations, compared with the CCTL and BCRP simulations, respectively. The warming effect that occurred in the reforested experiments was principally due to a decrease in the albedo of the forest land, since the darker forests could absorb more NSR and thus increase the surface local temperature accordingly. The relationships amongst temperature, surface albedo and NSR, showed that over the central and east regions of the plateau, where extensive crop lands were replaced by forests in the simulations, the captured albedo significantly decreased, but the NSR and temperature were significantly enhanced (Figures 8a–d). There were strong pattern correlation coefficients (PCCs) amongst the changes in the spatial distribution of the three climate variables, being -0.51 (CFOR) and -0.39 (BFOR) between the temperature and surface albedo, and 0.41 (CFOR) and 0.46 (BFOR) between the temperature and NSR.

The increase in ET flux captured over the eastern region of the plateau was spatially correlated with the simulated reforested areas (Fig. 8e–f). Forests favoured the generation of higher ET fluxes than crop lands, partially due to their deeper root layers than those in crop lands that could tap into water more effectively, as well as different water stress function between the two land surface types in the model (Jackson et al. 1996). Despite the fact that the increase in ET favoured an increase the latent heat flux and hence had a cooling effect on the surface temperature, on balance, a net warming effect on the local temperature was simulated. This suggests that, during the cold and dry season, radiative forcing was more dominant in causing the changes in temperature than hydrological forcing; this was also found in previous studies of regions subject to boreal winters (e.g., Betts 2000; Pielke 2001).

During the summer, the radiative forcing on the local temperature competed against the hydrological forcing to lead to the changes in climate associated with reforestation. Over the central and east regions of the plateau, the albedo experienced a significant decrease, associated with positive NSR changes locally (Fig. 9a–d). However, these positive changes to the surface radiation did not necessarily lead to an increase in temperature; a negative PCC between the NSR and the temperature spatial difference was found in these areas. Meanwhile, over these areas, the simulations captured significant increases in the ET fluxes when the crop lands were converted to forest; the highest absolute values of the PCCs between the ET flux and changes in temperature were -0.72 in the CFOR and -0.90 in the BFOR (Fig. 9e–f). This suggests that the increases in ET primarily explain the cooling effect of reforestation during the summer season over the plateau.

The increase in ET associated with the conversion from crop lands to forests also appeared to increase the total precipitation over the central and southeast regions of the plateau. This was validated by the high PCC values between the differences in the two variables, of 0.55 and 0.89 for the CFOR and BFOR simulations, respectively. The increase in ET made more water vapour available for precipitation, which was particularly important over this semi-arid region, where the water vapour was a limiting resource for precipitation (Fig. 9e–f).

The simulated medium climate responses using the CLM and the revised BATS are consistent with a series of previous studies that investigated the climate effects of the reforestation from non-irrigated crop lands. For example, Liu et al. (2008c) used an earlier version of the RegCM with the BATS to simulate the impact of reforestation in northern China; they found that, overall, reforestation increased precipitation but reduced temperature, together with increasing the ET, relative humidity, root layer soil moisture

and decreasing the wind speed over the reforested area. Zhao and Pitman (2002), using the NCAR CCM3 coupled with the BATS, also simulated a cooling effect of reforestation (around 0.5˚C) in northern China, from crop land. Fu and Yuan (2001) used a regional integrated environmental model system and found a cooling effect (by between 0.5˚C and 2.0˚C) of natural vegetation, and an increase of summer precipitation by about 1–2 mm day^{-1}, in comparison with crop land over the Loess Plateau region. The winter warming effect simulated as a result of reforestation in this study was also validated through several modelled and observed data sets over the temperate region, which suggested increases in radiation balance were the primary reason for this warming effect (e.g., Snyder et al. 2004; Jackson et al. 2005).

c. Roughness length and its impacts on the monsoon flow

Aside from the local changes in ET, the simulated precipitation responses to reforestation could also have been driven by the changes in atmospheric circulation, associated with changes in moisture advection over the reforestation region, particularly during summer. In the simulations that used the CLM, the increases in roughness length in the forests compared with the crop lands, favoured the development of an anomalous low-pressure system over the reforested area (Fig. 10b). As a consequence, an anomalous cyclonic circulation was demonstrated, accompanied by positive moisture advection into the reforested zone, resulted in increases in summer rainfall over the central and southeast plateau. Such changes in roughness length associated with changes in atmospheric circulation patterns, and their impacts on precipitation have also been captured in previous studies (e.g., Liu et al. 2008b, Chen et al. 2012).

In terms of the effects of reforestation simulated using the BATS, changes in the summer monsoon flow could also have impacted on the variation in precipitation. Similar

to the CLM, the roughness length increases in the forest category, which favoured the generation of an anomalous lower pressure system over the southeast regions of the plateau in the BFOR configuration, compared with the BCTL configuration (Fig. 10a). The lower pressure, accompanied by positive moisture advection, partially increased the precipitation in the region. Nevertheless, in general, over the southeast of the plateau with the conversion from irrigated crop lands to forests, precipitation appeared to decrease; this indicates that the decrease in the surface ET within the experiments was the most dominant forcing that influenced the surface water balance and reduction in precipitation, compared with the effects of roughness length changes.

The increases in the roughness length by converting crop land to forest, using both LSMs, also favoured the reduction in the wind speed as it moved over the reforested zone. This was primarily through the increase surface drag on the air flow by the forests, compared with the crop lands (Dorman and Sellers 1989). In particular, during the winter season, the higher roughness length of forest effectively reduced the prevailing north-westerly wind over the reforested area, resulting in increases of the southerly winds captured over the eastern region of the plateau in both reforestation experiments, using the two LSMs (Fig. 11). The increases in the southerly winds showed good agreement with the increases in temperature. This indicates the relatively important role of the changes in roughness length on the local climate during winter and was also found by Ma et al. (2013).

In summary, comparison of the BATS and CLM simulations has illustrated that the changes in surface ET, albedo and roughness length were the primary underlying mechanisms operating in both models that explain how reforestation affects the local climate over the Loess Plateau. For the BATS configuration which included the irrigated crop lands, the surface ET served as the critical link between the response of the surface

processes and atmospheric dynamics and physics, to reforesation. The soil water content of the irrigated region was much higher than that of the forest, which resulted in significantly higher ET in the irrigated crop lands than in the forest; this is because the soil water content was the limiting factor for ET rates over the semi-arid region. When the irrigated crop was converted to forest, the reduced soil water content, associated with the decreased ET flux, favoured the simulation of less water vapour for precipitation, as well as generating a shift from latent to sensible heat fluxes. This resulted in the apparent surface drying and warming effects over the plateau simulated by the configuration.

In the CLM, which did not include the irrigated crop land category, the land surface changes resulting from reforestation primarily affected the surface air temperature through changes in the albedo in winter, and surface ET and roughness length in summer. During the winter, with cold and dry conditions, the changes in the surface energy balance were largely controlled by the absorbed surface radiation; as the darker forests generally absorbed more net solar radiation compared to the crop lands, the simulated reforestation generated a net warming effect. During the summer season, with large monsoon rainfalls, the role of surface ET became critical; the increase in surface ET simulated with the forest was the primary factor that explained the surface cooling and increases in precipitation. Furthermore, the increases in precipitation with reforestation were also related to increases in the roughness length that may have enhanced the pattern of moisture convergence, thereby increasing precipitation.

The conversion from crop lands to forests also resulted in a higher roughness length that was assigned as a function of the canopy height in the CLM. The increases in roughness length often resulted in an increase in the turbulent fluxes (latent heat and sensible heat), and could therefore be another reason for the cooling effect simulated in the CFOR compared to the CCTL simulation.

d. Model uncertainties

The different climate responses to reforestation, simulated by using the two LSMs were associated with the dominance of different biophysical mechanisms induced by different representation of irrigated crop. Kueppers et al. (2008) performed an inter-comparison among a series of RCMs over the semi-arid region of the United States, simulating the climate effects of converting natural vegetation to agricultural lands. They found that the RegCM, with the irrigated crop category, had a significant cooling effect in agricultural lands compared with natural vegetation; the CLM, without the irrigated crop lands, only simulated a slight influence of the land surface conversions on surface air temperature. Furthermore, when irrigation was added to the CLM and coupled with the RegCM, in another study, a significant cooling effect of the irrigated crops was also simulated (Jin and Miller 2011); adding the irrigated crop in the CLM was primarily performed through changing the soil water content to a series of gradients. Thus, although the cooling effects in the CLM were largely consistent with the BATS simulations, the magnitude of the cooling simulated using the two LSMs was complex and varied in accordance with changes made to the soil moisture content, as well as to differences in the atmospheric dynamics, radiative transfer, soil texture, soil thermal diffusion, and surface albedo.

The primary results using rain-fed crop replacing irrigated crop in BATS showed that the revised BATS could alleviate cold biases and precipitation overestimation during winter, although during summer it also deteriorated warm biases and precipitation underestimation over the land surface altered region compared with the default BATS. In spite of such deteriorates, the revised BATS was closer to the real situation compared with the default BATS from the view of simulated soil moisture content which is one of the most critical factors impacting on local climate of this semi-arid region.

The revised BATS altered default water balances during model simulation and introduced different processes into interactions between land surface and atmosphere. The default BATS remained high soil moisture content by adding extra water fluxes into irrigated land surface, however, the revised BATS removed such supplementary, resulting in lower water fluxes in soil moisture content. As a result, the surface turbulent fluxes significantly changed (sensible heat fluxes largely increased at the cost of latent heat fluxes decreases) over the corresponding region, which tended to increase the local surface air temperature but decrease precipitation in the revised BATS. Due to these deteriorates of the revised BATS, more thoroughly improvement of BATS was necessary for the improvement of model simulation.

Clearly, irrigated crops and their associated soil moisture have an important role in the modelled climate responses to changes in the land surface; more detailed studies of the biophysical and hydrological properties of the irrigated crop land are needed. The irrigated crops in semi-arid regions have a much lower soil moisture content, compared to the irrigation field capacity in the BATS, and vary to a great extent during the year (since irrigation is only used to supplement soil water during the growing season, when there is a lack of reliable rainfall). The unnaturally high soil water in the BATS should be avoided, as it is associated with an exaggerated climate response to the land conversion from irrigated crops to natural vegetation.

5. Conclusion

In this study, we have explored the atmospheric dynamical responses to land surface changes, induced by reforestation programmes in the Loess Plateau region. The temporal scale from 1990 to 2009 was applied to cover the reforestation implementation period. The results were obtained using the RegCM version 4.3, coupled with two different land

surface models, that is, the BATS and the CLM. We have validated the model's performance using the two LSMs, with an emphasis on the simulation of surface temperatures and precipitation; both of the LSMs were able to reproduce the local climate. In particular, the configuration using the CLM was more consistent with observations, in simulating both winter climate features, as well as summer temperatures, compared with the configuration using the BATS.

Within this study, we have undertaken a series of analyses to identify the key climate responses to changes in the land surface, using the two LSMs. The main scenario used in this analysis was a change in the land surface type from agricultural land to forest (i.e., reforestation). A revised vegetation scenario of the configuration with the BATS was also implemented, in which the irrigated crop land was converted to non-irrigated crop land; this made the agricultural land surface before reforestation more similar to that within the CLM, and so allowed a better comparison between the BATS and CLM simulations. Comparisons amongst the simulations run with these vegetation scenarios revealed the key climate consequences and uncertainties, as well as the underlying mechanisms of climate change according to the two LSMs configurations.

Our results suggest that the impacts of reforestation on the local climate simulated by the model are similar between the two LSMs during winter. Reforestation over the Loess Plateau was found, on balance, to cause a warming effect using both LSMs, together with slight changes in precipitation. Large climate responses were mostly captured over the central and east regions of the plateau, where there are extensive areas of agricultural land, which were converted to forest in both LSM configurations. The climate responses in winter were predominantly caused by changes in the surface albedo radiation according to the configuration with the CLM, whereas in the BATS simulations, changes in ET played critical role.

The effects of reforestation on the climate during the summer were strikingly different between the experiments using the two LSMs. The critical reason for the differences in the climate responses were attributed to the different representation of irrigated crops between the two LSMs. Both irrigated and non-irrigated crops are included as categories within the BATS, but there is only one category for crops in the CLM, and these are effectively non-irrigated. Reforestation from the irrigated crop lands in the BATS primarily decreased the surface ET, which largely influenced the climate response over the semi-arid area. Thus, under the reforestation scenario using the BATS, the model consistently simulated climate features of pronounced warming and drying, particularly over the southeast region of the plateau. Unlike the model configuration with the BATS, the CLM simulations and the revised BATS simulations produced medium climate responses, with cooling and wetting effects during the summer season. The climate responses to reforestation in simulations using the CLM were mainly related to changes in the surface ET and roughness length.

Considering that the CLM does not parameterise irrigated crop lands, a more sophisticated surface model is needed. Even the BATS lacks sufficient skill to simulate variations in soil water content within irrigated lands, due to different vegetation and soil types, farming practices, or water availability. It is necessary to include such uncertainties in the regional climate model for more accurate simulations. Further, a series of other model simulation deficiencies were still captured that may have implications on the effects of changes in the land surface on the climate; as a result, simulating detailed local climate characteristics, in particular, needs further improvement in the future.

It is important to note that in our experiments of the potential climate effects of changing land surfaces through reforestation, all agricultural land across the Loess Plateau was converted to forest. The actual area that has been reforested across the plateau is more

complex and this may have introduced variation, compared to the effects that we have simulated. Over the next 50 years, the reforestation programme is planned for further expansion, through both planting trees and natural restoration approaches using local vegetation, such as bush land and grass land. Meanwhile, some existing reforestation areas have been in decline, due to a lack of sufficient water supply, or the conversion of natural vegetation to crop and urban lands (e.g., Cao 2008; Cao et al. 2011). Thus, in the future, modelling work is needed that uses a dynamical vegetation map coupled with the RegCM, to more accurately investigate the effects of reforestation.

Greenhouse gas increases have coincided with the expansion of reforestation in China. Expanding reforestation may have introduced an overlapping effect on temperature. The carbon uptake process of reforestation will have weakened the warming effect; however, the overall climate effect needs more investigation by using land surface schemes incorporated with photosynthesis processes (Foley et al. 1996).

Ultimately, the study applied a more sophisticated land surface model to predict the potential impacts of reforestation on the local climate, and compared with simulations using a relatively simple land surface model. This study is a part of the efforts in improving our understanding of the local climate over the Loess Plateau, which could provide important references for future reforestation strategies and help reduce economic and ecological losses, before embarking on large-scale reforestation in the northern semi-arid region of China.

Acknowledgement. The first author (LW) is supported by the China Scholarship Council, the International Macquarie Research Excellence Scholarship, and Higher Degree Research support fund from Macquarie University. Computational facilities are provided by Intersect Inc., NSW and the National Computational Infrastructure of Australia. We would like to thank Prof. C.-P. Chang of the US Naval Postgraduate School and the National Taiwan University for co-supervising LW and his many valuable comments on this work.

List of Tables

TABLE 1 The configuration of each simulation, in the RegCM4.3, used to identify the effects of reforestation on the Loess Plateau.

Experiment	Land surface scheme	Convective scheme	Land surface scenario	Forcing data
BCTL (Wang and Cheung 2015a, b)	Biosphere Atmosphere Transfer Scheme (BATS)	Grell Fritsch-Chapell (Grell, 1993)	Default land surface before reforestation	50-km BATSFC[a] over the China domain[b]
BFOR			All crop land, including irrigated crop land, converted to forest.	50-km BATSFC over the China domain
BCRP			Irrigated crop land converted to non-irrigated crop land (no reforestation)	50-km BATSFC over the China domain
CCTL	Community Land Model version 3.5 (CLM)	Emanuel (Emanuel 1991; Emanuel and Zivkovic-Rothman 1999)	Default land surface before reforestation	50-km CLMEM[c] over the China domain
CFOR			All crop land converted to forest	50-km CLMEM over the China domain

[a]The RegCM4.3 configuration using the BATS and the Grell Fritsch-Chapell convective scheme (Wang and Cheung 2015a, b); [b]This domain covered the entirety of China and its surrounding regions, it was centred at 107˚E, 35˚N with a grid size of 50-km and 110 × 144 grid points, which is close to that recommended by the East Asian portion of the COordinated Regional climate Downscaling EXperiment (CORDEX); [c]The RegCM4.3 configuration using the CLM and the Emanuel convective scheme (Wang and Cheung 2015c).

TABLE 2 The land cover characteristics used in the BATS (Dickinson et al. 1993) and the CLM3.5 (Bonan et al. 2002; Oleson et al. 2007).

Parameters	The BATS					The CLM		
	Crop	Irrigated	Forest	Conversion to forest		Crop	Forest	Conversion to forest from crop
				from crop	form irrigated			
Percentage vegetation coverage (Maximum)	0.85	0.80	0.80	-0.05	-	0.85	0.75	-0.05
Roughness length (m)	0.08	0.06	0.80	+0.72	+0.74	0.06	1.10	+1.04
Albedo for shortwave radiation (<0.7 nm)	0.10	0.08	0.06	-0.04	-0.02	0.24	0.13	-0.11
Albedo for long-wave radiation (>0.7 nm)	0.30	0.28	0.26	-0.04	-0.02	0.58	0.42	-0.16
Stomatal resistance (Minimum; s m^{-1})	45	45	120	+75	+75	2000	2000	-
Leaf area index (Maximum)	6.00	6.00	6.00	-	-	4.00	5.00	+1.00
Leaf area index (Minimum)	0.50	0.50	1.00	+0.50	+0.50	0	0	-
Depth of rooting zone soil layer (m)	1.00	1.00	2.00	+1.00	+1.00	-	-	-

TABLE 3 The critical climate variables simulated by the five experiments over the Loess Plateau of China during the winter months (December, January and February).

Variables	**Entire**	**BATS (Entire plateau)**		**BATS (Irrigated domain)**		**BATS (Entire plateau)**		**CLM (Entire plateau)**	
	OBS[a]	**BCTL (δ[b])**	**BFOR[c]**	**BCTL (δ)**	**BFOR**	**BCRP (δ)**	**BFOR**	**CCTL (δ)**	**CFOR**
Tmp[e] (˚C)	-4.55	-6.40 (0.87)	+0.14	0.05 (0.84)	+0.47	-6.32 (0.85)	+0.06	-5.65 (0.97)	-0.01
Tmax[f] (˚C)	2.24	-0.07 (0.86)	+0.21	5.82 (1.03)	+0.79	0.08 (0.85)	+0.06	-0.90 (0.86)	+0.20
Tmin[g] (˚C)	-9.69	-11.68 (0.94)	-0.02	-4.42 (0.87)	+0.02	-11.72 (0.92)	+0.02	-10.61 (1.13)	-0.19
Pre[h] (mm month^{-1})	7.17	16.87 (4.80)	+0.11	28.23 (12.86)	+0.38	16.66 (4.75)	+0.32	16.29 (4.06)	-0.54
PreC[i] (mm month^{-1})	1.98	0.18 (0.11)	+0.01	0.25 (0.55)	+0.06	0.18 (0.12)	+0.01	3.33 (0.52)	-0.05
PreS[j] (mm month^{-1})	9.03	16.69 (4.72)	+0.10	27.98 (12.63)	+0.32	16.47 (4.67)	+0.32	12.96 (3.60)	-0.49
NSR[k] (W m^{-2})	92.72	104.69 (4.25)	+1.26	119.43 (7.65)	+2.47	104.64 (4.02)	+1.31	108.39 (4.34)	+2.20
NLR[l] (W m^{-2})	76.57	77.12 (4.04)	+0.84	77.16 (6.81)	+3.24	77.73 (4.09)	+0.23	80.20 (3.96)	+0.42
SHF[m] (W m^{-2})	18.81	16.84 (2.21)	+2.17	19.64 (2.91)	**+6.94**	18.13 (2.58)	+0.88	14.46 (2.00)	+0.83
LHF[n] (W m^{-2})	10.36	14.45 (1.02)	**-1.06[d]**	26.04 (2.28)	**-5.77**	12.10 (1.28)	**+1.29**	12.38 (0.88)	+0.06
SM[o] (mm)	23.12	17.89 (1.32)	-1.31	29.25 (2.16)	**-5.92**	15.54 (1.77)	+1.04	14.20 (0.77)	-0.12
Cloud[p] (%)	40.92	42.07 (3.15)	+0.01	36.79 (5.49)	-0.45	41.93 (3.16)	+0.15	42.30 (2.76)	-0.38
Albedo[q]	-	0.18 (0.02)	-0.01	0.11 (0.03)	-0.02	0.19 (0.02)	**-0.02**	0.19 (0.02)	**-0.02**

[a] The spatial averaged values of the observational data (OBS) and control runs (BCTL, BCRP and CCTL); [b] Corresponding standard deviation; [c] Spatially averaged differences of the reforested runs (BFOR and CFOR) from the corresponding control runs; [d] Bold font indicates a statistically significant difference at the 90% level; [e] The mean surface air temperature; [f–g] Maximum and minimum temperatures, respectively; [h] Mean precipitation; [i–j] Convective and stratiform precipitation, respectively; [k–l] Net shortwave and net long-wave radiation, respectively; [m–n] Sensible and latent heat flux, respectively; [o] Soil moisture at the top layer; [p] Cloud coverage; [q] Surface albedo.

TABLE 4 The same as Table 3, but during the summer months (June, July and August).

Variables	**Entire**	**BATS (Entire plateau)**		**BATS (Irrigated domain)**		**BATS (Entire plateau)**		**CLM (Entire plateau)**	
	OBS	**BCTL (δ)**	**BFOR**	**BCTL (δ)**	**BFOR**	**BCRP (δ)**	**BFOR**	**CCTL (δ)**	**CFOR**
Tmp (˚C)	20.49	21.79 (0.55)	+0.56	25.23 (0.54)	**+2.42**	22.47 (0.64)	-0.12	20.43 (0.56)	-0.35
Tmax (˚C)	26.48	28.84 (0.66)	+0.61	31.28 (0.77)	**+2.93**	29.54 (0.74)	-0.09	25.67 (0.66)	+0.10
Tmin (˚C)	15.15	15.94 (0.39)	+0.30	20.86 (0.30)	**+1.13**	16.36 (0.46)	-0.12	15.73 (0.47)	**-0.61**
Pre (mm month^{-1})	95.07	82.35 (11.72)	+2.03	102.34 (25.93)	**-15.33**	83.17 (12.61)	+1.21	123.65 (13.34)	+5.66
PreC (mm month^{-1})	57.02	51.93 (7.11)	+1.50	82.83 (19.71)	**-11.43**	51.53 (8.15)	+1.90	81.86 (9.28)	+4.53
PreS (mm month^{-1})	52.39	30.42 (6.24)	+0.53	19.52 (10.28)	-3.90	31.64 (6.13)	-0.69	41.79 (5.06)	+1.13
NSR (W m^{-2})	198.88	228.26 (4.54)	+1.30	230.88 (9.61)	**+9.70**	228.81 (4.26)	+0.75	235.74 (5.06)	+1.59
NLR (W m^{-2})	76.93	84.07 (3.58)	+2.29	57.38 (4.56)	**+14.85**	87.79 (3.99)	-1.43	79.80 (2.76)	-1.67
SHF (W m^{-2})	46.35	68.24 (4.03)	**+7.93**	46.12 (5.08)	**+42.53**	76.57 (4.96)	-0.40	38.29 (1.94)	+1.88
LHF (W m^{-2})	69.11	73.08 (3.40)	**-7.37**	126.78 (4.14)	**-47.95**	63.97 (5.20)	+1.74	77.03 (3.42)	+0.74
SM (mm)	24.52	20.88 (0.72)	-0.01	26.58 (0.60)	**-3.68**	19.46 (0.85)	**+1.41**	23.79 (0.66)	+0.23
Cloud (%)	53.70	44.00 (2.26)	-0.79	47.40 (4.13)	**-5.49**	43.13 (2.32)	+0.08	43.81 (2.06)	+0.71
Albedo	-	0.12 (0.00)	0	0.09 (0.00)	**-0.01**	0.13 (0.00)	**-0.01**	0.10 (0.00)	0

List of Figures

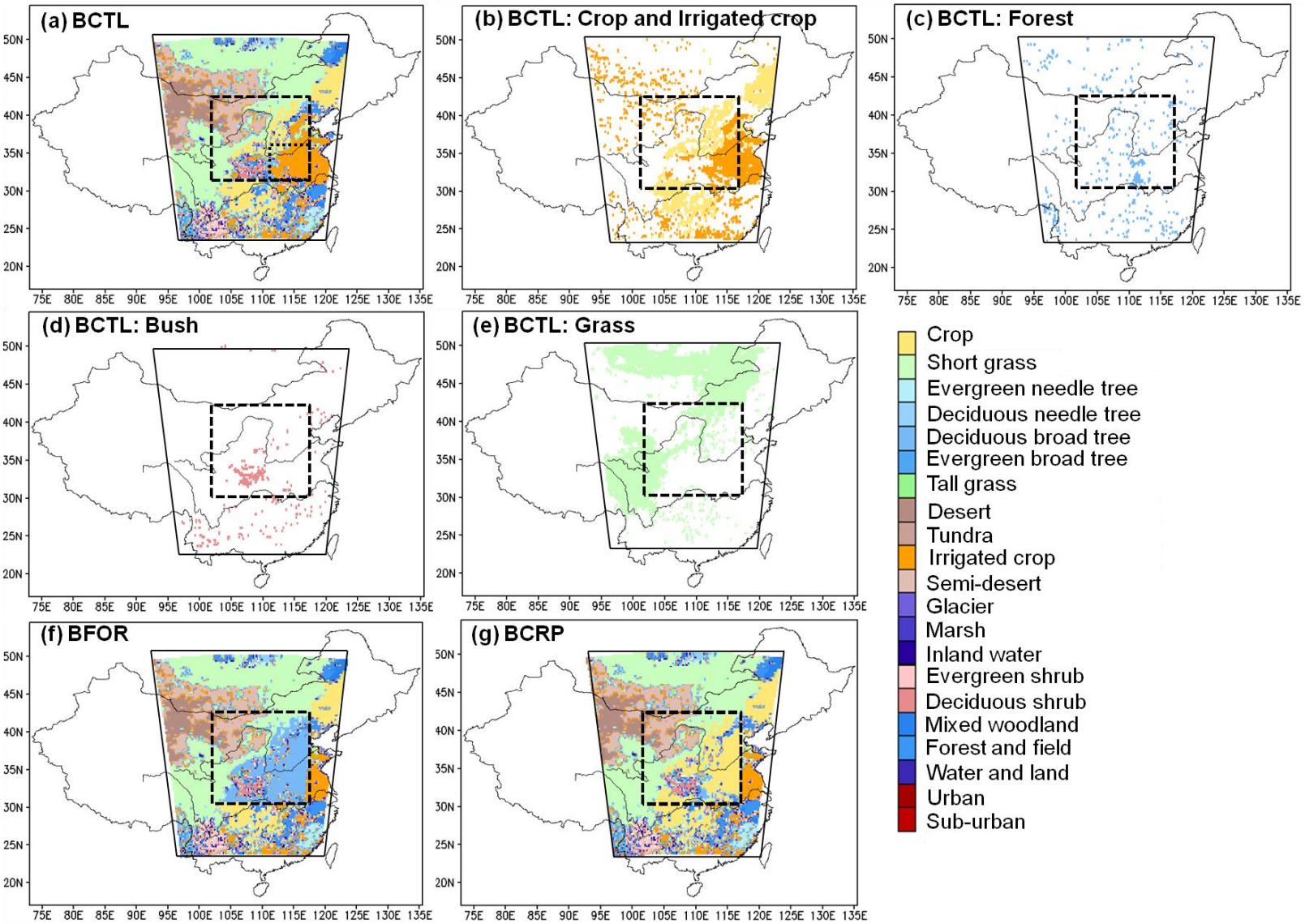
(a) BCTL
(b) BCTL: Crop and Irrigated crop
(c) BCTL: Forest
(d) BCTL: Bush
(e) BCTL: Grass
(f) BFOR
(g) BCRP
50N
45N
40N
35N
30N
25N
20N
75E 80E 85E 90E 95E 100E 105E 110E 115E 120E 125E 130E 135E
Crop
Short grass
Evergreen needle tree
Deciduous needle tree
Deciduous broad tree
Evergreen broad tree
Tall grass
Desert
Tundra
Irrigated crop
Semi-desert
Glacier
Marsh
Inland water
Evergreen shrub
Deciduous shrub
Mixed woodland
Forest and field
Water and land
Urban
Sub-urban

FIGURE 1 Land surface types and the scenarios of land surface change analysed using the BATS scheme within the Loess Plateau and its surrounding areas. The black dashed box denotes the entire plateau analysis domain and the black dotted box in (a) shows the irrigated analysis domain. (a) The BCTL land cover types for each grid cell, aggregated into the categories of the BATS; these comprise the distribution of (b) non-irrigated and irrigated crops, (c) forests, (d) bush land, and (e) grass land. (f) the BFOR land cover types for each grid cell, aggregated into the BATS categories, in which all of the agricultural land types were replaced by forest within the entire plateau analysis domain and (g) the BCRP land cover types for each grid cell, aggregated into the BATS categories, in which the irrigated crop grid cells were converted to crop land, within the entire plateau analysis domain.

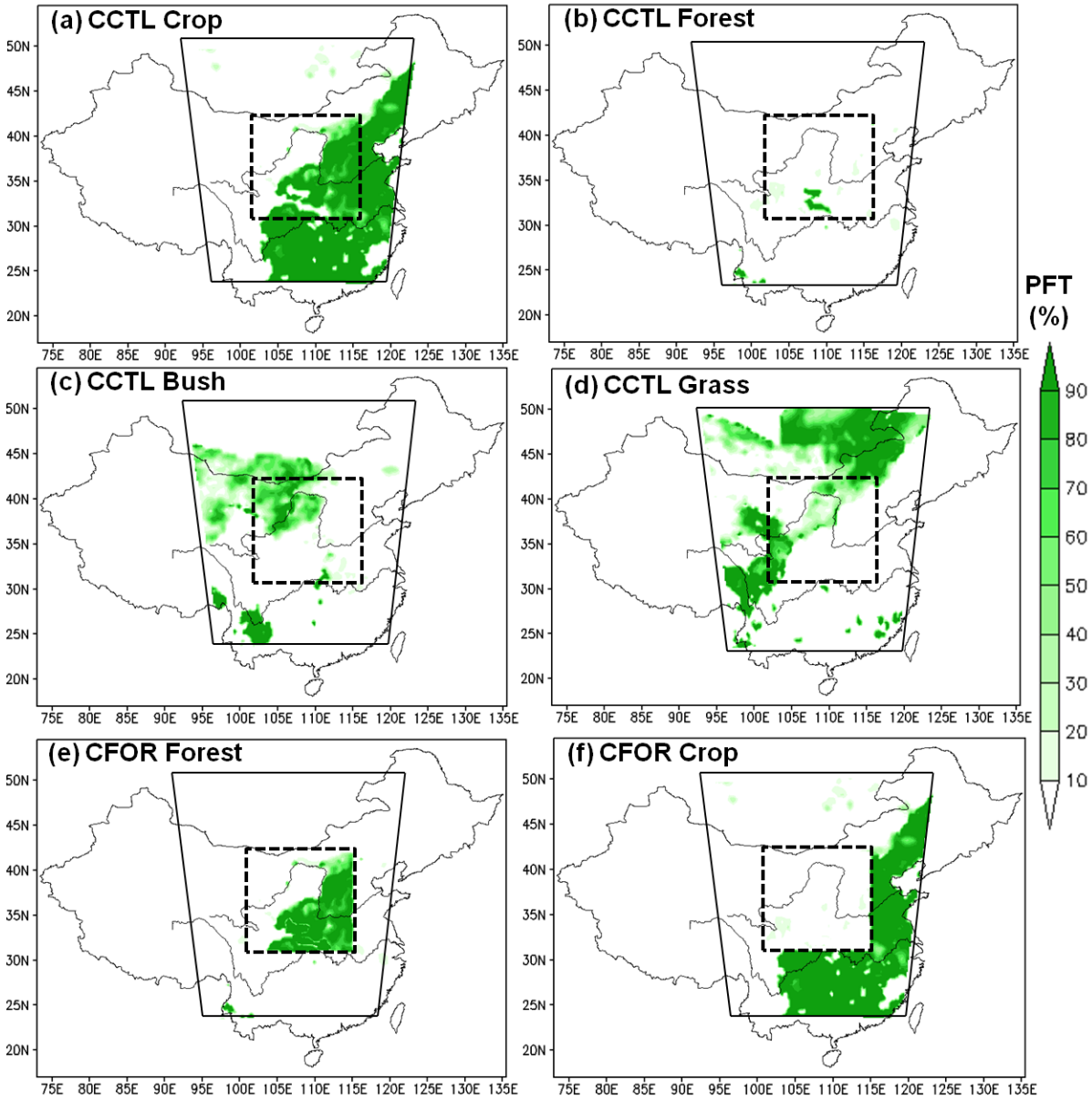

FIGURE 2 Land cover of the plant function types (PFTs) in the CLM and reforestation scenarios within the Loess Plateau and its surrounding areas. The black dashed box denotes the plateau analysis domain: Figures (a–d) show the PFT percentage in the CCTL simulation of (a) the crop land, (b) the temperate broadleaf deciduous tree (Forest), (c) the temperate broadleaf deciduous shrub (Bush) and (d) the C_3 grass (Grass); Figures (e–f) show the PFT percentage in the CFOR simulation of (e) the temperate broadleaf deciduous tree, which replaced all crop PFT in the plateau analysis domain, and (f) the crop land.

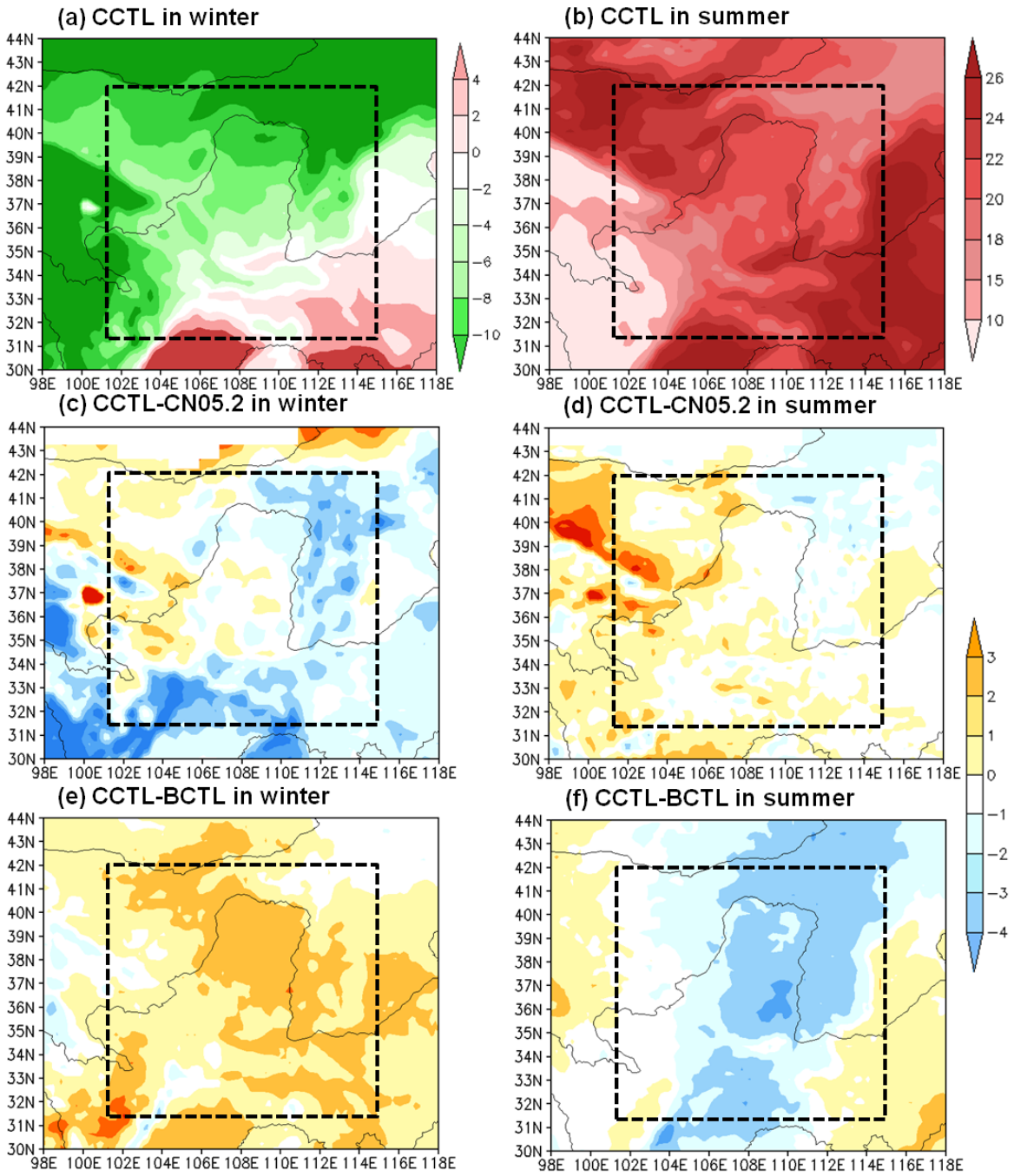

FIGURE 3 Spatial distribution of the surface temperatures (˚C) over the plateau analysis domain in the black dashed box for the CCTL in (a) winter, (b) summer, the differences between the CCTL and the CN05.2 observations in (c) winter, (d) summer, and the differences between the CCTL and the BCTL in (e) winter, (f) summer.

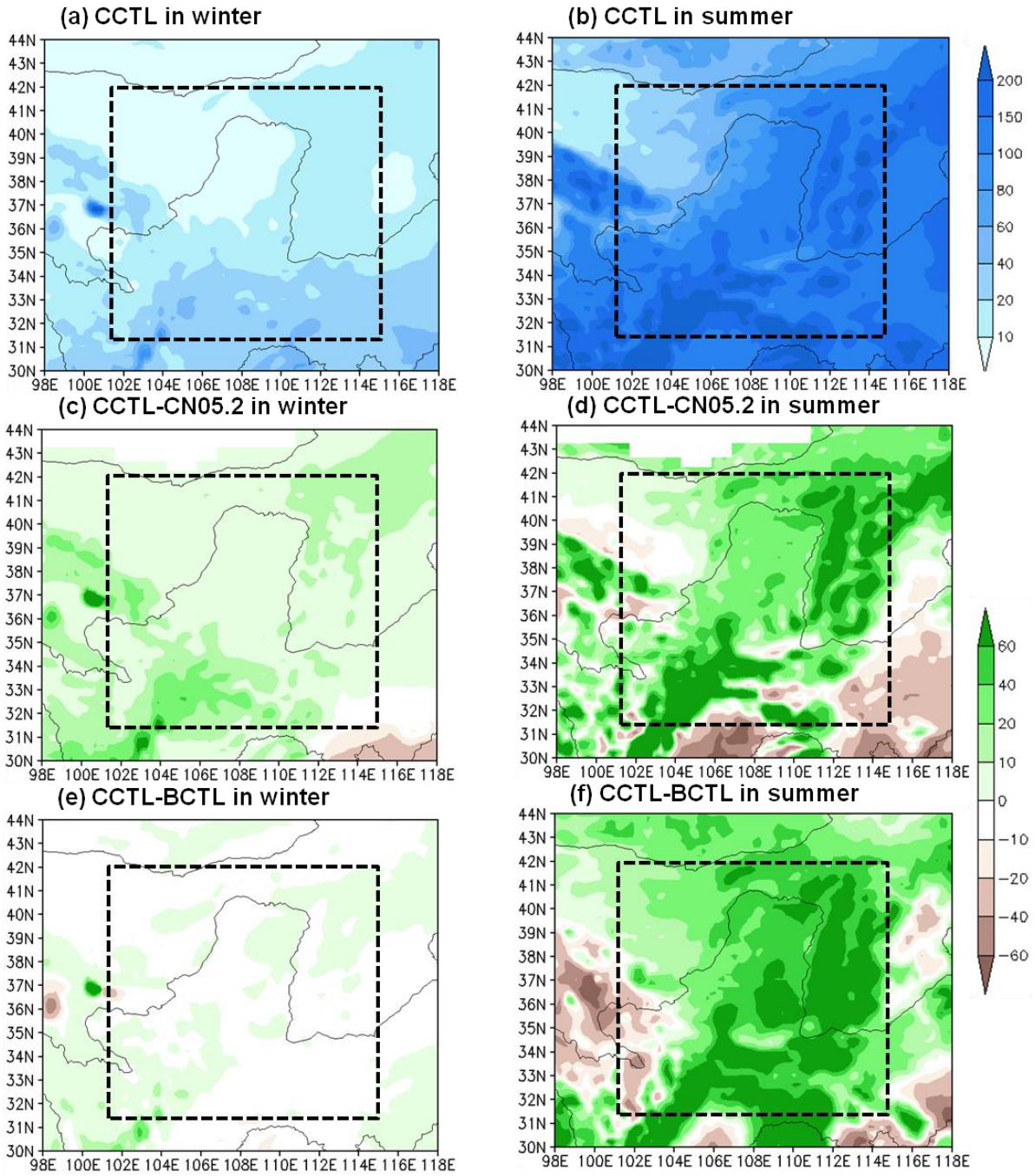

FIGURE 4 As in FIGURE 3, except for precipitation (mm month^{-1}).

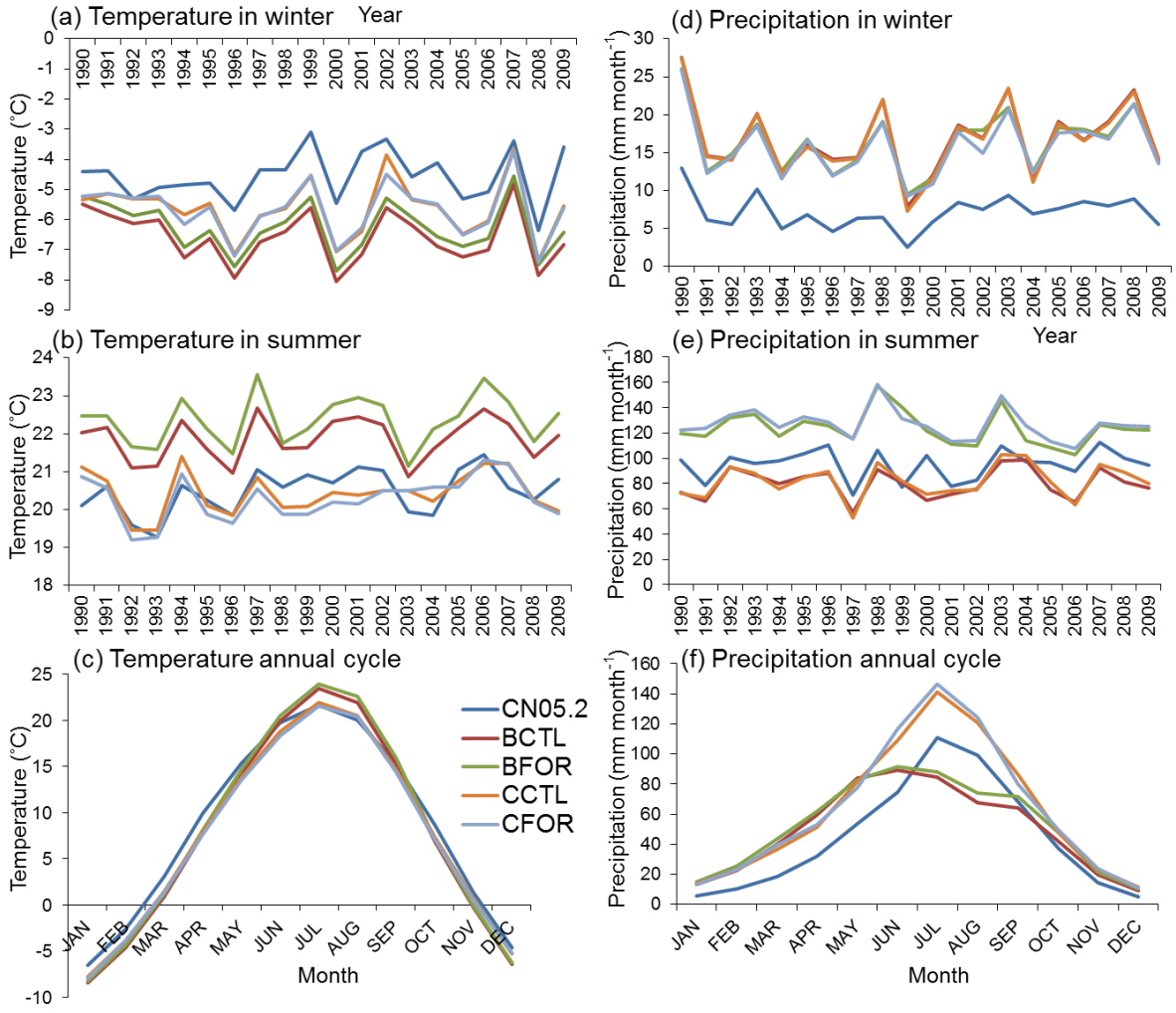

FIGURE 5 Time series of the observed and simulated (BCTL, BFOR, CCTL, and CFOR) (a) surface temperature (˚C) in (a) winter, (b) summer and (c) annual cycle of surface temperature, (d) – (f) As in (a) – (c) except for precipitation (mm month^{-1}).

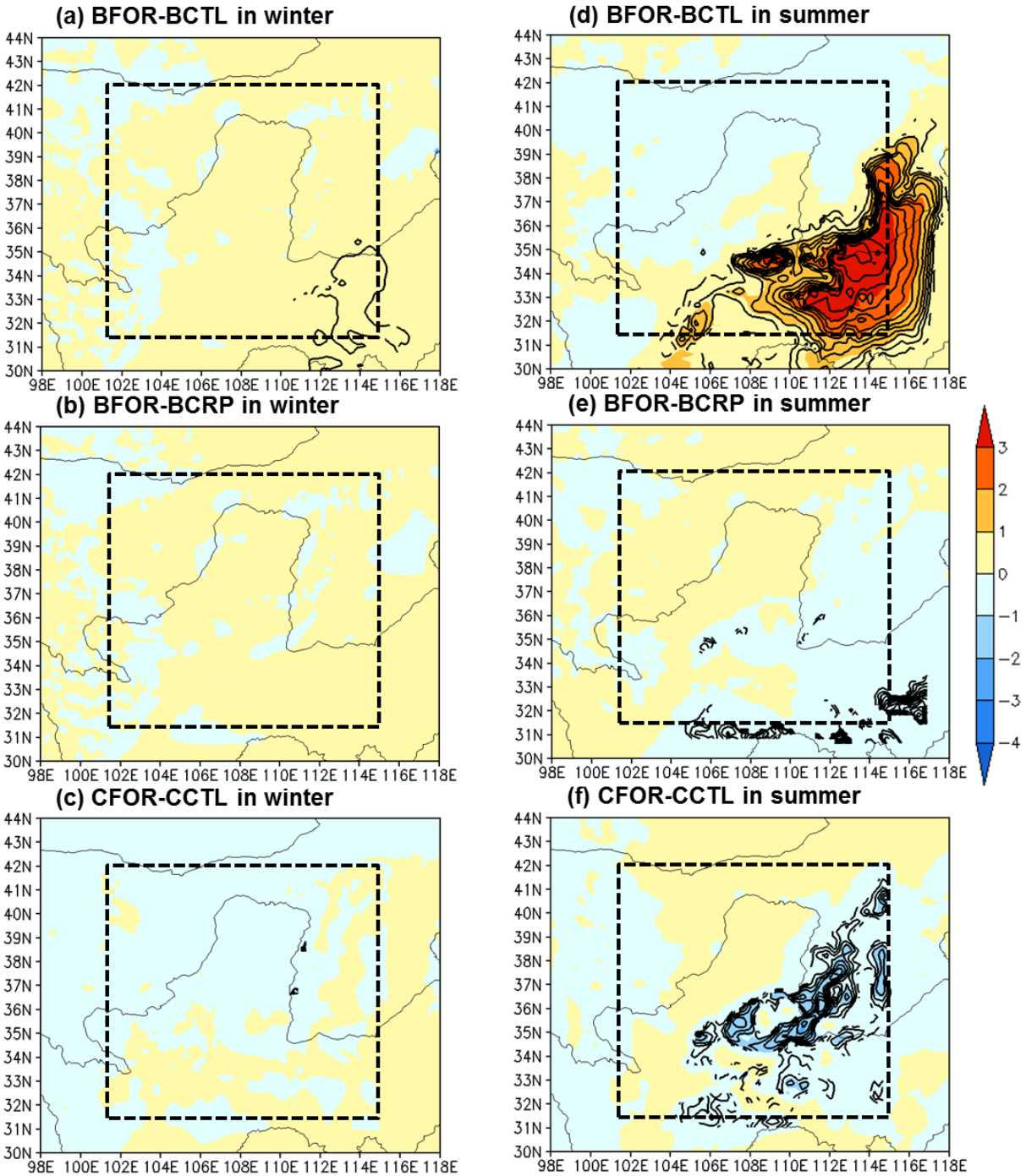

FIGURE 6 Differences in simulated surface temperature (˚C) between (a) the BFOR and the BCTL in winter, (b) the BFOR and the BCRP in winter, (c) the CFOR and the CCTL in winter, (d) the BFOR and the BCTL in summer, (e) the BFOR and the BCRP in summer, (f) the CFOR and the CCTL in summer. Contours represent changes that are statistically significant at the 90% confident level using the Student's *t*-test.

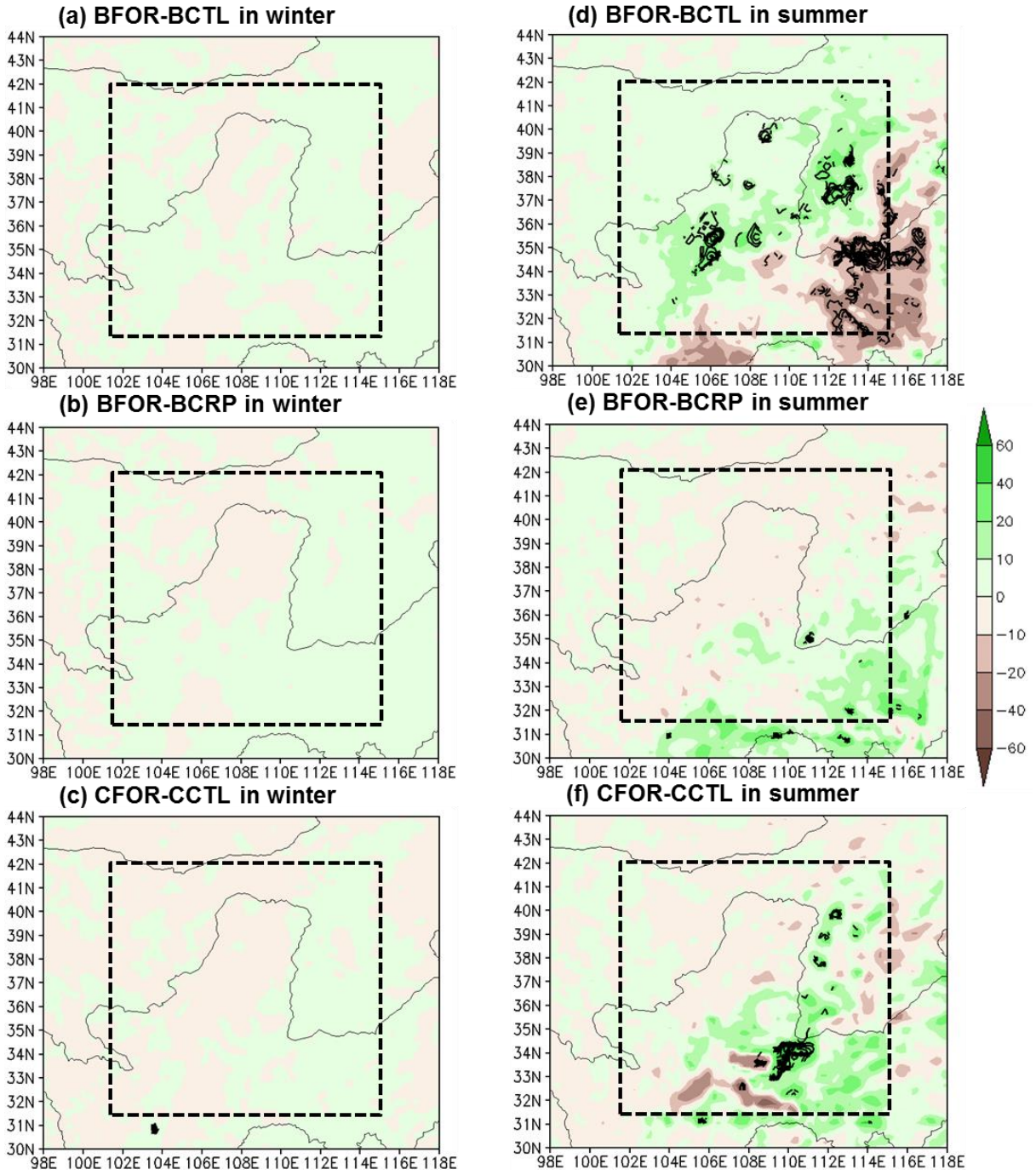

FIGURE 7 As in FIGURE 6, except for precipitation (mm month^{-1}).

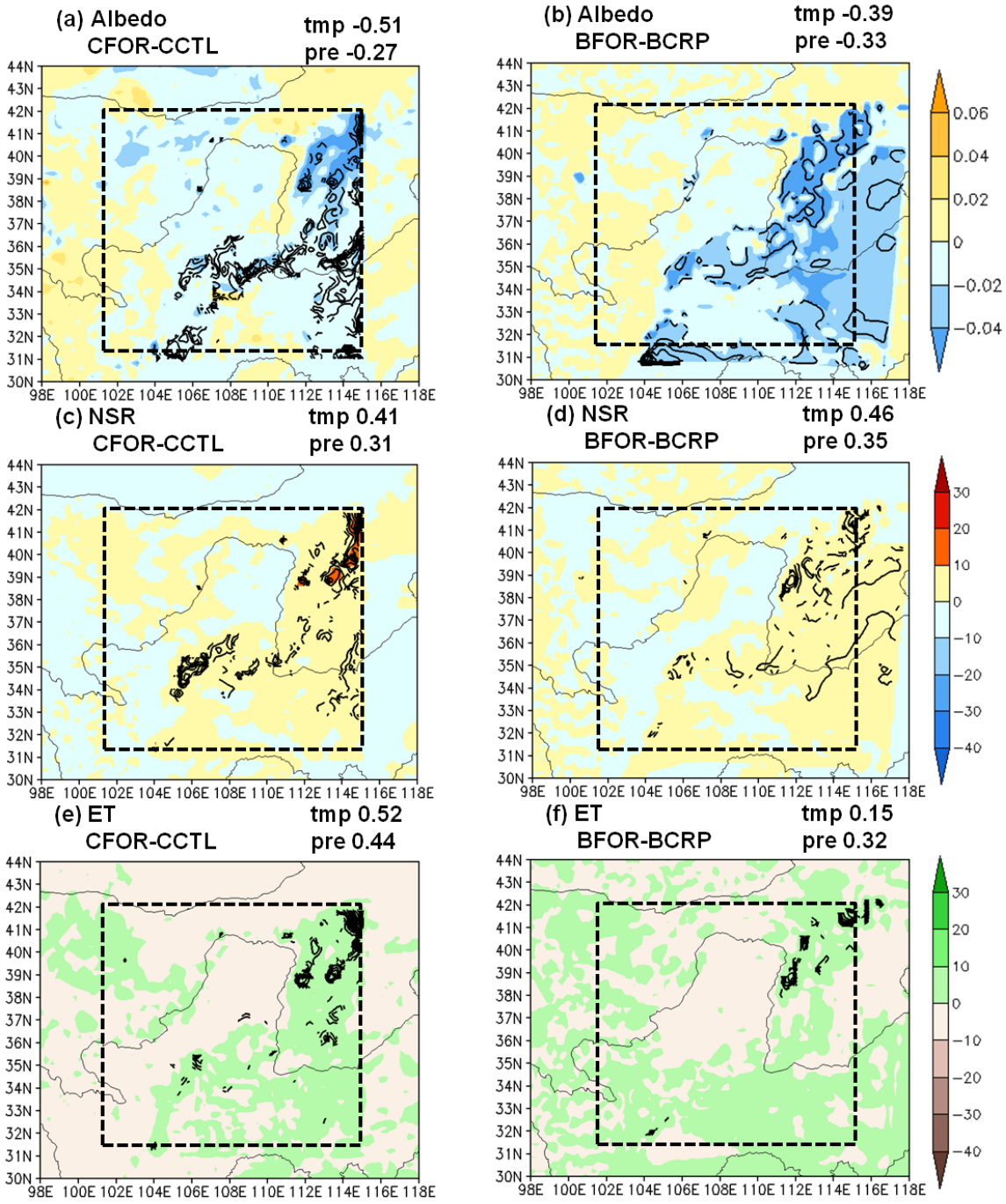

FIGURE 8 In the winter season, differences in surface albedo (a) between the CFOR and the CCTL, (b) between the BFOR and the BCRP; net solar radiation (W m^{-2}) (c) between the CFOR and the CCTL, (d) between the BFOR and the BCRP; evapotranspiration (mm $month^{-1}$) (e) between the CFOR and the CCTL, (f) between the BFOR and the BCRP. Contours represent changes that are statistically significant at the 90% confident level using Student's *t*-test. The pattern correlation coefficients between the differences in temperature (tmp) or precipitation (pre) and each respective variable are shown the top right corner of each figure.

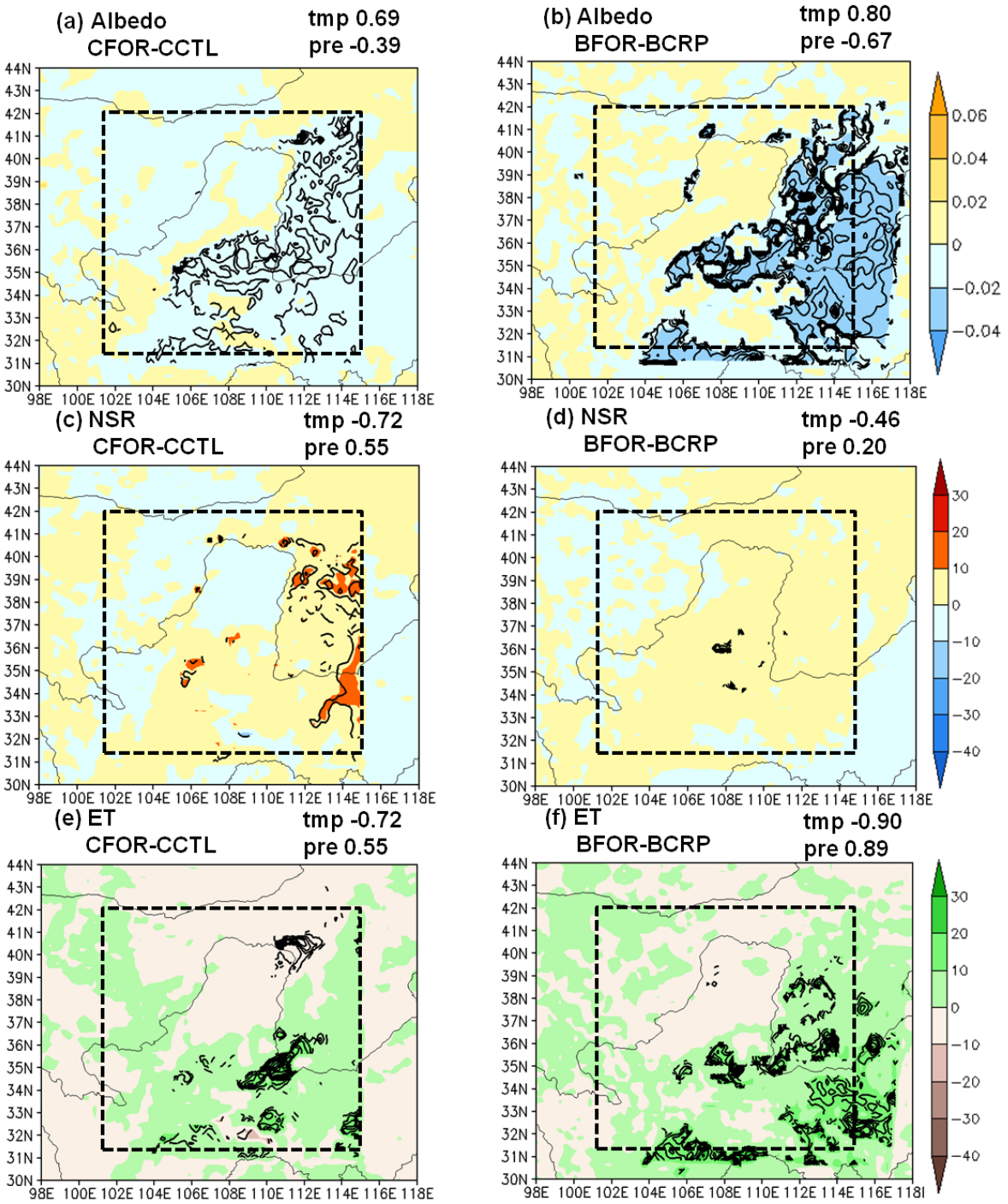

FIGURE 9 As in FIGURE 8, except for summer.

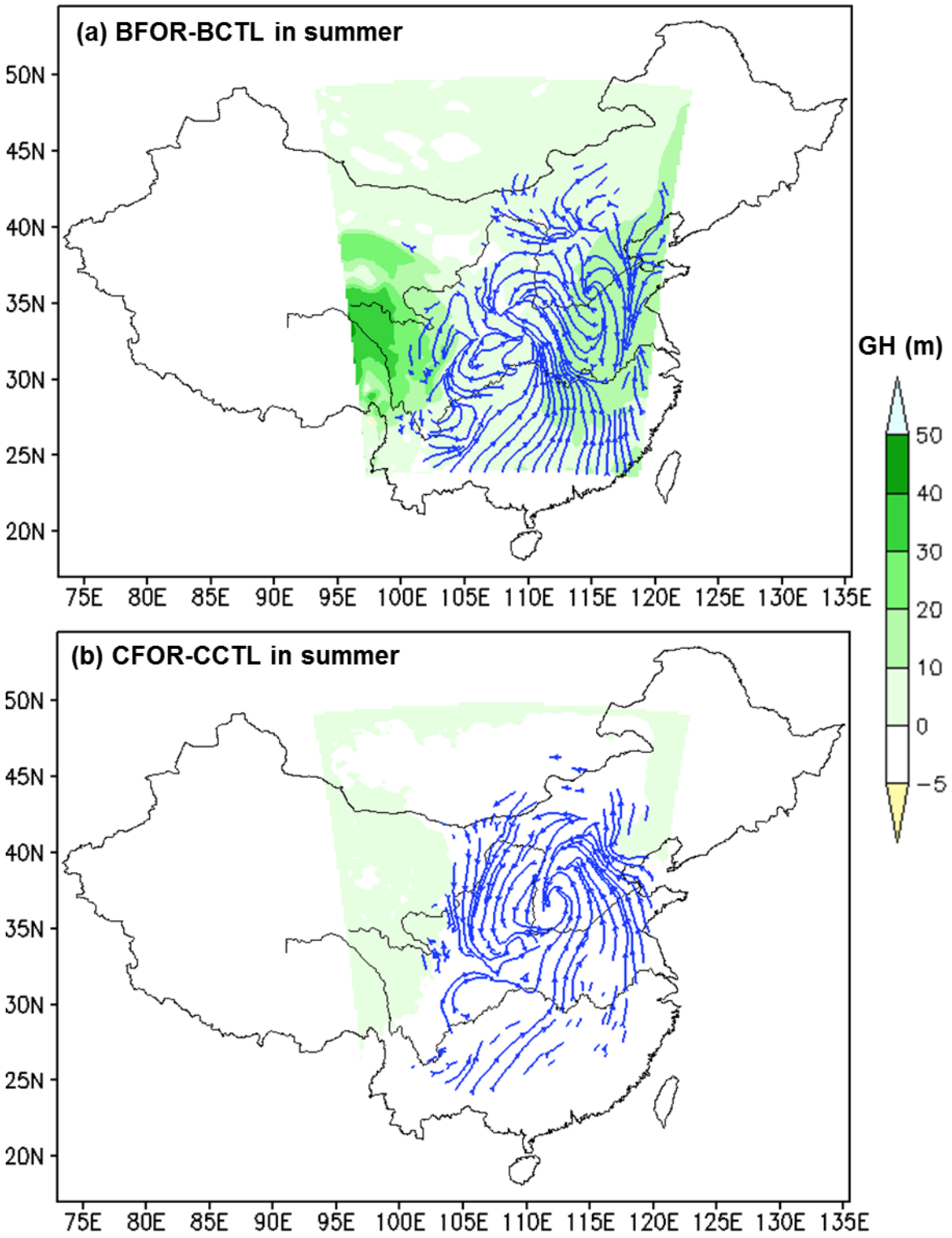

FIGURE 10 Differences in the 850-hPa wind (m s^{-1}) (steamline) and geopotential height (GH; m) in summer between (a) the BFOR and the BCTL, and (b) the CFOR and the CCTL.

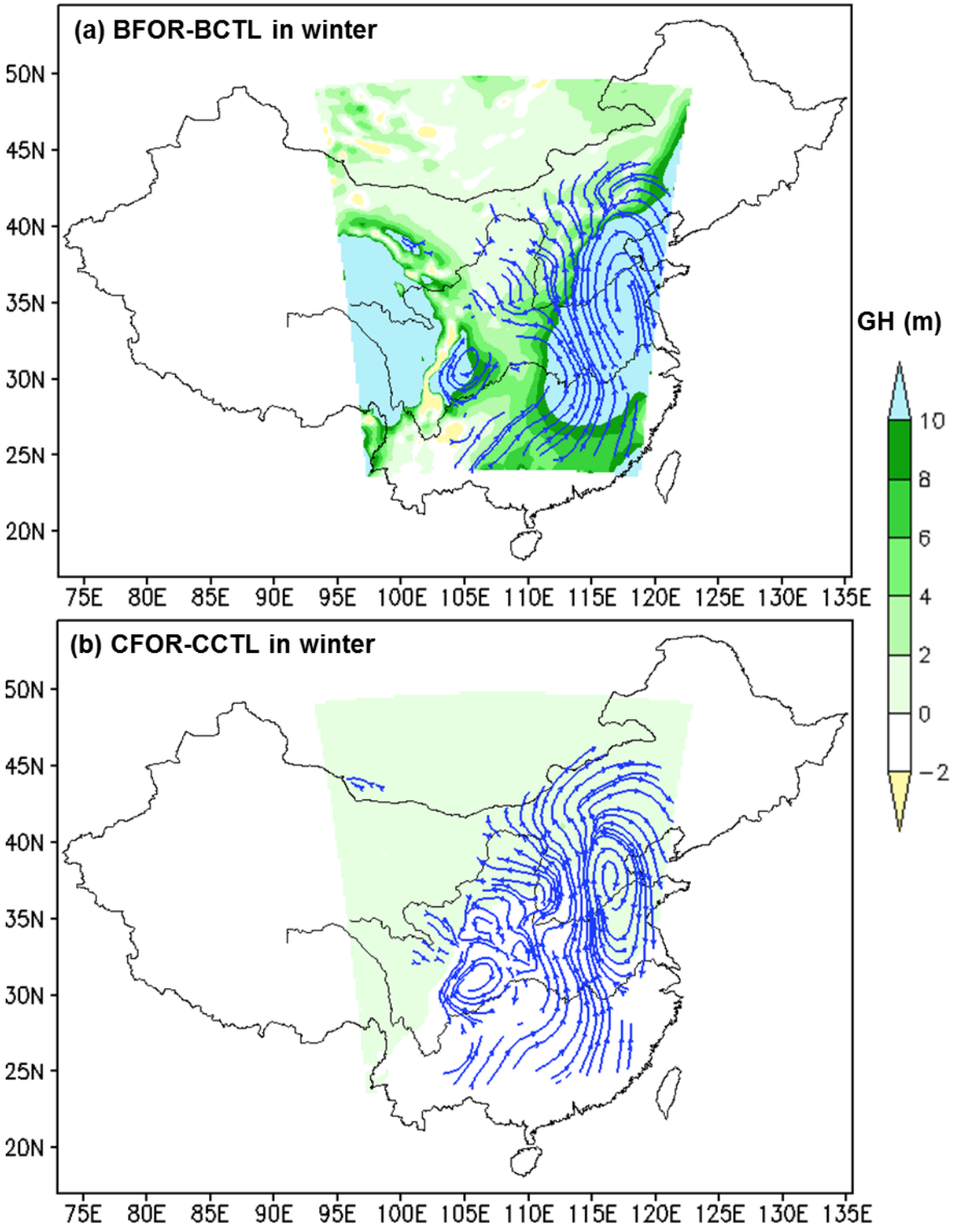

FIGURE 11 As in FIGURE 10, except in winter.

Chapter 6. Discussion

The discussion summarizes the findings of this research, and places it in context with other similar modelling studies and observational datasets. Within the chapter, future opportunities and directions for this research are also identified.

1. Major RegCM4.3 simulation biases

a. Simulated winter cold bias

The main deficiency of the RegCM4.3 simulation over the Loess Plateau was in the representation of the winter temperature with overall cold biases captured by all configurations that have been explored. In addition to the possible reason analyzed in Chapter 2 and Chapter 3, there were three other factors that may also contribute to the cold biases.

The first factor was the modified planetary boundary layer scheme of Holtslag et al. (1990), considering the temperature signal was largely determined by large-scale conditions. The original Holtslag scheme before modification in previous versions of the RegCM appeared to generate excessive vertical transport of heat, moisture, and momentum in the stable conditions, such as the winter season over the northern hemisphere high latitude regions (Giorgi et al. 2012). It was found that in such conditions, the scheme led to large warm winter biases (>10˚C) over several regions such as northern Siberia and northern Canada. To address this problem, the RegCM4.3 modified the Holtslag parameterization through weakening vertical transport of heat and momentum in high latitude winter conditions. Our simulation domain over China and surroundings included a part of such high latitude regions where the vertical transport was potentially limited by the modified Holtslag scheme. As a consequence, the winter temperature cold biases may be generated over the Loess Plateau in Northern China.

The other concern of the cold bias was the aerosol radiative transfer calculation. The radiatively interactive aerosols (particularly the desert dust) had substantial impacts on

long-term regional climate simulations. Solmon et al. (2012) and Zanis et al. (2012) studied of the Sahel and European region, respectively, both showing potential impacts of aerosols on their local temperature. The lack of the aerosols in the simulations may possibly result in the temperature bias over the Loess Plateau surrounded by desert and semi-desert regions.

Last but not least, high resolution simulations of the model were capable of capturing the fine-scale climatic signal in distinct climate regimes with complex topography. A sub-grid land surface configuration could be used for improving the temperature simulation over the Loess Plateau. The sub-grid configuration divides each grid in the model into a regular sub-grid and land surface processes are calculated at each sub-grid point taking into account the local topography and land cover. This scheme has been shown to be useful in model simulations particularly over mountainous areas (Giorgi et al. 2003b). However, the RegCM4.3 is still a hydrostatic model that limits its application for studies requiring very high resolution. The model is being developed for a new non-hydrostatic dynamical core as the base for the next version of the RegCM system.

b. Inconsistencies of the CLM coupled with RegCM4.3

The CLM coupled RegCM4.3 represented more realistic climate simulation than the BATS-coupled simulation over the Loess Plateau. However, the over-effective runoff in the CLM was the primary inconsistence of the simulated surface water budget. The over-effective runoff removed excessive surface water, which resulted in less water stored in the soil that in turn substantially decreased precipitation through the soil-precipitation

feedbacks. The decreased precipitation has been found in several other tests of the CLM within the RegCM framework, such as simulations over the West Africa monsoon region (Steiner et al. 2009), the Central America (Diro et al. 2012) and the center of the United States (Tawfik and Steiner 2011).

The other inconsistence of the CLM was the large amount of energy residual in the surface energy budget, which may also relate to the over-effective runoff. The over-effective runoff associated with dry soil conditions potentially led to surface latent heat fluxes decreases over this semi-arid region, which largely accounted for the redundant net surface energy in the CLM, since the other part of the energy budget remained similar values with observations. A further improvement of the runoff scheme in the CLM is needed especially for semi-arid regions with relatively weak surface flows.

2. Opposite climate responses to the reforestation between the CLM and the BATS simulations

The potential effects of reforestation on the local climate showed pronounced warm and dry conditions in the BATS-coupled simulation, while there were modest cooling and wetting conditions in the CLM during the summer. The warming signs in the BATS were consistent with the observed data from the local meteorology stations (Lü et al. 2012). However, the observations were the mixture of climatic effects of reforestation and greenhouse gases, as well as other sources such as aerosol and urbanization. It is hard to distinguish the climate changes induced by reforestation from the overall climatic effects, which requires further investigation. Meanwhile, the CLM simulated temperature response

was consistent with most modeled results over temperate regions (e.g., Xue et al. 1996; Jackson et al. 2005; Liu 2011; Chen et al. 2012; Zhang et al. 2009), as well as the simulated precipitation change with some of the model results (e.g., Chen et al. 2012; Zhang and Gao 2009).

The primarily reason for the opposite patterns of climate response could be the characteristic difference of the irrigated crop between the BATS and the CLM land surface schemes. It was evidenced by simulations that when the irrigation was added into the CLM as a land surface category, similar responses were achieved with the BATS simulation (Jin and Miller 2011). Similar results were obtained when the irrigation from the BATS was removed and keeping the non-irrigated crop land as the only agricultural land category; consistent climate responses were simulated as in the CLM configuration (Chapter 5).

Such opposite climate responses to similar land surface change were also captured by previous studies, and the dominant factors accounted for the opposite signs include land surface characteristics across regions and relative importance of land-atmosphere feedbacks across models and configurations. For example, the roughness length increase induced by reforestation played an important role in model responses. Chen et al. (2012) using the Community Climate System Model version 3.5 (CCSM3.5), Jackson et al. (2005) using the Regional Atmospheric Modelling System (RAMS), and Liu (2011) using the previous version of RegCM, all simulated the climatic effects of reforestation over the southeast United States and found various precipitation changes. Chen et al. (2012) found that the local precipitation increased with reforestation, which was primarily due to the anomalous ascent of the vertical motion. The anomalous ascent associated with

atmospheric moisture lift and condensation was largely attributed from the roughness length increase that effectively enhanced water vapour and heat exchanges between land surface and atmosphere in the CCSM3.5 system.

In contrast, the local precipitation was found to decrease in response to reforestation in studies of Jackson et al. (2005) and Liu (2011). Jackson et al. (2005) attributed such decrease to the lack of energy to lift the atmospheric moisture high enough to condense and form clouds over the temperate region in the RAMS, although the roughness length has been increased. Liu (2011) found that overall precipitation decreases were mainly caused by the reduction in the prevailing wind that transported moisture to the reforested area. The larger roughness substantially reduced the prevailing wind speed and therefore decreased the local precipitation. Such changes in prevailing wind associated with roughness length increases could also explain the opposite climate responses to reforestation over the East Asia in the studies of Zhang et al. (2009) and Zhang and Gao (2009) (Chapter 1 and Chapter 5). In addition, the SST alternation was found an important factor in the precipitation and temperature changes to reforestation in the study of Ma et al. (2013) over the East Asia monsoon region.

Therefore, it is necessary to thoroughly investigate the climatic effects of reforestation. The land surface change induced by reforestation is an extremely complex system with many processes operating simultaneously at large temporal and spatial scales. The simulated common and uncommon climate responses to reforestation could help improve understanding of land-atmosphere interactive processes using different models. Last but not least, reforestation resulted in cooling effects through bio-geophysical

feedbacks in the CLM-coupled simulation, which helped alleviate the global climate warming. However, the reforestation was also found resulting in dry soil layers over this semi-arid region (McVicar et al. 2007; He et al. 2003), as well as stream flow decline (Sun et al. 2006). With such changes, there will be increasing demand for water from planted trees and human beings, and current water resources will be continually overcommitted in the future. Therefore, future reforestation project requires careful considerations of the regional hydrology-land surface impacts over the semi-arid region of the Loess Plateau.

3. Conclusion

The Loess Plateau and its surrounding regions are considered one of the world's most climatic sensitive areas with complex topography and intensive anthropogenic activities. Recent years, the 'Grain for Green Project' (GGP) has been implemented over the Loess Plateau, with the primary goal of alleviating the local severe soil erosion. The GGP reforestation program primarily focussed on replacing the area of erodible agricultural lands by forest and other natural habitat. Consequently, the land surface over the Loess Plateau has been experiencing a significant change with decreases in agricultural land but increases in natural habitat. Over the next two decades, the GGP proposes to convert additional large erodible regions into natural vegetation. Such extensive land cover changes can have strong impacts on the local climate through their interactions with atmospheric system on a variety of spatial scales.

In this study, a series of simulations using the version 4.3 of RegCM were performed over the Loess Plateau to understand the regional climate features and predict the potential

effects of reforestation on the local climate. The period from 1990 to 2009 was applied to cover the GGP implementation plan. The large simulation domain covered the entire China and surrounding regions with 50-km horizontal resolution, while the inner simulation domain covered the Loess Plateau and surrounding areas with 20-km horizontal resolution using one-way nesting method downscaled from the large domain simulations.

First, the model validation showed that the model could reasonably capture the major climate features in both spatial distribution and temporal variability, including the surface temperature, precipitation, water and energy budgets, total cloud coverage and atmosphere circulation features. The main deficiency was in the overall cold biases during winter simulated by all configurations that have been explored. Using the EM convective scheme (Chapter 3 and 4), a finer horizontal resolution (Chapter 3) and/or the CLM land surface scheme (Chapter 4) can alleviate magnitudes of these cold biases, however, these biases are still a common problem in RegCM4.3 over such topographic complex region.

The bias origins were analysed in detail in Chapter 2 and Chapter 3, including deficiencies of the observed data and ECMWF reanalysis data, lack of greenhouse gases forcing, unrealistic altitudes and temperature laps rate, as well as deficiencies in interior dynamical processes of the model, such as cloud-radiation feedbacks and anomalous temperature advection.

Secondly, the present study analysed the major sensitivities of RegCM4.3 in simulating the regional climate over the Loess Plateau (Chapter 3). A series of simulations using different configurations were applied to investigate the model sensitivity to convective parameterization, horizontal resolution and domain choice. These simulations

revealed that the simulated surface air temperature and precipitation were substantially sensitive to the choice of convective parameterization. The Grell scheme with the Fritsch-Chappell closure assumption was the best suited scheme amongst the three convective experiments in the context of BATS.

The model was also found with more realistic representation at finer resolution of 20-km compared with the simulation at 50-km horizontal resolution. Particularly, the climate spatial pattern was improved over the orographically diverse area as well as the lower bias magnitudes; although certain biases remained in the finer resolution simulation.

The RegCM4.3 simulations were relatively less sensitive to domain size in comparison to the convective scheme and horizontal resolution. However, excluding the Tibetan Plateau from the domain degraded the model simulation. This indicated that the Tibetan Plateau had an important effect on the local climate than other surrounding terrains and should be retained in the simulation domain.

Thirdly, the model sensitivity to the recently coupled land surface scheme, the CLM version 3.5, was analysed over the Loess Plateau in China (Chapter 4). The CLM, in comparison with the default land surface scheme of BATS, applies more sophisticated physical representation of surface water and energy budgets, as well as its bio-geophysical parameterizations describing the heterogeneous land surface. It was found that the CLM represented more realistic climate simulation compared with the BATS, particularly in the surface air temperature and the winter precipitation. However, two inconsistencies in the CLM-coupled simulation were captured: the over-effective runoff in the surface water budget and the large amounts of energy residual in the surface energy budget. Particularly,

the over-effective runoff tended to preclude recharging of the soil moisture and the surface water budget, which potentially inhibited precipitation and latent heat flux in the CLM simulation.

Moreover, the CLM land surface model intensively interacted with convective schemes in the RegCM4.3. Couple with the Emmanuel convective scheme, the CLM could generate the most consistent simulation with the observation. However, when coupled with the Grell convective scheme using two different closure assumptions, the CLM appeared to produce large cold biases during the summer season.

Finally, the two best configurations in the RegCM4.3 system in simulating the regional climate over the Loess Plateau were used to study the climate responses to reforestation (Chapter 5). One configuration was the BATS land surface scheme using the Grell convective scheme with the Fritsch-Chappell closure assumption, the other was the CLM using the Emmanuel convective scheme. Both of them used 20-km horizontal resolution and replaced agricultural land by forest within the Loess Plateau region to simulate potential climatic effects of the reforestation.

Results suggested that the impacts of reforestation on the local climate were similar between the CLM and the BATS simulations during winter. Reforestation over the Loess Plateau was found to cause a warming effect using both land surface schemes, together with a slight decrease in precipitation according to the BATS simulation, but slight increase using the CLM. Large climate responses were mostly captured over the central and east regions of the plateau where there are extensive areas of agricultural land that were converted to forest in both configurations. The climate responses in winter were

predominantly caused by changes in the surface albedo radiation in the CLM configuration, whereas in the BATS simulation changes in ET played critical role.

Furthermore, the model simulated climate responses were strikingly different between the two configurations during summer. The BATS-coupled simulation showed a pronounced warm and dry local climate over the reforested area, while the CLM-coupled simulation showed a medium cooling and wetting climate correspondingly.

The critical reason for the differences in the climate responses were attributed to the different variations in ET, which were associated with the different representation of irrigated crops between the two land surface schemes. The BATS included both irrigated and non-irrigated crops as land categories, but there was only one category for non-irrigated crops in the CLM. Reforestation from the irrigated crop lands in the BATS significantly decreased the surface ET. The lower ET was associated with a shift from sensible to latent heat fluxes that substantially increased the surface air temperature. Meanwhile, the lower ET provided less water vapour to the atmosphere that favoured reducing the local precipitation in the BATS simulation.

The moderate climate responses to reforestation in the CLM simulation were mainly related to changes in the surface ET and roughness length during the summer. The forest generally led to higher ET and larger roughness length compared to the non-irrigated crop. The higher ET associated with higher latent heat fluxes and additional water vapour to atmosphere favoured decreasing surface air temperature and increasing precipitation locally. The larger roughness length tended to enhance the pattern of moisture convergence, which also contributed to precipitation increases.

Overall, this study explicitly examined the climatic features over the Loess Plateau and predicted the potential impacts of reforestation on the local climate using the regional climate model of RegCM version 4.3. This study improved on past studies by providing regional model simulation guidance regarding the performance in such climate transitional zones with very complex topography. This study has also revealed the model's strengths and weaknesses and identified the key mechanisms that drove the simulated biases, which could help to explore future modelling efforts to generate more accurate climate information.

The study also compared the potential impacts of reforestation on the local climate using a more sophisticated land surface model versus those using a relatively simple land surface model. Comparisons amongst these simulations revealed the key climate consequences and uncertainties as well as the underlying mechanisms of climate changes. The opposite climate responses from the two land surface models to reforestation highlights the need for better descriptions of land surface characteristics in climate models, to enable the reliable prediction of climate responses to land surface change. This study is a part of the efforts in improving our understanding of the local climate over the Loess Plateau, which could provide important references for future reforestation strategies and help reduce economic and ecological losses.

4. Future work

It should be noted that a number of processes related to regional simulations of climate and vegetation changes have not been included in this study and need further

improvement in the future. For example, the impacts due to dust and aerosol on regional climate were not identified. Neither does the model allow simulating the effect of land surface changes on carbon cycle and dynamic feedbacks between vegetation distributions and local climate. Furthermore, the vegetation scenarios used do not necessarily reflect the realistic vegetation changes occurred in this region. The opposite climate signs between the two land surface models posted a scientific challenge to predict accurate effects of reforestation on the climate.

Corresponding to those mentioned above, there are several ways in which future study could be expanded and improved. Firstly, employing an integrated regional Earth System Model is necessary to potentially increase confidence in model simulations through reducing biases in the representation of current climate and better characterizing uncertainties in predictions. Secondly, using larger domains, longer simulation times and combining with future climate projections would allow investigation of land surface changes effects on large-scale circulation, climate variability and extreme events. Additional field measurements could also improve the model results validation. Furthermore, it is worthwhile to include the carbon sequestration scheme and investigate the radiative and physiological effects of CO_2 on the regional climate. Meanwhile, the sign of the net local temperature effects of increased forest should be clarified from the overall surface air temperature changes in the future simulations.

References

References

Abiodun, B. J., Z. D. Adeyewa, P. G. Oguntunde, A. T. Salami, and V. O. Ajayi, 2012: Modeling the impacts of reforestation on future climate in West Africa. *Theor Appl Climatol.*, **110,** 77–96.

Afiesimama, E., J. Pal, B. Abiodun, W. Gutowski Jr and A. Adedoyin, 2006: Simulation of West African monsoon using the RegCM3. Part I: Model validation and interannual variability. *Theor. Appl. Climatol.,* **86,** 23–27.

Almazroui, M., 2012: Dynamical downscaling of rainfall and temperature over the Arabian Peninsula using RegCM4. *Clim. Res.,* **52,** 49–62.

An, Z., J. E. Kutzbach, W. L. Prell, and S. C. Porter, 2001: Evolution of Asian monsoons and phased uplift of the Himalaya-Tibetan plateau since Late Miocene times. *Nature,* **411,** 62–63, doi:10.1038/35075035.

Anderson, R. G., and Coauthors, 2010: Biophysical considerations in forestry for climate protection. *Front. Ecol. Environ.,* **9,** 174–182.

Anthes, R. A., 1977: A cumulus parameterization scheme utilizing a one-dimensional cloud model. *Mon. Wea. Rev.,* **105,** 1423–1438.

Anthes, R. A., 1984: Enhancement of convective precipitation by mesoscale variations in vegetative cover in semiarid regions. *J. Climate Appl. Meteor.,* **23,** 541–554.

Anthes, R. A., E. Y. Hsie, and Y. H. Kuo, 1987: Description of the Penn State/NCAR Mesoscale Model, Version 4 (MM4), NCAR Tech Note, NCAR/TN-282-STR, National Center for Atmospheric Research, Boulder, CO 80307.

Antic, S., R. Laprise, B. Denis, and R. de Elía, 2004: Testing the downscaling ability of a one-way nested regional climate model in regions of complex topography. *Clim. Dyn.,* **23,** 473–493.

Arakawa, A., and W. H. Schubert, 1974: Interaction of a cumulus cloud ensemble with the large-scale environment, Part I. *J. Atmos. Sci.*, **31**, 674–701.

Barnston, A. G., and P. T. Schichedanz, 1984: The effect of irrigation on warm season precipitation in the southern Great Plains. *J. Clim. Appl. Meteorol.,* **23,** 865–888.

Betts, R. A., 2000: Offset of the potential carbon sink from boreal forestation by decreases in surface albedo. *Nature,* **408,** 187–190.

Betts, R. A., R. L. Desjardins, and D. Worth, 2007: Impact of agriculture, forest and cloud feedback on the surface energy budget in BOREAS. *Agric. For. Maereorol.,* **142,** 156–169.

Boisier, J. P., N. de Noblet-Ducoudré, A. J. Pitman, F. T. Cruz, C. Delire, B. J. J. M. van den Hurk, M. K. van der Molen, C. Müller and A. Voldoire, 2012: Attributing the impacts of land-cover changes in temperate regions on surface temperature and heat fluxes to specific causes: Results from the first LUCID set of simulations. *J. Geophys. Res.*, **117,** D12116.

Bonan, G. B., 1996: A land surface model (LSM version 1.0) for ecological, hydrological, and atmospheric studies. *NCAR Tech. Note.*, NCAR/RN-417+STR, National Center for Atmospheric Research, Boulder. CO.

Bonan, G. B., 1997: Effects of land use on the climate of the United States. *Clim. Change,* **37,** 449–486.

Bonan, G. B., 2008: Forests and climate change: Forcings, feedbacks, and the climate benefits of forests. *Science,* **320,** 1444–1449.

Bonan, G. B., S. Levis, L. Kergoat, and K. W. Oleson, 2002: Landscape as patches of plant functional types: an intergrating concept for climate and ecosystem models. *Global Biogeochem. Cycles,* **16,** 1360–1384.

Boucher, O., G. Myhre, and A. Myhre., 2004: Direct human influence of irrigation on atmospheric water vapour and climate. *Clim. Dyn.,* **22,** 597–603.

Bounoua, L., 2002: Effects of land cover conversion on surface climate. *Clim. Change,* **52,** 29–64.

Bounoua, L., and T. N. Krishnamurti, 1993: Influence of soil moisture on the Sahelian climate prediction I. *Meteorol. Atmos. Phys.*, **52,** 183–203.

Bowen, I., 1926: The ratio of heat losses by conduction and by evaporation from any water surface. *Phys. Rev.*, **27,** 779–787.

Briegleb, B., P. Minnis, V. Ramanathan, and E. Harrison, 1986: Comparison of regional clear-sky albedos inferred from satellite observations and model calculations. *J. Clim. Appl. Meteorol.*, **25**, 214–226.

References

Brooks, C. E. P., 1928: The influence of forests on rainfall and runoff. *Quart. J. Roy. Meteor. Soc.,* **54,** 1–7.

Cao, S. X., 2008: Why large-scale afforestation efforts in China have failed to solve the desertification problem. *Enviro. Sci. Technol.,* **42,** 1826–1831.

Cao, S. X., L. Chen, D. Shankman, C. M. Wang, X. B. Wang, and H Zhang, 2011: Execessive reliance on afforestation in China's arid and semi-arid regions: Lessons in ecological restoration. *Earth Sci. Rev.,* **104,** 240–245.

Chang, C. P., 2004: East Asian monsoon. World scientific series on meteorology of East Asia. Singapore: World Scientific, 2.

Chang, C. P., and T. N. Krishnamurti, 1987: Monsoon meteorology. New York: Oxford University Press.

Charney, J. G., 1975: Dynamics of deserts and drought in the Sahel. *Quart. J. Roy. Meteorol. Soc.,* **101,** 193–202.

Charney, J. G., W. J. Quirk, S. H. Chow, and J. Kornfield, 1977: A comparative study of the effects of albedo change on drought in semi-arid regions. *J. Atmos. Sci.,* **34,** 1366–1385.

Chase, T. N., R. A. Pielke, T. G. F. Kittel, R. Nemani, and S. W. Running, 1996: Sensitivity of a general circulation model to global changes in leaf area index. *J. Geophys. Res.,* **101,** 7393–7408.

Chase, T. N., R. A. Pielke, T. G. F. Kittel, R. R. Nemani, and S. W. Running, 2000: Simulated impacts of historical land cover changes on global climate in northern winter. *Clim. Dyn.,* **16,** 93–105.

Chazdon, R. L., 2008: Beyond deforestation: Restoring forests and ecosystem services on degraded lands. *Science,* **320,** 1458–1460.

Chen, G. S., M. Notaro, Z. Y. Liu, and Y. Q. Liu, 2012: Simulated local and remote biophysical effects of afforestation over the Southeast United States in Boreal summer. *J. Climate,* **25,** 4511–4522.

References

Chow, K., J. C. L. Chan, J. S. Pal, and F. Giorgi, 2006: Convective suppression criteria applied to the MIT cumulus parameterization scheme for simulating the Asian summer monsoon. *Geophys. Res. Lett.*, **33,** L24709.

Christensen, J. H., T. R. Carter, and F. Giorgi, 2002: PRUDENCE employs new methods to assess European climate change. *EOS Trans. Amer. Geophys. Union*, **83**, 147.

Christensen, J. H., T. R. Carter, M. Rummukainen, and G. Amanatidis, 2007: Evaluating the performance and utility of regional climate models: the PRUDENCE project. *Clim. Change*, **81,** 1–6.

Copeland, J. H., R. A. Pielke, and T. G. F. Kittel, 1996: Potential climatic impacts of vegetation change: A regional modeling study. *J. Geophys. Res.*, **101,** 7409–7418.

Coppola, E., and F. Giorgi, 2010: An assessment of temperature and precipitation change projections over Italy from recent global and regional climate model simulations. *Int. J. Climatol.*, **30,** 11–32.

Cotton, W. R., and Coauthors, 2003: RAMS 2001: Current status and future directions. *Meteorol. Atmos. Phys.*, **82,** 5–29.

Cox, S., P. Stackhouse, S. Gupta, and J. Mikovitz, 2004: The NASA/GEWEX Surface Radiation Budget Project: Results and analysis, In IRS 2004: Current Problems in Atmospheric Radiation, paper presented at the Inter-national Radiation Symposium, Busan, South Korea, 23–27 pp.

Cui, X., G. Huang, and W. Chen, 2008: Notes of numerical simulation of summer rainfall in China with a regional climate model REMO. *Adv. Atmo. Sci.*, **25,** 999–1008. doi: 10.1007/s00376-008-0999-z.

Da Rocha, R., S. V. Cuadra , M. S. Reboita, L. F. Kruger, T. Ambrizzi, and N. Krusche, 2012: Effects of RegCM3 parameterizations on simulated rainy season over South America. *Clim. Res.*, **52,** 253–265.

Dai, Y., and Q. Zeng, 1996: A land surface model (IAP94) for climate studies part I: Formulation and validation in off-line experiments. *Adv. Atmos. Sci.*, **14,** 433–460.

Dai, Y., X. B. Zeng, R. E. Dickinson, and Coauthors, 2003: The Common Land Model. *Bull. Amer. Meteor. Soc.*, **84,** 1013–1023.

References

Daniela, J., and Coauthors, 2007: An inter-comparison of regional climate models for Europe: model performance in present-day climate. *Clim. Change,* **81,** 31–52.

Dash, S., M. S. Shekhar, and G. P. Singh, 2006: Simulation of Indian summer monsoon circulation and rainfall using RegCM3. *Theor. Appl. Climatol.,* **86,** 161–172.

Davis, N., J. Bowden, F. Semazzi, L. Xie, and B. Onol, 2009: Customization of RegCM3 regional climate model for eastern Africa and a tropical Indian Ocean domain. *J. Climate,* **22,** 3595–3616.

de Noblet-Ducoudré N., J-P. Boisier, A. J. Pitman, and coauthors, 2012: Determining Robust Impacts of Land-Use-Induced Land Cover Changes on Surface Climate over North America and Eurasia: Results from the First Set of LUCID Experiments. *J. Climate,* **25,** 3261–3281.

Deardoff, J., 1978: Efficient prediction of ground surface temperature and moisture with inclusion of a layer of vegetation. *J. Geophys. Res.,* **83,** 1889–1903.

Dee, D. P., S. M. Uppala, A. J. Simmons, and Co-authors, 2011: The ERA-Interim reanalysis: configuration and performance of the data assimilation system. Q.J.R. Meteorol. Soc., 137, 553–597, doi: 10.1002/qj.828.

Deque, M., R. Jones, M. Wold, and F. Giorgi, 2005: Global high resolution versus limited area model climate change projections over Europe: quantifying confidence level from PRUDENCE results. *Clim. Dyn.,* **25,** 653–670.

Dickinson, R. E., 1988: The force-restore model for surface temperatures and its generalizations. *J. Climate,* **1,** 1086–1097.

Dickinson, R. E., 1995: Land-atmosphere interaction. *Rev. Geophys.,* **33**, 917–922.

Dickinson, R. E., and A. Henderson-Sellers, 1988: Modelling tropical deforestation: A study of GCM land-surface parameterizations. *Q. J. R. Meteorol. Soc.,* **114,** 439–462.

Dickinson, R. E., R. M. Errico, F. Giorgi, and G. T. Bates, 1989: A regional climate model for the western United States. *Clim. Change,* **15,** 383–422.

Dickinson, R. E., A. Henderson-Sellers, and P. J. Kennedy, 1993: Biosphere-atmosphere transfer scheme (BATS) version 1 as coupled to the NCAR Community Climate Model. *NCAR Tech. Note,* **33,** L24709.

Dirmeyer, P. A., and J. Shukla, 1994: Albedo as a modulator of climate response to tropical deforestation. *J. Geophys. Res.,* **99,** 20863–20877.

Diro G. T., S. A. Rauscher, F. Giorgi, and A. M. Tompkins, 2012: Sensitivity of seasonal climate and diurnal precipitation over Central America to land and sea surface schemes in RegCM4. *Clim. Res.,* **52,** 31–48.

Dorman, J. L., and P. J. Sellers, 1989: A global climatology of albedo, roughness length and stomatal resistance for atmospheric general circulation models as represented by the simple biosphere model (SiB). *J. Appl. Meteorol.,* **28,** 833–855.

Elguindi, N., X. Q. Bi, and F. Giorgi, 2011: Regional Climate Model RegCM User Manual Version 4.3. The Abudus Salam International Centre for Theoretical Physics, Trieste, Italy.

Emanuel, K. A., 1991: A scheme for representing cumulus convection in large-scale models. *J. Atmos. Sci.,* **48,** 2313–2329.

Emanuel, K. A., and R. Pierrehumber, 1996: Microphysical and dynamical control of tropospheric water vapour. *Clouds, Chemistry and Climate,* P. J. Crutzen and V. Ramanathan, Eds., Springer, 264.

Emanuel, K. A., and M. Zivkovic-Rothman, 1999: Development and evaluation of a convection scheme for use in climate models. *J. Atmos. Sci.,* **56,** 1766–1782.

Evans, J. P., and B. F. Zaitchik, 2008: Modeling the large-scale water balance impact of different irrigation systems. *Water Resour. Res.,* **44,** W08448.

Evans, J. P., J. L. McGregor and K. McGuffie, 2012: Future Regional Climates, in *The Future of the World's Climate,* edited by A. Henderson-Sellers and K. McGuffie. Elsevier, New York, 223–252pp.

Fan X. G., Z. G. Ma, Q. Yang, Y. H. Ha, R. Mahmood, Z. Y. Zheng ZY, 2015a: Land use/land cover changes and regional climate over the loess plateau during 2001−2009. Part I: observational evidence. *Clim Chang.,* **129,** 427−440.

Fan X. G., Z. G. Ma, Q. Yang, Y. H. Ha, R. Mahmood, Z. Y. Zheng ZY, 2015b: Land use/land cover changes and regional climate over the loess plateau during 2001−2009. Part II: interrelationship from observations. *Clim Chang.*, **129,** 441−455.

Fang, J. Y., A. P. Chen, C. H. Peng, S. Q. Zhao, and L. J. Ci, 2001: Changes in forest biomass carbon storage in China between 1949 and 1998. *Science,* **292,** 2320–2322.

Feddema, J. J., K. W. Oleson, G. B. Bonan, L. O. Mearns, L. E. Buja, G. A. Meehl, and W. M. Washington, 2005: The importance of land-cover change in simulating future climates. *Science,* **310,** 1674–1678.

Fernandez, J., S. H. Franchito, and V. B. Rao, 2006: Simulation of the summer circulation over South America by two regional climate models. Part I: Mean climatology. *Theor. Appl. Climatol.*, **86**, 247–260.

Field, C. B., D. B. Lobell, H. A. Peters, and N. R. Chiariello, 2007: Feedbacks of terrestrial ecosystems to climate change. *Annu. Rev. Environ. Resour.,* **32,** 1–29.

Findell, K. L., E. Shevliakova, P. C. D. Milly, and R. J. Stouffer, 2007: Modeled impact of anthropogenic land cover change on climate. *J. Climate,* **20,** 3621–3634.

Foley, J. A., I. C. Prentice, N. Ramankutty, S. Levis, D. Pollard, S. Sitch, and A. Haxeltine, 1996: An integrated biosphere model of land surface processes, terrestrial carbon balance, and vegetation dynamics. *Global Biogeochem. Cycles,* **10,** 603–628.

Foley, J. A., M. H. Costa, C. Delire, N. Ramankutty, and P. Snyder, 2003: Green surprise? How terrestrial ecosystems could affect earth's climate. *Front. Ecol. Environ.,* **1,** 38–44.

Foley, J. A., R. DeFries, G. P. Asner, C. Barford, and G. Bonan, 2005: Global consequences of land use. *Science,* **309,** 570–574.

Frei, C., R. Schöll, S. Fukutome, J. Schmidli, and P. L. Vidale, 2006: Future change of precipitation extremes in Europe: Intercomparison of scenarios from regional climate models. *J. Geophys. Res.,* **111,** D06105.

Fritsch, J. M., and C. F. Chappell, 1980: Numerical prediction of convectively driven mesoscale pressure systems. Part I: Convective parameterization. *J. Atmos. Sci.,* 37, 1722–1733.

Fu, B., Y. Liu, and Y. H. Lu, 2011: Assessing the soil erosion control service of ecosystems change in the Loess Plateau of China. *Ecol. Complexity,* **8,** 284–293.

References

Fu, C., and Coauthors, 2005: Regional Climate Model Intercomparison Project for Asia. *Bull. Amer. Meteor. Soc.,* **86,** 257–266.

Fu, C., and H. Yuan, 2001: A virtual numerical experiment to understand the impacts of recovering natural vegetation on the summer climate and environmental conditions in East Asia. *Chin. Sci. Bull.,* **46,** 1199–1203.

Fu, C., H. Harasawa, V. Kasyanov, J. Kim, D. Ojima, Z. Wan, and S. Zhao, 2002: Regional-global interactions in East Asia. Tyson P., R. Fuchs, C. Fu, L. Lebel, A. P. Mitra, E. Odada, J. Perry, W. Steffen, H. Virji (Eds.), *Global-Regional Linkages in the Earth System*, Springer, Berlin, 109–149 pp.

Gao, X., Z. Zhao, Y. Ding, R. Huang, and F. Giorgi, 2001: Climate change due to greenhouse effects in China as simulated by a regional climate model. *Adv. Atmos. Sci.* **18,** 1224–1230.

Gao, X., Z. Zhao, and F. Giorgi, 2002: Changes of extreme events in regional climate simulations over East Asia. *Advan. Atmos. Sci.,* **19,** 927–942.

Gao, X., Y. Luo, W. Lin, Z. Zhao, and F. Giorgi, 2003: Simulation of effects of land use change on climate in China by a regional climate model. *Adv. Atmos. Sci.,* **20**, 583–592.

Gao, X., Y. Xu, Z. Zhao, J. Pal, and F. Giorgi, 2006: On the role of resolution and topography in the simulation of East Asia precipitation. *Theor. Appl. Climatol.*, **86**, 1–4.

Gao, X., D. F. Zhang, Z. Chen, J. Pal, and F. Giorgi, 2007: Land use effects on climate in China as simulated by a regional climate model. *Science in China Ser. D. Earth Sci*, **50,** 620–628.

Gao, X., Y. Shi, R. Song, F. Giorgi, Y. Wang, and D. Zhang, 2008: Reduction of future monsoon precipitation over China: comparison between a high resolution RCM simulation and the driving GCM. *Meteo. Amer. Phys.,* **100,** 73–86.

Gao, X., Y. Shi and F. Giorgi, 2011: A high resolution simulation of climate change over China. *Sci. China Earth Sci.,* **54,** 462–472.

Gao, X., Y. Shi, D. Zhang, J. Wu, and F. Giorgi, 2012: Uncertainties in monsoon precipitation projections over China: results from two high-resolution RCM simulations. *Clim. Res.*, **52**, 213–226.

George, R. J., R. A. Nulsen, R. Ferdowsian, and G. P. Raper, 1999: Interactions between trees and groundwaters in recharge and discharge areas – A survey of Western Australian sites. *Agric. Water Manage.*, **39,** 91–113.

Gianoti, R., D. Zhang and E. Eltahir, 2012: Assessment of the Regional Climate Model Version 3 over the Maritime Continent Using different cumulus parameterization and land surface schemes. *J. Climate.*, **25,** 638–656.

Giorgi, F., 1991: Sensitivity of simulated summertime precipitation over the western United States to different physics parameterizations. *Mon. Wea. Rev.,* **119,** 2870–2888.

Giorgi, F., and G. T. Bates, 1989: The climatological skill of a regional model over complex terrain. *Mon. Wea. Rev.*, **117,** 2325–2347.

Giorgi, F., and L. O. Mearns, 1991: Approaches to the simulation of regional climate change: A review. *Rev. Geophys.*, **29,** 191–216.

Giorgi, F., M. Marinucci, and G. Bates, 1993a: Development of a second generation Regional Climate Model (RegCM2). Part I: Boundary layer and radiative transfer processes. *Mon. Wea. Rev.*, **121**, 2794–2813.

Giorgi, F., R. M. Maria, and T. B. Gary, 1993b: Development of a second generation Regional Climate Model (RegCM2). Part II: Convective processes and assimilation of lateral boundary conditions. *Mon. Wea. Rev*., **121**, 2814–2832.

Giorgi, F., C. B. Shields, and G. T. Bates, 1994: Regional climate change scenarios over the United States produced with a nested regional climate model: Spatail and seasonal characteristics. *J. Climate,* **7,** 375–399.

Giorgi, F., and M. Marinucci, 1996: An investigation of the sensitivity of simulated precipitation to model resolution and its implications for climate studies. *Mon. Wea. Rev.*, **124**, 148–166.

References

Giorgi, F., and R. Avissar, 1997: The representation of heterogeneity effects in earth system modeling: Experience from land surface modeling. *Rev. Geophys.,* **35,** 413–438.

Giorgi, F., J. W. Hurrell, M. R. Marinucci, and M. Beniston, 1997: Elevation dependency of the surface climate change signal: a model study. *J. Climate,* **10,** 288–296.

Giorgi, F., L. Mearns, C. Shields, and L. McDaniel, 1998: Regional nested model simulations of present day and 2 x CO_2 climate over the Central Plains of the U.S.. *Clim. Change*, **40**, 457–493.

Giorgi, F., and L. Mearns, 1999: Introduction to special section: Regional climate modeling revisited. *J. Geophys. Res.*, **104**, 6335–6352.

Giorgi, F., Y. Huang, K. Nishizawa, and C. Fu, 1999: A seasonal cycle simulation over eastern Asia and its sensitivity to radiative transfer and surface processes. *J. Geophys. Res.*, **104**, 6403–6423.

Giorgi, F., X. Q. Bi, and Y. Qian, 2003a: Indirect vs. Direct Effects of Anthropogenic Sulfate on the Climate of East Asia as Simulated with a Regional Coupled Climate-Chemistry/Aerosol Model. *Clim. Change,* **58,** 345–376.

Giorgi F., R. Francisco and J. Pal, 2003b: Effects of a Subgrid-Scale Topography and Land Use Scheme on the Simulation of Surface Climate and Hydrology. Part I: Effects of Temperature and Water Vapor Disaggregation. *J. Hydrometeor,* **4,** 317–333.

Giorgi, F., X. Bi, and J. Pal, 2004: Mean, interannual variability and trends in a regional climate change experiment over Europe. I. Present-day climate (1961–1990). *Clim. Dyn.*, **22**, 733–756.

Giorgi, F., C. Jones, and G. R. Asrar, 2009: Addressing climate information needs at the regional level: the CORDEX framework. *WMO Bulletin*, **58,** 175–183.

Giorgi, F., and Coauthors, 2012: RegCM4: model description and preliminary tests over multiple CORDEX domains. *Clim. Res.,* **52,** 7–29.

Global Soil Data Task, 2000: Global Soil Products CD-ROM (IGBP-DIS). CD-ROM. International Geosphere-Biosphere Programme, Data and Information System, Potsdam, Germany. [Available online at http://www.daac.ornl.gov]

Gochis, D., W. Shuttleworth, and Z. Yang, 2002: Sensitivity of the modeled North American monsoon regional climate to convective parameterization. *Mon. Wea. Rev.*, **130**, 1282–1298.

Grell, G. A., 1993: Prognostic evaluation of assumptions used by cumulus parameterizations. *Mon. Wea. Rev.*, **121**, 764–787.

Grell, G., J. Dudhia, and D. Stauffer, 1994: A description of the fifth generation Penn State/NCAR Mesoscale Model (MM5). *NCAR Tech. Note,* NCAR/TN-398+STR, 121pp.

Gu, H. H., G. L. Wang, Z. B. Yu, and R. Mei, 2012: Assessing future climate changes and extreme indicators in east and south Asia using the RegCM4 regional climate model. *Clim. Change*, **114**, 301–317.

Halenka, T., J. Kalvova, Z. Chladova, A. Demeterova, K. Zemankova, and M. Belda, 2006: On the capability of RegCM to capture extremes in long term regional climate simulation comparison with the observations for Czech Republic. *Theor. Appl. Climatol.*, **86**, 125–145.

He, X., B., Zhan, M., Hao, K., Tang, and F. Zheng, 2003: Down-scale analysis for water scarcity in response to soil-water conservation on Loess Plateau of China. Agric. *Ecosyst. Environ.,* **94,** 355–361.

Henderson-Sellers, A., and M. Wilson, 1983: Surface albedo data for climate modeling. *Rev. Geophys.*, **21**, 1743–1778.

Henderson-Sellers, A., K. McGuffie, and A. Pitman, 1996: The Project for Intercomparison of Land-surface Parametrization Schemes (PILPS): 1992 to 1995. *Clim. Dyn.,* **12,** 849–859.

Hirakuchi, H., and F. Giorgi, 1995: Multiyear present-day and 2 x CO_2 simulations of monsoon climate over eastern Asia and Japan with a regional climate model nested in a general circulation model. *J. Geophys. Res.*, **100**, 21105–21125.

Holtslag, A. A., E. de Bruijn, and H. Pan, 1990: A high resolution air mass transformation model for short-range weather forecasting. *Mon. Wea. Rev.*, **118**, 1561–1575.

References

Hong, S.-Y., and J. Choi, 2006: Sensitivity of the simulated regional climate circulations over East Asia in 1997 and 1998 summers to three convective parameterization schemes. *J. Korean. Meteor. Soc.*, **42,** 361–378.

Hong S.-Y. and M. Kanamitsu, 2014: Dynamical downscaling: Fundamental issues from an NWP point of view and recommendations. *Asia-Pacific J. Atmos. Sci.*, **50,** 83–104.

Huang, J., and Coauthors, 2008: An overview of the semi-arid climate and environment research observatory over the Loess Plateau. *Adv. Atmos. Sci.*, **25**, 906–921.

Huang, W. R., J. C. L. Chan, and A. Y. M. Au-Yeung, 2013: Regional climate simulations of summer diurnal rainfall variations over East Asia and Southeast China. *Clim. Dyn.*, **40,** 1625–1642.

IGBP (International Geosphere Biosphere Programme) Terrestrial Carbon Working Group, 1998: The terrestrial carbon cycle: Implications for the Kyoto Protocol. *Science,* **280,** 1393–1394.

Im, E. S., E. Park, W. Kwon, and F. Giorgi, 2006: Present climate simulation over Korea with a regional climate model using a one-way double-nested system. *Theor. Appl. Climatol.,* **86,** 187–200.

Im, E. S., J. Ahn, A. Remedio, and W. Kwow, 2008: Sensitivity of the regional climate of East/Southeast Asia to convective parameterizations in the RegCM3 modelling system. Part 1: focus on the Korean. *Int. J. Climatol.,* **28,** 1861–1877.

Im, E. S., E. Coppola, F. Giorgi, and X. Bi, 2010: Validation of a high-resolution regional climate model for the Alpine region and effects of a subgrid-scale topography and land use representation. *J. Climate*, **23**, 1854–1873.

Im, E. S., R. L. Gianotti, and E. A. B. Eltahir, 2014: Improving the simulation of the West African Monsoon using the MIT Regional Climate Model. *J. Climate,* **27,** 2209–2229.

Jackson, R. B., J. Canadell, J. R. Ehleringer, H. A. Mooney, O. E. Sala, and E. D. Schulze, 1996: A global analysis of root distributions for terrestrial biomes. *Oecologia,* **108,** 389–411.

Jackson, R. B., E. G. Jobbágy, R. Avissar, and S. Baidya Roy, D. J. Barrett, C. W. Cook, K. A. Farley, D. C. le Maitre, B. A. McCarl, and B. C. Murray, 2005: Trading water for carbon with biological carbon sequestration. *Science,* **310,** 1944–1947.

Jacob, D., and Coauthors, 2007: An inter-comparison of regional climate models for Europe: model performance in present-day climate. *Clim. Change,* **81,** 31–52.

Jarvis, P., 1976: The interpretation of the variations in leaf water potential and stomatal conductance found in canopies in the field. *Philos. T. Roy. Soc.,* **273,** 593–610.

Jin, J. M., and N. L. Miller, 2011: Regional simulations to quantify land use change and irrigation impacts on hydroclimate in the California Central Valley. *Theor. Appl. Climatol.,* **104,** 429–442.

Jobbagy, E. G., and R. B. Jackson, 2004: Groundwater use and salinization with grassland afforestation. *Global Change Biol.*, **10,** 1299–1312.

Jones, R. G., J. M. Murphy, and M. Noguer, 1995: Simulation of climate change over Europe using a nested regional climate model. I: Assessment of control climate, including sensitivity to location of lateral boundaries. *Q. J. R. Meteorol. Soc.*, **121**, 1413–1449.

Juang, H., and M. Kanamitsu, 1994: The NMC nested regional spectral model. *Mon. Wea. Rev.,* **122,** 3–26.

Kato, H., H. Hirakuchi, K. Nishizawa, and F. Giorgi, 1999: Performance of NCAR RegCM in the simulation of June and January climates over eastern Asia and the high-resolution effect of the model. *J. Geophys. Res.*, **104**, 6455–6476.

Kaufmann, R. K., L. Zhou, R. B. Myneni, C. J. Tucker, D. Slayback, N. V. Shabanov, and J. Pinzon, 2003: The effect of vegetation on surface temperature: A statistical analysis of NDVI and climate data. *Geophys. Res. Lett.*, **30,** 2147, doi:10.1029/2003GL018251, 22.

Kiehl, J. T., J. J. Hack, G. B. Bonan, B. A. Boville, and B. P. Briegleb, 1996: Description of the NCAR Community Climate Model (CCM3). *NCAR Tech. Note*, NCAR/TN-464+STR, 152, *National Center for Atmospheric Research*. 2006, Boulder, CO.

Kim, J., and J. Lee, 2003: A multiyear regional climate hindcast for the Western United States using the Mesoscale Atmospheric Simulation model. *J. Hydrometeor*, **4**, 878–890.

Koster, R. D., and Coauthors, 2004: Regions of strong coupling between soil moisture and precipitation. *Science*, **305,** 1138–1140.

Kueppers, L. M., M. A. Snyder, and L. C. Sloan, 2007: Irrigation cooling effect: Regional climate forcing by land-use change. *Geophys. Res.*, 34, L03703.

Kueppers, L. M., M. A. Snyder, L. C. Sloan, D. Cayan, J. Jin, and H. Kanamaru, 2008: Seasonal temperature responses to land-use change in the western United States. *Glob. Planet. Chang.*, **60,** 250–264.

Laprise, R., D. Caya, A. Frigon, and D. Paquin, 2003: Current and perturbed climate as simulated by the second-generation Canadian Regional Climate Model (CRCM-II) over northwestern North America. *Climate Dyn.*, **21,** 405–421.

Laprise, R., and Coauthors, 2008: Challenging some tenets of Regional Climate Modelling. *Meteorol. Atmos. Phys.*, **100,** 3–22.

Laval, K., and L. Picon, 1986: Effect of a change of the surface albedo of the Sahel on climate. *J. Atmos. Sci.*, **43,** 2418–2429.

Lawrence, P., and T. Chase, 2007: Representing a new MODIS consistent land surface in the Community Land Model (CLM3.0). *J. Geophys. Res.*, **112,** G01023.

Lawston, P. M., A. S. Jr. Joseph, F. Z. Benjamin, and R. Matthew, 2015: Impact of Irrigation Methods on Land Surface Model Spinup and Initialization of WRF Forecasts. *J. Hydrometeor*, **16,** 1135–1154.

Lenton, T. M., and N. E. Vaughan, 2009: The radiative forcing potential of different climate geoengineering options. *Atmos. Chem. Phys.*, **9,** 5539–5561.

Leung, L. R., S. J. Ghan, Z. Zhao, Y. Luo, W. Wang, and H. Wei, 1999: Intercomparison of regional climate simulations of the 1991 summer monsoon in eastern Asia. *J. Geophys. Res.*, **104**, 6425–6454.

Leung, L. R., L. O. Mearns, F. Giorgi, and R. L. Wilby, 2003: Regional climate research needs and oppotunities. *Bull. Amer. Meteor. Soc.*, **84,** 89–95.

References

Li, R., 2001: One of report of China's Six Key Forestry Programs: visiting of Sand Control Programs for areas in the vicinity of Beijing and Tianjin. *Forestry and Humans,* **9,** 14–18 (in Chinese).

Li, S., Z. Zhong, W. Guo, and W. Lu, 2014: Modifications on the surface layer scheme in RegCM4.3.5-CLM. *Clim. Dyn.,* **44,** 2249–2265.

Li, W., 2004: Degradation and restoration of forest ecosystems in China. *Forest Ecol. Manage.,* **201,** 33–41.

Li, Z., F. Zheng, W. Liu and D. C. Flanagan, 2010: Spatial distribution and temporal trends of extreme temperature and precipitation events on the Loess Plateau of China during 1961–2007. *Quat. Int.,* **226,** 92–100.

Li, Z., W. Z. Liu, and X. C. Zhang, 2011: Assessing the site-specific impacts of climate change on hydrology, soil erosion and crop yields in the Loess Plateau of China. *Clim. Change,* **105,** 223–242.

Liang, X., and Coauthors, 2012: Regional Climate-Weather Research and Forecasting Model. *Bull. Amer. Meteor. Soc.,* **93,** 1363–1387.

Linda, O., R. A. Mearns, and B. Sebastien, 2012: The North American Regional Climate Change Assessment Program: Overview of Phase I Results. *Bull. Amer. Meteor. Soc.,* **93,** 1337–1362.

Liu, C., and Y. Zeng, 2004: Changes of pan evaporation in the recent 40 years in the Yellow River Basin. *Water Int.,* **29**, 510–516.

Liu, J., S. Li, Z. Ouyang, C. Tam, and X. Chen, 2008a: Ecological and socioeconomic effects of China's policies for ecosystem services. *PNAS,* **105,** 9477–9482.

Liu, Q., Z. Yang, and B. Cui, 2008b: Spatial and temporal variability of annual precipitation during 1961–2006 in Yellow River Basin, China. *J. Hydrol.,* **361,** 330–338.

Liu, Y., 2011: A numerical study on hydrological impacts of forest restoration in the southern United States. *Ecohydrol.,* **4,** 299–314.

Liu, Y., F. Giorgi, and W. M. Washington, 1994: Simulation of summer monsoon climate over East Asia with an NCAR regional climate model. *Mon. Wea. Rev.*, **122**, 2331–2348.

Liu, Y., J. Stanturf, and H. Lu, 2008c: Modeling the potential of the Northern China forest shelterbelt in improving hydroclimate conditions. *J. Amer. Water Res. Assoc.*, **44,** 1176–1192.

Liu, Z. Y., M. Notaro, J. Kutzbach, and N. Z. Liu, 2006: Assessing global vegetation-climate feedbacks from observations. *J. Climate,* **19,** 787–814.

Lobell, D. B., G. Bala, and P. B. Duffy, 2006: Biogeophysical impacts of cropland management changes on climate. *Geophys. Res. Lett.*, **33,** L06708.

Loveland, T., B. Reed, J. Brown, D. Ohlen, Z. Zhu, L. Yang, and J. Merchant, 2000: Development of a global land cover characteristics database and IGBP DISCover from 1 km AVHRR data. *Int. J. Remote Sens.,* **21,** 1303–1330.

Lü Y. H., B. J. Fu, X. M. Feng, Y. Zeng, Y. Liu, R. Y. Chang, G. Sun, B. F. Wu, 2012: A policy-driven large scale ecological restoration: Quantifying ecosystem services changes in the Loess Plateau of China. *Plos One,* **7,** e31782.

Ma, D., M. Notaro, Z. Y. Liu, G. S. Chen, and Y. Q. Liu, 2013: Simulated impacts of afforestation in East China monsoon region as modulated by ocean variability. *Clim. Dyn.*, **41,** 2439–2450.

Martinez-Castro, D., R. da Rocha, A. Bezanilla-Morlot, L. Alvarez-Escudero, J. P. Reyes-Fernandez, Y. Silva-Vidal, and R. W. Arritt, 2006: Sensitivity studies of the RegCM3 simulation of summer precipitation, temperature and local wind field in the Caribbean Region. *Theor. Appl. Climatol.*, **86**, 5–22.

Mass, C., D. Ovens, K. Westrick, and A. Colle, 2002: Does increasing horizontal resolution produce more skillful forcasts? Bull. *Amer. Meteor. Soc.*, **83,** 407–430.

McDonald, A., 1997: Lateral boundary conditions for operational regional forecast models: A review. *HIRLAM Technical Report No.32,* HIRLAM Project, Norrköping, Sweden, 31 pp.

McGregor, J. L., 1997: Regional climate modelling. *Meteorol. Atmos. Phys.,* **63,** 105–117.

McGregor, J. L., J. J. Katzfey, and K. C. Nguyen, 1998: Fine resolution simulations of climate change for Southeast Asia: Final report for a research project commissioned by Southeast Asian Regional Committee for START (SARCS), Aspendale, VIC, Australia: CSIRO Atmospheric Research VI, 35 pp.

McVicar, T., L. Li, T. Van Niel, and Coauthors, 2007: Developing a decision support tool for China's re-vegetation program: Simulating regional impacts of afforestation on average annual streamflow in the Loess Plateau. *Forest Ecol. Manage.,* **251,** 65–81.

Mearns, L. O., and Coauthors, 2012: The North American regional climate change assessment program: Overview of phase I results. *Bull. Amer. Meteor. Soc.,* **93,** 1337–1362.

Mei, R., G. Wang, and H. Gu, 2013: Summer land-atmosphere coupling strength over the United States: Results from the Regional Climate Model RegCM4-CLM3.5. *J. Hydrometeor.,* **14,** 946–962.

Metz B., O. R. Davidson, P. R. Bosch, R. Dave, and L. A. Meyer, 2007: Climate change 2007: mitigation of climate change. *Contribution of working group III to the Fourth assessment report of the intergovernmnetal panel on climate change,* Cambridge University Press, Cambridge, United Kingdom and New York, USA.

Mitchell, T., and D. Jones, 2005: An improved method of constructing a database of monthly climate observations and associated high-resolution grids. *Int. J. Climatol.*, **25,** 693–712.

Moss R. H., J. A. Edmonds, K. A. Hibbard, and co-authors, 2010: The next generation of scenarios for climate change research and assessment. *Nature,* **463,** 747–756, doi: 10.1038.

Myneni R. B., S. Hoffman, Y. Knyazikhin, and coauthors, 2002: Global products of vegetation leaf area and fraction absorbed PAR from year one of MODIS data. *Remote Sens. Environ.*, **83,** 214–231.

Nabuurs, G., O. Masera, K. Anderasko, and P. Benitez-Ponce, 2007: Climate change 2007: mitigation of climate change. B. Metz, O. R. Davidson, P. R. Bosch, R. Dave, and L. A. Meyer (eds.), *Contribution of working group III to the Fourth assessment report*

of the intergovernmnetal panel on climate change, Cambridge University Press, Cambridge, United Kingdom and New York, USA.

NDRC (National Development and Reform Commission), MWR (Ministry of Water Resources), MA (Ministry of Agriculture), and SFA (State Forestry Administration), People's Republic of China, 2010: Programming for Comprehensive Management of the Loess Plateau (2010–2030), **69,** 8–10.

New, M., M. Hulme, and P. Jones, 2000: Representing twentieth-century space-time climate variability. Part II: Development of 1901–96 monthly grids of terrestrial surface climate. *J. Climate*, **13**, 2217–2238.

Niu, G., Z. L. Yang, R. E. Dickinson, and L. E. Gulden, 2005: A simple TOPMODEL-based runoff parameterization (SIMTOP) for use in global climate models. *J. Geophys. Res.,* **110,** D21106.

Nobre, C. A., P. J. Sellers, and J. Shukla, 1991: Amazonian deforestation and regional climate change. *J. Climate,* **4,** 957–988.

Notaro, M., Z. Liu, and J. W. Williams, 2006: Observed vegetation-climate feedbacks in the United States. *J. Climate,* **19,** 763–786.

Notaro, M., and Z. Liu, 2008: Statistical and dynamical assessment of vegetation feedbacks on climate over the boreal forest. *Climate Dyn.,* **31,** 691–712.

Oleson, K. W., G. B. Bonan, S. Levis, and M. Vertenstein, 2004a: Effects of land use change on North American climate: impact of surface datasets and model biogeophysics. *Climate Dyn.,* **23,** 117–132.

Oleson, K. W., and Coauthors, 2004b: Technical description of the Community Land Model (CLM). *NCAR Tech. Note*, NCAR/TN-461+STR, Natl. Cent. for Atmos. Res..

Oleson, K. W., and Coauthors, 2007: CLM3.5 Documentation. UCAR, 34pp. [Available online at http://www.cgd.ucar.edu/tss/clm/distribution/clm3.5/CLM3_5_documentation.pdf.]

Oleson, K. W., G. Y. Niu, Z. L. Yang and D. M. Lawrence, 2008: Improvements to the Community Land Model and their impact on the hydrologic cycle. *J. Geophys. Res.,* **113,** G01021.

Otte, T. L., 1999: Developing Meteorological Fields, *Atmospheric Modeling Division*, National Exposure Research Laboratory U. S. Environmental Protection Agency, Washington, DC, pp 6–7.

Pal, J. S., E. E. Small, and E. Eltahir, 2000: Simulation of regional-scale water and energy budgets: Representation of subgrid cloud and precipitation processes within RegCM. *J. Geophys. Res.*, **105**, 29579–29594.

Pal, J. S., and Coauthors, 2007: The ICTP RegCM3 and RegCNET: Regional climate modeling for the developing world. *Bull Amer. Meteor. Soc.*, **88**, 1359–1409.

Pan, Z., J. H. Christensen, R. W. Arritt, W. J. Gutowski Jr., E. S. Takle, and F. Otieno, 2001: Evaluation of uncertainties in regional climate change simulations. *J. Geophys. Res.*, **106,** 17735–17751.

Park, E., S. Hong, and H. Kang, 2008: Characteristics of an East-Asian summer monsoon climatology simulated by the RegCM3. *Meteo. Atmos. Phys.*, **100,** 139–158.

Pawson, S., R. S. Stolarski, A. R. Douglass, P. A. Newman, J. E. Nielsen, S. M. Frith, and M. L. Gupta, 2008: Goddard Earth Observing System chemistry-climate model simulations of stratospheric ozone temperature coupling between 1950 and 2005. *J. Geophys. Res.*, **113,** D12103, doi: 10.1029/2007JD009511.

Peng, M., J. Ridout, and T. Hogan, 2004: Recent modifications of the Emanuel convective scheme in the Navy Operational Global Atmospheric Prediction Scheme. *Mon. Wea. Rev.*, **132,** 1254–1268.

Piao, S. L., P. Ciais, Y. Huang, and Coauthors, 2010: The impacts of climate change on water resources and agriculture in China. *Nature*, **467,** 43–51.

Pielke, R. A., 2001: Influence of the spatial distribution of vegetation and soils on the prediction of cumulus convective rainfall. *Rev. Geophys.*, **39**, 151–177.

Pielke, R. A., and R. Avissar, 1990: Influence of landscape structure on local and regional climate. *Landscape Ecol.*, **4**, 133–155.

Pielke, R. A., M. Raupach, A. J. Dolman, X. Zeng, and A. S. Denning, 1998: Interactions between the atmosphere and terrestrial ecosystem: Influence on weather and climate. *Global Change Biol.*, **4,** 461–475.

Pielke, R. A., G. Marland, R. Betts, T. N. Chase, and J. L. Eastman, 2002: The influence of land-use change and landscape dynamics on the climate system: relevance to climate-change policy beyond the radiative effect of greenhouse gases. Philos. *Trans. R. Soc. Lond.,* **360,** 1705–1719.

Pinker, R. T., and I. Laszlo, 1992: Modeling surface solar irradiance for satellite applications on a global scale. *J. Appl. Meteor.,* **31**, 194–211.

Pitman, A., 1999: Key results and implications from phase 1(c) of the Project for Intercomparison of Land-Surface Parametrization schemes. *Clim. Dyn.,* **15,** 673–684.

Pitman, A. J., 2003: The evolution of, and revolution in, land surface schemes designed for climate models. *Int. J. Climatol.,* **23,** 479–510.

Pitman, A. J., and G. T. Narisma, 2005: The role of land surface processes in regional climate change: a case study of future land cover change over south western Australia. *Meteor. Atmos. Phys.,* **89,** 235–249.

Pitman, A. J. and N. de Noblet-Ducoudré, 2011: Human effects on climate through land-use induced land cover change, *Chapter 4 of The Future of the World's Climate,* edited by A. Henderson-Sellers and K. McGuffie 77–95 pp, Elsevier Amsterdam.

Pitman A. J., N. de Noblet-Ducoudré, F. T. Cruz and co-authors, 2009: Uncertainties in climate responses to past land cover change: first results from the LUCID intercomparison study. *Geophys. Res. Lett.,* **36,** L14814.

Pitman, A., F. B. Avila, G. Abramowitz, Y. P. Wang, S. J. Phipps, and de N. Noblet-Ducoudre, 2011: Importance of background climate in determining impact of land-cover change on regional climate. *Nat. Climate Change*, **1,** 472–475.

Pitman, A. J., N. de Noblet-Ducoudré, F. B. Avila, and co-authors, 2012: Effects of land cover change on temperature and rainfall extremes in multi-model ensemble simulations. *Earth Syst. Dynam.,* **3,** 213–231.

Qian, W., and Y. Zhu, 2001: Climate change in China from 1880 to 1998 and its impact on the environmental condition. *Clim. Change*, **50**, 419–444.

Qian, Y., F. Giorgi, Y. Huang, W. L. Chameides, and C. Luo, 2001: Simulation of anthropogenic sulfur over East Asia with a regional coupled chemistry-climate model. *Tellus,* **53B,** 171–191.

Ratnam, J., and K. Kumar, 2005: Sensitivity of the simulated monsoons of 1987 and 1988 to convective parameterization schemes in MM5. *J. Climate*, **18**, 2724–2743.

Reboita, M., J. P. R. Fernandez, M. P. Llopart, R. P. da Rocha, L. A. Pampuch, and F. T. Cruz., 2014: Assessment of RegCM4.3 over the CORDEX South America domain: sensitivity analysis for physical parameterization schemes. *Clim. Res.*, **60,** 215–234.

Ribaudo, M. O., D. Colacicco, L. L. Langner, S. Piper, G. D. Schaible, 1990: Natural resources and users benefit from the Conservation Reserve Program. *Agricultural Economic Report, Economic Research Service, U. S. Department of Agriculture, Washington, DC,* **627,** 51 pp.

Rogers, R., and M. Yau, 1989: A short course in cloud physics. *Int. Ser. Nat. Philos.,* **113,** 3rd ed., Elsevier, New York, 290 pp.

Rossow, W., and R. Schiffer, 1999: Advances in understanding clouds from ISCCP. *Bull. Amer. Meteor. Soc.*, **80**, 2261–2287.

Rummukainen, M., 2010: State-of-the-art with regional climate models. *WIREs Clim. Change*, **1,** 82–96.

Schmidli, J., C. M. Goodess, C. Frei, M. R. Haylock, Y. Hundecha, J. Ribalaygua, and T. Schmith, 2007: Statistical and dynamical downscaling of precipitation: An evaluation and comparison of scenarios for the European Alps. *J. Geophys. Res.*, **112,** D04105.

Sellers, P. J., 1992: Biophysical models of land surface processes. In: *Climate System Modelling, Trenberth K. E. (Ed.)*. Cambridge University Press, Cambridge, 451–490 pp.

Sen, O. L., Y. Wang, and B. Wang, 2004: Impact of Indochina deforestation on the East Asian Summer Monsoon. *J. Climate,* **17,** 1366–1380.

Seneviratne, S. L., I. D. Luthi, M. Litschi, and C. Schar, 2006: Land-atmosphere coupling and climate change in Europe. *Nature*, **443,** 205–209.

Seth, A., and F. Giorgi, 1998: The effects of domain choice on summer precipitation simulation and sensitivity in a regional climate model. *J. Climate,* **11,** 2698–2712.

Seth, A., S. A. Rauscher, S. J. Camargo, J. Qian, and J. S. Pal, 2007: RegCM3 regional climatologies for South America using reanalysis and ECHAM global model driving fields. *Clim. Dyn.,* **28,** 461–480.

Shukla, J., and Y. Mintz, 1982: Influence of land-surface evaportranspiration on the Earth's climate. *Science,* **125,** 1498–1501.

Siebert, S. and P. Döll, 2001: A digital global map of irrigated areas-An update for Latin America and Europe. *Kassel World Water Ser. 4, Cent. for Environ. Syst. Res.*, University of Kassel, Germany, 14 pp. http://www.geo.uni-frankfurt.de/fb/fb11/ipg/ag/dl/f_publikationen/2001/siebert_doell_kwws4.pdf.

Siebert, S., P. Döll, J. Hoogeveen, J.-M. Faures, K. Frenken and S. Feick, 2005: Development and validation of the global map of irrigation areas. *Hydrol. Earth Sys. Sci. Discuss.,* **2,** 1299–1327.

Singh, G. P., J. H. Oh, J. Y. Kim, and O. Y. Kim, 2006: Sensitivity of summer monsoon precipitation over East Asia to convective parameterization schemes in RegCM3. *SOLA,* **2,** 29–32.

Snyder, P. K., C. Delire, and J. A. Foley, 2004: Evaluating the influence of different vegetation biomes on the global climate. *Climate Dyn.,* **23,** 279–302.

Solmon F., N. Elguindi, and M. Mallet, 2012: Radiative and climatic effects of dust over West Africa, as simulated by a regional climate model. *Clim. Res.*, **52,** 97–113.

Stackhouse, P. W., S. K. Gupta, S. J. Cox, J. C. Mikowitz, T. Zhang, and M. Chiacchio, 2004: 12-year surface radiation budget data set. No. 4 International GEWEX Project Office, Silver Spring, MD, *GEWEX News*, **14**, 10–12 pp.

Stebbings, E., 1935: The encroaching Sahara. *Geogr. J.*, **86,** 509–510.

Steiner, A., J. S. Pal, F. Giorgi, R. Dickinson and W. Chameides, 2005: The coupling of the common land model (CLM0) to a regional climate model (RegCM). *Theor. Appl. Climatol.,* **82,** 225–243.

Steiner, A., J. S. Pal, S. Rauscher, J. Bell, S. D. Noah, A. Boone, L. C. Sloan and F, Giorgi, 2009: Land surface coupling in regional climate simulations of the West African monsoon. *Clim. Dyn.,* **33,** 869–892.

Stieglitz, M., D. Rind, J. Famiglietti, and C. Rosenzweig, 1997: An effective approach to modeling the topographic control of surface hydrology for regional and global climate modeling. *J. Climate,* **10,** 118–137.

Stocker T. F., D. Qin, G.-K. Plattner and co-authors, 2013: *Climate change 2013: the physical science basis. Contribution of Working Group I to the Fifth Assessment Report of the Intergovernmental Panel on Climate Change.* Cambridge University Press, Cambridge.

Sud, Y. C., and M. Fennessy, 1982: A study of the influence of surface albedo on July circulation in semi-arid regions using the glas GCM. *J. Climatol.,* **2,** 105–125.

Sud, Y. C., J. Shukla, and Y. Mintz, 1988: Influence of land surface roughness on atmospheric circulation and precipitation: A sensitivity study with a general circulation model. *J. Appl. Meteor.,* **27,** 1036–1054.

Sun, G., G. Zhou, Z. Zhang, X. Wei, and S. McNulty, 2006: Potential water yield reduction due to forestation across China. *J. Hydrology,* **328,** 548–558.

Sun, Q., C. Miao, Q. Duan, D. Kong, A. Ye, Z. Di, and W. Gong, 2014: Would the 'real' observed dataset stand up? A critical examination of eight observed gridded climate datasets for China. *Environ. Res. Lett.,* **9,** 1–9.

Sundqvist, H., E. Berge, and J. Kristjansson, 1989: Condensation and Cloud Parameterization Studies with a Mesoscale Numerical Weather Prediction Model. *Mon. Wea. Rev.*, **17**, 1641–1657.

Sylla, M. B., E. Coppola, L. Mariotti, F. Giorgi, P. M. Ruti, A. Dell'Aquila, and X. Bi, 2010: Multiyear simulation of the African climate using a regional climate model (RegCM3) with the high resolution ERA-interim reanalysis. *Clim. Dyn.*, **35,** 231–247.

Takle, E., and Coauthors, 1999: Project to intercompare regional climate simulations (PIRCS): Description and initial results. *J. Geophys. Res.*, **104**, 19443–19461.

Tawfik A. B., and A. L. Steiner, 2011: The role of soil ice in land-atmosphere coupling over the United States: A soil moisture-precipitation winter feedback mechanism. *J. Geophys. Res.,* **116,** D02113.

Taylor, K., 2001: Summarizing multiple aspects of model performance in a single diagram. *J. Geophys. Res.,* **106,** 7183–7192.

Torma, C., E. Coppola, F. Giorgi, J. Bartholy, and R. Pongracz, 2011: Validation of a High-Resolution Version of the Regional Climate Model RegCM3 over the Carpathian Basin. *J. Hydrometeorol.,* **12,** 84–100.

Troy, T., and E. Wood, 2009: Comparison and evaluation of the gridded radiation products across northern Eurasia. *Env. Res. Lett.,* **4**, 045008.

Unruh, J., 1995: Agroforestry, reforestry, and the carbon problem: The role of land and tree tenure. *Interdiscipl. Sci. Rev.,* **20,** 215–227.

Uppala, S., D. Dee, S. Kobayashi, P. Berrisford, and A. Simmons, 2008: Towards a climate data assimilation system: status update of ERA-interim. *ECMWF Newsletter*, **115**, 12–18.

von Storch, H, H. Langenberg, and F. Feser, 2000: A spectral nudging technique for dynamical downscaling purposes. *Mon. Wea. Rev.,* **128,** 3664–3667. doi: http://dx.doi.org/10.1175/1520-0493(2000)128<3664:ASNTFD>2.0.CO;2.

Walker, G. R., L. Zhang, T. W. Ellis, T. J. Hatton, and C. Petheram, 2002: Estimating impacts of changed land use on recharge: review of modelling and other approaches appropriate for management of dryland salinity. *Hydrogeology J.,* **10,** 68–90.

Wang, D., C. Menz, T. Simon, C. Simmer, and C. Ohlwein, 2013: Regional dynamical downscaling with CCLM over East Asia. *Meteorol. Atmos. Phys.*, **121,** 39–53. doi: 10.1007/s00703-013-0250-z.

Wang, G., J. L. Innes, J. Lei, S. Dai, and S. W. Wu, 2007: China's forestry reforms. *Science,* **318,** 1556–1557.

Wang, H., A. J. Pitman, M. Zhao, and R. Leemans, 2003: The impact of land-cover modification on the June meteorology of China since 1700, simulated using a Regional Climate Model. *Int. J. Climatol.,* **23,** 511–527.

Wang, L., and K. K. W. Cheung, 2015a: A regional climate modeling study over the Loess Plateau, China. Part I: Model validation. *J. Climate* (submitted).

Wang, L., and K. K. W. Cheung, 2015b: A regional climate modeling study over the Loess Plateau, China. Part II: Sensitivity tests. *J. Climate* (submitted).

Wang, L., and K. K. W. Cheung, 2015c: A regional climate modeling study over the Loess Plateau, China. Part III: Impacts from the Community Land Model. *J. Climate* (in preparation).

Wang, S. Y., R. R. Gillies, E. S. Takle, and W. J. Gutowski Jr., 2009: Evaluation of precipitation in the Intermountain Region as simulated by the NARCCAP regional climate models. *Geophys. Res. Lett.*, **36**, L11704.

Wang, S. Z., and E. T. Yu, 2013: Simulation and projection of changes in rainy season precipitation over China using the WRF model. *Acta Meteorol. Sin.*, **27,** 577–584. doi: 10.1007/s13351-013-0406-2.

Wang, Y. Q., L. R. Leung, J. L. McGregor, D.-K. Lee, W. C. Wang, Y. Ding, and F. Kimura, 2004: Regional climate modelling: Progress, Challenges, and Prospects. *J. Meteorol. Soc. Japan*, **82,** 1599–1628.

Wang, Z. Q., A. M. Duan, and G. X. Wu, 2014: Impacts of boundary layer parameterization schemes and air-sea coupling on WRF simulation of the East Asian summer monsoon. *Sci. China Earth Sci.*, **57,** 1480–1493.

Warner, T. T., R. A. Peterson, and R. E. Treadon, 1997: A tutorial on lateral boundary conditions as a basic and potentially serious limitation to regional numerical weather prediction. *Bull. Amer. Meteor. Soc.*, **78,** 2599–2617.

Watson, R. T., 2009: Climate plan calls for forest expansion. *USA Today, 19 August.* [Available online at http://usatoday30.usatoday.com/news/nation/environment/2009-08-19-forest_N.htm]

Watson, R. T., I. R. Noble, B. Bolin, N. H. Ravindranath, and D. Verado, 2000: *Intergovernmental Panel on Climate Change Special Report; Land Use, Land-Use Change and Forestry.* Cambridge University Press, Cambridge.

Winter, J., J. S. Pal, and E. A. B. Eltahir, 2009: Coupling of Integrated Biosphere Simulator to Regional Climate Model version 3. *J. Climate,* **22,** 2743–2757.

World Bank, 2000: Argentina-Water resources management-policy elements for sustainable development in the 21st century. Washington, DC: World Bank. [Available online at http://documents.worldbank.org/curated/en/2000/08/693215/argentina-water-resources-management-policy-elements-sustainable-development-21st-century]

Wu, J. and X. Gao, 2013: A gridded daily observation dataset over China region and comparison with the other datasets. *Chinese J. Geophys. (in Chinese),* **56,** 1102–1111, doi: 10.6038/cjg20130406.

Wu, J., Gao, F. Giorgi, Z. Chen and D. Yu, 2012: Climate effects of the Three Gorges Reservoir as simulated by a high resolution double nested regional climate model. *Quat. Int.,* **282,** 27–36.

Xiao, J., T. Nakamura, H. Lu, and G. Zhang, 2002: Holocene climate changes over the desert/loess transition of north-central China. *Earth Planet. Sci. Lett.,* **197,** 11–18.

Xu, Y., X. Gao, Y. Shen, C. Xu, Y. Shi, and F. Giorgi, 2009: A daily temperature dataset over China and its application in validating a RCM simulation. *Adv. Atmos. Sci.,* **26**, 763–772.

Xue, Y., 1996: The impact of desertification in the Mongolian and the Inner Mongolian grassland on the regional climate. *J. Climate,* **9,** 2173–2189.

Xue, Y., and J. Shukla, 1996: The influence of land surface properties on Sahel climate. Part II: Afforestation. *J. Climate,* **9,** 3260–3275.

Xue, Y., M. J. Fennessy and P. J. Sellers, 1996: Impact of vegetation properties on U.S. summer weather prediction. *J. Geophys. Res.*, **101,** 7419–7430.

Xue, Y., and M. Fennessy, 2002: Under what conditions does land cover change impact regional climate? In Reynolds, J. F. and D. M. Stafford Smith (Eds.), *Global desertification: Do human causes deserts?* Dahlem University Press, Berlin, Germany, 59–73 pp.

Xue, Y., H. Juang, W. Li, S. Prince, R. DeFries, Y. Jiao, and R. Vasic, 2004: Role of land surface processes in monsoon development: East Asia and West Africa. *J. Geophys. Res.,* **109,** D03105.

Yang, H., 2004: Land conservation campaign in China: integrated management, local participation and food supply option. *Geoforum,* **35,** 507–518.

Yang, Z., and R. Dickinson, 1997: Description of the Biosphere-Atmosphere Transfer Scheme (BATS) for the Soil Moisture Workshop and evaluation of its performance. *Global Planet. Change,* **13,** 117–134.

Yhang, Y., and S. Hong, 2008: Improved Physical Processes in a Regional Climate Model and Their Impact on the Simulated Summer Monsoon Circulations over East Asia. *J. Climate,* **21,** 963–979.

Zanis, P., C. Douvis, I. Kapsomenakis, I. Kioutsioukis, D. Melas, and J. Pal, 2009: A sensitivity study of the regional climate model (RegCM3) to the convective scheme with emphasis in Central Eastern and Southeastern Europe. *Ther. Appl. Climatol.,* **97,** 327–337.

Zanis P., C. Ntogras, A. Zakey, I. Pytharoulis, and T. Karacostas, 2012: Regional climate feedback of anthropogenic aerosols over Europe using RegCM3. *Clim. Res.,* **52,** 267–277.

Zeng, N., J. D. Neelin, K. M. Lau, and C. J. Tucker, 1999: Enhancement of interdecadal climate variability in the Sahel by vegetation interaction. *Science,* **286,** 1537–1540.

Zeng, X., M. Zhao, and R. Dickinson, 1998: Intercomparison of bulk aerodynamic algorithms for the computation of sea surface fluxes using the TOGA COARE and TAO data. *J. Climate,* **11,** 2628–2644.

Zhang, G. J., 2002: Convective quasi-equilibrium in midlatitude continental environment and its effect on convective parameterization. *Clim. Dyn.,* **107,** 12–16.

Zhang, H., A. Henderson-Sellers, and K. McGuffie, 2001: The compounding effects of tropical deforestation and greenhouse warming on climate. *Clim. Change,* **49,** 309–338.

Zhang, H., and X. Gao, 2009: On the atmospheric dynamical responses to land-use change in East Asian monsoon region. *Clim. Dyn.,* **33,** 409–426.

Zhang, H., X. Gao, and Y. Li, 2009: Climate impacts of land-use change in China and its uncertainty in a global model simulation. *Clim. Dyn.,* **32**, 473–494.

Zhang, J., L. Wu, and W. Dong, 2011: Land-atmosphere coupling and summer climate variability over East Asia. *J. Geophys. Res.,* **116,** D05117.

Zhang, Y., W. B. Rossow, and P. W. Stackhouse Jr., 2006a: Comparison of different global information sources used in surface radiative flux calculation: Radiative properties of the near-surface atmosphere. *J. Geophys. Res.*, **111**, D13106.

Zhang, Y., W. B. Rossow, and P. W. Stackhouse Jr, 2007: Comparison of different global information sources used in surface radiative flux calculation: Radiative properties of the surface. *J. Geophys. Res.*, **112**, D01102.

Zhang, Y. Q., 2000: Deforestation and forest transition: theory and evidence from China. Palo, M. and H. Vanhanen (Eds.), In: World Forests from Deforestation to Transition? *World Forests,* **2,** 41–65.

Zhang, Y., Y. Xu, W. Dong, L. Cao, and M. Sparrow, 2006b: A future climate scenario of regional changes in extreme climate events over China using the PRECIS climate model. *Geophy. Res. Lett.*, **33,** L24702.

Zhao, M., and A. J. Pitman, 2002: The regional scale impact of land cover change simulated with a climate model. *Int. J. Climatol.,* **22,** 271–290.

Zhao, M., and A. J. Pitman, 2005: The relative impact of regional scale land cover change and increasing CO_2 over China. *Adv. Atmos. Sci.,* **22,** 58–68.

Zheng, Y., G. Yu, Y. Qian, M. Miao, X. Zeng and H. Liu, 2002: Simulations of regional climatic effects of vegetation change in China. *Q. J. R. Meteorol. Soc.,* **128,** 2089–2114.

Zhou, X., Y. Ding, and P. Wang, 2010: Moisture transport in the Asian summer monsoon region and its relationship with summer precipitation in China. *J. Meteor. Res.,* **24,** 31–42.

Zobler, L., 1999: Global Soil Types, 1-Degree Grid (Zobler). Data set from Oak Ridge National Laboratory Distributed Active Archive Center, Oak Ridge, Tennessee, U.S.A. [Available online at http://www.daac.ornl.gov]